EPA-460/3-73-001

DEVELOPMENT OF LOW EMISSION POROUS-PLATE COMBUSTOR FOR AUTOMOTIVE GAS TURBINE AND RANKINE CYCLE ENGINES

U.S. ENVIRONMENTAL PROTECTION AGENCY
Office of Air and Water Programs
Office of Mobile Source Air Pollution Control
Alternative Automotive Power Systems Division
Ann Arbor, Michigan 48105

EPA-460/3-73-001

DEVELOPMENT OF LOW EMISSION POROUS-PLATE COMBUSTOR FOR AUTOMOTIVE GAS TURBINE AND RANKINE CYCLE ENGINES

by

Mr. Richard J. Rossbach
General Electric Co.
Energy Systems Programs
P.O. Box 15132
Cincinnati, Ohio 45215

Contract No. 68-01-0461

Project Officers:

Mr. Thaddeus S. Mroz (NASA - Lewis)
Mr. William C. Cain (EPA)

Prepared for

U.S. ENVIRONMENTAL PROTECTION AGENCY
Office of Air and Water Programs
Office of Mobile Source Air Pollution Control
Alternative Automotive Power Systems Division
Ann Arbor, Michigan 48105

September 1973

This report is issued by the Office of Mobile Source Air Pollution Control, Office of Air and Water Programs, Environmental Protection Agency, to report technical data of interest to a limited number of readers. Copies of this report are available free of charge to Federal employees, current contractors and grantees, and non-profit organizations - as supplies permit - from the Air Pollution Technical Information Center, Environmental Protection Agency, Research Triangle Park, North Carolina 27711 or may be obtained, for a nominal cost, from the National Technical Information Service, 5285 Port Royal Road, Springfield, Virginia 22151.

This report was furnished to the U.S. Environmental Protection Agency by The General Electric Company in fulfillment of Contract No. 68-01-0461 and has been reviewed and approved for publication by the Environmental Protection Agency. Approval does not signify that the contents necessarily reflect the views and policies of the agency. The material presented in this report may be based on an extrapolation of the "State-of-the-art." Each assumption must be carefully analyzed by the reader to assure that it is acceptable for this purpose. Results and conclusions should be viewed correspondingly. Mention of trade names or commercial products does not constitute endorsement or recommendation for use.

Publication No. EPA-460/3-73-001

CONTENTS

	Page
SUMMARY	1
INTRODUCTION	5
ABSTRACT	17
CONCLUSIONS AND RECOMMENDATIONS	19
GAS TURBINE COMBUSTOR	31
Discussion	31
Combustor Loading and Emission Analysis	33
Combustor Concept Feasibility Development	105
Fuel-Air Mixture Supply Development	147
Porous Plate Combustor Fabrication Development	167
Combustor Configuration and Engine Integration Design	180
RANKINE CYCLE COMBUSTOR	189
Discussion	189
Preliminary Burner-Vapor-Generator Design	191
Bench Tests	200
REFERENCES	232
APPENDIX	235
ACKNOWLEDGEMENT	244

LIST OF FIGURES

Figure No.		Page
1	Schematic of Porous Plate Burner.	9
2	Effect of Unburned Gas Superficial Velocity and Equivalence Ratio Upon Flame Temperature.	11
3	NO Formation Rate From Hot-Air Mechanism.	13
4	Calculated NO_2 Formation Rates as a Function of Porous Plate Superficial Velocity and Equivalence Ratio. . . .	14
5	Air-Cooled Porous-Plate Burner Concept.	21
6	Schedule for Gas-Turbine Porous-Plate Combustor	22
7	Conceptual Design of Porous-Plate Burner-Vapor Generator for Rankine System.	26
8	Schedule for Rankine Porous-Plate Combustor	28
9	Low NO_x Frit Plate Gas Turbine Combustor (Fuel Inside).	34
10	Fuel Scheduling of Base Line Engine	37
11	Hot-Side Burner Temperature: Primary Air from Compressor Discharge	38
12	Hot-Side Burner Temperature: Primary Air from Compressor Discharge	39
13	Hot-Side Burner Temperature: Primary Air from Regenerator Discharge	41
14	Hot-Side Burner Temperature: Primary Air from Regenerator Discharge	42
15	Hot-Side Burner Temperature	43
16	Effect of Emissivity on Burner Temperatures	45
17	Burned Gas Temperature of Radiation Cooled Combustor at Steady State Points.	48
18	Burned Gas Temperature of Radiation Cooled Combustor at Steady State Points.	49
19	Burned Gas Temperature of Radiation Cooled Combustor at Steady State Points.	50
20	Burned Gas Temperature of Radiation Cooled Combustor at FDC Points.	51
21	Burned Gas Temperature of Radiation Cooled Combustor at FDC Points.	52
22	Burned Gas Temperature of Radiation Cooled Combustor at FDC Points.	53
23	Burned Gas Temperature of Radiation Cooled Combustor at Steady State Wide Open Throttle Points.	54

Figure No.		Page

24	Burned Gas Temperature of Radiation Cooled Combustor at Steady State Wide Open Throttle Points.	55
25	Burned Gas Temperature of Radiation Cooled Combustor at Steady State Wide Open Throttle Points.	56
26	Surface Temperature of Radiation Cooled Combustor at Steady-State Points	57
27	Surface Temperature of Radiation Cooled Combustor at Steady-State Points	58
28	Surface Temperature of Radiation Cooled Combustor at Steady State Points	59
29	Surface Temperature of Radiation Cooled Combustor at FDC Points.	60
30	Surface Temperature of Radiation Cooled Combustor at FDC Points.	61
31	Surface Temperature of Radiation Cooled Combustor at FDC Points.	62
32	Surface Temperature of Radiation Cooled Combustor at Steady State Wide Open Throttle Points.	63
33	Surface Temperature of Radiation Cooled Combustor at Steady State Wide Open Throttle Points.	64
34	Surface Temperature of Radiation Cooled Combustor at Steady State Wide Open Throttle Points.	65
35	Surface Temperature of Radiation Cooled Combustor at Steady State Points	66
36	Surface Temperature of Radiation Cooled Combustor at Steady State Points	67
37	Surface Temperature of Radiation Cooled Combustor at Steady State Points	68
38	Surface Area of Radiation Cooled Combustor at FDC Points.	69
39	Surface Temperature of Radiation Cooled Combustor at FDC Points.	70
40	Surface Temperature of Radiation Cooled Combustor at FDC Points.	71
41	Surface Temperature of Radiation Cooled Combustor at Steady State Wide Open Throttle Points.	72
42	Surface Temperature of Radiation Cooled Combustor at Steady State Wide Open Throttle Points.	73
43	Surface Temperature of Radiation Cooled Combustor at Steady State Wide Open Throttle Points.	74
44	Superficial Velocity Along Steady State Power Match Line.	76

Figure No.		Page

45 Combustor Temperature Along Steady State Power Match Line. 77

46 NO_x Emission Index Along Steady State Power Match Line. 78

47 CO Emission Index Along Steady State Power Match Line. 79

48 Nodal System for Transient Thermal Analysis 82

49 Time-Dependent Gas Generator Speed During 3 Wide-Open-Throttle Transients (WOT) at 85°F 85

50 Fuel Scheduling of Base Line Engine During the Four Transients. 86

51 Configuration or Materials in Porous Burner (for Transient Analysis) 88

52 Schedule of Burner Area and Equivalence Ratio During the 4 Transients. 89

53 Calculated Thermal Response of the Porous Combustor During WOT From Idle. 90

54 Undiluted Burned Gas Temperature During the WOT Transient From Idle to 100% Gas Generator Speed of the Base Line Engine. 92

55 Conditions at the Burner Surface During WOT From Idle to 100% Gas Generator Speed 93

56 Heat Fluxes Back to the Burner Surface During WOT from Idle to 100% Gas Generator Speed 94

57 Thermal Response of Porous Combustor to a Hypothetical Transient 96

58 Calculated Thermal Response of the Porous Combustor During the WOT Transient from 40% Engine Power. 97

59 Burned Gas Temperature During the WOT Transient from 40% Engine Power of the Base Line Engine. 98

60 Calculated Thermal Response of the Combustor During the WOT Transient from 60% Engine Power of Base Line Engine. 99

61 Burned Gas Temperature During the WOT from 60% Engine Power of the Base Line Engine 100

62 Combustor Response to Cold Start Transient. 101

63 Burned Gas Temperature During Cold Start Transient of Base Line Engine 102

64 Predicted NO_2 Emissions Index Based on the Hot Air Mechanism 103

65 Predicted CO Emissions Index. 104

66 Gas Turbine Porous-Plate Combustor Test Section 106

67 SiC Spring Loaded Configuration 108

Figure No.		Page

68 Metallic Combustor Configurations 110

69 Kanthal-Wrapped Burner. 112

70 Kanthal-Wrapped Burner with Zirconia Cloth and Cerapaper Insulation. 113

71 Emission Measurements from Burner S/N 102 117

72 Configuration With SiC Rings Over Mullite Cylinder. . . 118

73 Schematic of Preignition Test Setup 119

74 Preignition Test Rig Hardware 120

75 Upstream Face Temperature Leading to Preignition at 3 Atmospheres 124

76 Impending Preignition at P = 4 Atmospheres. 125

77 Radiant Heat Flux From A Burner 128

78 Calculated Maximum Wall Temperatures for Air-Cooled Burner for Cooling Air Initial Temperature, 400°F . . . 129

79 Calculated Maximum Wall Temperatures for Air-Cooled Burner for Cooling Air Initial Temperature, 1400°F. . . 130

80 Heat Flux Back to the Porous Burner as a Function of Pressure and of Superficial Gas Velocity (V_{25}). 132

81 Design of Air-Cooled Porous Burner 106. 133

82 Air-Cooled Burner #106 During Fabrication 136

83 Schematic of Gas Turbine Combustor Test Facility. . . . 138

84 Scott Exhaust Gas Analyzer. 140

85 Emissions from Air-Cooled Burner S/N 106 at 1 Atm. Pressure. 142

86 NO_2 Measurements at 1 to 4 Atmospheres on Air-Cooled Burner. 143

87 Burner 107 Pressure Drop. 144

88 Measurements of CO and NO_x Emissions on Burner 107. . . 146

89 Measured CO Emissions on Burner 108M with Both Heated and Unheated Air. 148

90 Measured NO_x Emissions on Burner 108M with Both Heated and Unheated Air. 149

91 Fuel Vaporizer for Gas Turbine Combustor. 151

92 "Sonicore" Fuel Vaporizer 153

93 Estimated Performance of Fuel Vaporizer for Gas Turbine Combustor 157

94 Vaporizer and Inlet and Exhaust Lines 159

95 Vaporizer and Inlet and Exhaust Lines 161

96 Vaporizer Air and Fuel Supply System. 162

97 Experimental Vaporization Quality as a Function of the B Group Parameter 166

Figure No.		Page

98 Weight Gain of Fe-25Cr-4Al-Y Alloy During Oxidation Testing in Air. 174

99 Poroloy Permeability Retention After Exposure at 1800 and 2000°F (982 and 1093°C) in Air. Alloys GE 1541 and H 875 175

100 Nichrome Porous Cylinder No. 3 As Sintered at 2350°F. . 181

101 Porous Cylinder No. 3 with Tube Sheets Brazed on Each End 182

102 Air-Cooled Porous-Plate Burner Concept. 185

103 Conceptual Design of Porous-Plate Burner-Vapor Generator for Rankine System. 192

104 Fuel-Air Mixer and Fuel Vaporizer Double-Swirl Carbureting Concept 195

105 Preliminary Installation Configurations 196

106 Rankine Engine Fuel-Air Mixer Cup Flow Characteristics. 198

107 Estimated Vaporizer Performance 199

108 Half-Filled Copper Shot Burner, Illustrating Burner Construction and Coolant Tube Manifolding 201

109 Schematic Diagram of Burner Test and Gas Sampling Arrangement 202

110 Burner Heat Flux Back to the Burner from the Flame; Propane-Air Mixtures. 213

111 Burner Heat Flux Back to the Burner from the Flame; Gasoline (EPA)-Air Mixtures 214

112 Comparison of Gasoline (EPA) and Propane-Air Burned Gas Temperatures. 215

113 CO Analyses from Two Flames 220

114 CO Experimental Measurements on Water-Cooled Burners with 20 Milliseconds Residence Time 222

115 Variation of NO Formation Rate from "Hot-Air" Mechanism as a Function of Reciprocal Absolute Temperature. NO Formation Rate Adjusted to 2% Molar O_2. 224

116 NO_2 Experimental Measurements on Water-Cooled Burners with 20 Milliseconds Residence Time 230

A-1 GDF I Combustor Test Facility 236

A-2 Test Cell Heaters and Flow Metering Sections. 237

A-3 Fuel Storage and Pumping. 239

A-4 Heater Control Console. 240

A-5 Facility Control Console. 241

A-6 Scott Exhaust Gas Analyzer. 243

LIST OF TABLES

Table No.		Page
1	Base Line Engine Combustor Test Points	36
2	Summary of Calculations	47
3	Silicon Carbide Combustor Configurations	109
4	Metallic Combustor Configurations	114
5	Preignition Tests	122
6	Parts List of Air-Cooled Porous Burner Shown in Figure 81	134
7	Air-Cooled Burners (Cylindrical)	137
8	Gas Turbine Fuel Vaporizer Test Data	165
9	Porous Combustor Materials	168
10	Candidate Alloys for Combustor Components	170
11	Tensile Properties of Candidate Alloys for Combustor Components	173
12	Critical Thermal Properties of Selected Ceramics	176
13	Porous Rankine Combustor	193
14	Rankine Model Burner Test Results	216
15	Rankine Model Burner Emission Results	219

SUMMARY

The requirements of the 1970 Clean Air Act Amendments were that the Environmental Protection Agency enforce stringent exhaust emission standards for new automobiles on unburned hydrocarbons and carbon monoxide in the 1975 model year and on nitrogen oxides in the 1976 model year (although these requirements may be relaxed for a time). As the standards originally stood, the most difficult standard to meet was that relating to NO_x, especially since it is difficult to obtain low NO_x and low CO together. Experiments with porous-plate combustors previous to this contract had shown very low NO_x levels, so further development work was undertaken. The purpose of this contract was to evaluate analytically and experimentally the use of the porous-plate combustor for use in the gas-turbine or Rankine-cycle advanced automobile engines to control exhaust emissions.

By providing a uniform mixture of fuel and air (pre-mixed) and passing it through a porous plate, combustion is initiated and a uniform flame can be stabilized on the downstream surface of the porous material. Because of the closeness of the flame to the plate and short flame height (1-4 mm), heat is transferred from the flame to the plate, cooling the flame and preventing the adiabatic flame temperature from being attained. The heat transferred to the plate must be removed by radiation or a coolant in the case of the gas-turbine combustor and by the working fluid in the case of the Rankine-cycle combustor. This combustion process virtually eliminates unburned hydrocarbon emissions as long as there is

a small excess of oxygen. The reduction of the flame temperature from the adiabatic to some lower temperature dramatically reduces the NO_x emissions. The CO emission can be traded off with the very low NO_x emissions in terms of residence time to make them low also.

THE GAS TURBINE COMBUSTOR

The following conclusions were drawn concerning the porous-plate gas turbine combustor from the work described herein:

1. Analytical work indicates that the combustor equivalence ratio and the porous-plate burner area must be variable in order for the engine to operate between the steady-state level-road load fuel requirements and the wide-open-throttle acceleration fuel requirements.
2. The operational temperature of the downstream side of the porous plate must be limited to a specific value at the higher power levels to prevent flashback through the porous plate and pre-ignition of the fuel air mixture. Air cooling of the porous plate matrix, in addition to radiation cooling, is required to avert this condition.
3. Models of air-cooled porous-plate combustors have successfully been made from sintered nichrome and tested.
4. Emission measurements with propane-air mixtures at inlet temperatures of approximately 400°F and one atmosphere were favorable. The NO_x emission index was below the 1976 Federal Standards and the CO emission index was below the Standards at combustor conditions corresponding to light engine loads but somewhat above it at heavier loads. The unburned hydrocarbon values were at about the detection level which is much below the Standard.

5. Tests of a fuel atomizer and vaporizer using an air assist fuel nozzle spraying into a swirling flow resulted in all but a few points having 93% or more of the fuel vaporized.

Based upon these results, a full size porous-plate combustor concept has been developed for the Baseline Engine having a total porous plate area of 2.2 ft^2 and which extends only 2 inches higher vertically than the conventional combustor for the engine. In this concept, the total porous surface is made up of a number of air-cooled wedge-shaped flat-plate segments. It is recommended that this combustor be designed, fabricated, and tested with gasoline.

THE RANKINE CYCLE COMBUSTOR

The following conclusions were drawn concerning the porous-plate Rankine-cycle combustor from the work described herein:

1. The Arrhenius plots of superficial velocity versus reciprocal absolute flame temperature at constant equivalence ratio which are used to design porous-plate combustors were confirmed for five fuels including gasoline.
2. Both the emissions indexes for NO_x and CO increased with superficial velocity at constant equivalence ratios and for liquid fuels were only below the Standard at conditions corresponding to moderate engine loads.
3. The unburned hydrocarbon emission indexes were very low, about at the detection level.
4. The fuel atomizer and vaporizer developed for the gas turbine combustor are adequate for the Rankine combustor. All but a few of the test points indicated 93% or more fuel vaporization.

The original Rankine-cycle combustor concept is unchanged. Since the sintered copper water-cooled porous-plate combustors are successfully being made by the General Electric Company and based upon the above results, it is recommended that the full-size water-cooled Rankine combustor be designed, fabricated, and tested using gasoline.

INTRODUCTION

The purpose of the work under this contract was to evaluate the use of the porous plate combustor systems for gas turbine and Rankine cycle advanced automotive engines.

Evaluation of this unique combustion system included emission levels, burning limits, air and fuel requirements, response to transients, general operating characteristics, start up, durability, sensitivity to degree of inlet fuel vaporization, and pressure drop. This work was intended to provide proof of feasibility of use of porous plate burners by demonstrating adequate performance in the following areas:

- Emission characteristics of the model or segments as developed
- Definition of start up characteristics
- A complete combustor operating map sufficient to define full scale combustor designs. The information to be generated includes mixture quality control requirements, mixture distribution requirements, combustor active area control, means of controlling equivalence ratio, etc.

The approach to the gas turbine and Rankine cycle combustor development included the following tasks:

<u>Gas Turbine Combustor Development</u>

IB. Combustor loading and emission analysis

IIB. Combustor configuration and engine integration design

IIIB. Combustor concept feasibility development

IVB. Fuel-air mixture supply development

VB. Porous plate combustor fabrication development

VIB. Prepare recommendations

Rankine Cycle Combustor Development

IR. Preliminary burner vapor generator design

IIR. Bench tests

IIIR. Engineering test unit

IVR. Prepare recommendations

The development of the Rankine Cycle Combustion system was performed in parallel to the gas turbine combustor development. A complete interchange of technology was made, generated on either gas turbine or Rankine cycle burners.

The requirements of the 1970 Clean Air Act Amendments are that the Environmental Protection Agency enforce stringent exhaust emission standards for new automobiles on unburned hydrocarbons and carbon monoxide in the 1975 model year and on nitrogen oxides in the 1976 model year. The original 1976 standards are as follows:

Unburned hydrocarbons, grams/mile	0.41
Carbon monoxide, grams/mile	3.4
Nitrogen oxides, grams/mile	0.4

Although the automobile industry is attempting to meet the emission standards with the conventional automobile reciprocating engine, there are several other promising engine types which have a high potential of meeting the 1976 emission Standards. Both the gas turbine and the Rankine cycle engines have the potential for low exhaust emissions. The combustor for each engine can be designed separately for efficient and controlled

combustion while still being integrated into the engine configuration. Currently, combustors designed for these two engine types still have emissions problems, especially with difficulty in obtaining low NO_x emissions. Many conventional combustors burn from sprayed droplets.[1,2,3] The result is that large variations in the local equivalence ratio can exist in the primary combustion zone due to inefficient atomization and mixing; for an overall lean equivalence ratio, part of the combustion can occur at near-stoichiometric conditions, resulting in high peak flame temperatures, with attendant high NO_x production rates, while the rest of the combustion occurs at a very lean equivalence ratio at lower flame temperatures with lower NO_x production rates. The overall result is high NO_x, since the NO_x production rate increases logarithmically with temperature; the areas of low NO_x production cannot balance the areas of high NO_x production.

In order to minimize NO_x emissions, both the flame temperature and the residence time at temperature must be controlled. The flame temperature determines the NO_x production rate, while the residence time is the time over which the NO_x production rate is operative. The flame temperature should not be excessively depressed; if the flame temperature is too low, then the CO decay rate is also low, and not enough CO will be burned off to form CO_2, for a given residence time. Similarly, flame temperatures that are too low will also result in high emissions of unburned hydrocarbons, since the burn-off rates depend strongly on flame temperature.

Previously, experiments with a porous plate combustor had shown very low NO_x levels, so further development work was undertaken. By providing a uniform mixture of fuel and air and passing it through a

porous plate, a uniform flame can be stabilized on the downstream surface of the porous material. Because of the closeness of the flame to the plate, heat is transferred from the flame to the plate, cooling the flame and preventing the adiabatic flame temperature from being attained. The heat transferred to the plate must be removed by radiation or a coolant in the case of the gas-turbine combustor and by the working fluid in the case of the Rankine-cycle combustor. The evenness of the flame virtually eliminates unburned hydrocarbon emissions as long as there is a small excess of oxygen. The reduction of the flame temperature from the adiabatic to some lower temperature dramatically reduces the NO_x emissions. The emission of CO can be traded off with the very low NO_x emissions in terms of residence time and flame temperature to make them low also.

The porous burner is shown schematically in Figure 1. Premixed fuel and air pass through a porous matrix. A substantial amount of heat is conducted from the flame back to the cooled porous matrix, since the flat laminar flame is maintained close to the metal surface. The burned gas (flame) temperature obtained with the porous burner varies from the adiabatic flame temperature down to about 1500°F (2340°F) as the superficial velocity is decreased from the adiabatic flame velocity. NO_x production rates decrease logarithmically with burned gas temperature; hence, since burned gas temperatures with the porous combustor are lower than the adiabatic flame temperature, NO_x production rates are advantageously lower than in conventional combustors at the same combustion rates.

The characteristics of flames burning on cooled porous plugs have been discussed from various points of view.[4,5,6] The operating principle of the porous combustor relative to NO_x production rates is that a very

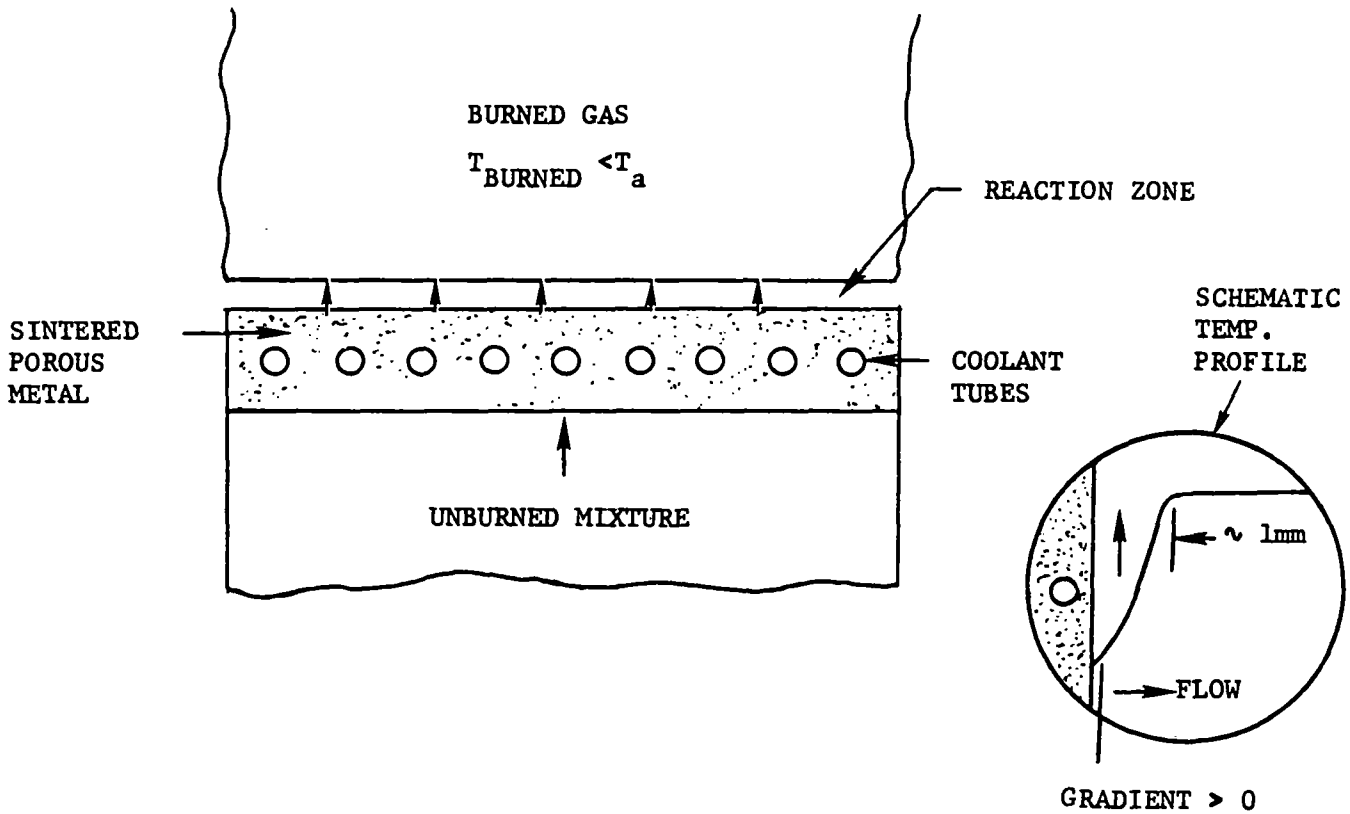

Figure 1. Schematic of Porous Plate Burner

uniform, flat, laminar flame, about 1 mm high, is formed on the surface of the porous combustor. This flame is non-adiabatic, with a predictable and appreciable fraction of its heat release being transferred from the unburned side of the flame back to the porous plate. Since the flame is non-adiabatic, the burned gas temperature can be selected by design at a value below the adiabatic temperature so as to control NO_x production rates; NO_x production rates are extremely temperature dependent, and reductions in burned gas temperatures result in significant reductions in NO_x production rates. The heat absorbed by the porous plate can be removed either by allowing the plate to operate at a high temperature such that heat removal is accomplished by thermal radiation and preheating of inlet unburned gas mixture or by incorporating cooling tubes in the porous matrix for compressor discharge air in the case of the gas turbine or for the working fluid in the Rankine application.

Measurements of burned gas temperature (T) with the porous burner are related to superficial unburned gas velocity through the burner (V_{25}) and equivalence ratio (R) by straight lines on a log V_{25} versus 1/T plot, yielding a single line for each value of R; data from Kaskan[6] is shown in Figure 2. The four porous burner combustion lines are independent of gas inlet temperature, to a first approximation. The lines at which adiabatic combustion occurs are also shown for two different unburned gas inlet temperatures. The inlet temperature of the fuel-air mixture has a significant effect on the maximum velocity above which the flame lifts off the porous surface. The points of intersection of the adiabatic and porous burner lines determine the unburned gas velocities at which the flat flame will begin to lift off the porous plate, the upper limit

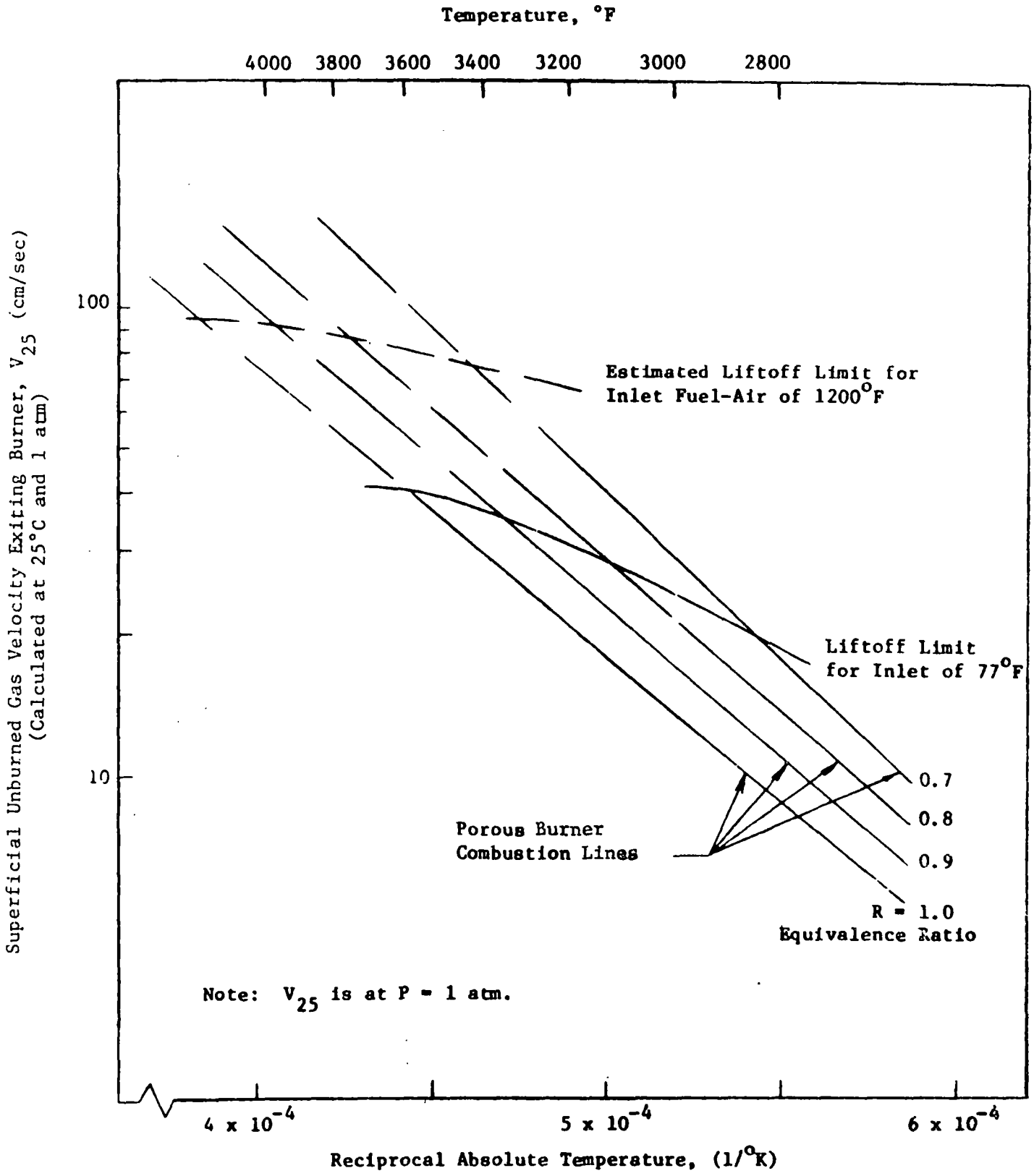

Figure 2. Effect of Unburned Gas Superficial Velocity and Equivalence Ratio Upon Flame Temperature.

of operation. The lower limit of operation (or flame extinguishment) is the gas velocity at which the burned gas temperature drops below that required to sustain the flame reaction, which occurs at about 4 cm/sec.

As seen in Figure 2, the flame temperature obtained with the porous burner can be considerably below the adiabatic flame temperature by varying the unburned gas velocity, independent of equivalence ratio.

Shown in Figure 3 are NO formation rates based on the "hot-air" mechanism. These rates are derived from the basic kinetic data used by Fenimore[7]. It can be seen that significant reductions in NO formation rates can be achieved by lowering the actual flame temperatures by only several hundred degrees. For example, a temperature reduction of 360°F (200°C) reduces the NO production rate by a factor of 20.

The porous burner produces a very uniform, stable flame; hydrocarbon and particulate emissions from lean flames on this burner have been measured, and are approximately zero. CO emissions can be kept at a low level by providing sufficient burned gas residence time at temperature to allow decay to CO_2. However, the gas temperature after dilution must be low enough so that the NO_x production rates are low. The emissions design of the porous plate burner therefore simplifies at first approximation to selection of a flame temperature low enough to limit NO formation. The NO production rates of Figure 3 can then be used to compute NO formation rates as a function of superficial velocity V_{25} from the flame temperature data of Figure 2; Figure 4 presents the NO_x formation rates thereby estimated as a function of V_{25}. The extreme reductions of NO_x that can be obtained with the porous combustor are apparent.

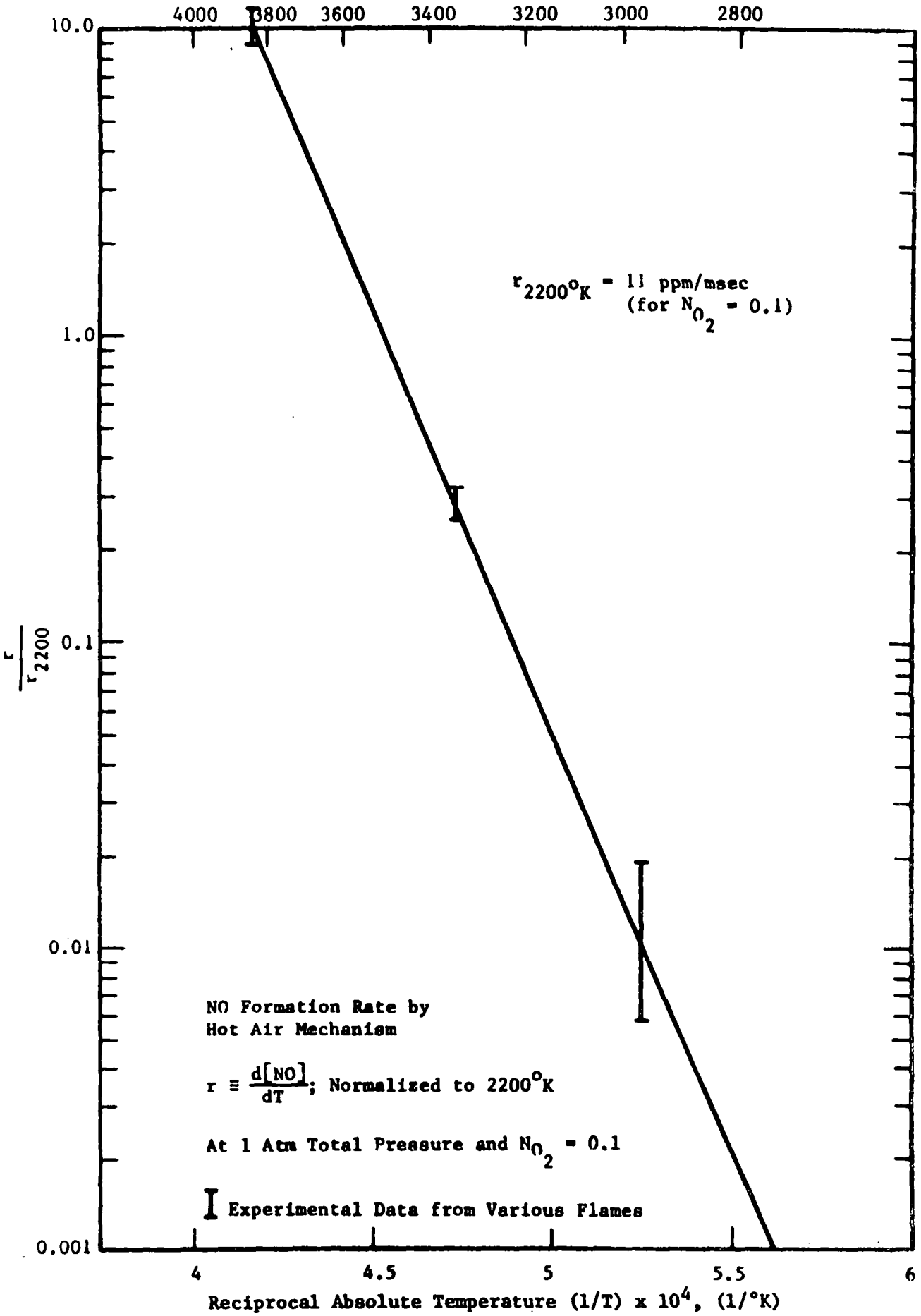

Figure 3. NO Formation Rate From Hot-Air Mechanism.

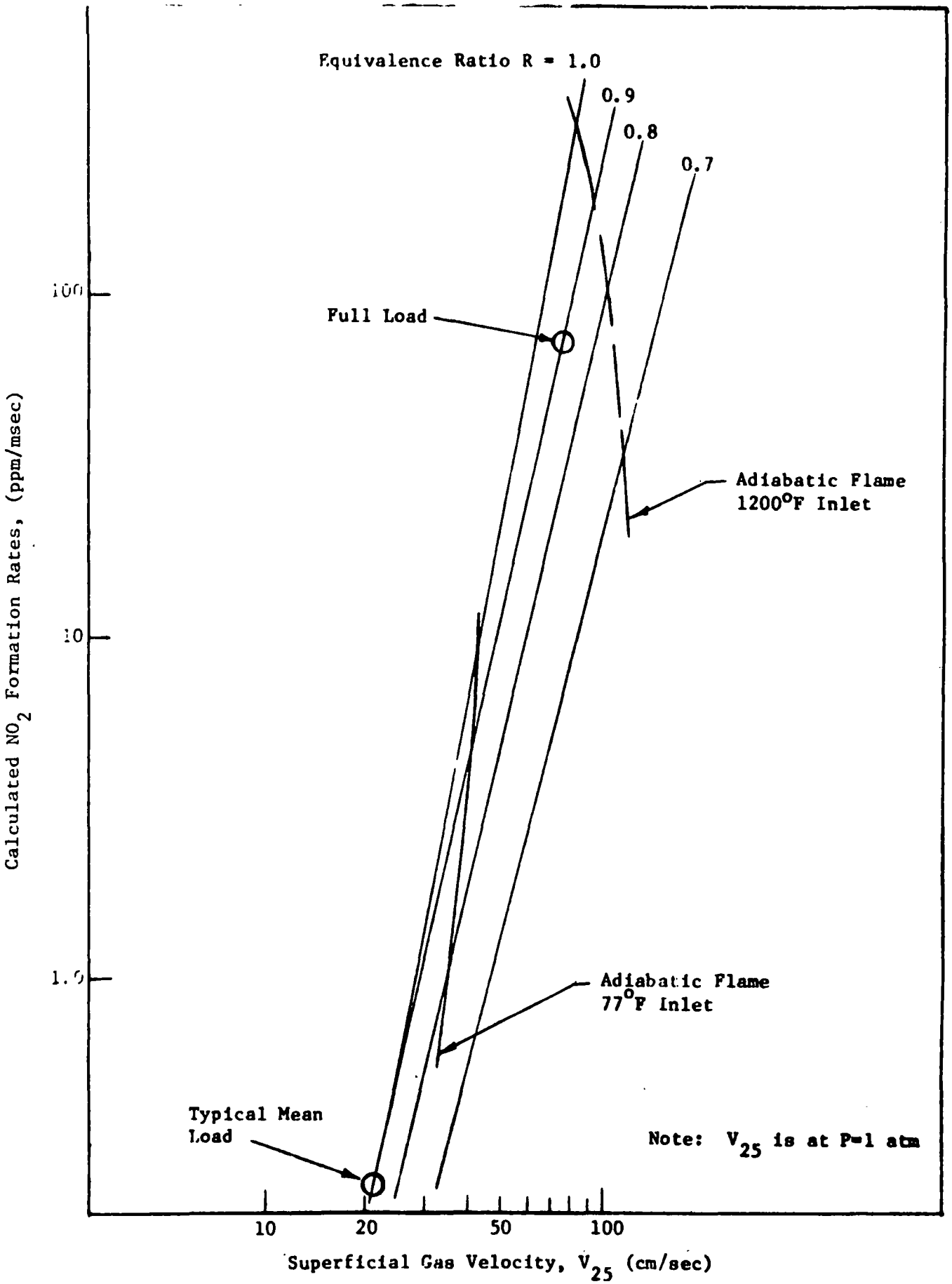

Figure 4. Calculated NO_2 Formation Rates as a Function of Porous Plate Superficial Velocity and Equivalence Ratio.

Both analytical and experimental techniques were employed to evaluate the feasibility of the porous-plate combustor for both gas turbine and Rankine automobile engines. As regards the gas turbine application, this report contains analytical results on the burner area requirements for the various operating conditions of the Baseline Engine as well as exhaust emission predictions. The design concept of an air-cooled, variable-area combustor for this engine is presented. Operational and emissions data on several experimental combustors are presented along with the fabrication development leading to these combustors. Finally the demonstration results for a full-scale fuel-air mixture system are presented.

With regard to the automotive Rankine engine application, heat load and emissions data are presented for propane and four liquid fuels. Although the fuel-air mixture system developed for the gas turbine combustor is directly applicable, alternate systems were investigated. Finally recommendations for the development of both gas turbine and Rankine combustors are presented.

ABSTRACT

Experiments with porous-plate combustors previous to this contract had shown very low NO_x levels, so further development work was undertaken. The purpose of this contract was to evaluate analytically and experimentally the use of the porous-plate combustor for use in the gas-turbine or Rankine-cycle advanced automobile engines to control exhaust emissions.

For the porous-plate combustor for the gas turbine, the following conclusions were drawn: (1) Analytical work indicates that the burner area must be variable in order to meet the fuel flow requirements for operation between steady-state load and wide-open-throttle acceleration; (2) Air-cooling of the porous burner (in addition to radiation cooling) is required to avoid flashback; (3) Models of air-cooled porous-plate combustors have been successfully built from nichrome and tested; (4) Emission measurements of NO_x, CO and unburned hydrocarbons with propane-air mixtures at inlet temperatures of approximately 400°F and one atmosphere were favorable; (5) Tests of a fuel atomizer and vaporizer resulted in all but a few points having 93% or more of the fuel vaporized.

For the porous plate combustor for the Rankine-cycle expander, the following conclusions were drawn: (1) The Arrhenius plots of superficial velocity versus reciprocal absolute flame temperature at constant equivalence ratio were confirmed for five fuels including gasoline; (2) Both the emission indexes for NO_x and CO increased with superficial velocity

at constant equivalence ratios and for liquid fuels (including gasoline) were only below the Standard at conditions corresponding to moderate engine loads; (3) The emission indexes for unburned hydrocarbons were at about the detection level, well below the Standards; (4) The fuel atomizer and vaporizer developed for the gas turbine combustor are adequate for the Rankine combustor.

CONCLUSIONS AND RECOMMENDATIONS

THE GAS TURBINE COMBUSTOR

The following conclusions were drawn concerning the porous-plate gas turbine combustor from the work described herein:

1. Analytical work indicates that the combustor equivalence ratio and the porous-plate burner area must be variable in order for the engine to operate between the steady-state level-road load fuel requirements and the wide-open-throttle acceleration fuel requirements.
2. The operational temperature of the downstream side of the porous plate must be limited to a specific value at the higher power levels to prevent flashback through the porous plate and pre-ignition of the fuel air mixture. Air-cooling of the porous plate matrix, in addition to radiation cooling, is required to avert this condition.
3. Models of air-cooled porous-plate combustors have successfully been made from sintered nichrome and tested.
4. Emission measurements with propane-air mixtures at inlet temperatures of approximately 400°F and one atmosphere were favorable. The NO_x emission index was below the 1976 Federal Standards and the CO emission index was below the Standards at combustor conditions corresponding to light engine loads but somewhat above it at heavier loads. The unburned hydrocarbon values were at about the detection level which is much below the Standard.

5. Tests of a fuel atomizer and vaporizer using an air-assist fuel nozzle spraying into a swirling flow resulted in all but a few points having 93% or more of the fuel vaporized.

As a result of these accomplishments, it is recommended that the full scale air-cooled porous-plate combustor shown in Figure 5 for the Base Line Engine be designed, fabricated and tested with gasoline in the General Electric Combustor Test Facility described in Appendix A. A schedule for the recommended work is shown in Figure 6.

The full size porous-plate combustor concept shown in Figure 5 and developed for the Baseline engine has a total porous plate area of 2.2 ft^2 and extends only 2 inches higher vertically than the conventional combustor for the engine. In this concept, the total porous surface is made up of a number of air cooled wedge-shaped flat-plate segments.

Development Plans

The air-cooled porous-plate combustor for the automotive gas turbine engine has been developed thus far by means of 1/5 scale models. Tests to date (at lower values of combustor inlet temperature than would be the case in the engine) have shown NO_x emission levels considerably below the Federal Standard and UHC levels at or below the detection level. CO emissions are either below or above the Standard depending upon operating conditions. By adjusting residence time and/or dilution staging, the CO values can be lowered with the expectation that the NO_x emissions will increase somewhat but still be below the Standard. It is now appropriate to test a module of the full-scale porous plate combustor at combustor inlet conditions commensurate with engine operating conditions, followed by testing of the full-scale combustor. The recommended work would be carried out in the following four tasks:

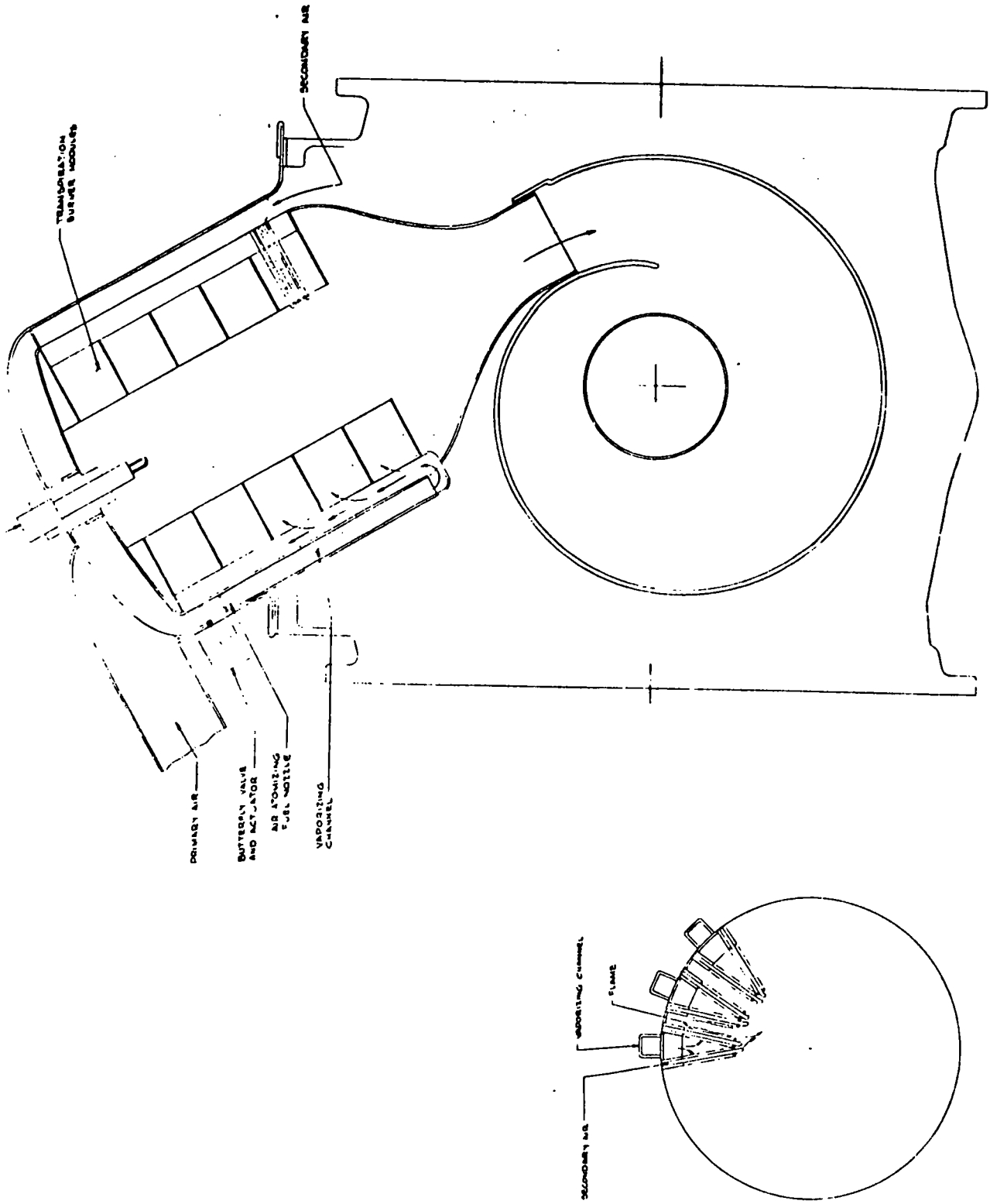

Figure 5. Air-Cooled Porous-Plate Burner Concept

Master Schedule Sheet

BASE LINE ENGINE FULL SIZE POROUS COMBUSTOR DEMONSTRATION

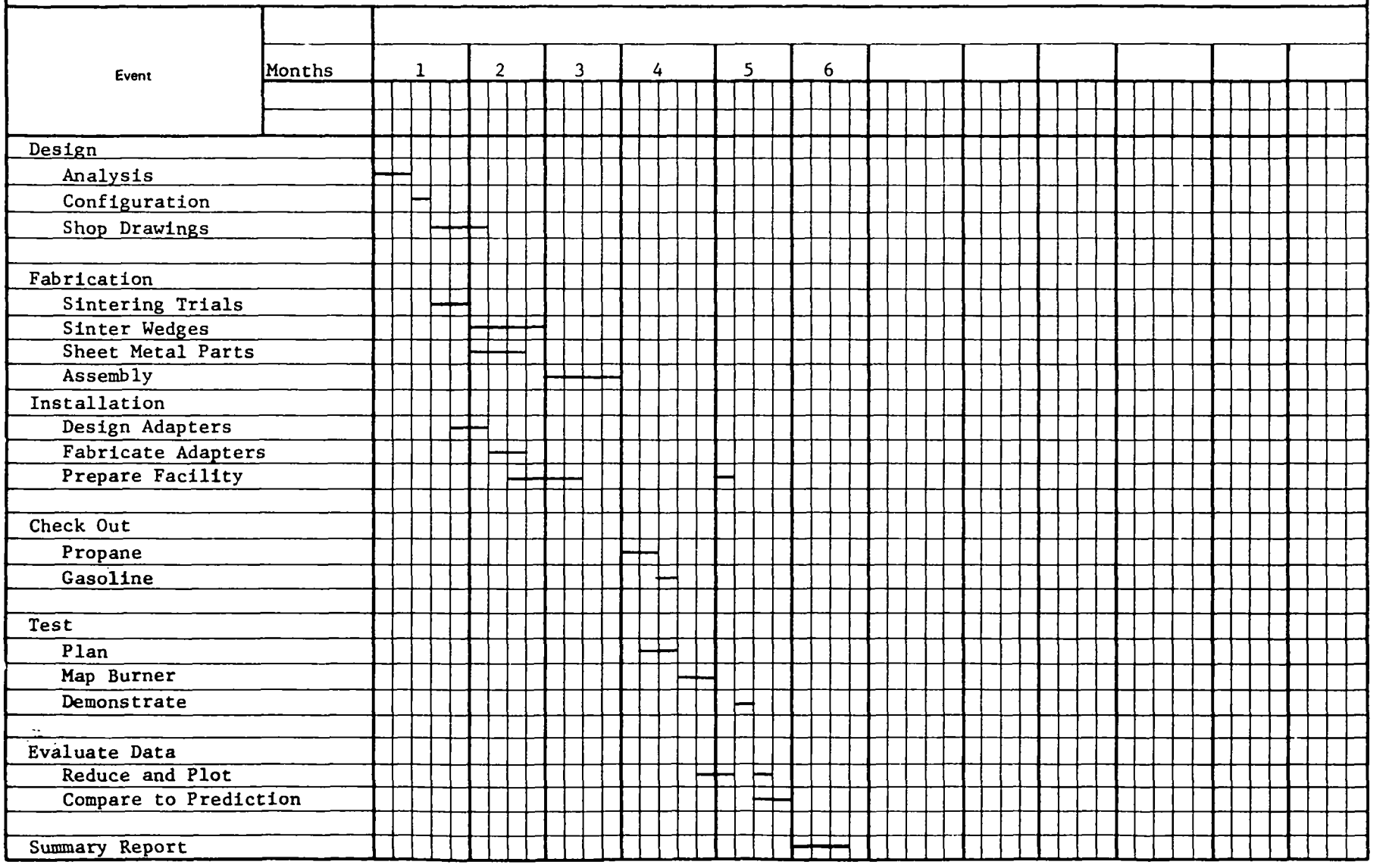

NS 1318

Figure 6. Schedule for Gas-Turbine Porous-Plate Combustor

Task I - Design and Fabrication of the Full Scale Combustor - Making use of the design analysis and the test results on the air-cooled porous plate combustor described above, a full scale combustor will be designed to the operating conditions of the Base Line Engine. More than one combustor will be fabricated having cooling tubes embedded in the sintered nichrome porous surface. Modules of the full-scale porous plate combustor will also be designed for the purpose of confirming emission measurements and module integrity under cycle conditions. In addition, all adapters will be made for installation in the General Electric GDF-I Combustor Facility described in the Appendix. In the fabrication of the combustor, care will be taken to properly control particle size distribution, sintering temperature, braze proportions and mixing and dimensions. Completion of the combustor will include the integrated fuel-air mixture supply, joining of the porous plates to the remainder of the combustor structure and insulation upstream of the porous plate to prevent preignition of the fuel-air mixture.

Task II - Installation and Checkout - After assembly of the full scale combustor it will be installed in the ESP GDF-I combustor test facility. Adapters and complete instrumentation will be provided to the facility. Provisions for measurement will include inlet flow rates, temperatures and pressures, outlet temperatures and emissions. The emissions will be measured using the Scott Dilute Exhaust Gas Emission Analyzer which is capable of accurately measuring, on a continuous basis, NO, NO_2, CO, CO_2 and unburned hydrocarbons. The facility will provide 2.5 lbm/sec of air flow in two streams, one being capable of being heated and controlled to temperatures up to 1400°F and the other to 500°F. The facility provides air at the test section at pressures up to 4 atmospheres.

Following installation of the combustor and calibration of the instrumentation, exploratory tests of the combustor will be made to assure that all required conditions of the test can be met and that all facility controls are functioning properly. The necessary adjustments to the facility will be made that are required for the test program.

Task III - Test and Evaluation - The operating performance of the combustor, including pressure drop, exit temperature, and emissions will be mapped over the appropriate ranges of burned gas velocity (V_{25}), equivalence ratio, temperature and pressure level. Testing of full-scale modules of the combustor will precede testing of the full-scale combustor. After this, the test points delineated in EPA Test procedure for Low NO_x Combustor Final Evaluation will be established and full measurements including emissions will be made. These data will be obtained at the airflow and fuel-flow rates, inlet temperature and pressure values specified in the EPA Test Procedure for Low NO_x Combustor Final Evaluation. The appropriate equivalence ratio established for each test point will also be set.

The reduced test data will be evaluated in terms of the Base Line Engine requirements. The exhaust emissions data will be interpreted in terms of emission index for the combustor performance map. However, for the points specified by the EPA Test Procedure for Low NO_x Combustor Final Evaluation, the data will be presented in terms of grams of pollutant per mile, using the mutually agreed upon schedule of fuel economy.

Task IV - Summary Report - The analysis, design and combustor test data will be documented at the end of the program along with appropriate drawings and specifications.

THE RANKINE CYCLE COMBUSTOR

The following conclusions were drawn concerning the porous-plate Rankine-cycle combustor from the work described herein:

1. The Arrhenius plots of superficial velocity versus reciprocal absolute flame temperature at constant equivalence ratio which are used to design porous-plate combustors were confirmed for five fuels including gasoline.
2. Both the emissions indexes for NO_x and CO increased with superficial velocity at constant equivalence ratios for all fuels tested and for liquid fuels were only below the Standard at conditions corresponding to moderate engine loads.
3. The unburned hydrocarbon emission indexes were very low, about at the detection level.
4. The fuel atomizer and vaporizer developed for the gas turbine combustor are adequate for the Rankine combustor. All but a few of the test points indicated 93% or more fuel vaporization.

The tin-coated copper porous-plate burners tested on this program were available from previous General Electric research programs. It was not necessary to develop the sintering techniques because they are established and available for use. The liquid-cooled porous-plate burner operates at temperatures below 700°F and as a result the thermal stresses are moderate. The Rankine cycle porous-plate combustor operates at atmospheric pressure which limits the heat flux conducted back to the porous plate from the flame, limiting the heat load.

Based on the above accomplishments, it is recommended that the full-scale water-cooled porous-plate combustor shown in Figure 7 for the

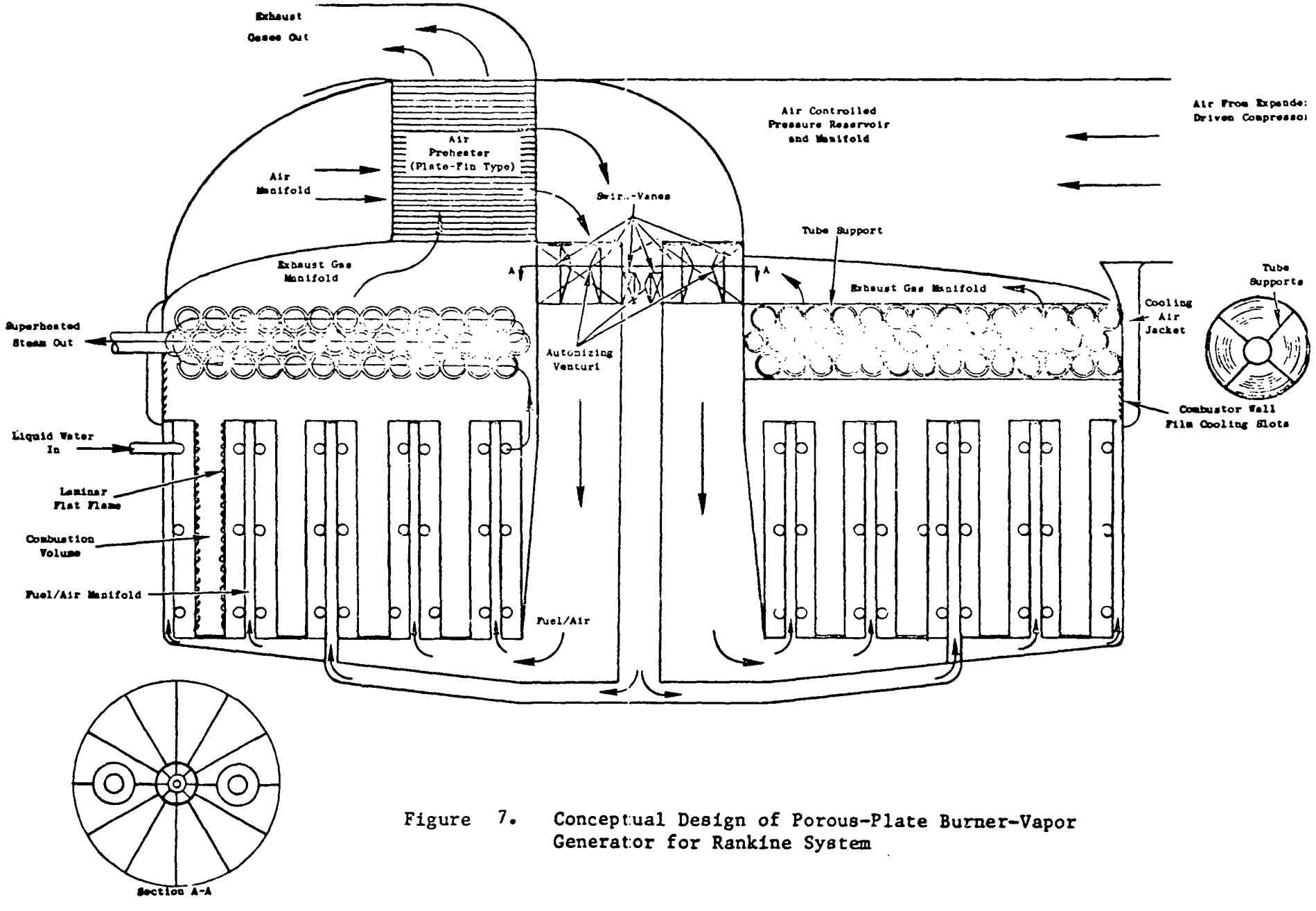

Figure 7. Conceptual Design of Porous-Plate Burner-Vapor Generator for Rankine System

Rankine-cycle engine be designed, fabricated, and tested with gasoline. The schedule for the recommended work is shown in Figure 8.

Development Plans

The water-cooled porous-plate combustor for the automotive Rankine-cycle engine has been developed thus far by means of bench tests on flat burner models. Tests to date suggest NO_x emission levels below the Federal Standard at most points and unburned hydrocarbon levels at or below the detection level. CO emissions may be either below or above the Standard depending upon operating conditions. By adjusting residence time and/or dilution staging, the CO values can be lowered with the expectation that the overall average of NO_x emissions over the cycle will increase somewhat but still be below the Standard. It is now appropriate to test a full-scale porous-plate combustor. The recommended work would be carried out in the following four tasks:

Task I - Design and Fabrication of the Full Scale Combustor - Making use of the design analysis and the test results on the water-cooled porous-plate combustor described above, a full-scale combustor will be designed to the operating conditions of a specified full-size Rankine engine. The combustor will be fabricated having cooling tubes embedded in the sintered copper porous surface. In the fabrication of the combustor, care will be taken to properly control particle size distribution, sintering temperature, braze proportions and mixing and dimensions. Completion of the combustor will include the integrated fuel-air mixture supply including the air preheater, joining of the porous plates to the remainder of the combustor structure, and a tube bundle.

Task II - Installation and Checkout - After assembly of the full scale combustor, it will be installed in a test facility which can supply air,

Master Schedule Sheet

BASE LINE ENGINE FULL SIZE POROUS COMBUSTOR DEMONSTRATION

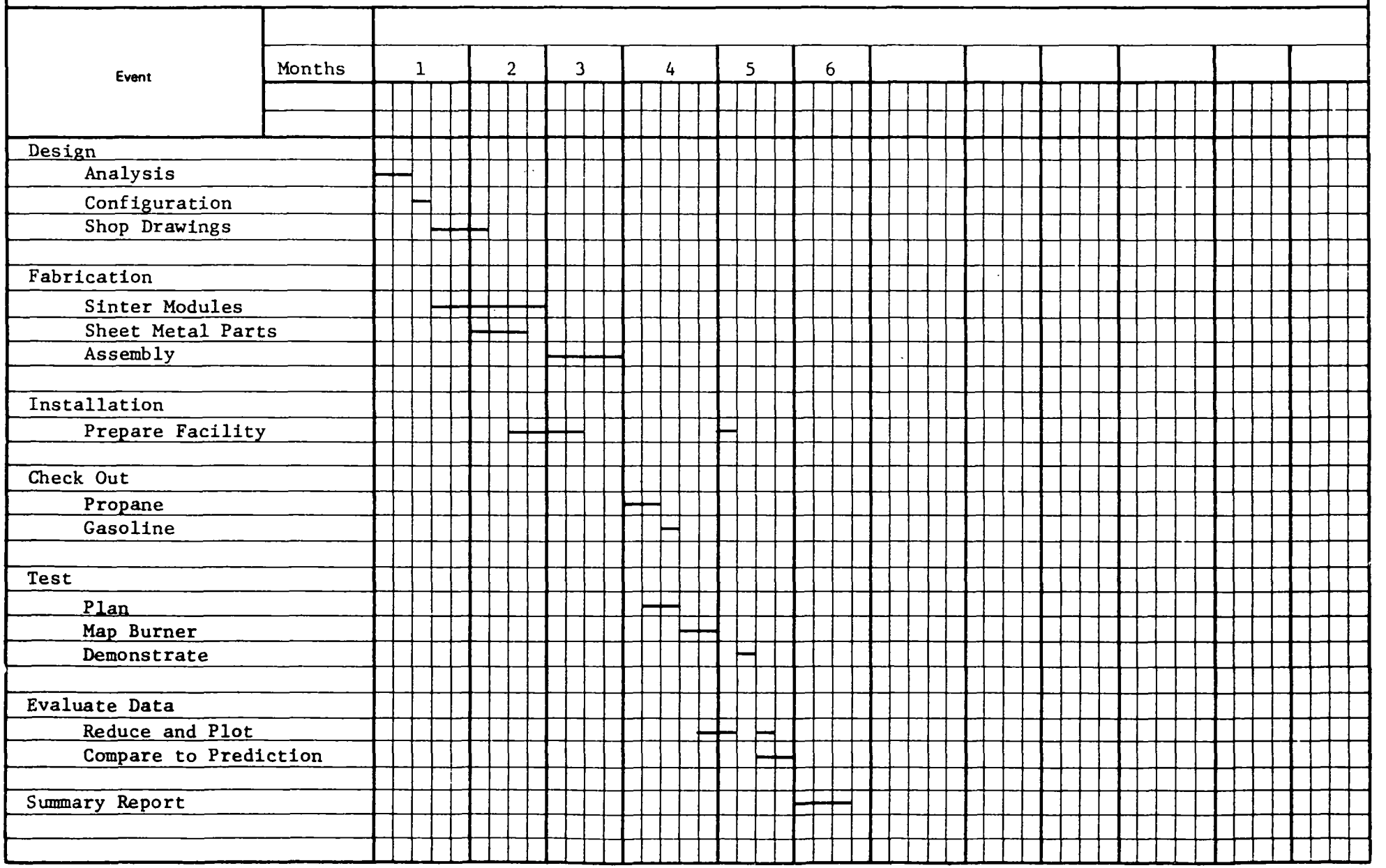

NS 1318 B

Figure 8. Schedule for Rankine Porous-Plate Combustor

water, and fuel at the appropriate conditions. Provisions for measurement will include inlet flow rates, temperatures and pressures, outlet temperatures and emissions. The emissions will be measured using the Scott Dilute Exhaust Gas Emission Analyzer which is capable of accurately measuring, on a continuous basis, NO, NO_2, CO, CO_2 and unburned hydrocarbons.

Following installation of the combustor and calibration of the instrumentation, exploratory tests of the combustor will be made to assure that all required conditions of the test can be met and that all facility controls are functioning properly. The necessary adjustments to the facility will be made that are required for the test program.

Task III - Test Evaluation - The operating performance of the combustor, including pressure drop, exit temperature, and emissions will be mapped over the appropriate ranges of burned gas velocity (V_{25}), equivalence ratio, temperature and pressure level. After this, mutually acceptable test points covering the expected range of operation of a specified Rankine cycle engine will be established and full measurements including emissions will be made. The appropriate equivalence ratio established for each test point will also be set.

The reduced test data will be evaluated in terms of the specified Rankine cycle engine requirements. The exhaust emissions data will be interpreted in terms of emission index for the combustor performance map.

Task IV - Summary Report - The analysis, design and combustor test data will be documented at the end of the program along with appropriate drawings and specifications.

GAS TURBINE COMBUSTOR

DISCUSSION

Conventional combustors for the gas turbine engine often have low emissions of CO and unburned hydrocarbons at high power levels; but the NO_x emissions are often high. In conventional gas turbine combustors, fuel from atomizing nozzles is sprayed into the primary combustion zone, and combustion occurs as the fuel vaporizes off the droplets. The local equivalence ratio of this combustion is uncontrollable, and the NO_x production rates are high because of the variable local equivalence ratio. The equivalence ratio has a string effect on flame temperature. Since NO_x production rates have a logarithmic temperature dependence, the NO_x rates at low temperatures can not offset the NO_x rates at high temperatures. Furthermore, for regenerated cycles, the combustor inlet temperature is usually the regenerator exit temperature; this high temperature also results in high NO_x production rates, since the resulting flame temperature is high.

With conventional combustors, efforts to reduce the NO_x emissions often result in increased emissions of CO and unburned hydrocarbons. At the same equivalence ratio and inlet air temperature, the flame temperature with the porous-plate combustor can be independently controlled and maintained below the adiabatic flame temperature. This independent control of flame temperature is not possible with conventional combustors.

With a porous plate combustor, the lean uniform flame eliminates unburned hydrocarbons; the controllable reduction in flame temperature

below the adiabatic flame temperature results in reduced emissions of NO_x and allows design freedom in controlling the CO. The flame temperature can be controlled so that the NO_x production rates are very low, while the CO decay rates are high enough with the available residence time to reduce the CO in the exhaust gas.

There are several design problems with the porous-plate combustor for the gas turbine application. At pressure levels of four atmospheres, the heat flux back to the burner which must be removed by the heat sink can be large, depending on the operating point. Possible cooling methods to remove this heat flux include independent air cooling with tubes embedded in the matrix and also radiation to a sink. The cooling can be done with cold-side regenerator discharge air, which is cooler than the flame temperature. A value of equivalence ratio approaching unity without violating the temperature limitations of the burner materials is desirable from the standpoint of minimum flow bypass around the regenerator. As the equivalence ratio increases towards unity, the amount of compressor discharge air required for combustion is favorably reduced, but the hot-side burner temperatures increase toward material limitations. In addition to materials limitations at the higher equivalence ratios, the problem of pre-ignition upstream of the burner also increases. Insulation on the upstream side of the burner is employed to prevent pre-ignition. Materials for both the porous burner matrix and the insulation must be suitable for high temperature operation. The porous-plate combustor also requires a fuel vaporizer, since a pre-mixed fuel-air charge is necessary for operation.

Another problem that must be met for combustors for the automotive gas turbine is that there is a wide range of fuel flow required to meet

all of the transient flow conditions. For the porous plate combustor, this means a wide range in superficial velocity (V_{25}) of the fuel-air mixture, and hence a wide range in heat flux back to the burner which must be removed by the cooling sink. Because of the fact that the flame can lift off the porous-plate burner if the superficial velocity becomes too high, sufficient porous-plate surface must be provided for the complete operating range of the engine.

Illustrated in Figure 9 is the general design concept of a cylindrical porous combustor for the gas turbine. The pre-mixed fuel-air mixture provided by a device which atomizes and vaporizes the flow is introduced to the inside of the combustor. The laminar flat flame burns on the outside of the cylinder where it is immediately quenched by the diluent air. The porous plate made either of metal or ceramic material radiates the heat removed from the flame to the diluent baffle, which is cooled by the diluent air. Also shown in Figure 9 are tubes embedded in the matrix of the porous combustor for air cooling in the event that radiation heat transfer can not provide enough cooling.

COMBUSTOR LOADING AND EMISSION ANALYSIS

In order to investigate the burner temperatures during operation and the limits imposed by the allowable range of superficial velocity, a steady-state combustor performance analysis was done. Estimates were made of the exhaust emissions of NO_x and CO. Then, the thermal response of the combustor to four engine transients was calculated.

Steady-State Combustor Performance Analysis

The results of a combustor performance analysis in parametric form are based upon the Test Procedure for Base Line Engine Combustor Final Evaluation on the Test Rig provided by EPA which specified the combustor

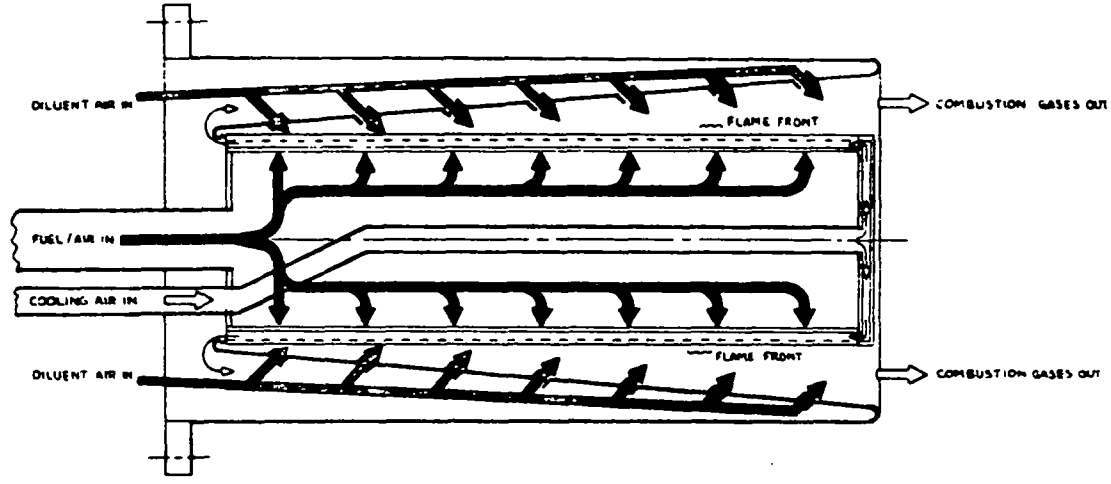

Figure 9. Low NO_x Frit Plate Gas Turbine Combustor (Fuel Inside)

test points shown in Table 1. Later, the transient fuel-flow map of the Base Line Engine, shown in Figure 10 became available. Steady state calculations for the points shown on Figure 10 were then done.

A computer code for the thermal analysis of radiation-cooled porous combustors was developed and used to perform parametric analyses. The assumptions made to calculate temperatures of the porous burner include:

- One dimensional, steady-state heat transfer
- Experimental relationship between superficial velocity, V_{25}, burned-gas temperature, and equivalence ratio according to Kaskan[6]
- Lift off at the adiabatic flame velocity
- Configuration: Hollow cylinder
- Engine data from the Base Line Engine.

The following values were assigned for the parametric study of burner temperatures with the computer code:

Porous Plate Emissivity	0.9
Radiation Receptor Emissivity	0.9
Gas Emissivity	0.0
Minimum Stable Flame Superficial Velocity, cm/sec	4.0
Burned Gas Specific Heat, Btu/lb-°F	0.38
Porous Material	SiC
Porous Plate Thickness, in.	0.125
Porous Plate Effective Conductivity, Btu/(hr-ft-°F)	13.8
Pore Size, microns	100
Porosity, %	20

Shown in Figures 11 and 12 is the hot-side burner temperature as a function of burner area for equivalence ratios (R) of 0.7, 0.8, and 0.9 with primary

Table 1. BASELINE ENGINE COMBUSTOR TEST POINTS

BE.1 Simulated Federal Driving Cycle

Fuel Flow Wf (pph)	Combustor Pressure P1 (psig)	Heat Exchanger Exit Temperature T1 (°F)	Turbine Inlet Temperature T2 (°F)	Total Air Flow Wa (lb/sec)
6	27	1380	1450	1.50
10	8	900	1100	0.85
12	8	1000	1250	0.85
13	8	1100	1370	0.85
16	10	1380	1680	0.95
65	16	1100	2100	1.15

BE.2 Steady Speed Mode

Wf (pph)	P1 (psig)	T1 (°F)	T2 (°F)	Wa (lb/sec)	Veh. Speed (MPH)
12	8	1100	1350	0.85	30
14	8	1200	1490	0.85	40
16	10	↑	1500	0.95	50
25	16		1590	1.15	60
31	20		1620	1.30	70
39	25		1680	1.45	80
48	29		1730	1.60	90
59	35		1780	1.80	100
69	40		1810	2.00	108
82	47	↓	1850	2.30	119

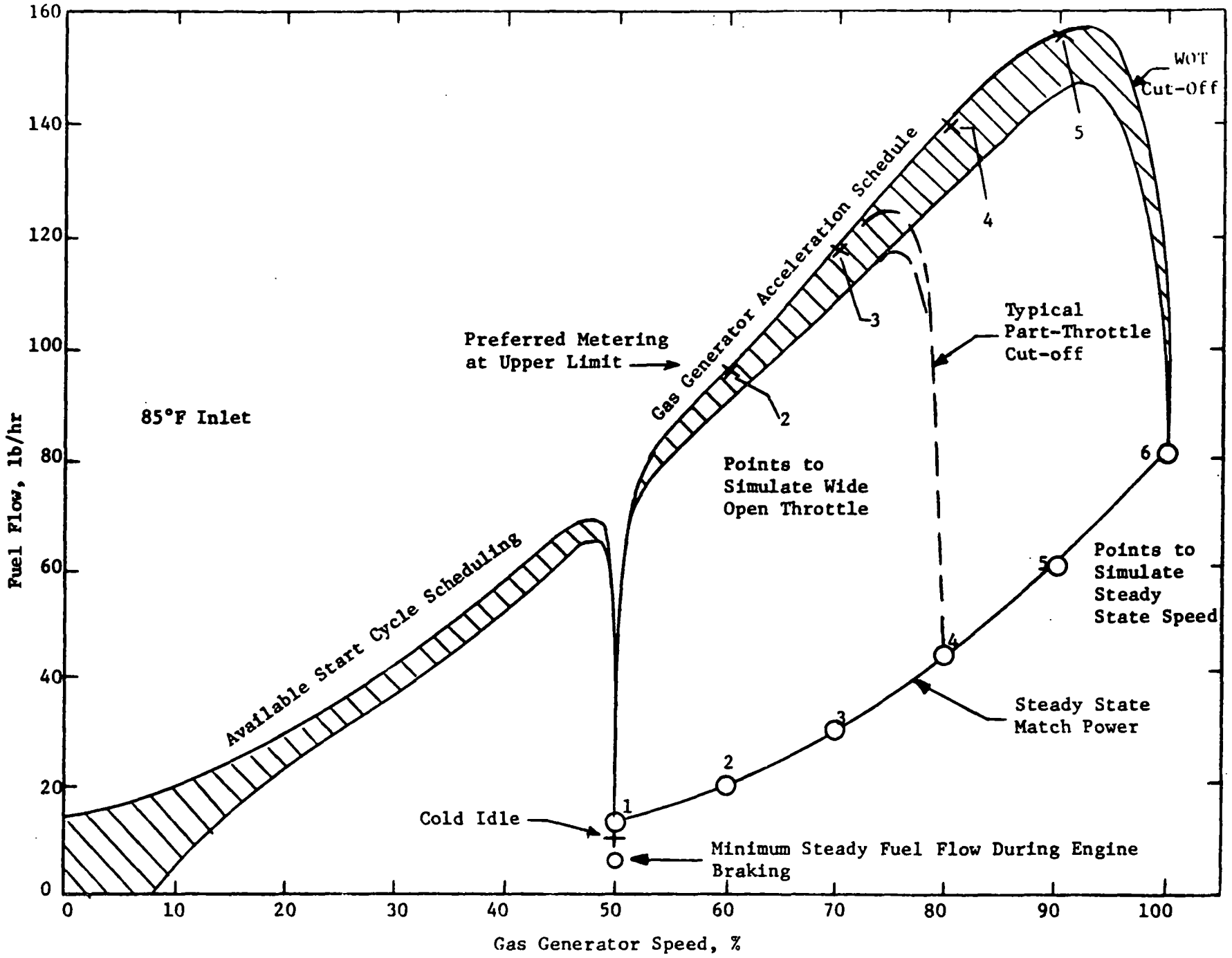

Figure 10. Fuel Scheduling of Base Line Engine

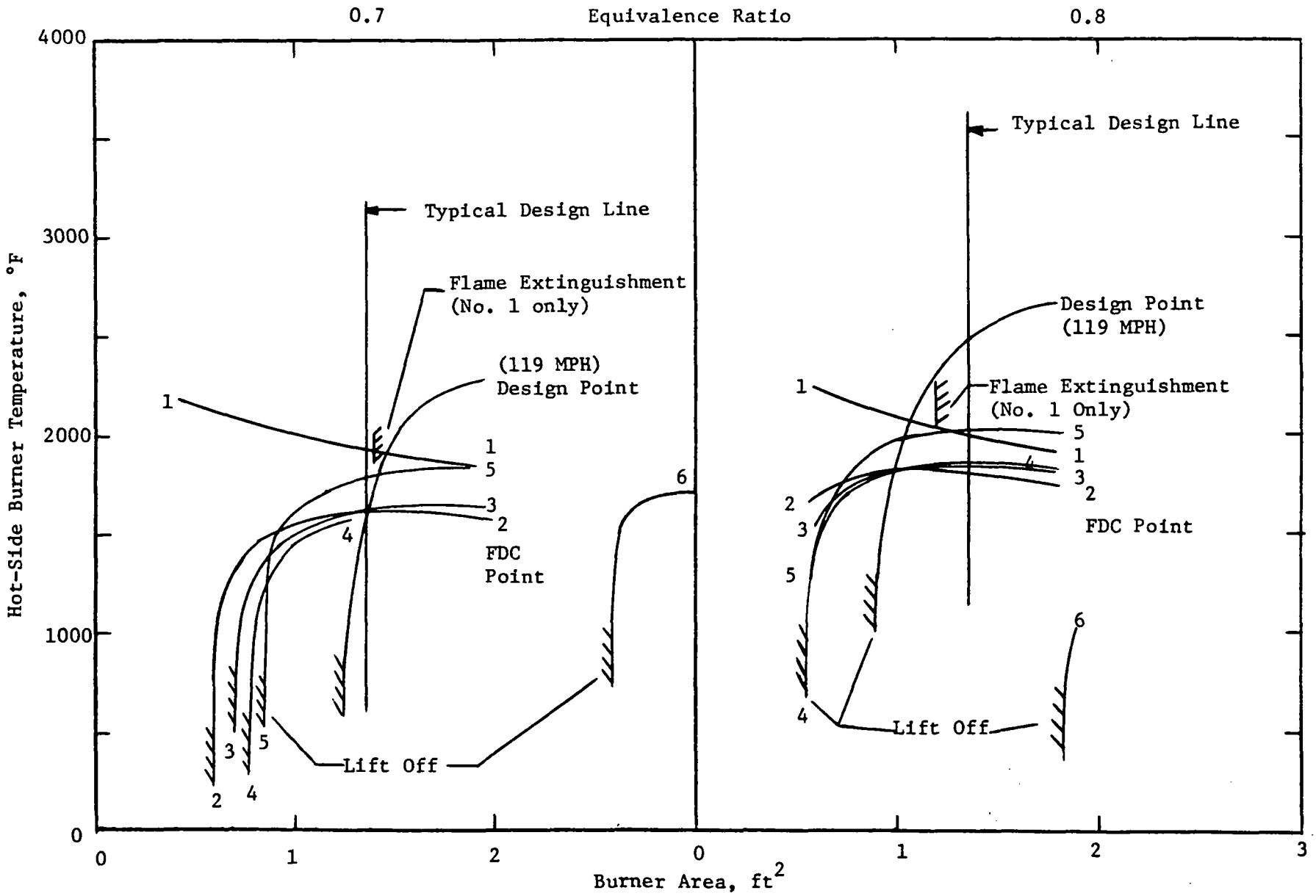

Figure 11. Hot-Side Burner Temperature: Primary Air from Compressor Discharge

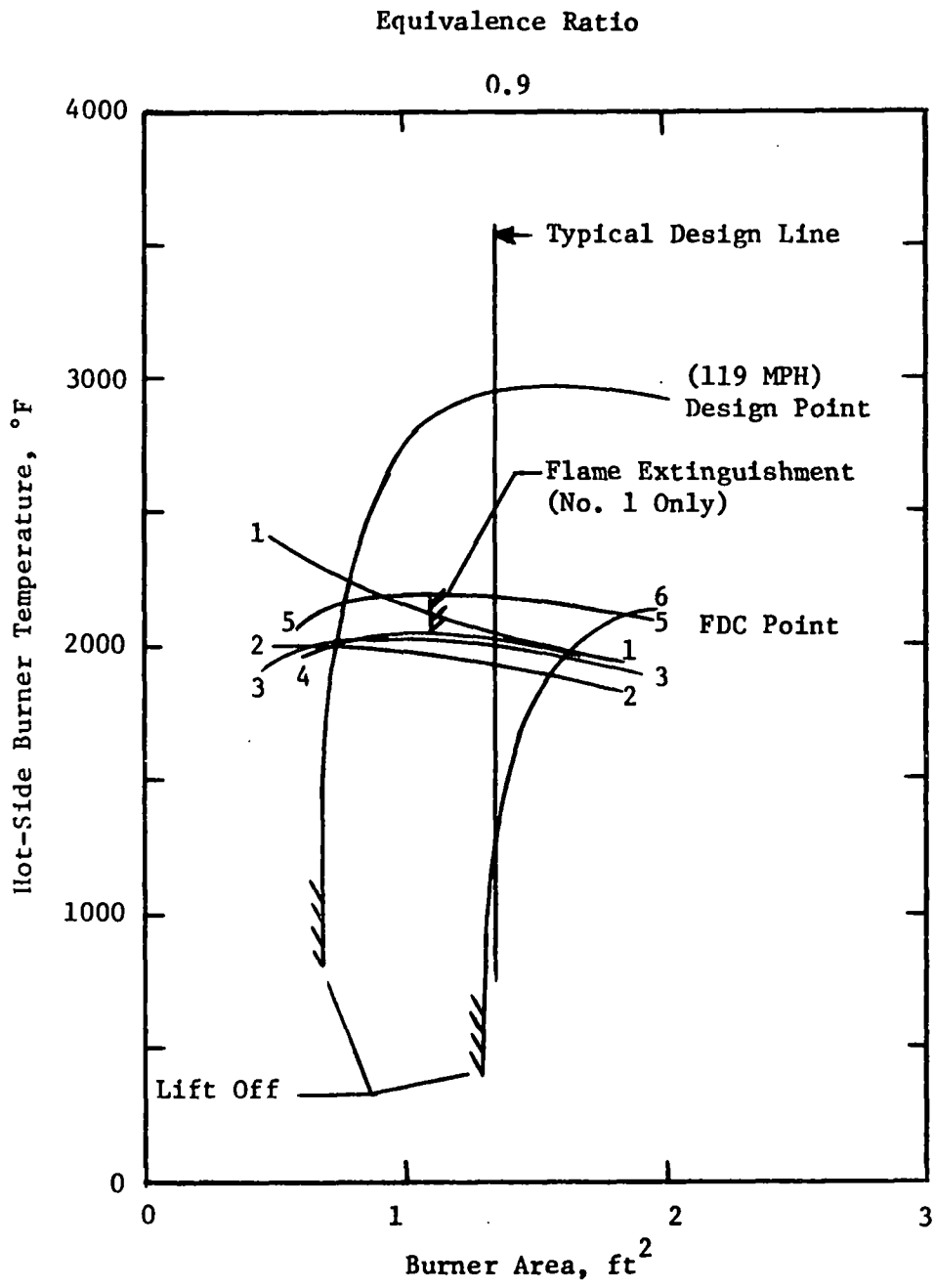

Figure 12. Hot-Side Burner Temperature:
Primary Air from Compressor Discharge

air to the combustor coming from the compressor discharge. Shown are lines for the six Federal Driving Cycle (FDC) points as well as the Design Point (119 mph) taken from Table 1. The maximum area above which flame extinguishment is assumed to occur (V_{25} = 4 cm/sec) is shown; the problem of flame extinguishment occurs only with the first FDC point. Also shown is the minimum area to avoid lift-off. The velocity, V_{25}, is the superficial velocity of the unburned gas based on the porous plate upstream area, and referred to the density of the fuel-air mixture at 25°C (76°F) and at pressure. A typical design line corresponding to a fixed area is shown on the figures. The conclusions from Figures 11 and 12 with the primary air being compressor discharge are that:

- Decreasing equivalence ratio from 0.9 to 0.7 generally increases required burner area and decreases the hot-side surface temperature level.
- A given design (fixed area) usually cannot be accommodated by a constant equivalence ratio.

Similarly, the variation of hot-side burner temperature is shown in Figures 13 and 14 as a function of burner area for equivalence ratios of 0.5, 0.7, 0.8 and 0.9 when the primary air is from the regenerator discharge; an equivalence ratio of less than 0.7 is required to keep the burner temperatures below 2000°F.

Shown in Figure 15 is a comparison of the case of primary air at R = 0.7 being the compressor discharge from Figure 11 and of the case of the primary air at R = 0.5 being the regenerator discharge from Figure 13. From Figures 13 and 15, it can be concluded that:

- At an equivalence ratio of 0.5 using regenerator air, the hot-side surface temperatures are generally higher than for an

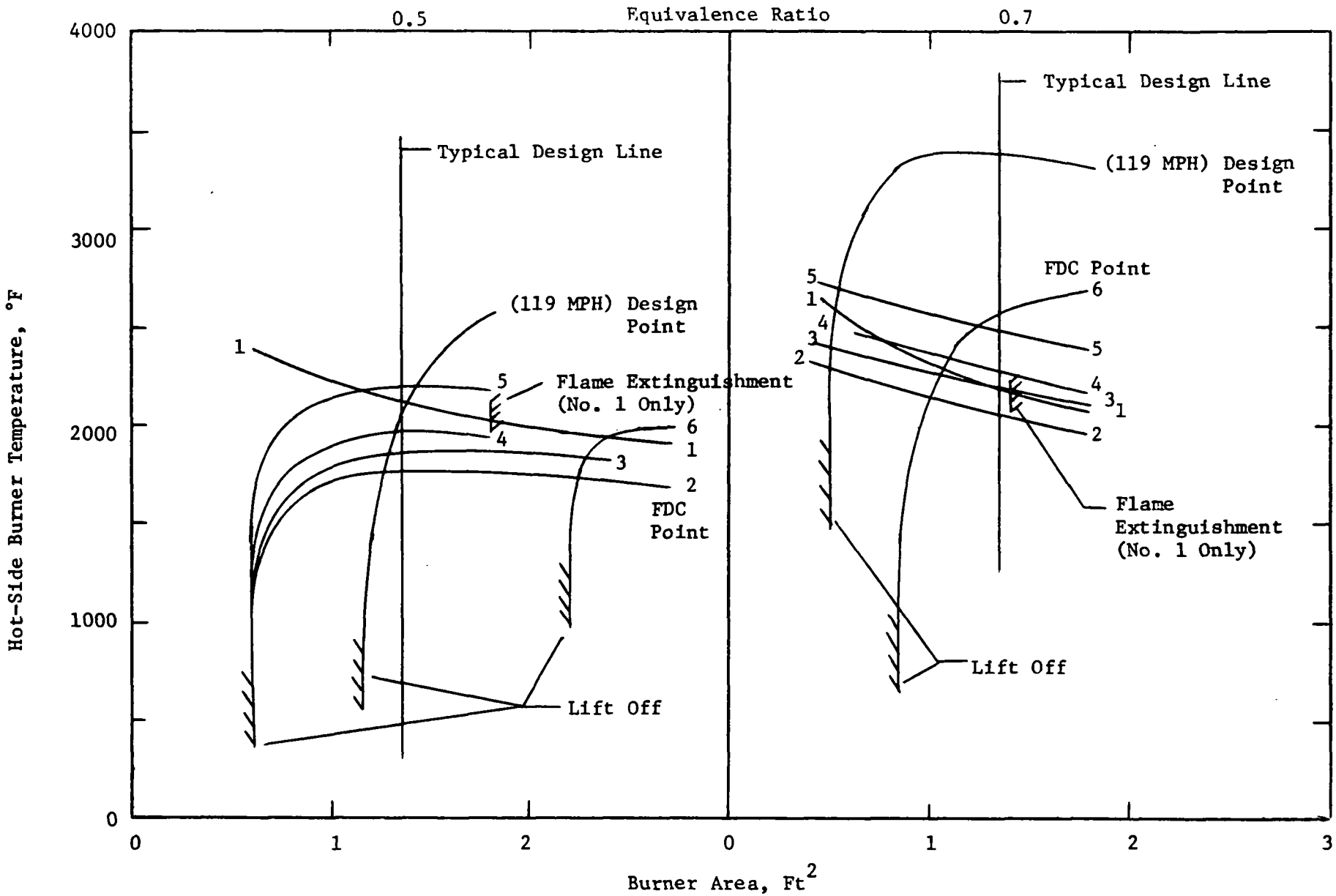

Figure 13. Hot-Side Burner Temperature:Primary Air From Regenerator Discharge

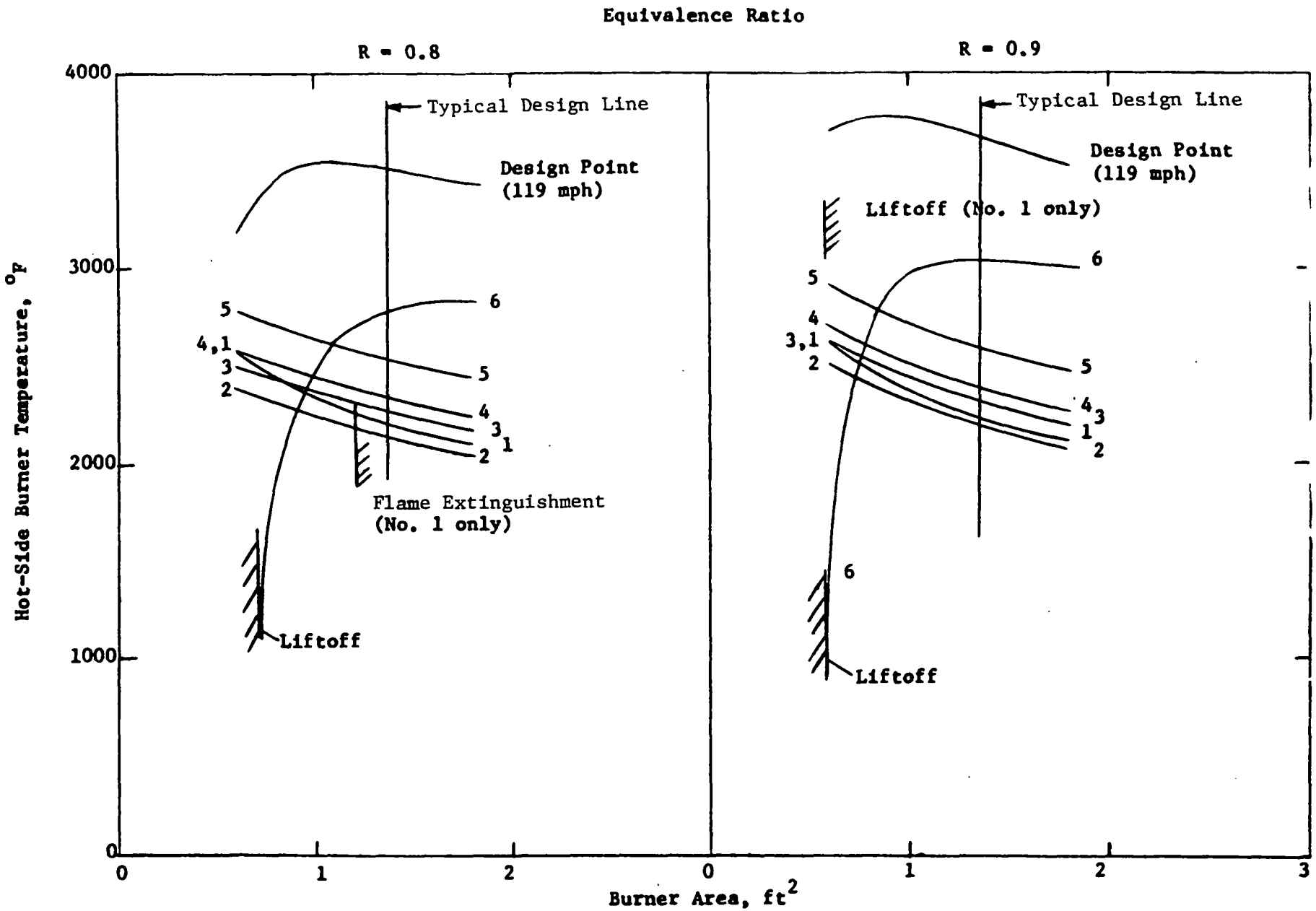

Figure 14. Hot-Side Burner Temperature: Primary Air From Regenerator Discharge

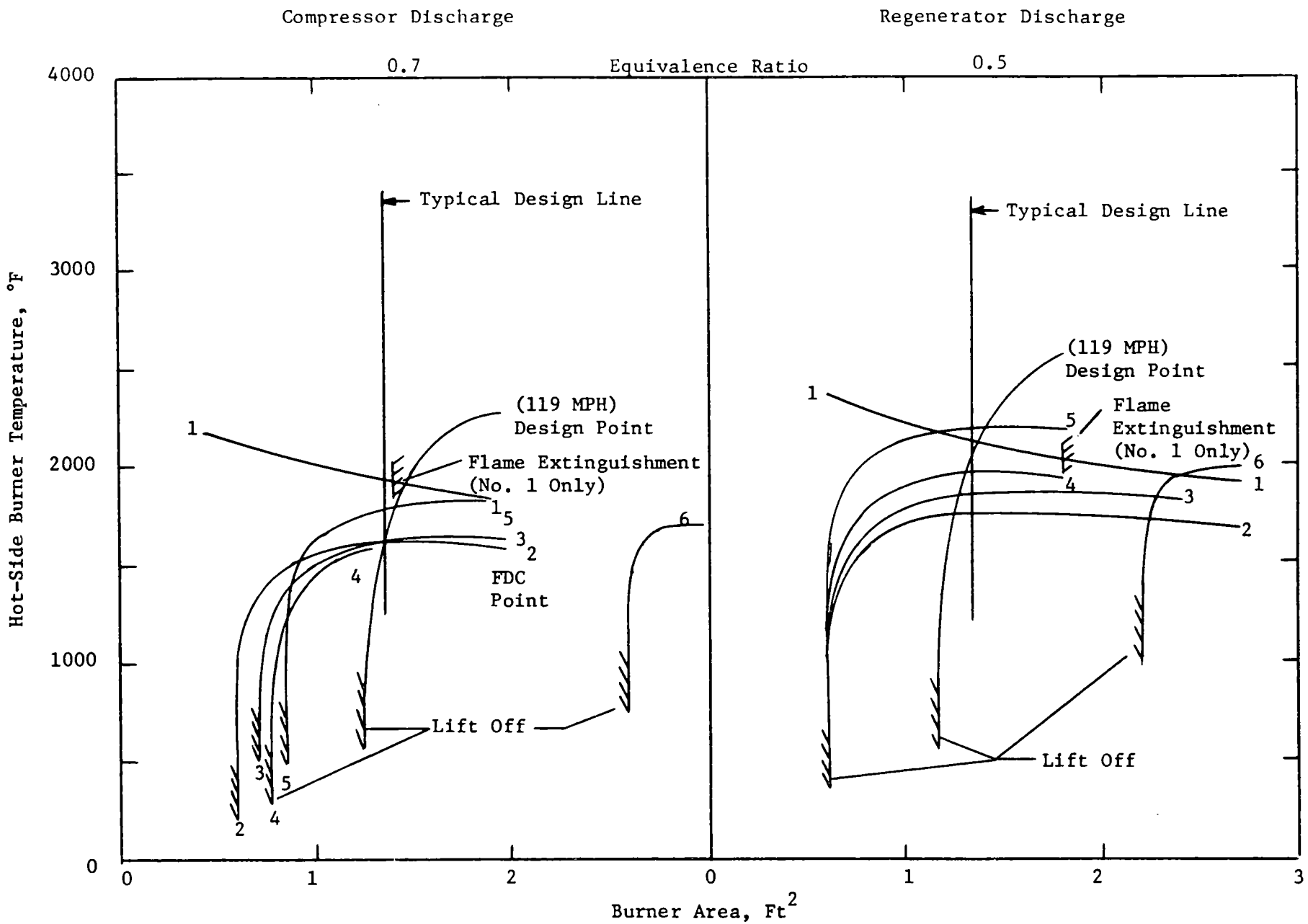

Figure 15. Hot-Side Burner Temperature

equivalence ratio of 0.7 using compressor discharge air.

- Decreasing equivalence ratio generally increases burner area and decreases surface temperature level.
- A variable equivalence ratio permits limiting surface temperatures, while staying within (V_{25}) velocity limits.

Calculated burner temperatures at one burner area (1.15 ft^2) are shown in Figure 16 for the FDC points and the steady-state vehicle speed points for the Base Line Engine for an SiC burner operated at an equivalence ratio of 0.8. The peak hot-side burner temperature occurs at 119 mph at this burner area. With the burner area fixed at 1.15 ft^2, the first FDC point has a V_{25} at 4.2 cm/sec, which is near flame extinguishment; the sixth FDC point has a V_{25} above the adiabatic lift-off data of Dugger.[8]

The effect of emissivity on hot-side temperature is shown in Figure 16. If the emissivity is only 0.75 instead of 0.9, then the hot-side burner temperature is about 2544°F at this burner area of 1.15 ft^2 (or almost 300°F higher than the case of 0.9 emissivity).

Combustor Analysis Using Base Line Engine Fuel Schedule - The code for steady-state analysis of burner temperatures mentioned previously was used to perform parametric analyses of 18 engine cycle points. These points are: a) six steady-state operating points from idle to full power, b) the six Federal Driving Cycle (FDC) points, and c) six engine points simulating wide-open-throttle (WOT). Figure 10 is the fuel flow map for the Chrysler Base Line Engine which shows the six steady-state operating points selected and the six engine points simulating wide-open throttle; the six FDC points are shown in Table 1. The corresponding air

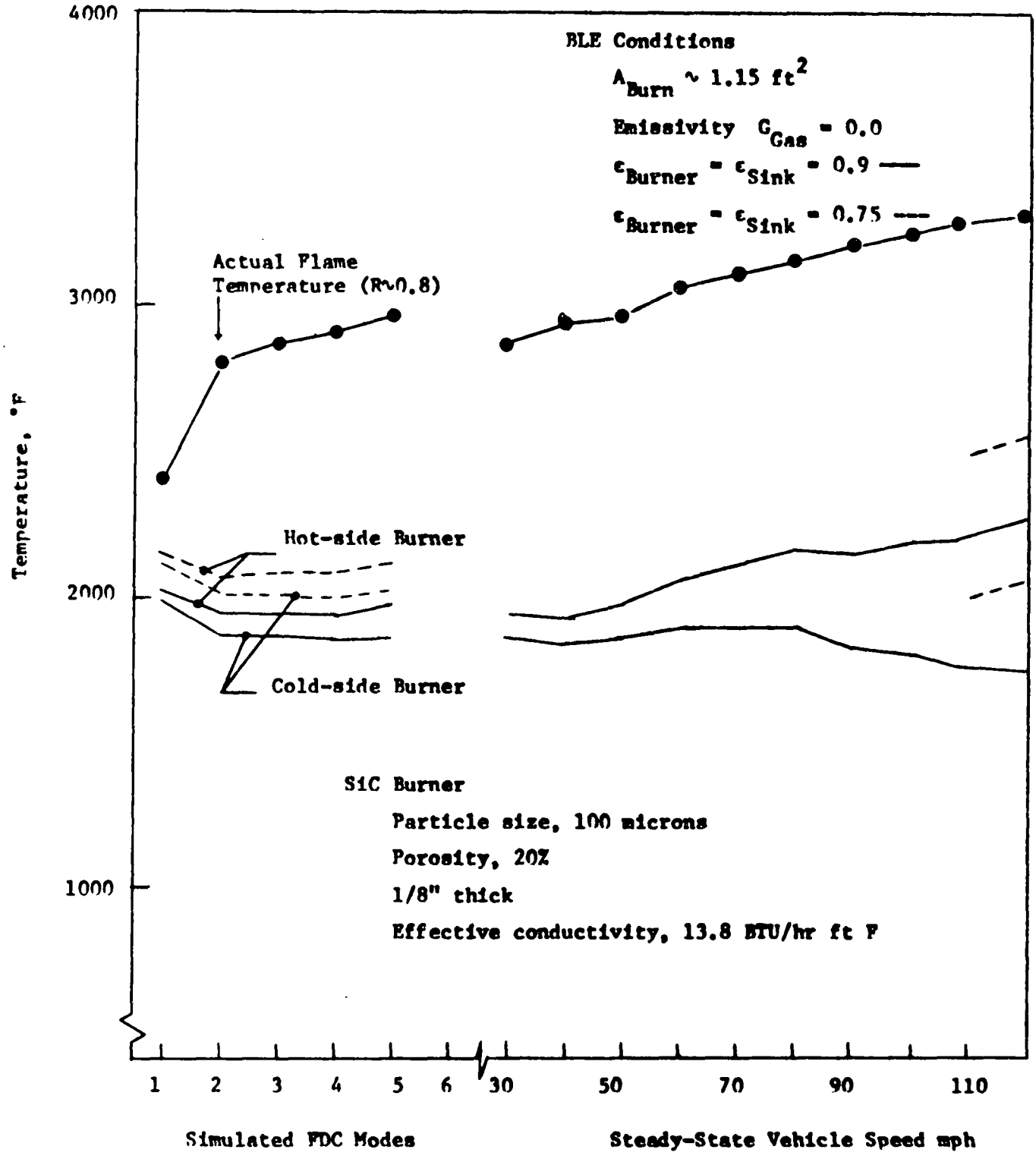

Figure 16. Effect of Emissivity on Burner Temperatures

flow rates and temperatures shown for each engine point are used in the analysis. Compressor discharge air is used as the primary air for combustion, and the diluent air is cold-side regenerator discharge air. The analysis for each of the three sets of six operating points was done for emissivities of the burner and radiation receptor of 0.9 and 0.7, and for equivalence ratios of 0.9, 0.8 and 0.7. At each of the 18 operating points, the burner area was varied from areas that correspond to flame extinguishment (at superficial velocity, V_{25} = 5 cm/sec) to areas that correspond to the lower of either 50 cm/sec or the lift-off velocity for each condition (as determined from the combustor inlet temperature and the equivalence ratio). These calculations are for mixtures of propane-air, since data for V_{25} versus 1/T with gasoline were not available. The specific heat of the burned gas in the flame was taken as 0.38 Btu/lbm-°F.

Table 2 summarizes the calculations of burned gas temperatures which are given in Figures 17 to 25 and of hot-side burner temperatures which are given in Figures 26 to 43. The burned gas temperature is determined solely by the superficial velocity V_{25} and the equivalence ratio, R, according to available data; hence, the emissivity of the burner has no effect on the burned gas temperatures.

The values of V_{25} at the operating points are indicated by the appropriate symbol on each of the figures.

On the figures of hot-side burner temperatures, operating envelopes corresponding to a hot-side temperature limit of 2300°F and of burner areas between 1 ft^2 and 2.5 ft^2 are shown. The 2300°F limit for steady-state operation on the hot-side is selected based on results from flashback tests at Energy Systems Programs and Corporate Research and Development which indicated that hot-side burner temperatures in the range of 2000°F to 2732°F (1500°C) can cause flashback. Burner areas up to 2.5 ft^2 are considered reasonable for packaging considerations.

Table 2. SUMMARY OF CALCULATIONS

Equivalence Ratio	Emissivity	Steady-State Operating Points: Burned Gas Temperatures	Steady-State Operating Points: Hot Side Burner Temperatures	FDC Points: Burned Gas Temperatures	FDC Points: Hot Side Burner Temperatures	WOT Points: Burned Gas Temperatures	WOT Points: Hot Side Burner Temperatures
0.9	0.9	Fig. 17	Fig. 26	Fig. 20	Fig. 29	Fig. 23	Fig. 32
0.8	↓	18	27	21	30	24	33
0.7	↓	19	28	22	31	25	34
0.9	0.7	17	35	20	38	23	41
0.8	↓	18	36	21	39	24	42
0.7	↓	19	37	22	40	25	43

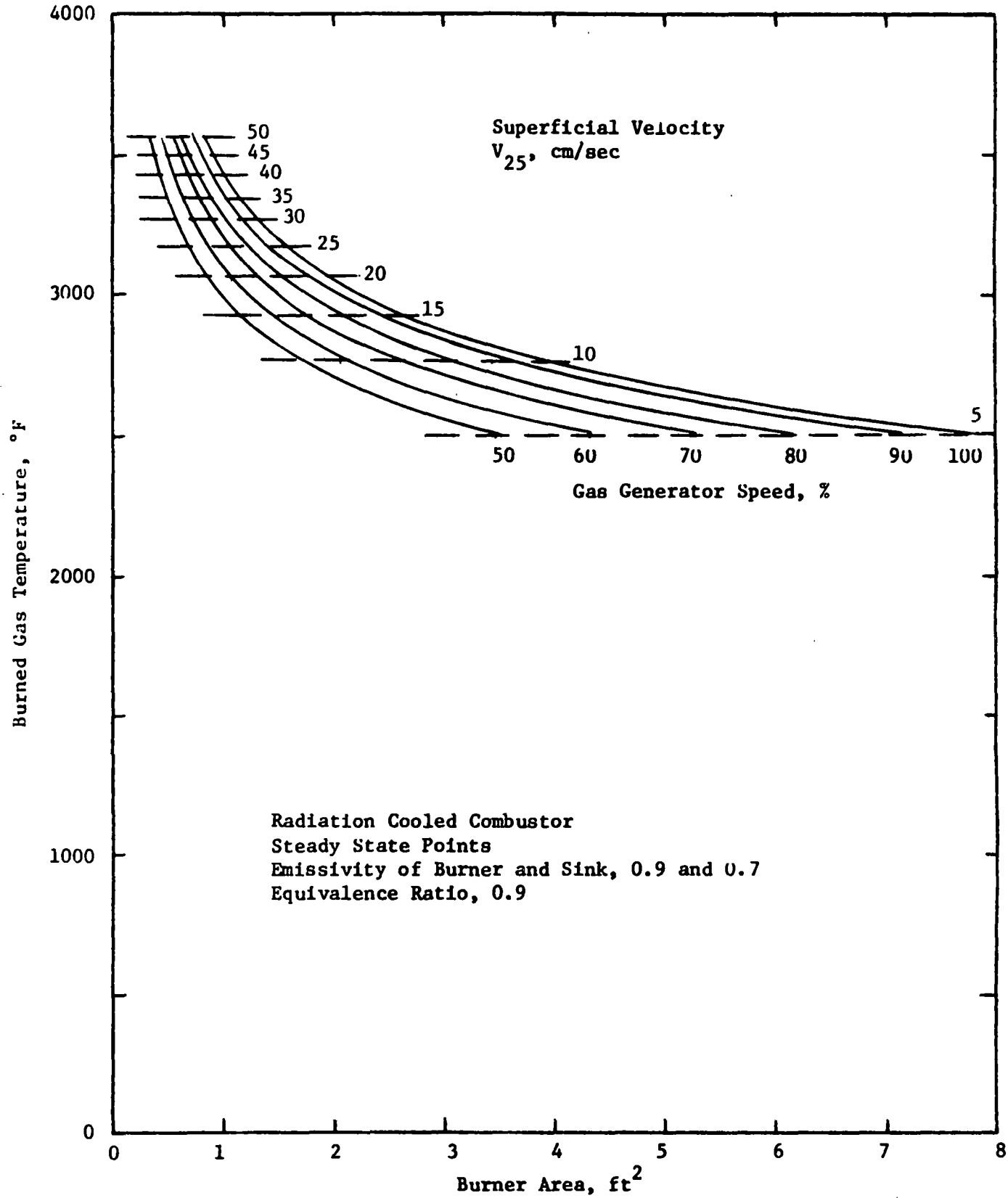

Figure 17. Burned Gas Temperature of Radiation Cooled Combustor at Steady State Points

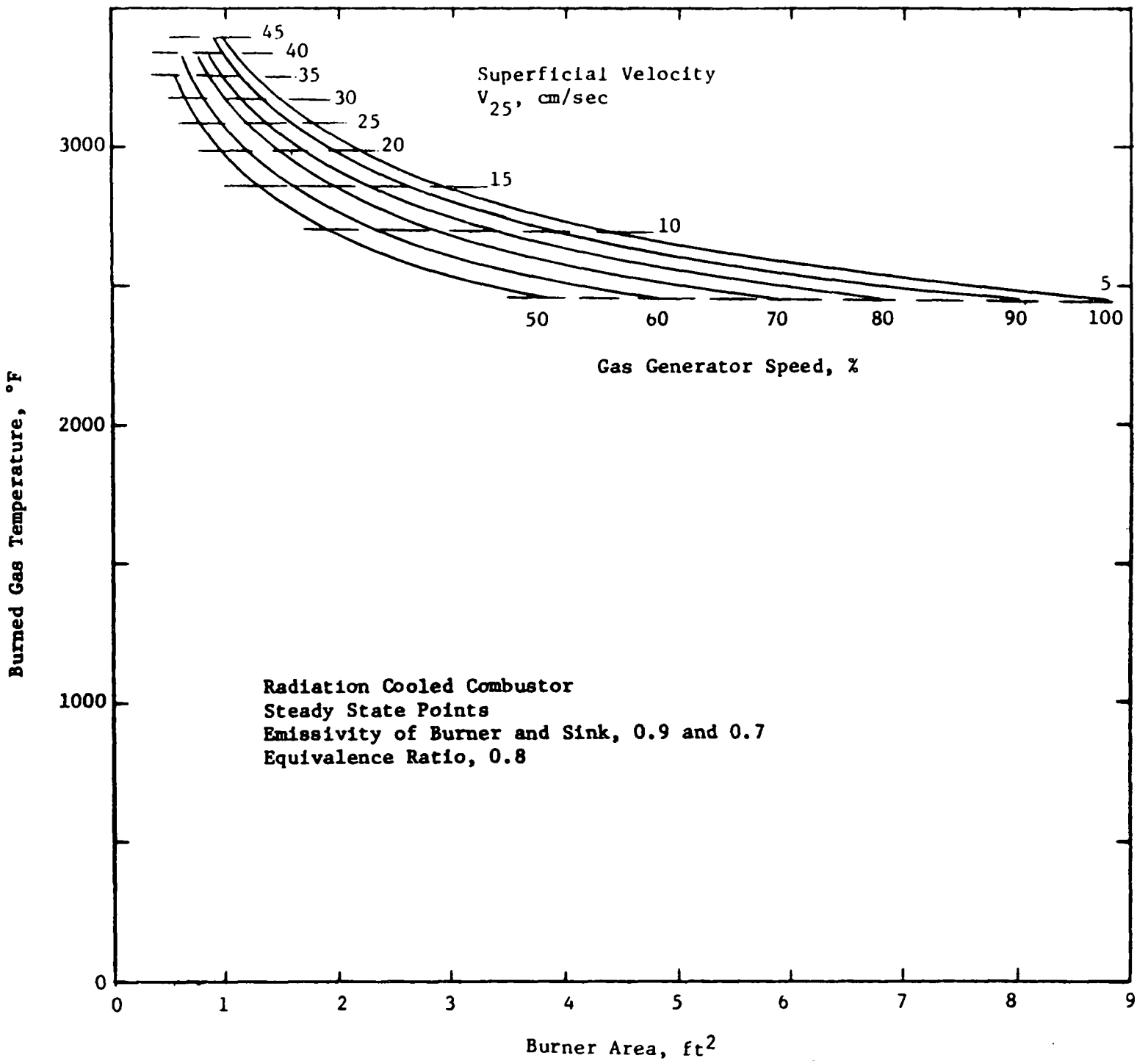

Figure 18. Burned Gas Temperature of Radiation Cooled Combustor at Steady State Points

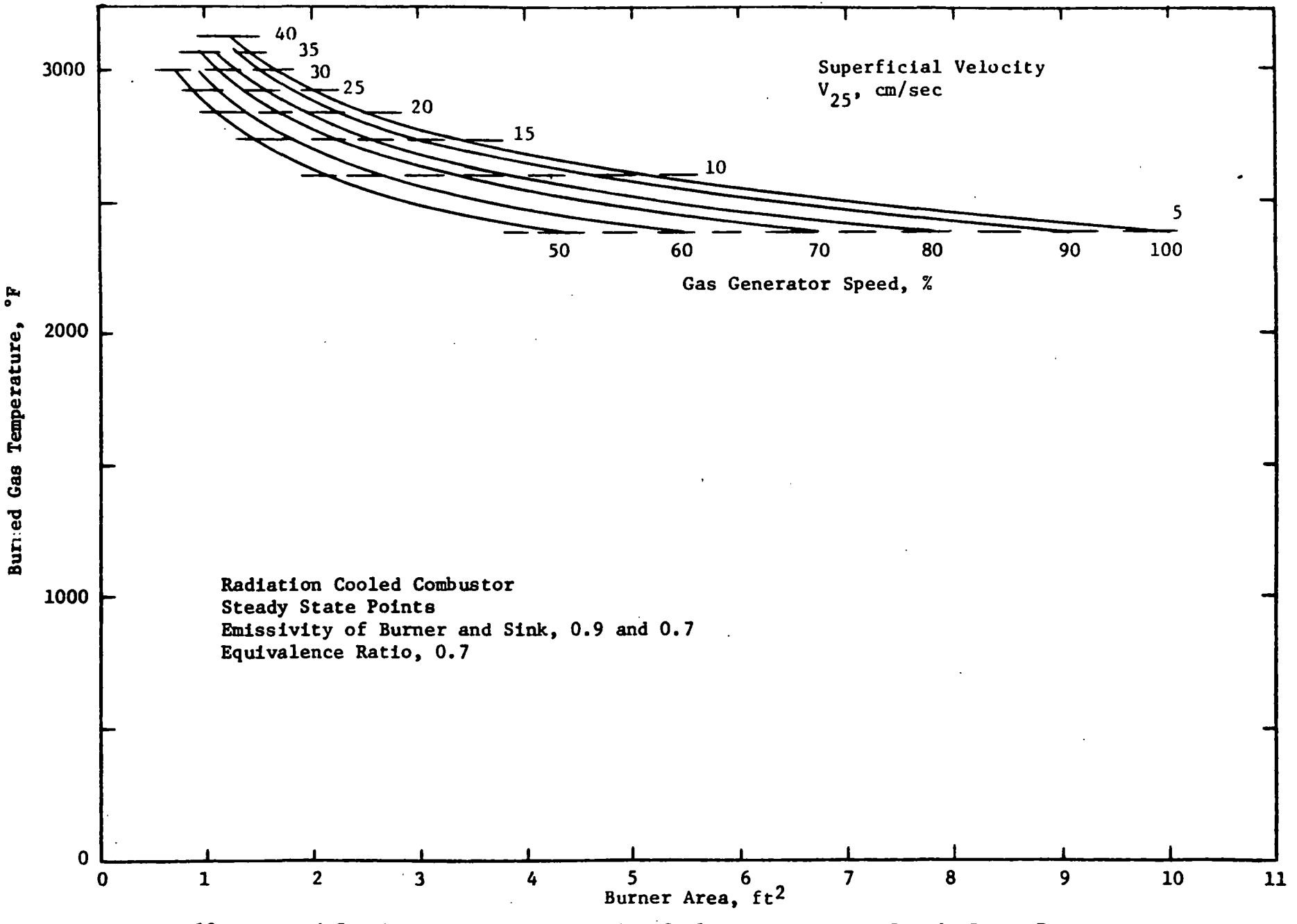

Figure 19. Burned Gas Temperature of Radiation Cooled Combustor at Steady State Points

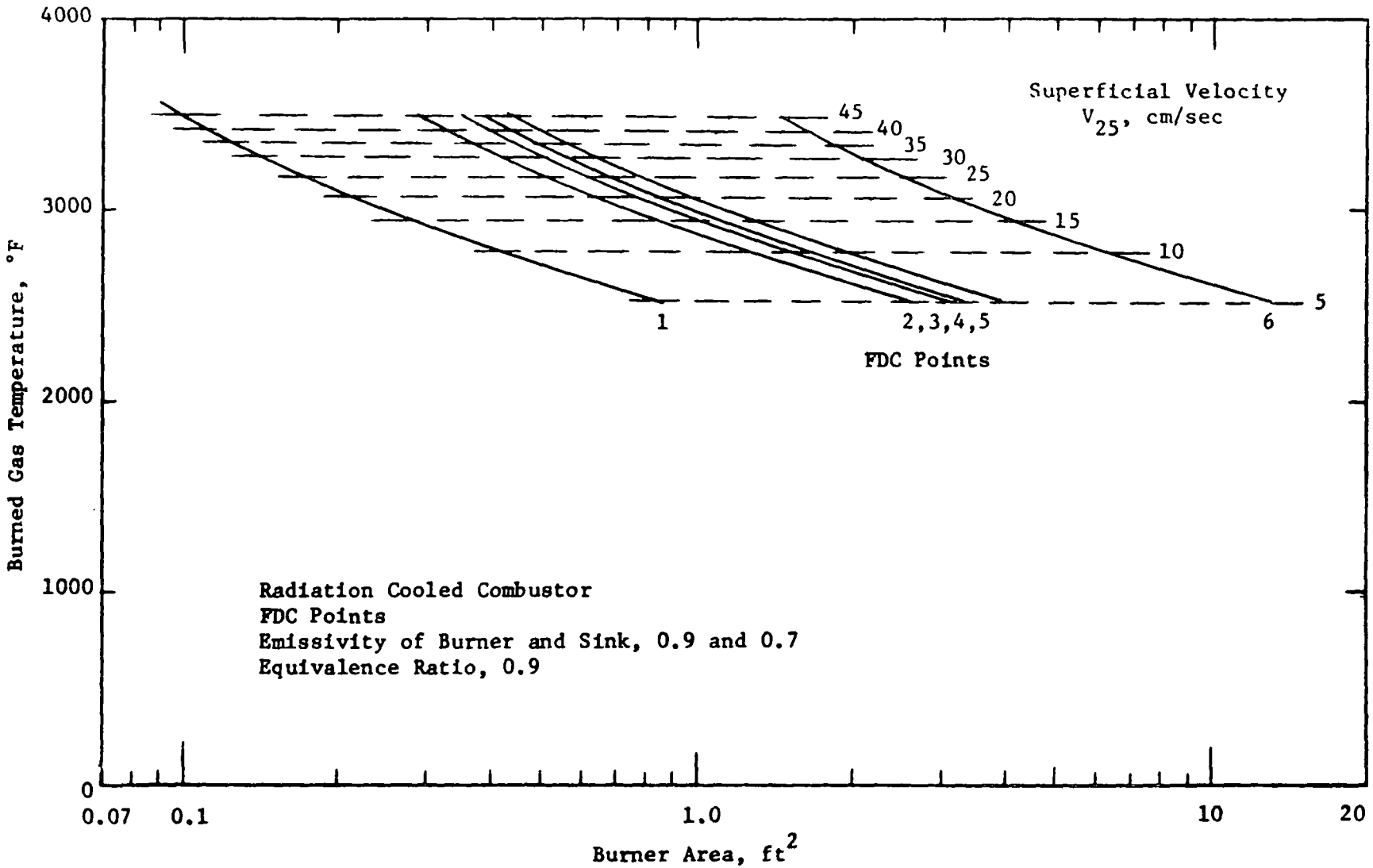

Figure 20. Burned Gas Temperature of Radiation Cooled Combustor at FDC Points

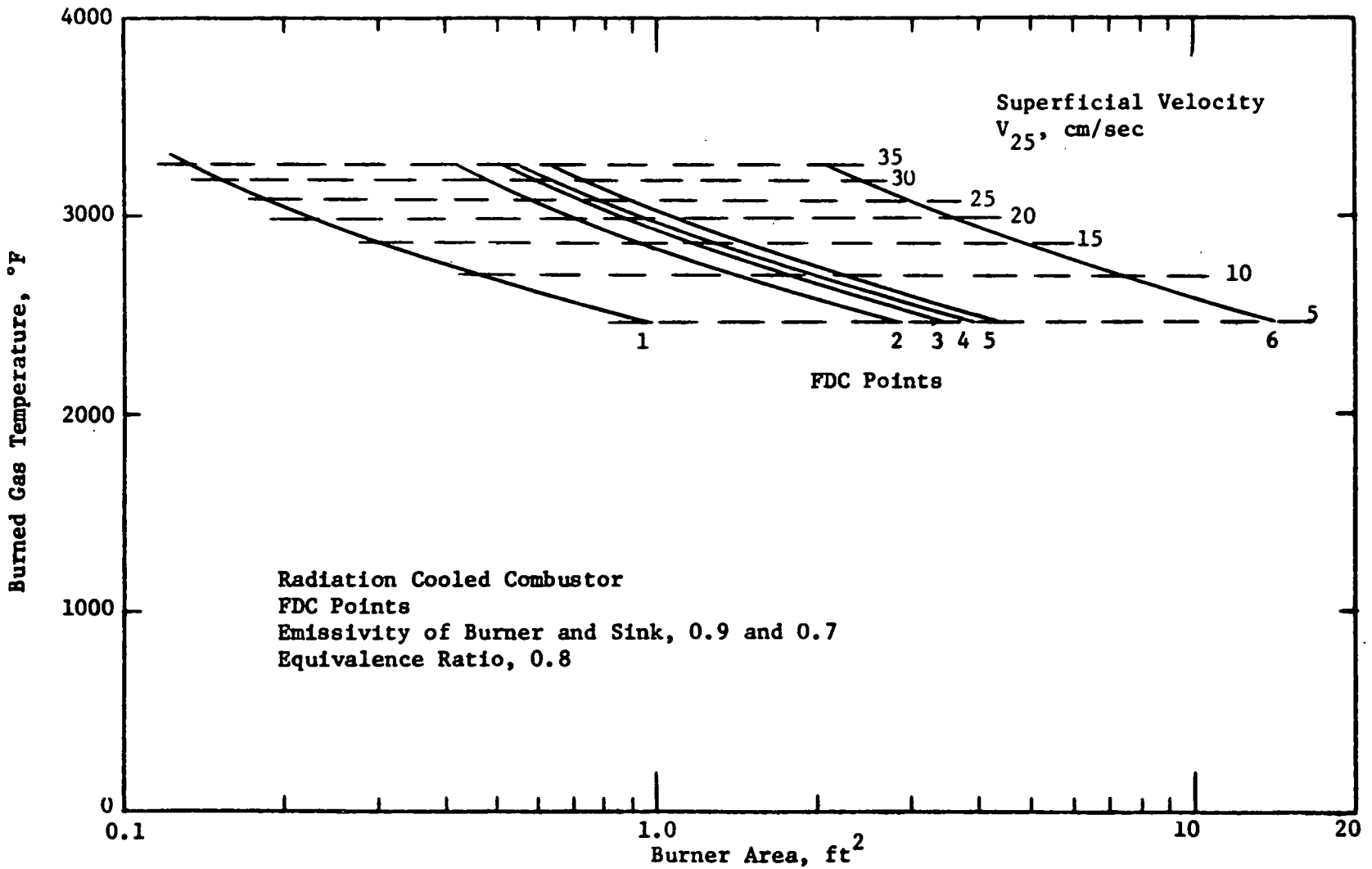

Figure 21. Burned Gas Temperature of Radiation Cooled Combustor at FDC Points

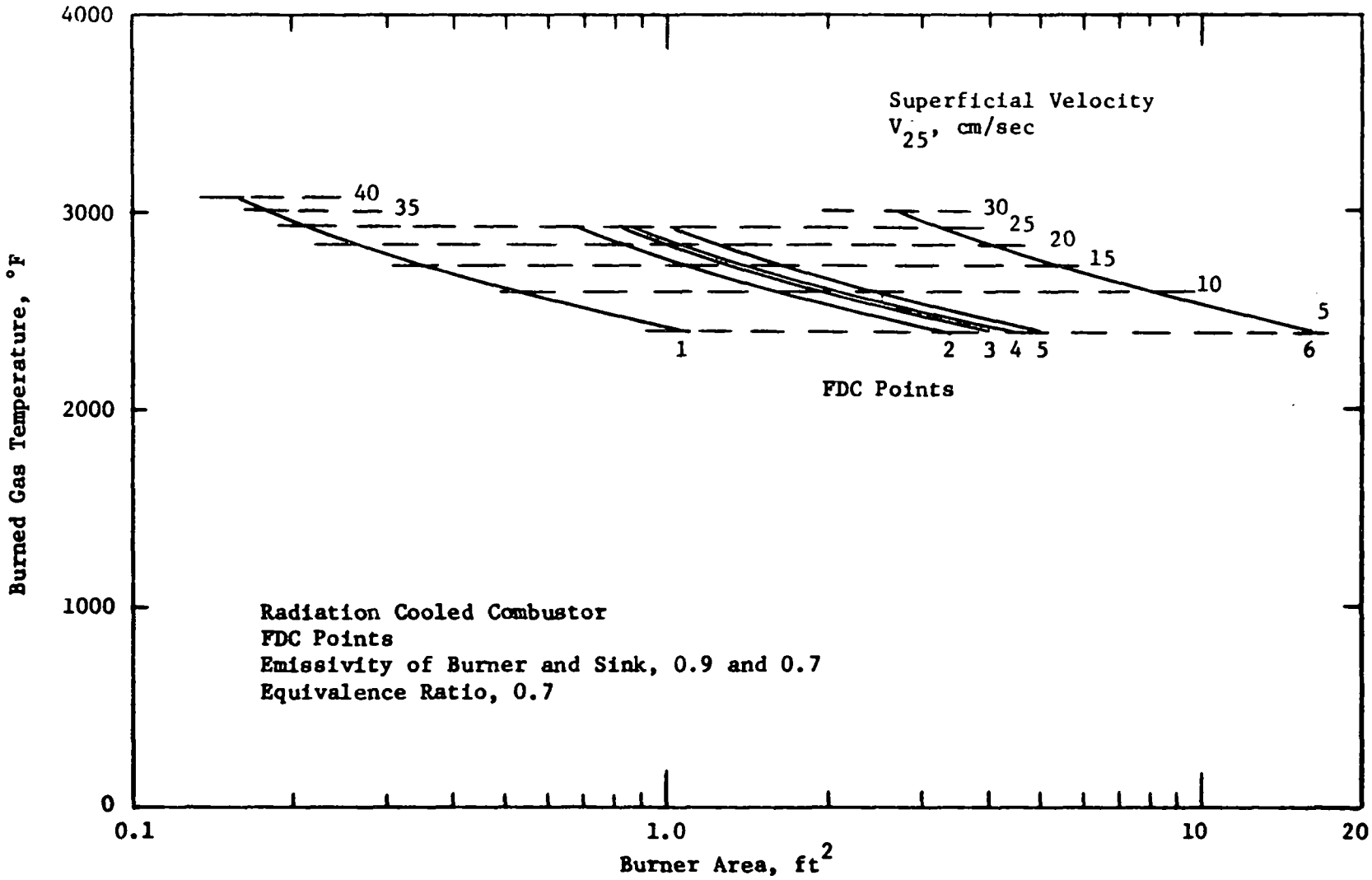

Figure 22. Burned Gas Temperature of Radiation-Cooled Combustor at FDC Points

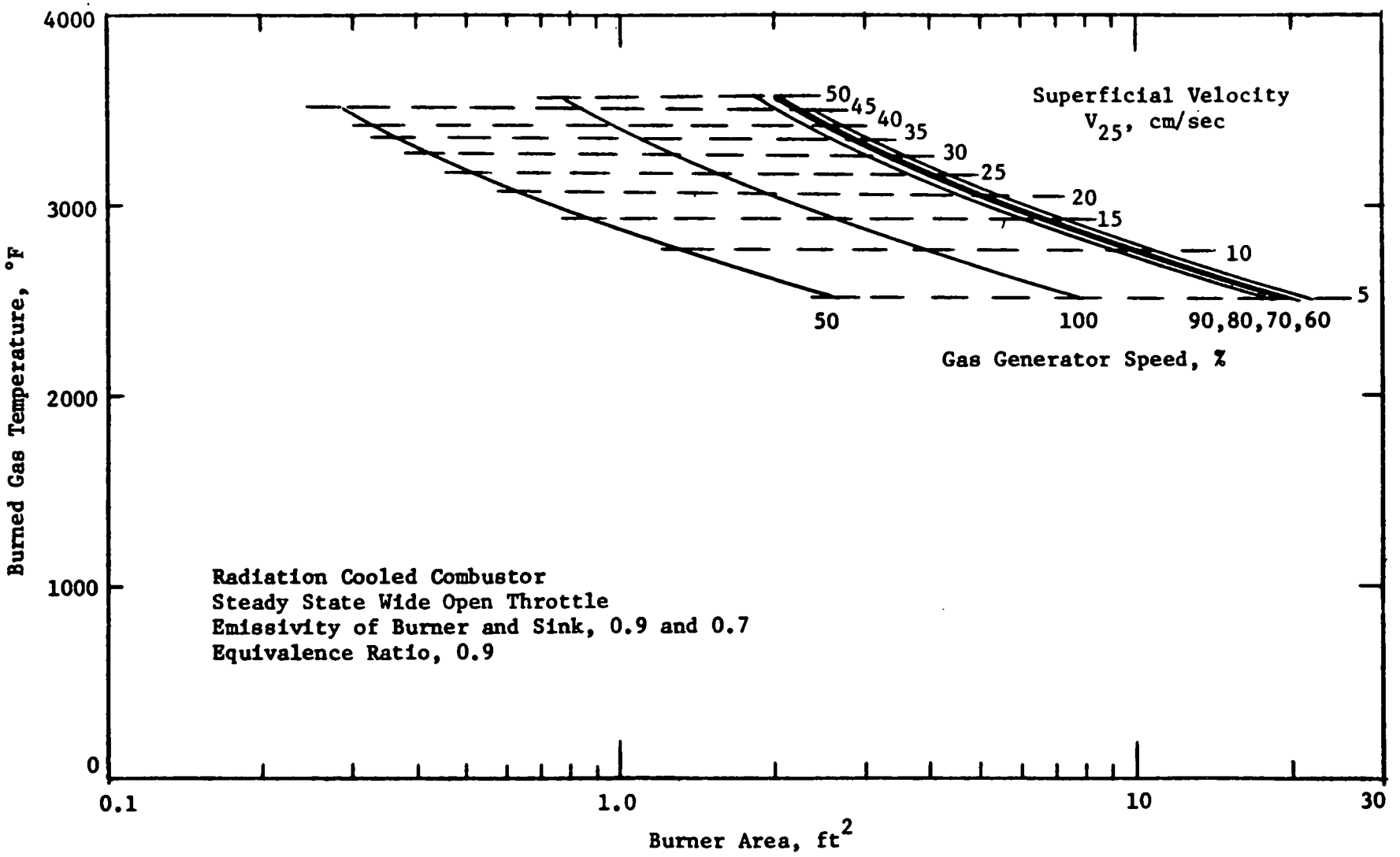

Figure 23. Burned Gas Temperature of Radiation Cooled Combustor at Steady State Wide Open Throttle Points

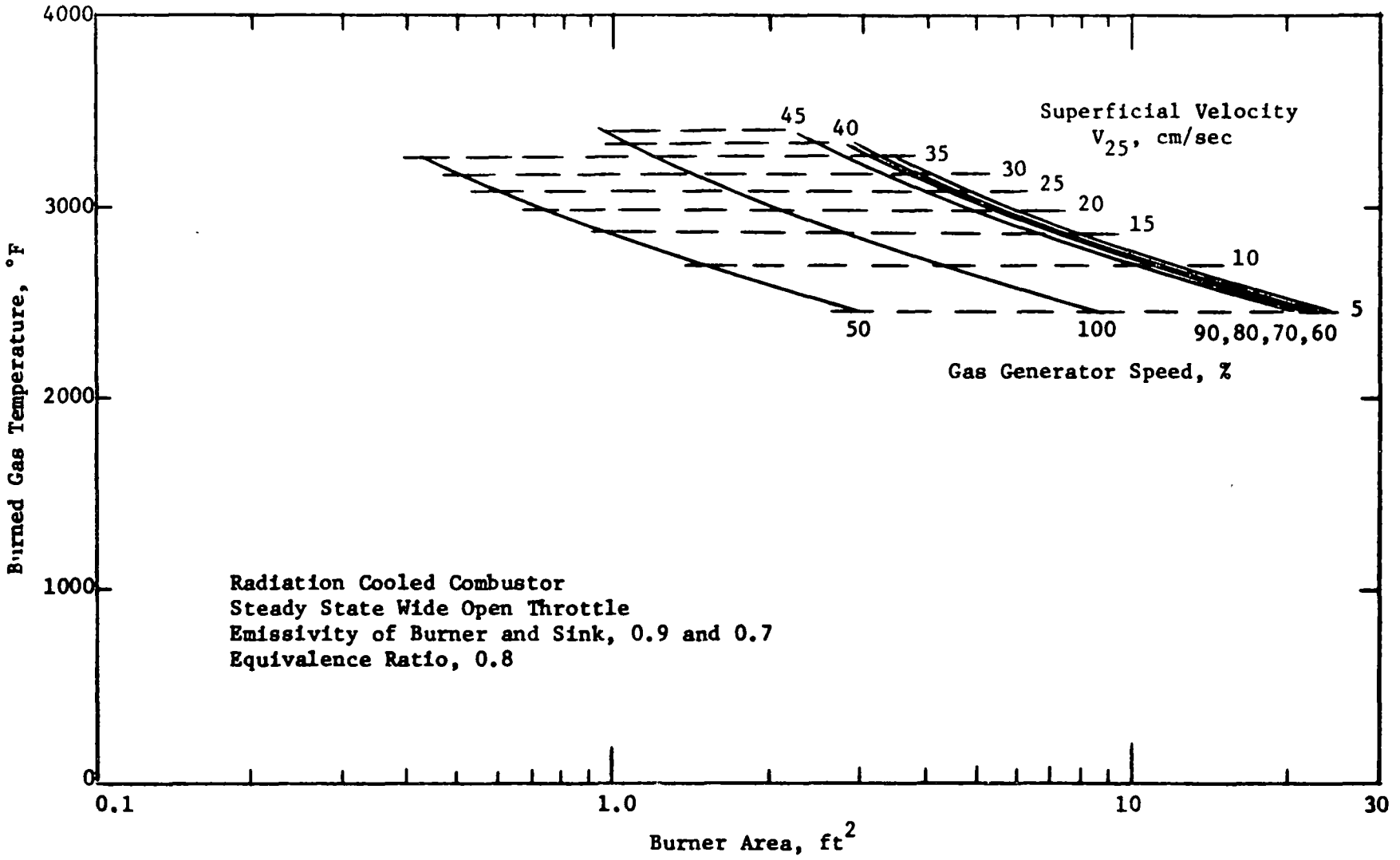

Figure 24, Burned Gas Temperature of Radiation Cooled Combustor at Steady State Wide Open Throttle Points

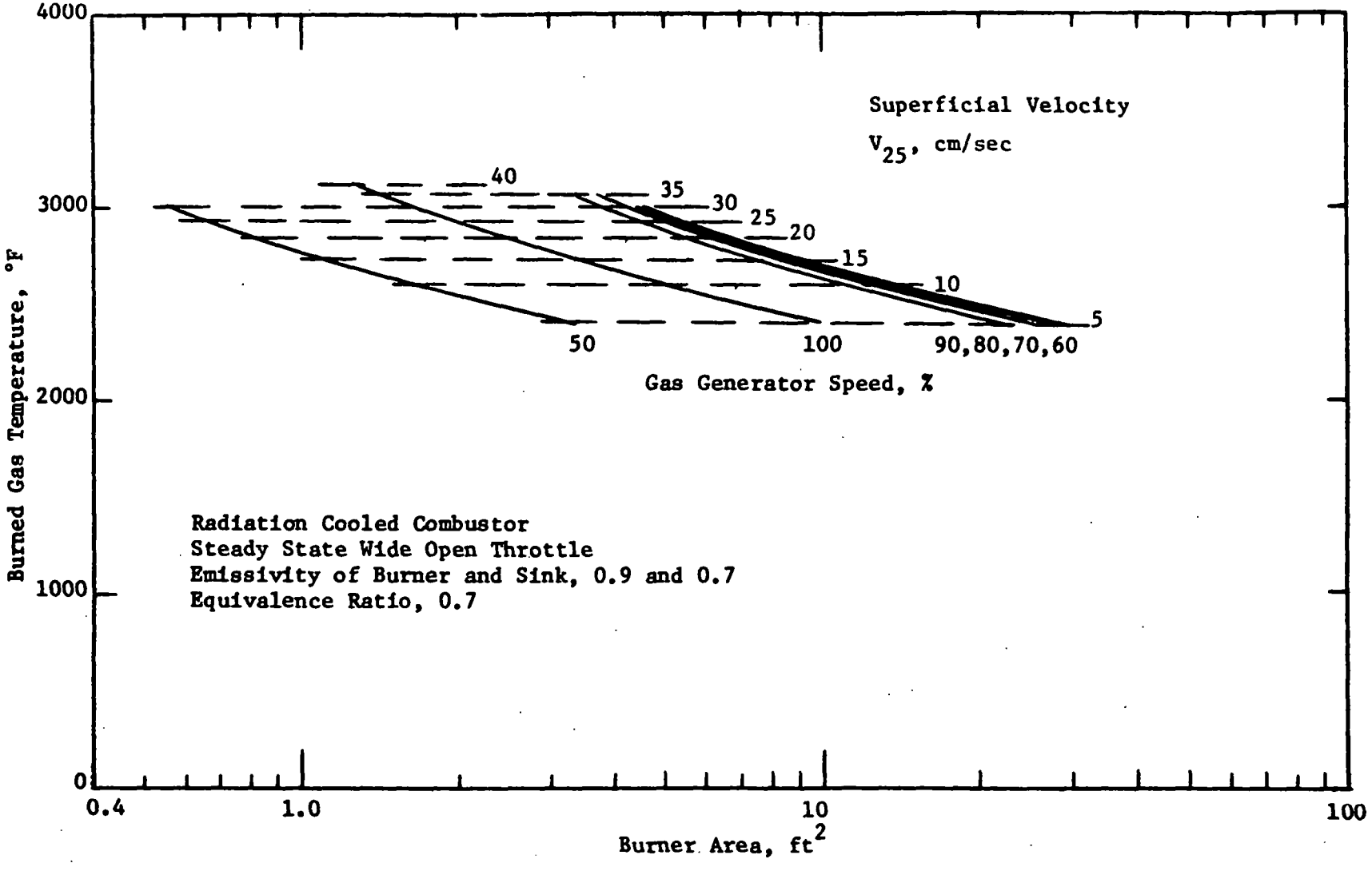

Figure 25. Burned Gas Temperature of Radiation Cooled Combustor at Steady State Wide Open Throttle Points

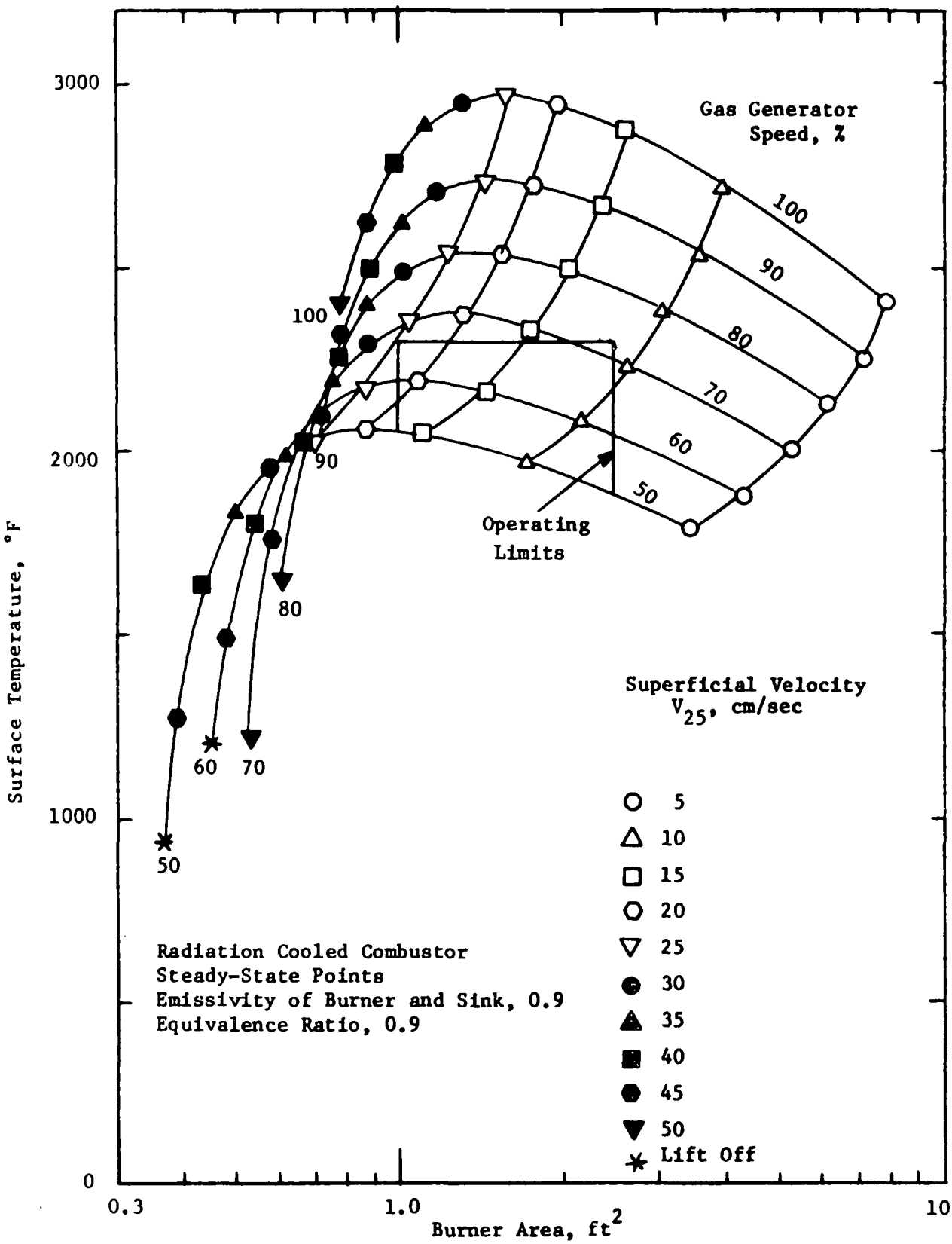

Figure 26. Surface Temperature of Radiation-Cooled Combustor at Steady-State Points

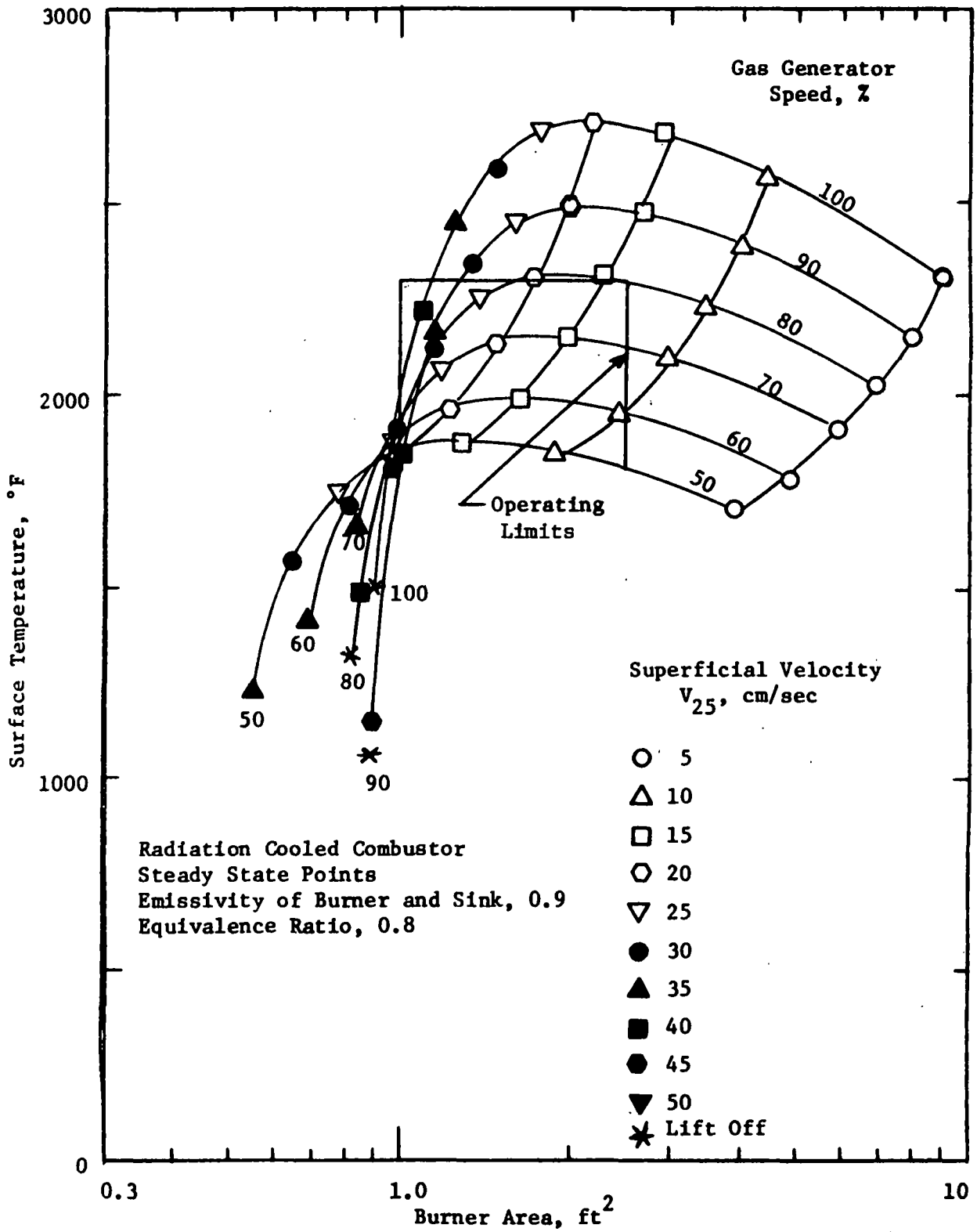

Figure 27. Surface Temperature of Radiation-Cooled Combustor at Steady-State Points

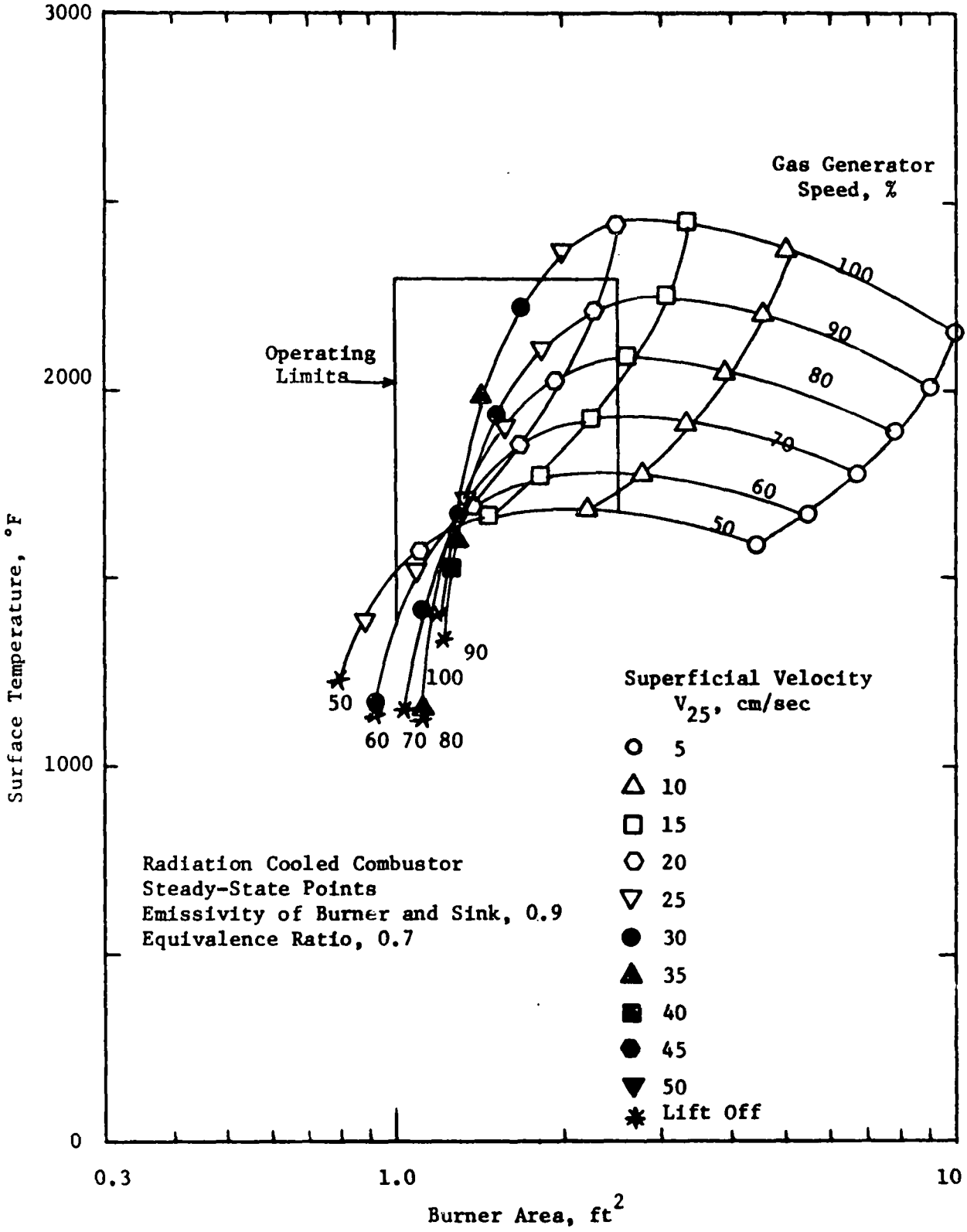

Figure 28. Surface Temperature of Radiation Cooled Combustor at Steady State Points

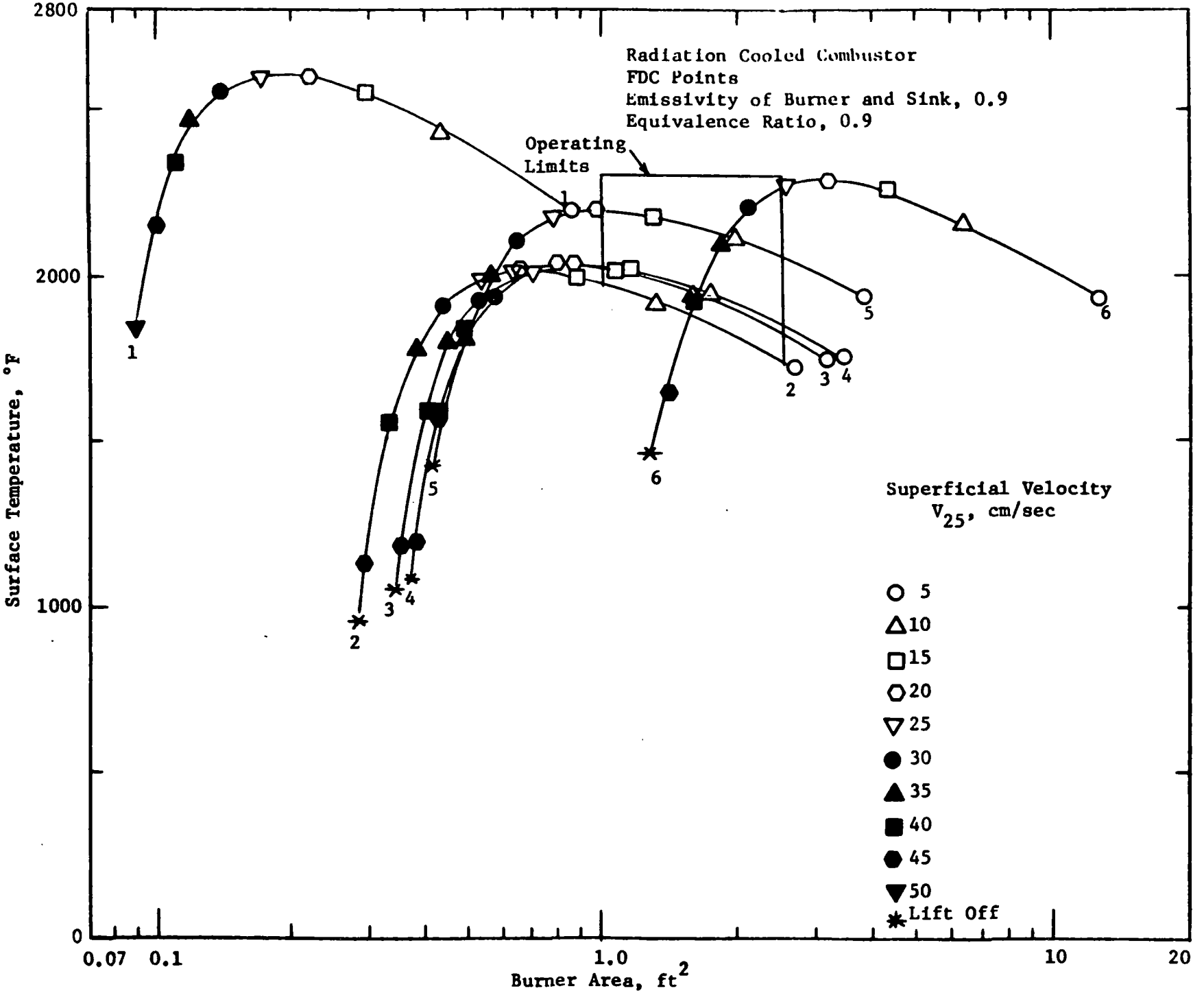

Figure 29. Surface Temperature of Radiation Cooled Combustor at FDC Points

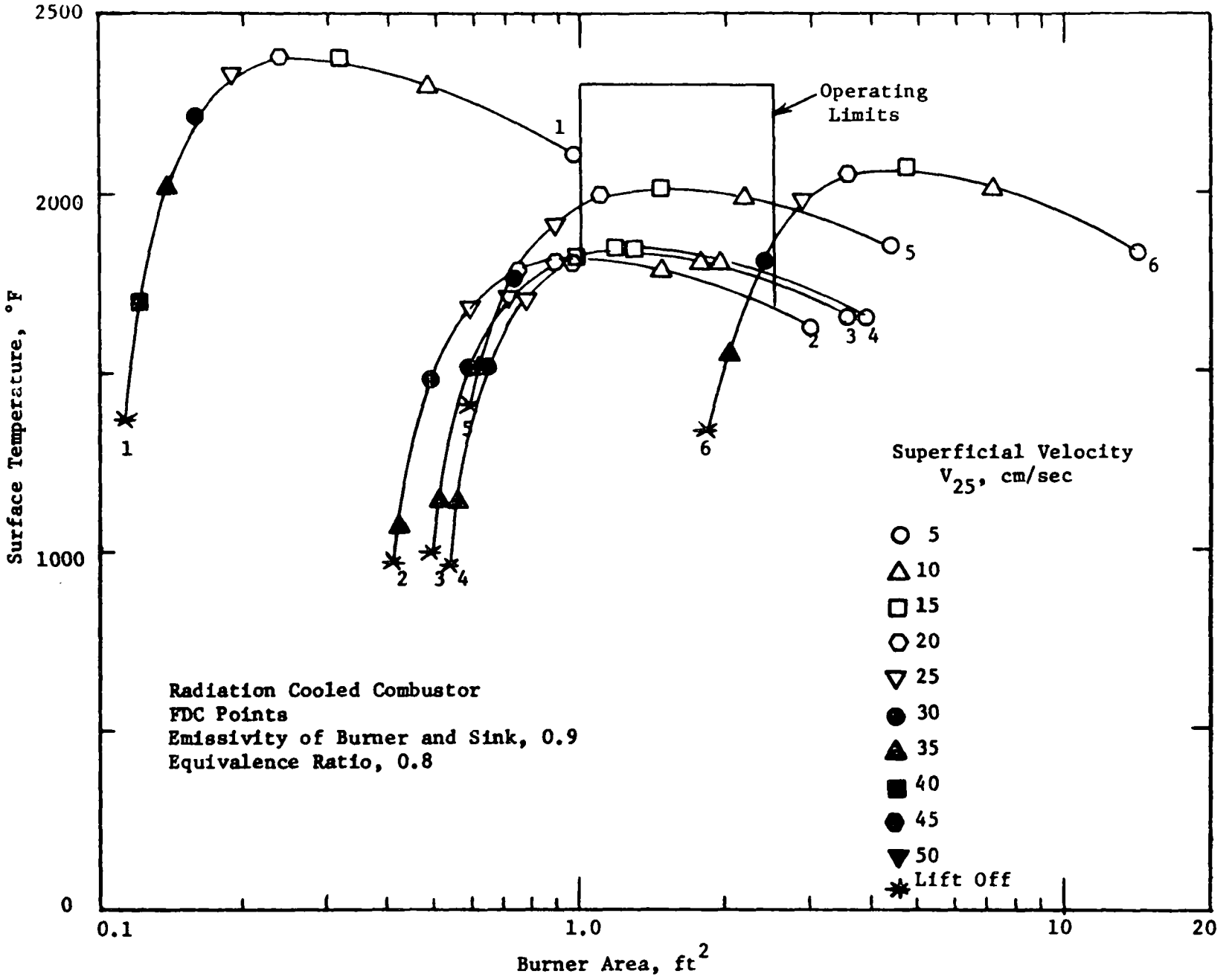

Figure 30. Surface Temperature of Radiation Cooled Combustor at FDC Points

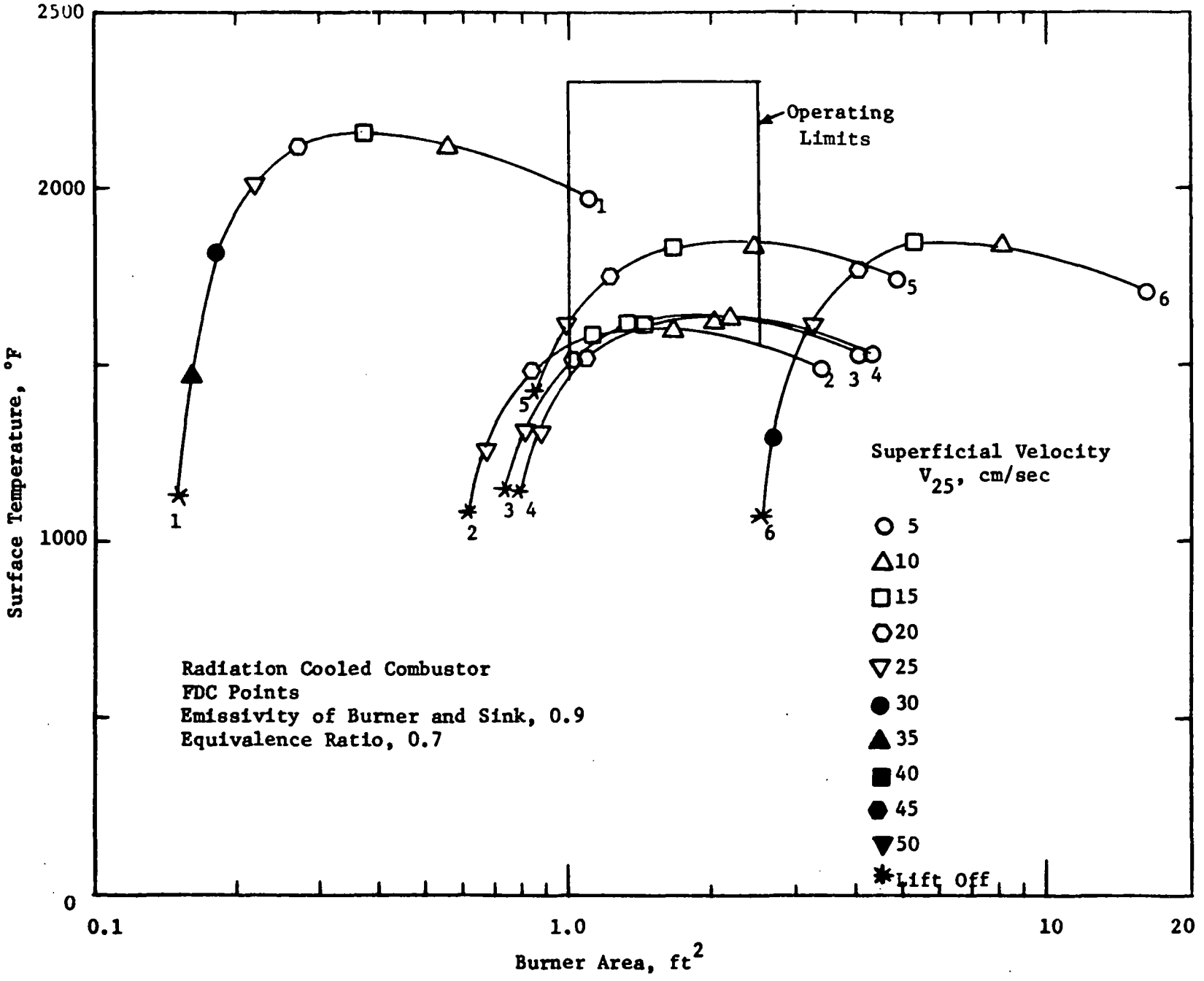

Figure 31. Surface Temperature of Radiation Cooled Combustor at FDC Points

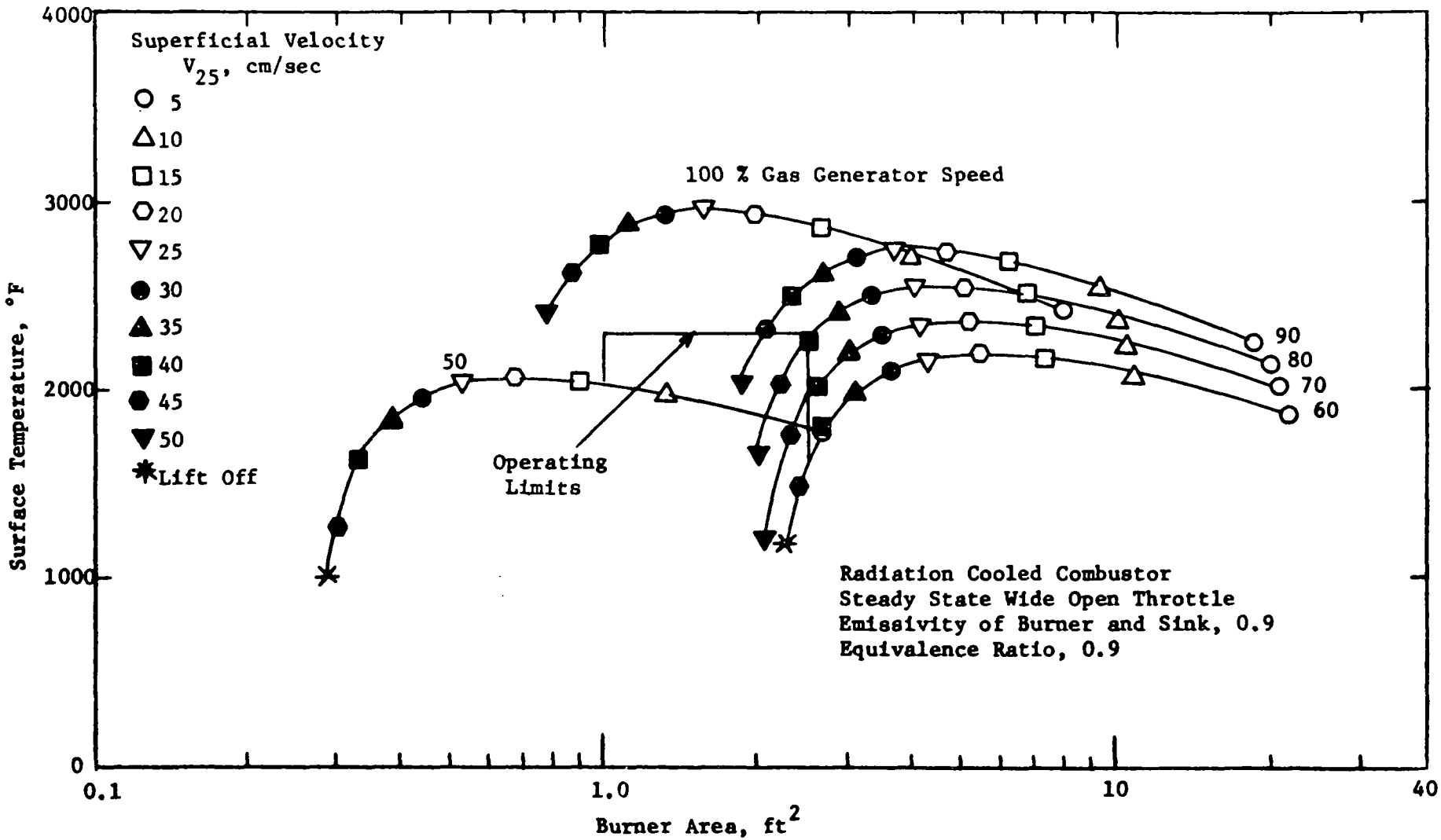

Figure 32. Surface Temperature of Radiation Cooled Combustor at Steady State Wide Open Throttle Points

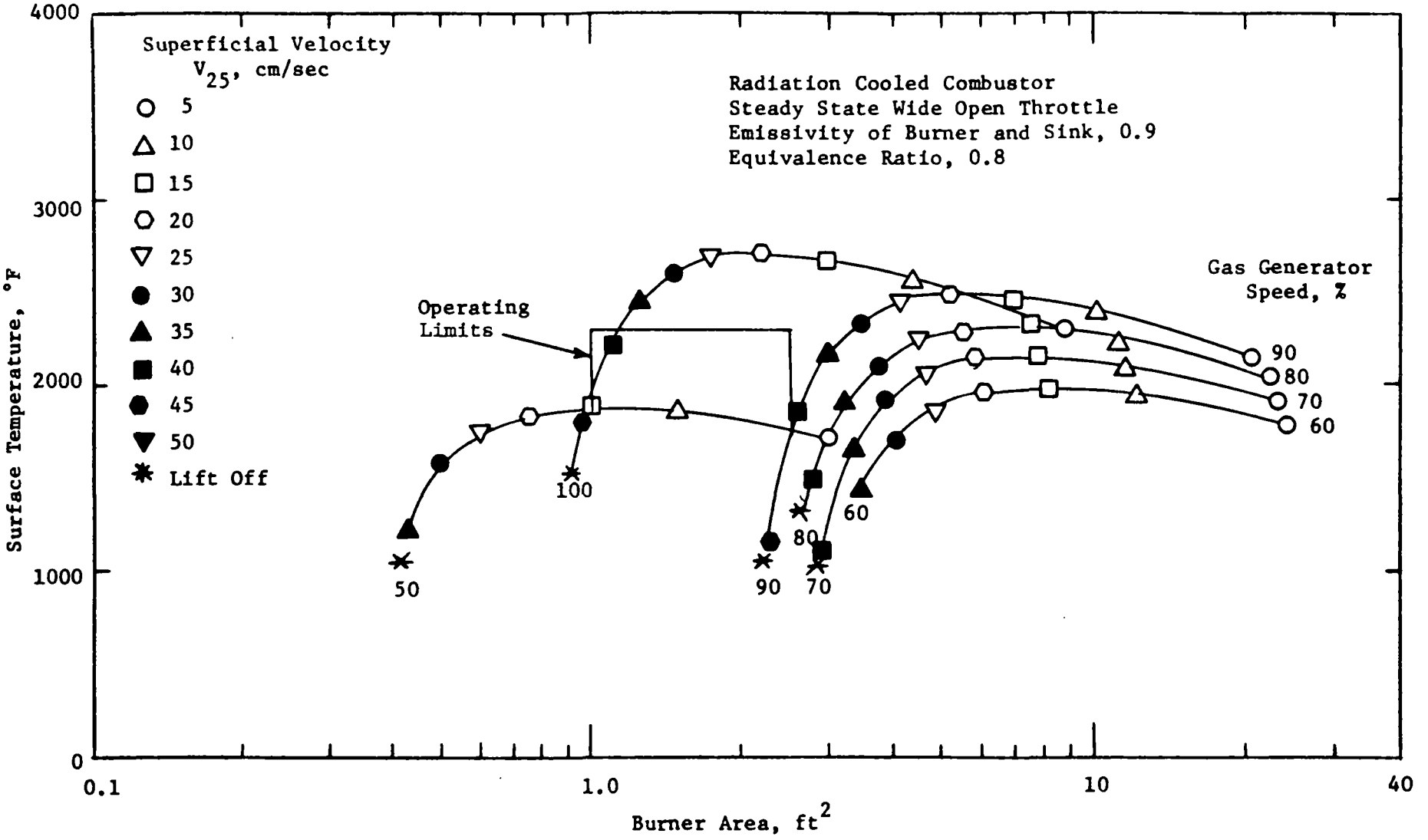

Figure 33. Surface Temperature of Radiation Cooled Combustor at Steady State Wide Open Throttle Points

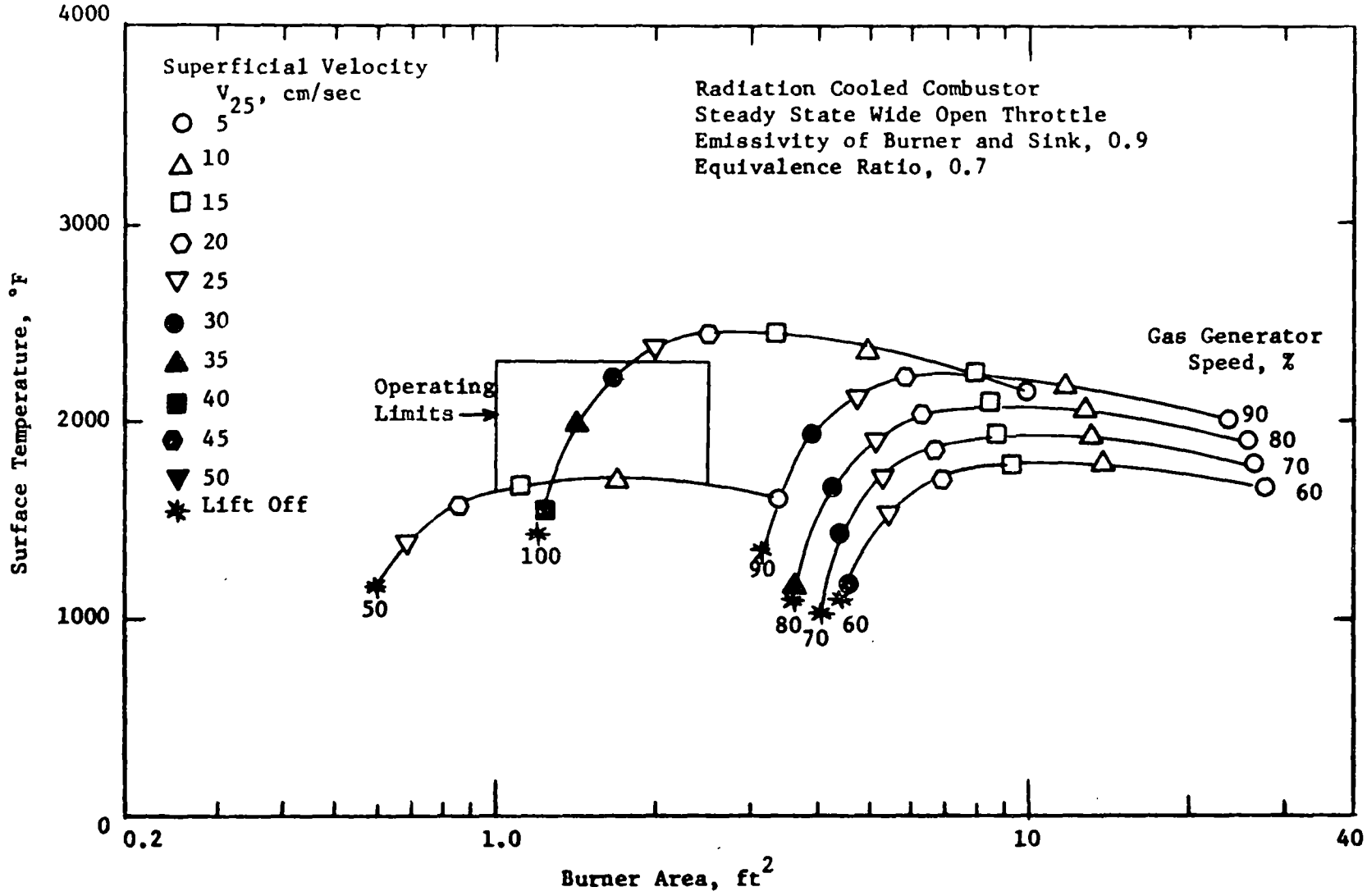

Figure 34. Surface Temperature of Radiation Cooled Combustor at Steady State Wide Open Throttle Points

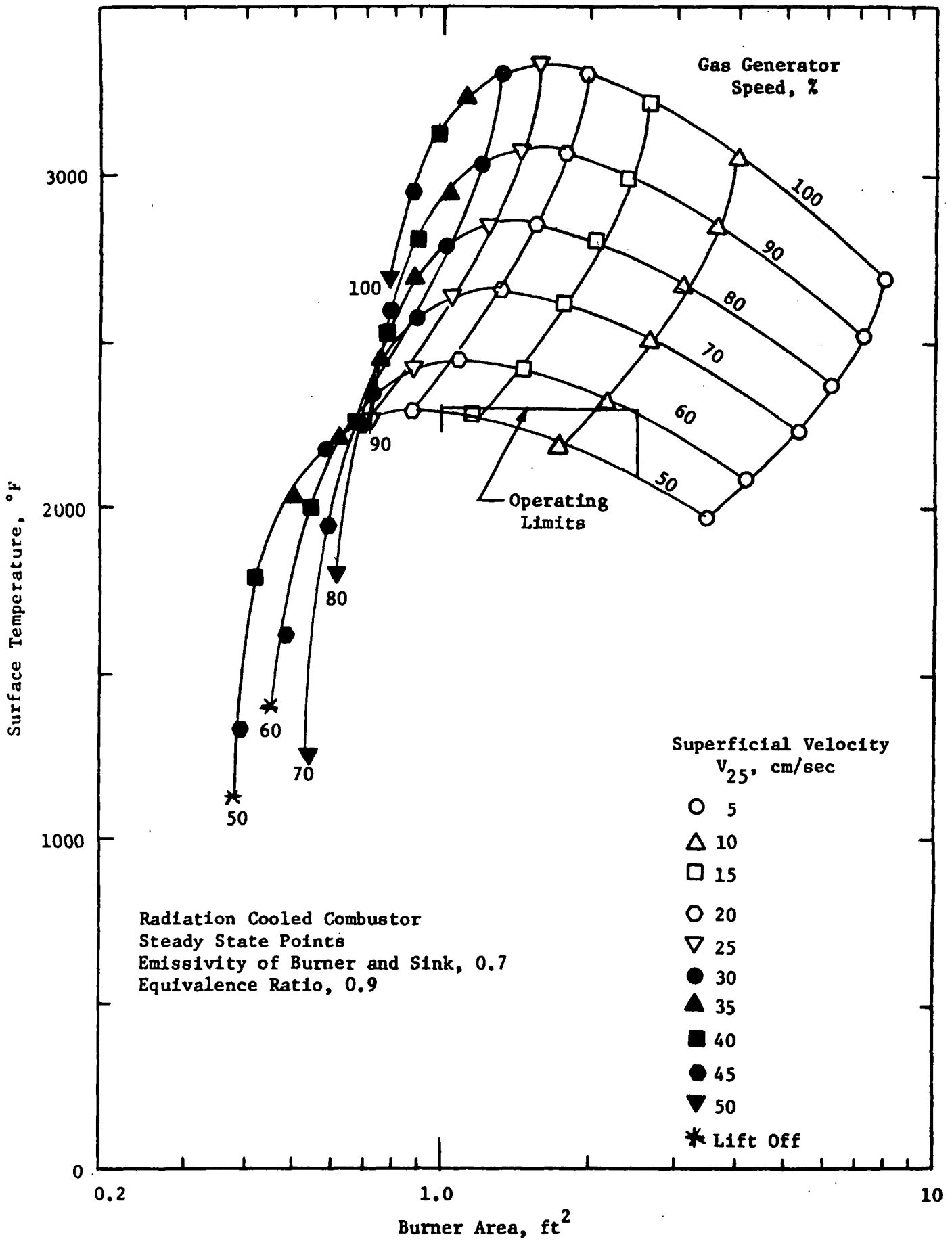

Figure 35. Surface Temperature of Radiation Cooled Combustor at Steady State Points

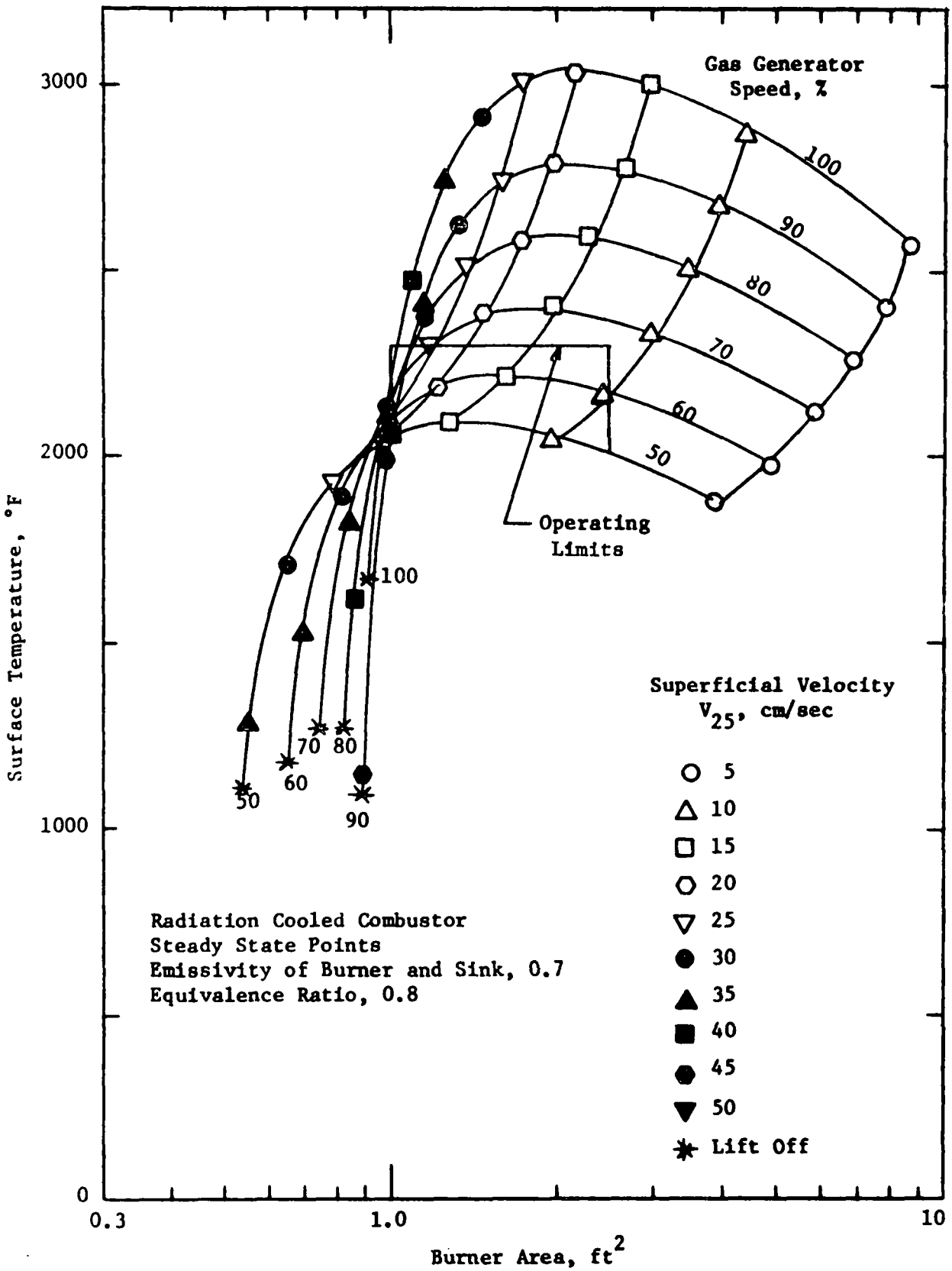

Figure 36. Surface Temperature of Radiation Cooled Combustor at Steady State Points

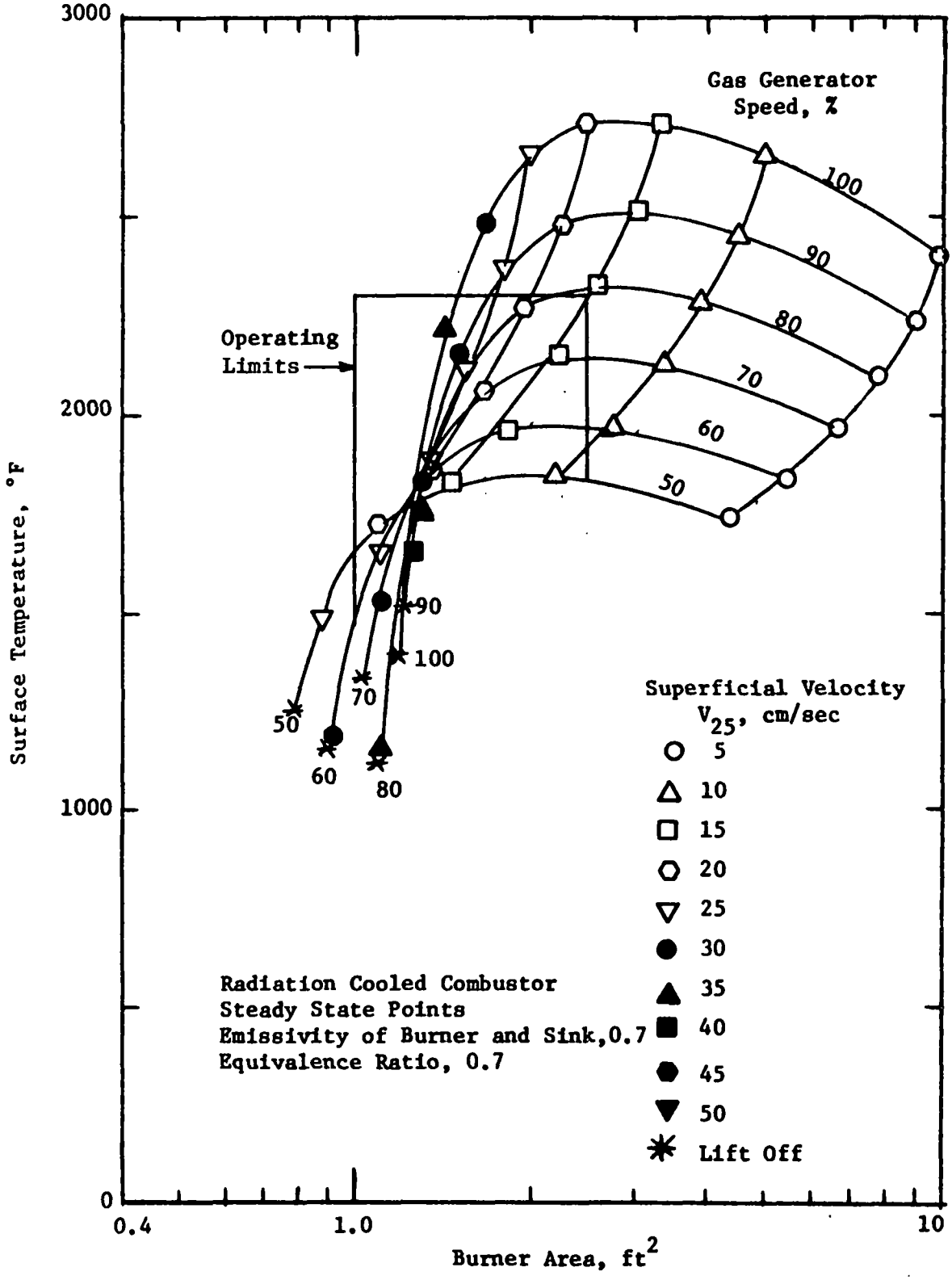

Figure 37. Surface Temperature of Radiation Cooled Combustor at Steady State Points

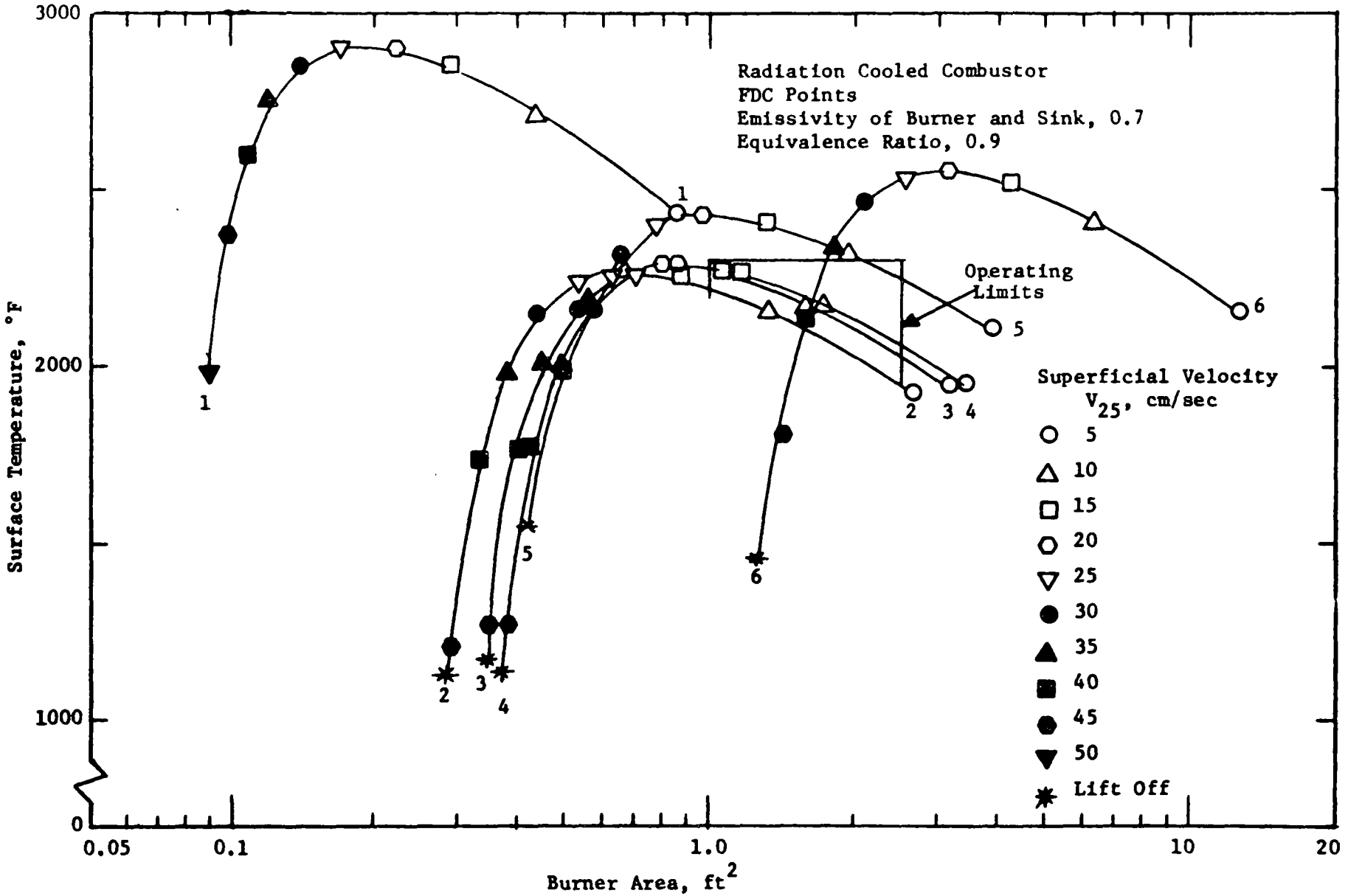

Figure 38. Surface Area of Radiation Cooled Combustor at FDC Points

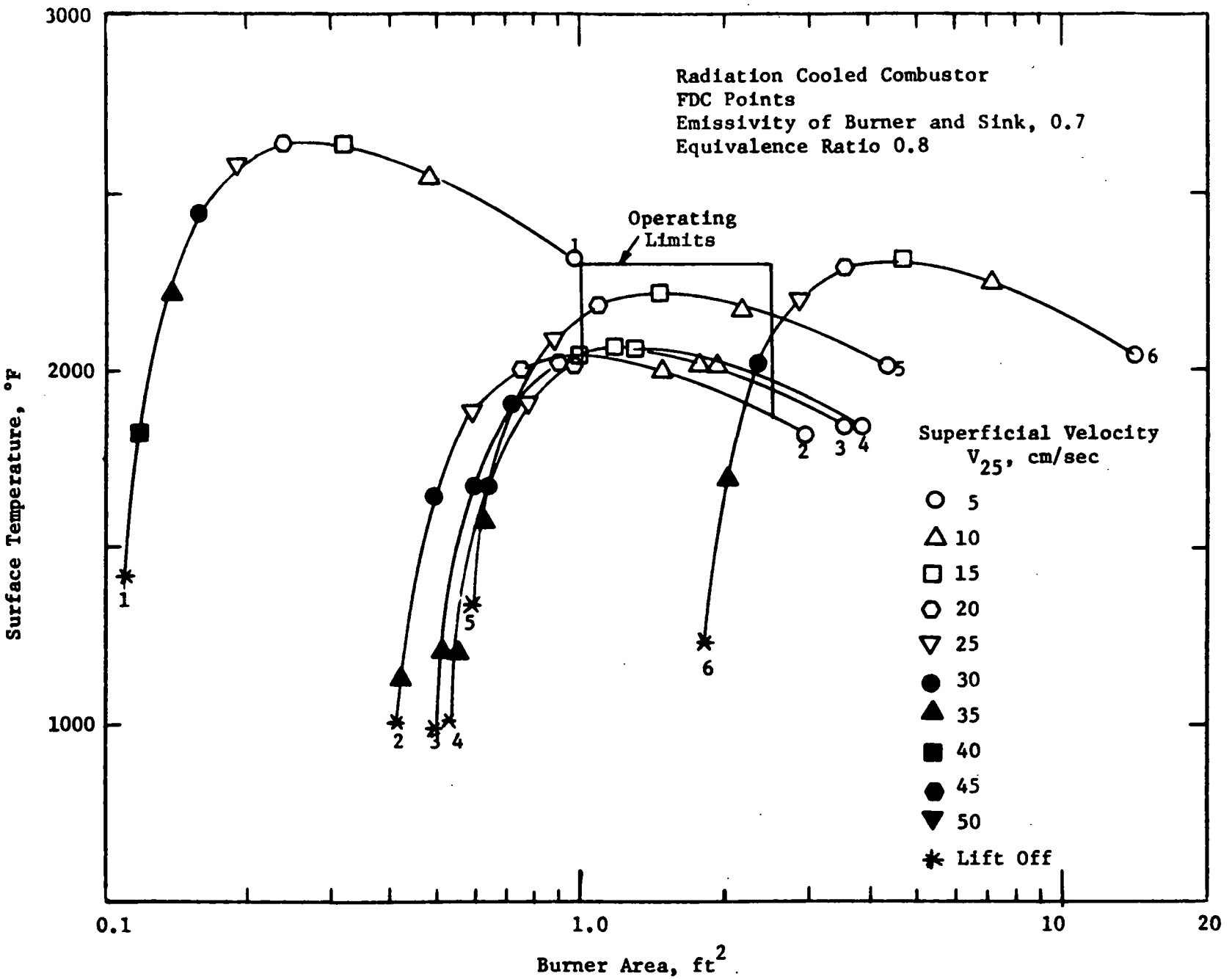

Figure 39. Surface Temperature of Radiation Cooled Combustor at FDC Points

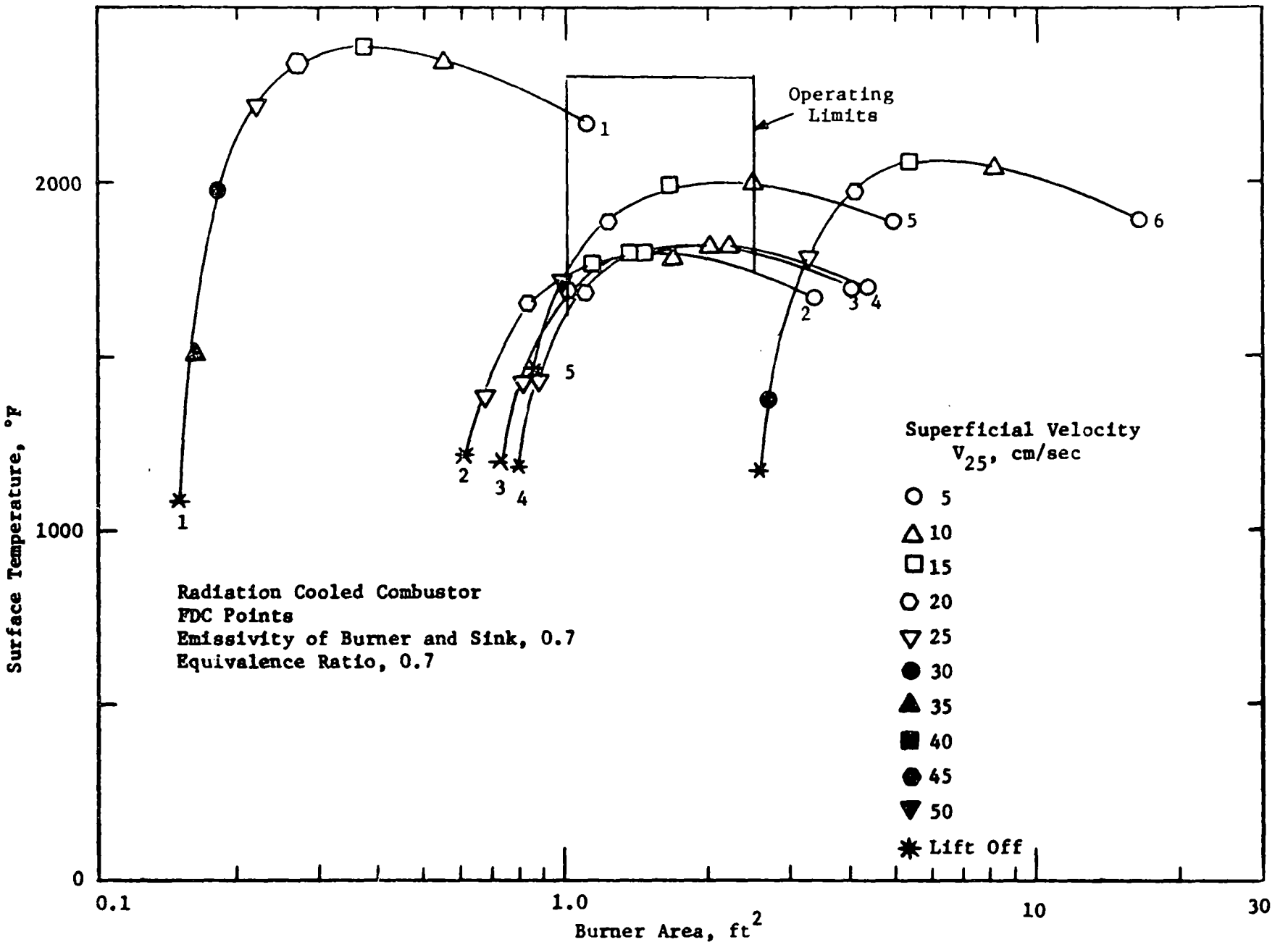

Figure 40. Surface Temperature of Radiation Cooled Combustor at FDC Points

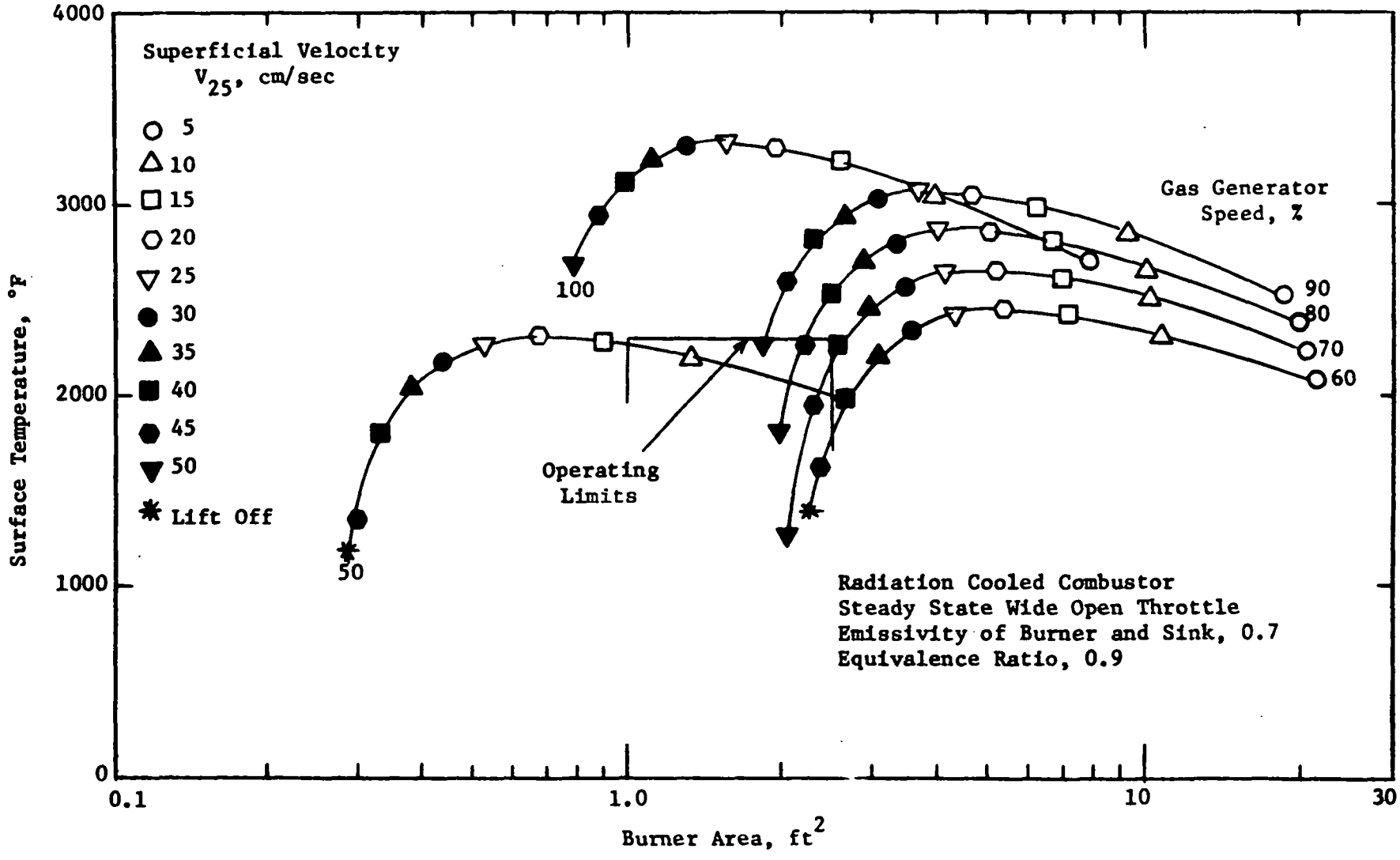

Figure 41. Surface Temperature of Radiation Cooled Combustor at Steady State Wide Open Throttle Points

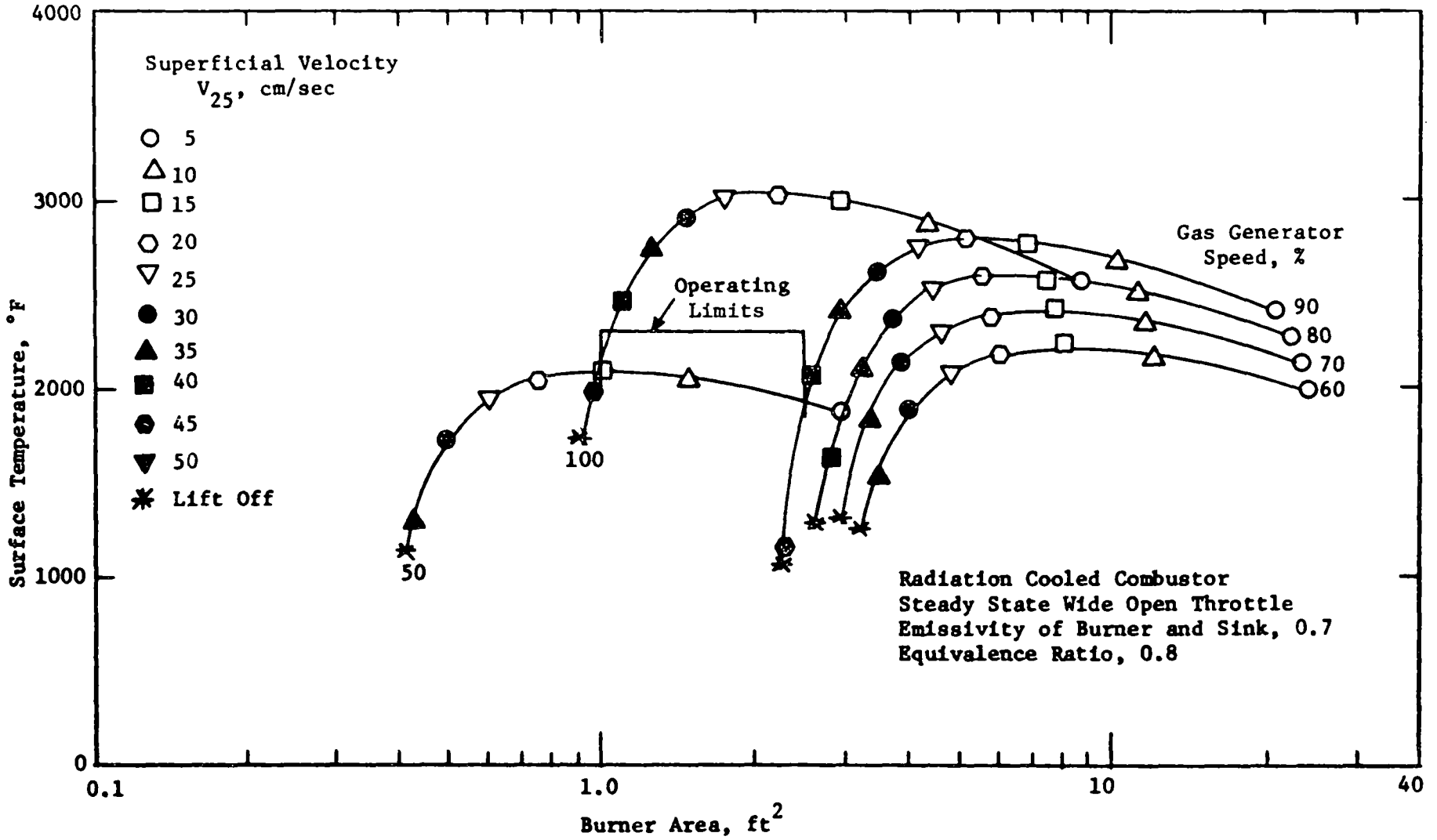

Figure 42. Surface Temperature of Radiation Cooled Combustor at Steady State Wide Open Throttle Points

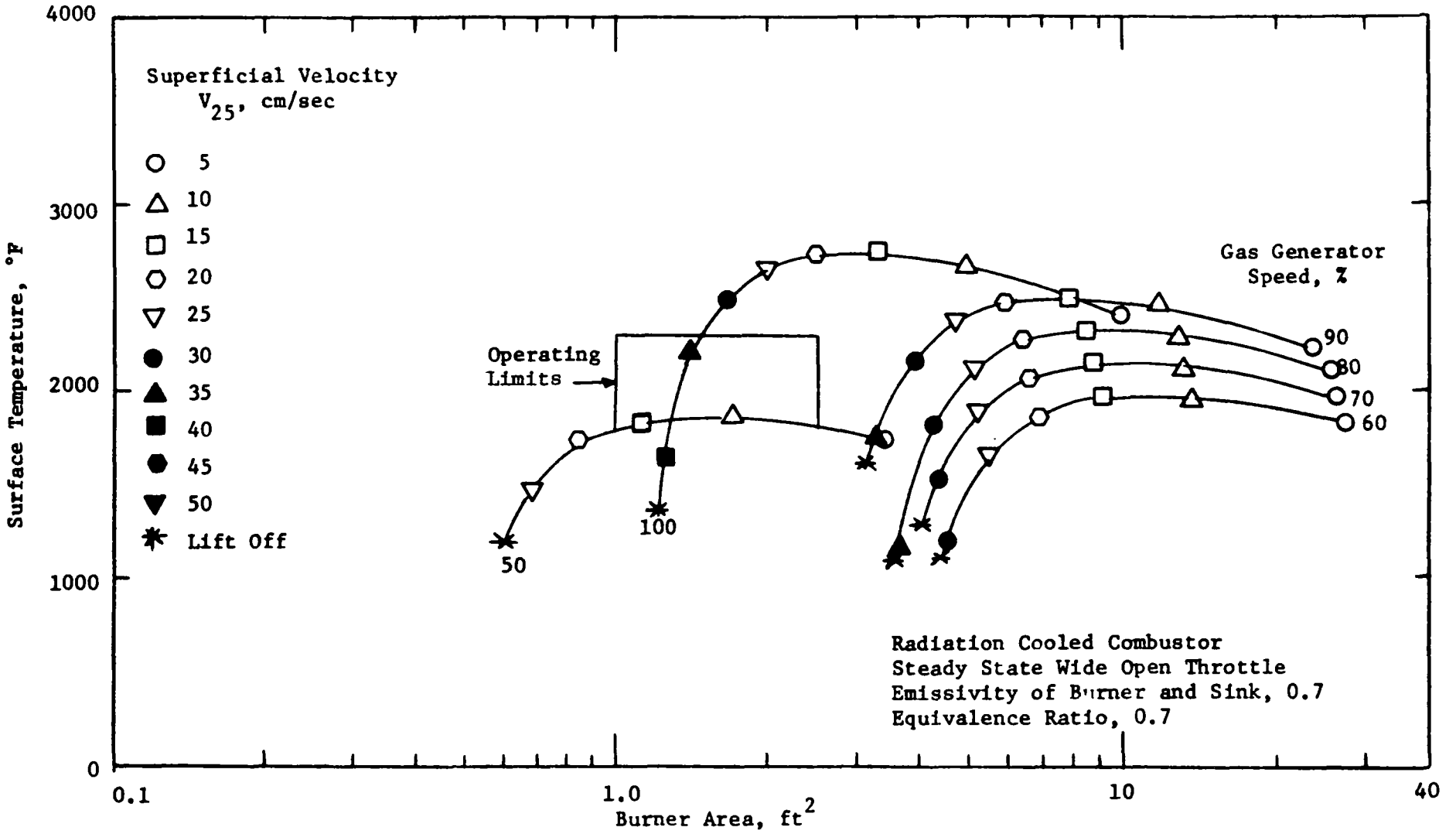

Figure 43. Surface Temperature of Radiation Cooled Combustor at Steady State Wide Open Throttle Points

Examination of the operating envelopes shows that all 18 operating points fall within the envelopes over a range of equivalence ratios from 0.7 to 0.9 and over a range of burner areas from 1.0 to 2.5 ft^2.

For the plots of hot-side burner temperature for the WOT, the hot-side burner temperature shown in the plots would be reached only if the burner were to remain in the steady-state at these pressures and fuel flow rates.

An analysis was made at an area of 1.15 ft^2 and an equivalence ratio of 0.8 along the steady state power matching line of Figure 10. Figure 44 shows the range of V_{25} over the range of power from idle to full power, on the line of steady-state match points. The operating velocity of 38.3 cm/sec at 100% gas generator speed is below the lift-off velocity of 48.3 cm/sec. Shown in Figure 45 are the burned gas temperatures, the hot-side burner temperatures, and the inside burner temperatures, all at steady state. The burner has a high-conductivity outer layer of 1/8" thick silicon-carbide (K about 10 Btu/hr-ft-°F) and an inside layer of 1/8" thickness and low thermal conductivity (K about 1.5 Btu/hr-ft-°F). Figure 46 shows the emission index for NO_2 emission; the calculation uses the hot-air model for NO_2 production rates, as shown earlier in Figure 3. Prompt NO_2 is not included in the calculation. A stratified-plug flow model is used to estimate residence time, with a six-inch residence length and an exit flow area of 34 in^2. This simplified model with stratified plug-flow assumes that the velocity profile is uniform, with the primary air from the flame and the secondary air assumed to be unmixed while in the combustor. In reality, the flows would be mixed, with the mixture at a lower temperature; the lower mixture temperature would have a lower NO_2 production rate. Figure 47 shows the CO emission index, calculated with a CO decay rate based on the flame temperature

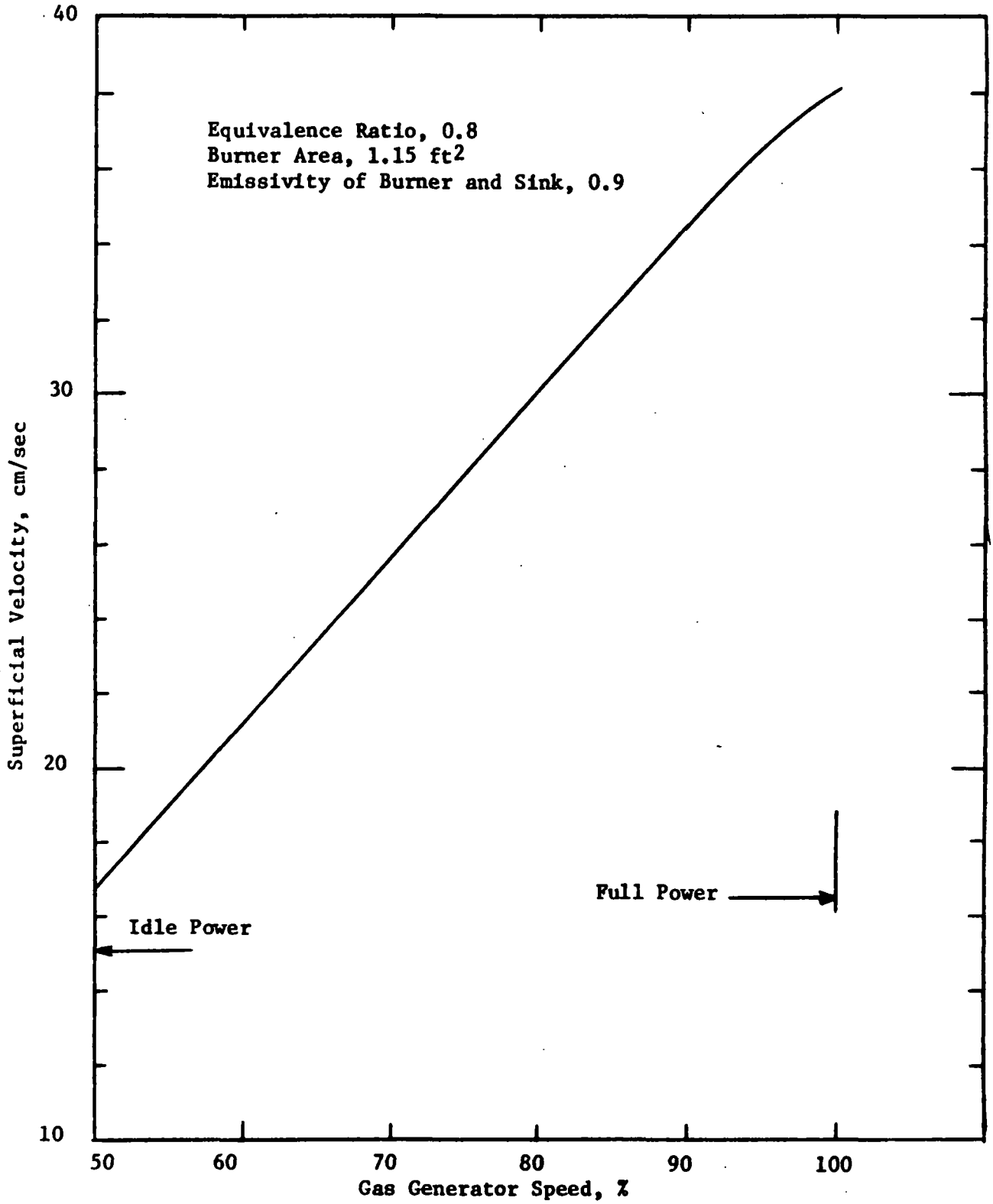

Figure 44. Superficial Velocity Along Steady State Power Match Line

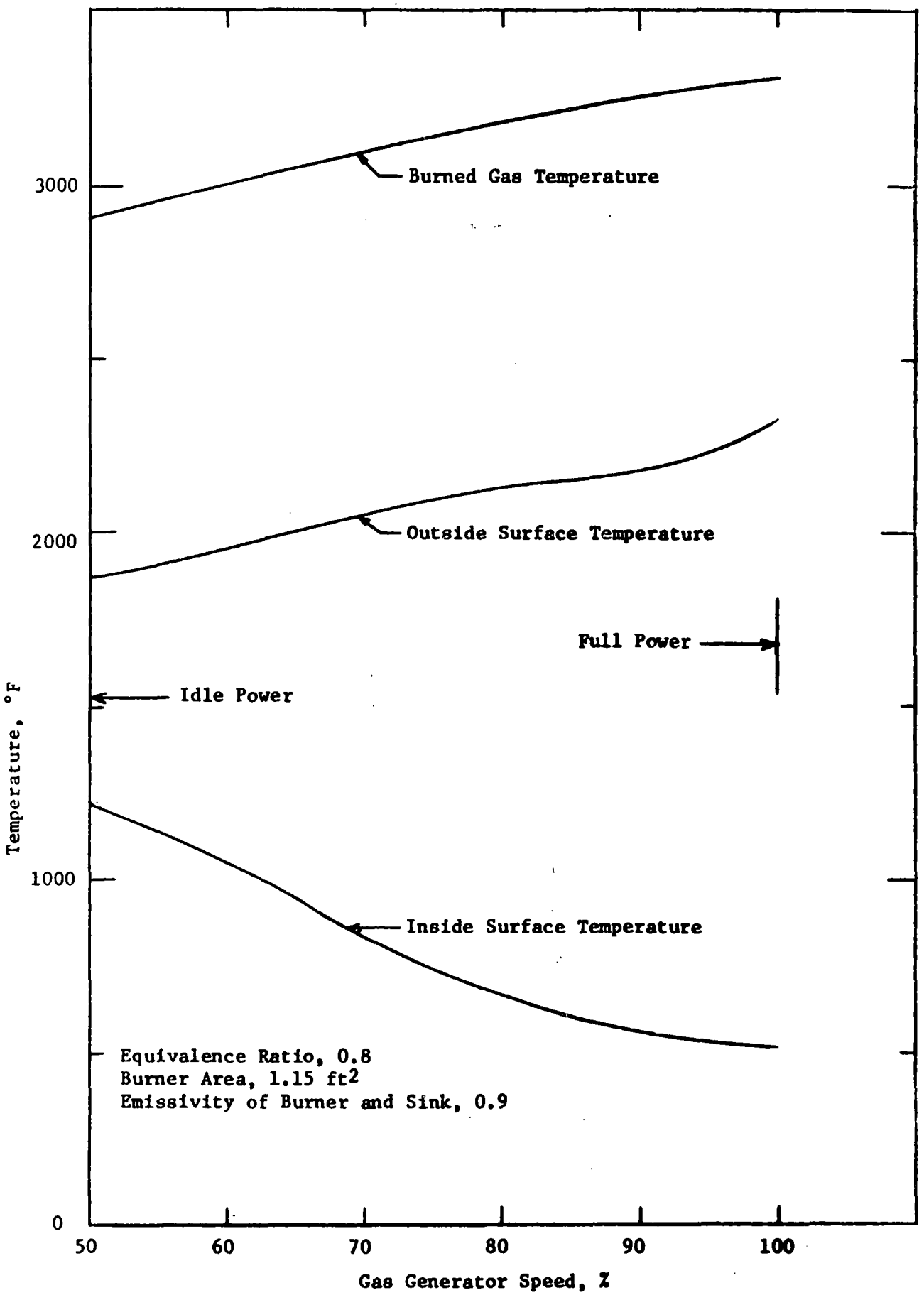

Figure 45. Combustor Temperature Along Steady State Power Match Line

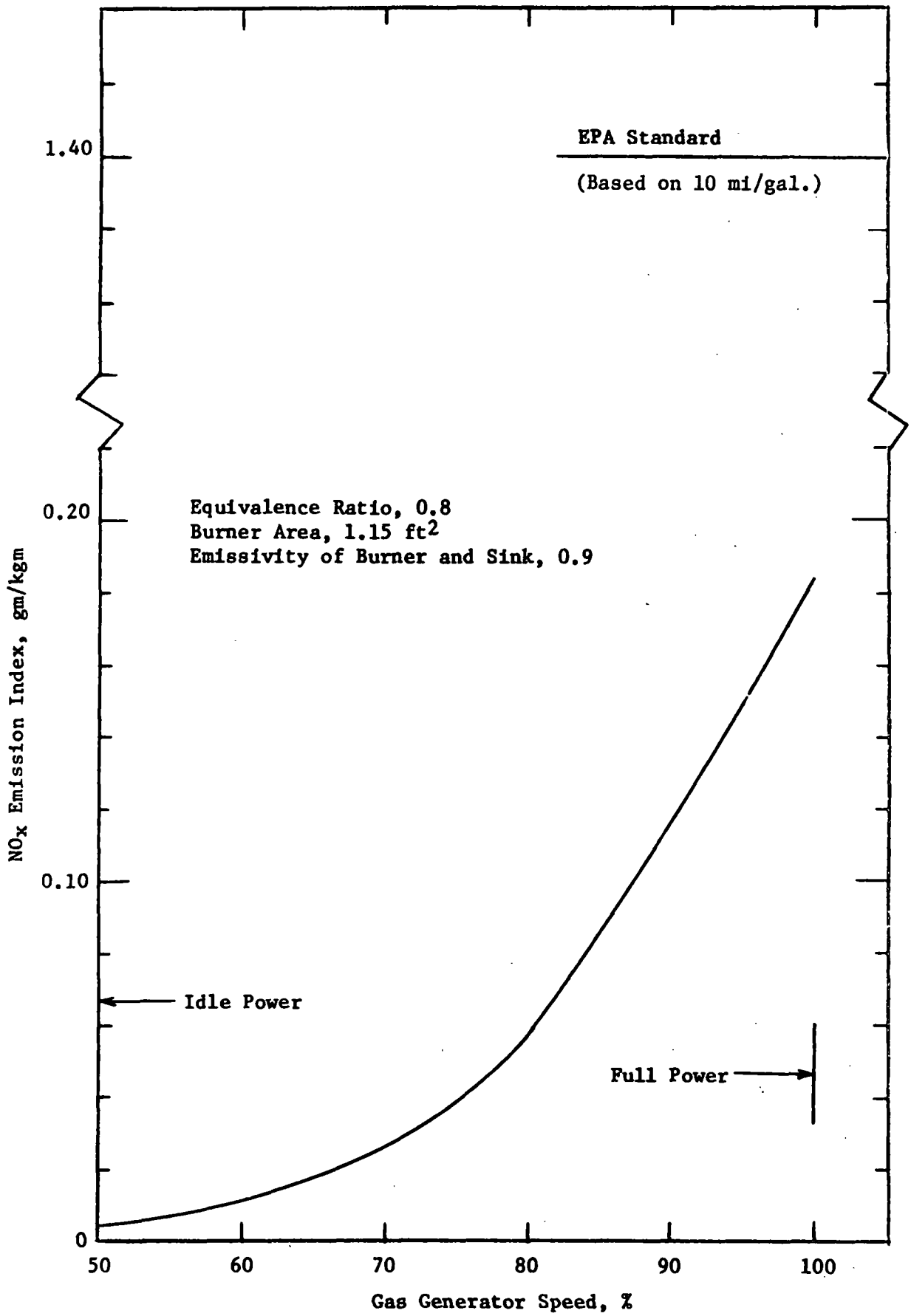

Figure 46. NO_x Emission Index Along Steady State Power Match Line

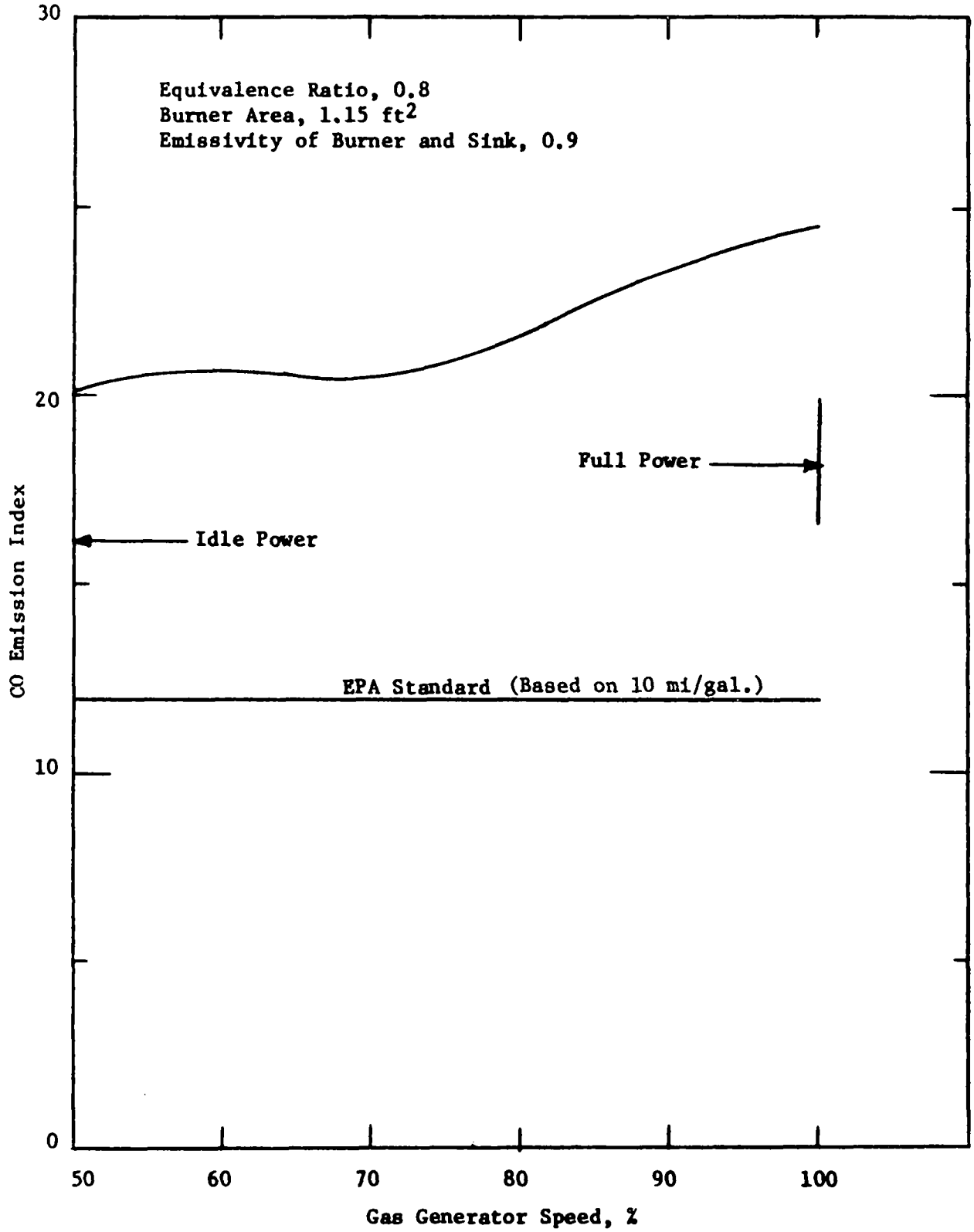

Figure 47. CO Emission Index Along Steady State Power Match Line

and with the stratified plug-flow model for residence time. For both Figures 46 and 47 the Federal Standard is indicated for the case of an average fuel consumption of 10 mpg. Although all of the steady-state NO_x points are lower than the Standard, the CO values are higher. By increasing the residence time and/or staging the diluent air the low NO_x values can be traded off with the high CO values. It is characteristic of porous-plate flames that only traces of unburned, hydrocarbon are produced as long as there is some excess air.

Transient Combustor Performance Analysis

A computer code for the transient thermal response of radiation-cooled burners was developed and used to analyze three Wide-Open-Throttle (WOT) accelerations and a cold start transient.

Analytical Methods - The approach was to use a finite difference marching-time (or explicit) formulation. The burner slab was divided into nodes, and a heat balance was written on each node to include conduction through the matrix, the enthalpy fluxes, and the heat from the flame for the case of the node on the hot-side surface. For the node on the cold-side surface, the heat out was balanced with the temperature increase in the gas just upstream of the burner by conduction in the gas. The code allows for 2 layers of porous materials with different properties to be used in a composite burner. Following the approach of Schneider[9], the local gas temperature within the porous material was taken as equal to the local metal temperature, because of the good heat transfer coefficient and the high volumetric density of heat transfer area in the matrix. Furthermore, the initial steady-state temperature profile in the solid was calculated using the steady-state results of Schneider[9] for a cooled porous plate.

The initial condition for each of the transients is assumed to be the steady state condition when the transient begins; for example, the initial condition of the WOT acceleration is the gas generator at 50% speed and at a fuel flow of 10 lbm/hr.

Looking at the nodal system as shown in Figure 48, the transient heat going into the hot-side node at an instant of time is:

$$Q_{In} = Q_{Air} + Q_{Fl} - Q_{RAD} \tag{1}$$

The first term on the right-hand side of Eq. 1 is:

$$Q_{Air} = W_{Pri}\ C_{Pg} \left(T'_B(1) - T_{A_{in}}\right) \tag{2}$$

The transient heat rate, Q_{Air}, is the heat that is required to heat the primary air flow, W_{Pri}, from its combustor inlet temperature, $T_{A_{in}}$, (which is the compressor exit temperature) to the hot-side burner exit temperature which is taken as identical to the hot-side burner temperature, $T'_B(1)$. The prime refers to the temperature of the node at the previous instant of time, since very small time increments with a typical size of 0.01 seconds are used in the marching time solution. C_{Pg} is the specific heat of the unburned fuel-air mixture.

The second term is:

$$Q_{Fl} = W_{Pri}(h^*-h) \tag{3}$$

This transient heat rate, Q_{Fl}, represents the net cooling of the flame by the sink and is calculated from Kaskan's data[6] as a function of the superficial gas velocity, V_{25}, and the equivalence ratio, R. The enthalpy difference of the fuel-air mixture in the parentheses is the enthalpy h* at the adiabatic flame temperature less the enthalpy h at the actual flame

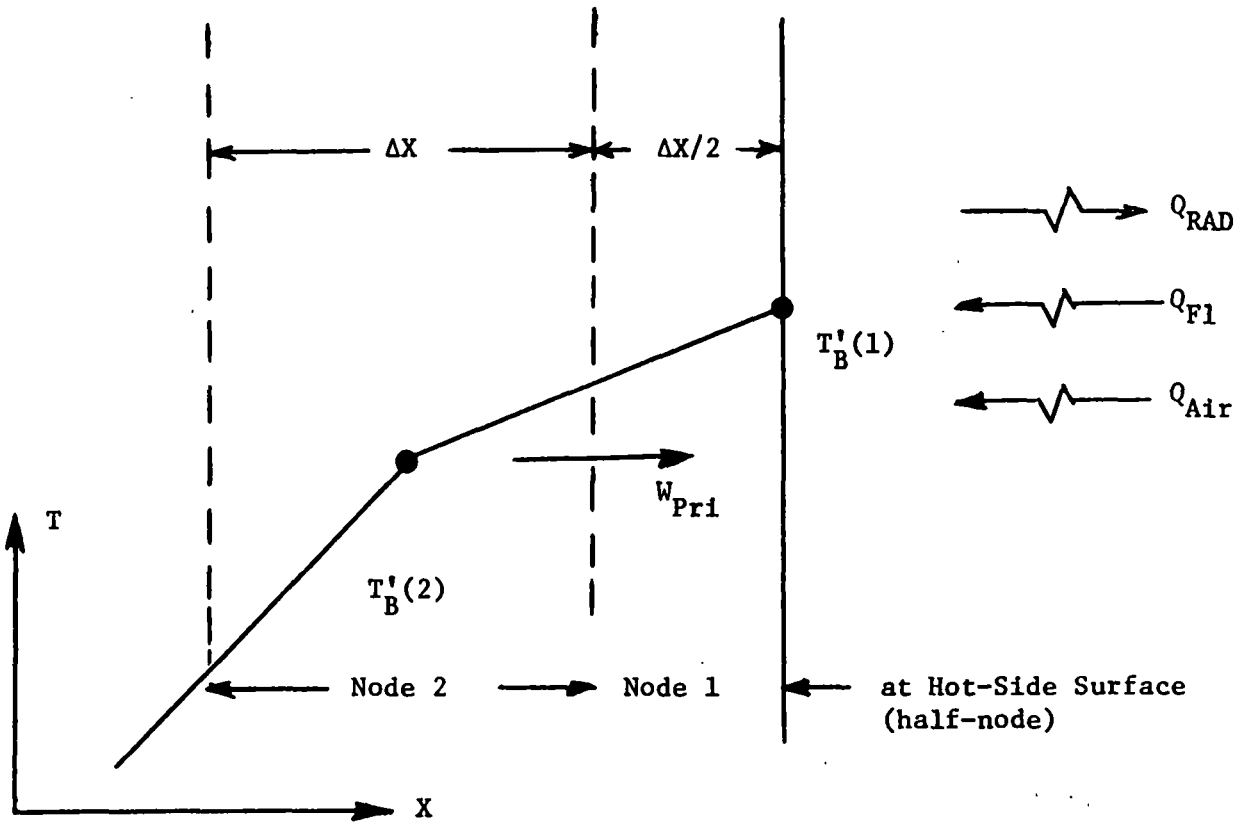

$$Q_{In} = Q_{Air} + Q_{Fl} - Q_{RAD}$$

where $Q_{Air} = W_{Pri}\ C_{Pg}\left(T'_B(1) - T_{A_{In}}\right)$

$$Q_{Fl} = W_{Pri}\ (h^* - h)$$

$$Q_{RAD} = A_{Burn}\ \sigma\ F \left\{ \left[T'_B(1)\right]^4 - T^4_{Sink} \right\}$$

Figure 48. Nodal System for Transient Thermal Analysis

temperature which is a function of V_{25} as shown earlier in Figure 2.

The third term is the transient radiation flux from the hot-side burner temperature, $T_B'(1)$, to the sink, T_{Sink}, and is calculated with:

$$Q_{RAD} = A_{Burn}\ \sigma\ F \left\{ \left[T_B'(1) \right]^4 - T_{Sink}^4 \right\} \tag{4}$$

σ is the Stefan-Boltzmann constant, and F is the overall view factor (including emissivities) from the burner to the sink. A_{Burn} is the frontal area of the burner.

The conduction flux out of node 1 into node 2 is approximated in the finite difference approach with Fourier's conduction law as:

$$Q_{1-2} = K_B\ A_{Burn}\ \frac{T_B'(1) - T_B'(2)}{\Delta X} \tag{5}$$

where K_B is the effective thermal conductivity of the burner, and ΔX is the node thickness and also the thickness over which the gradient $T_B'(1) - T_B'(2)$ is obtained.

The enthalpy flux of the air flow out of node 1 is:

$$Q_W\Big)_{Out} = W_{Pri}\ C_{Pg} \left(T_B'(1) - T_{Ref} \right) \tag{6}$$

while the enthalpy flux of the air flow into node 1 is taken as:

$$Q_W\Big)_{In} = W_{Pri}\ C_{Pg} \left(\frac{T_B'(2) + T_B'(1)}{2} - T_{Ref} \right) \tag{7}$$

The temperature, T_{Ref}, is an arbitrary reference temperature for the enthalpy which drops out of the calculation method.

Then, since the "heat in" less the "heat out" represents the heat left to increase the temperature of the node, the following heat balance holds:

$$Q_{In} + Q_W\Big)_{In} - Q_{1-2} - Q_W\Big)_{Out} = \frac{M_B\ C_{PB}\left\{T_B(1) - T_B'(1)\right\}}{\Delta t} \tag{8}$$

where Δt is the increment in time. For this half-node, the burner mass is $M_B = \rho_B \frac{\Delta X}{2} A_{Burn}$. The effective density and specific heat of the burner material are ρ_B and C_{PB}, respectively. The burner temperature of the node, $T_B(1)$ is the new temperature of the node at the end of the time increment, Δt; $T_B'(1)$ is the temperature of the node at the beginning of the time increment. Hence, the transient heat balance results in the following algebraic equation for the node temperature at the current instant of time in terms of the known temperatures from the previous instant of time:

$$T_B(1) = T_B'(1) + \frac{2Q_{In}\ \Delta t}{\rho_B\ C_{PB}\ \Delta X\ A_{Burn}} - \frac{2K\ \Delta t}{\rho_B\ C_{PB}\ (\Delta X)^2}\left\{T_B'(1) - T_B'(2)\right\}$$
$$- \frac{W_{Pri}\ C_{Pg}\ \Delta t}{A_{Burn}\ \Delta X\ \rho_B\ C_{PB}}\left\{T_B'(1) - T_B'(2)\right\} \tag{9}$$

For the interior nodes, similar heat balances are applied which also result in algebraic equations for temperatures of the nodes; the heat fluxes in and out of the interior nodes are calculated with Fourier's conduction equation.

Input Data - Time-dependent values of fuel flow, total air flow, and temperatures were taken from the supplied Chrysler Base Line Engine data. For the WOT acceleration from Idle, the gas generator speed is shown in Figure 49 as a function of time as supplied for the Chrysler Base Line Engine; this plot in conjunction with the plot of fuel flow as a function of gas generator speed shown in Figure 50 was used to obtain the time dependent fuel flow. Similar plots were utilized to obtain the time dependent values of pressure level, total gas flow, compressor exit tem-

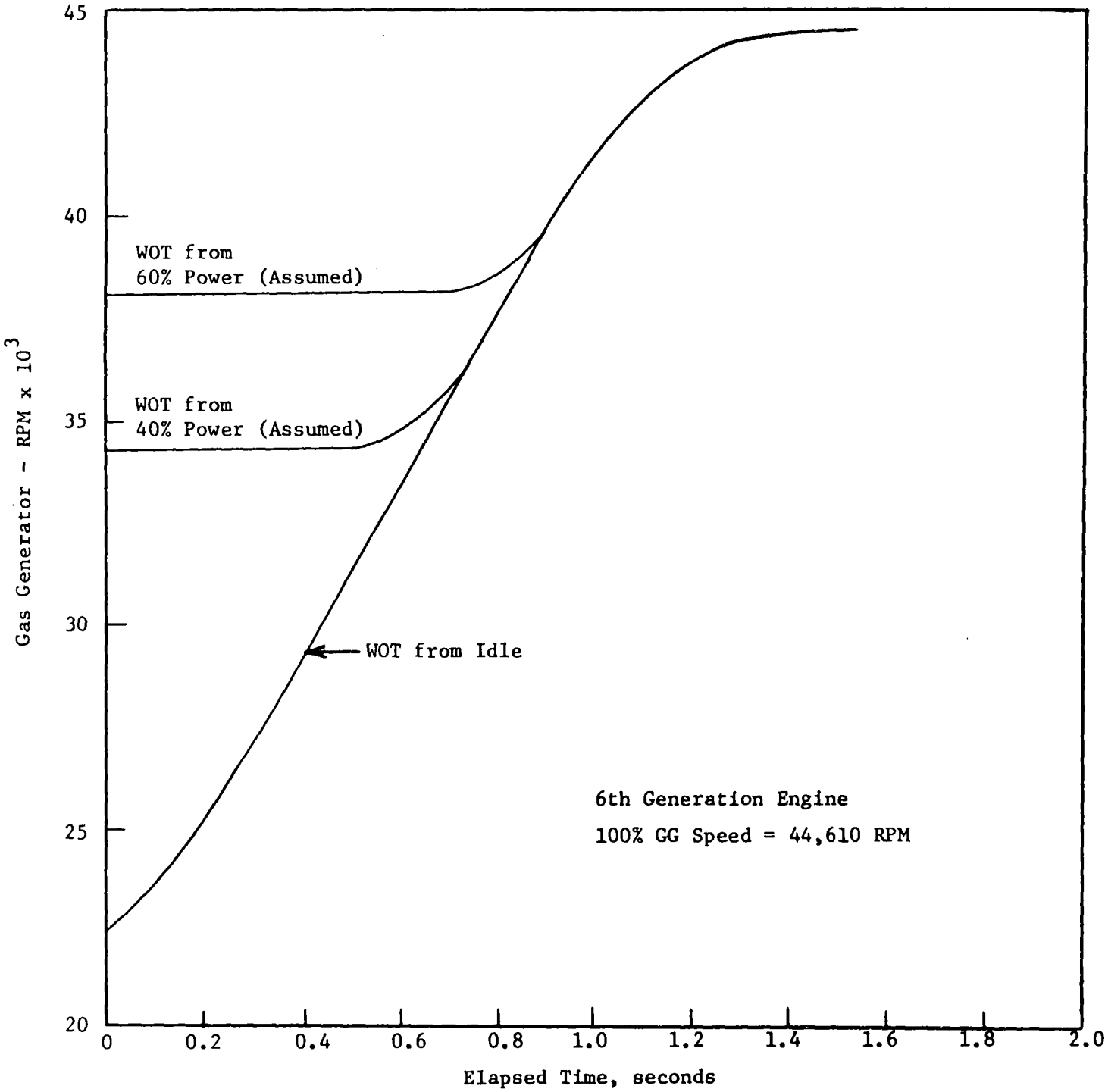

Figure 49. Time-Dependent Gas Generator Speed During 3 Wide-Open-Throttle Transients (WOT) at 85°F

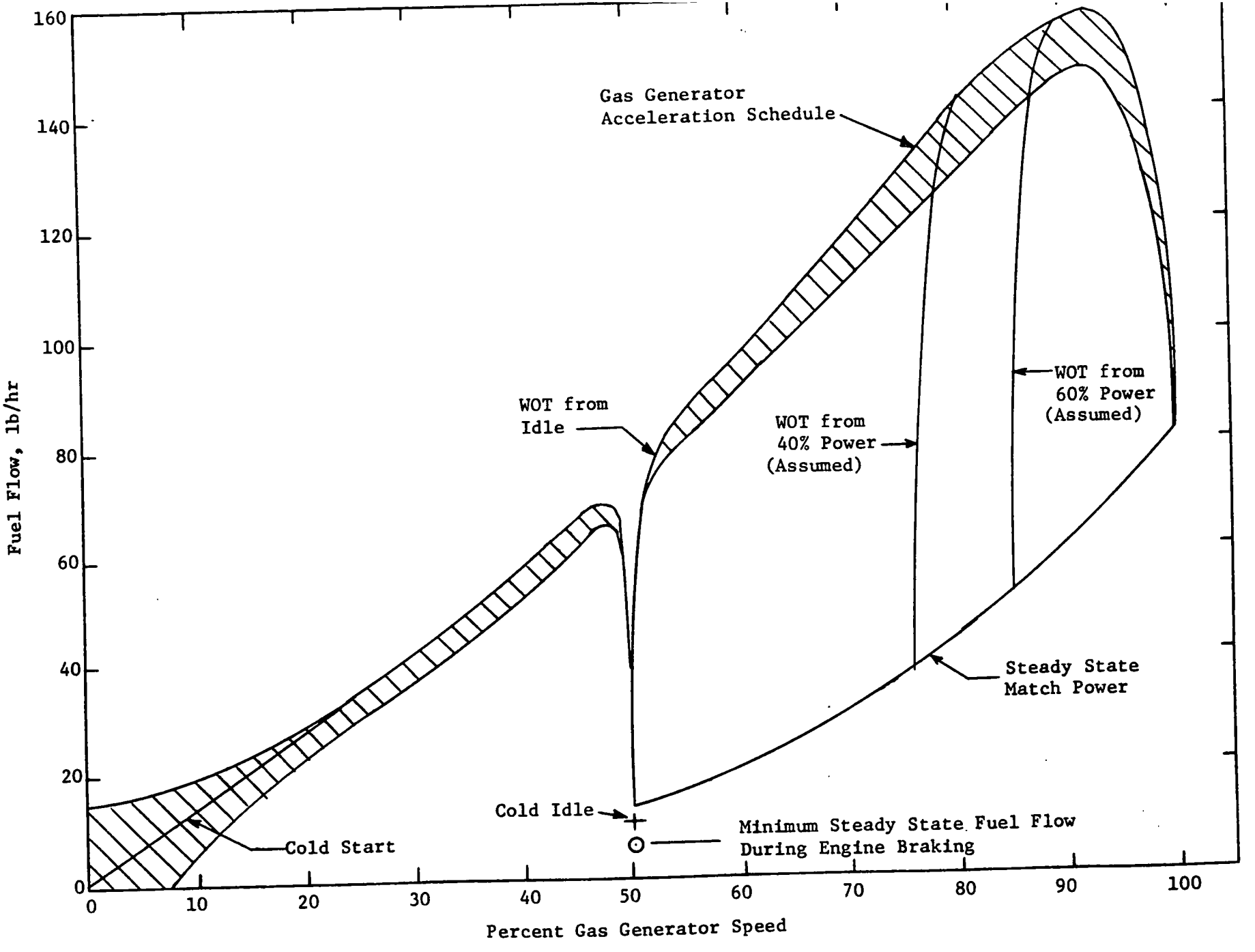

Figure 50. Fuel Scheduling of Base Line Engine During the Four Transients

perature, and regenerator exit temperature. The gas generator speed during the cold start transient was also supplied.

For the WOT transients from 40% engine power and 60% engine power, the transient gas generator speeds were approximated as shown in Figures 49 and 50 since they were not supplied.

For the transient calculations discussed herein, the configuration of materials and their thermophysical properties are shown in Figure 51. On the flame side of the burner is a slab of Silicon Carbide (SiC) of 1/8" thickness; it is selected because of its high-temperature capabilities. On the air inlet side is a slab of low-conductivity material which acts as an insulator to prevent auto-ignition upstream of the burner; the thickness of this slab was arbitrarily taken as 1/8", but the thickness may need to be increased to prevent auto-ignition of gasoline which has a lower ignition temperature than propane.

The schedules of burner area and of equivalence ratio during the four transients are shown in Figure 52. These arbitrary schedules were selected to avoid both lift-off and flame extinguishment during the transients; the steady-state temperatures at both the beginning and the end of the transient with these schedules are sufficiently within materials limitations. At the start of the transient, the equivalence ratio undergoes a step increase to 1.0 from 0.8, and the burner area has a simultaneous step increase to 2.20 ft^2 from 1.15 ft^2. At the end of the transients, the equivalence ratio undergoes a step decrease to 0.8, as does the burner area to 1.15 ft^2.

Results - Shown in Figure 53 is the calculated thermal response of the porous combustor at three locations during the WOT fuel transient from

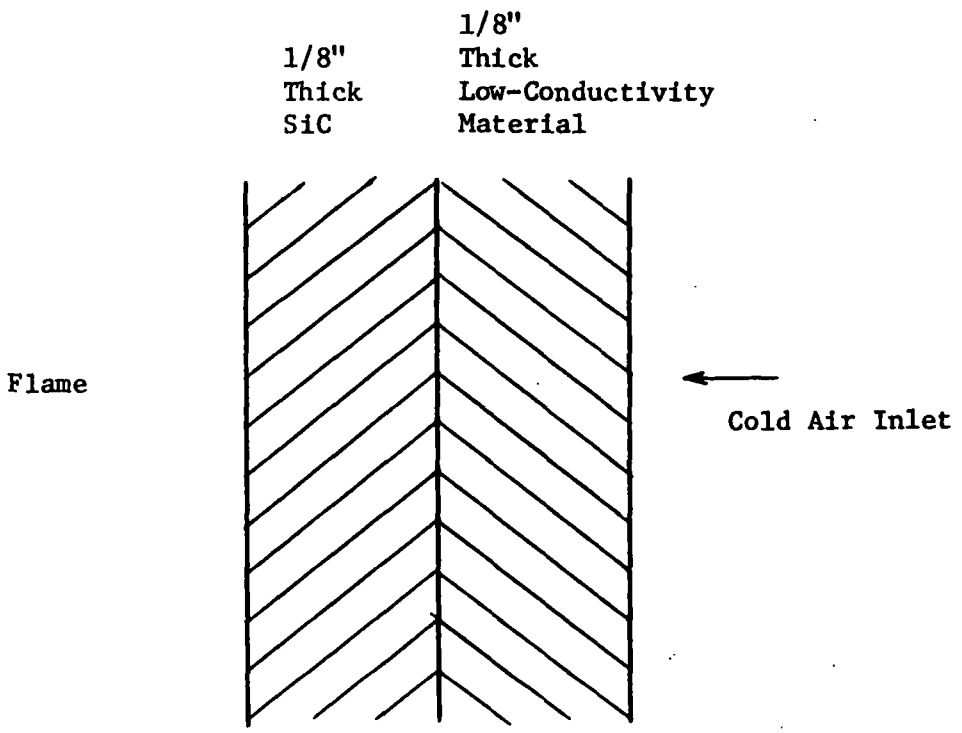

Thermal Conductivity	10	1.5	BTU/hr-ft-°F
Specific Heat	0.3	0.3	BTU/lbm-°F
Density	162.	112.	lbm/ft^3

Figure 51. Configuration of Materials in Porous Burner (for Transient Analysis)

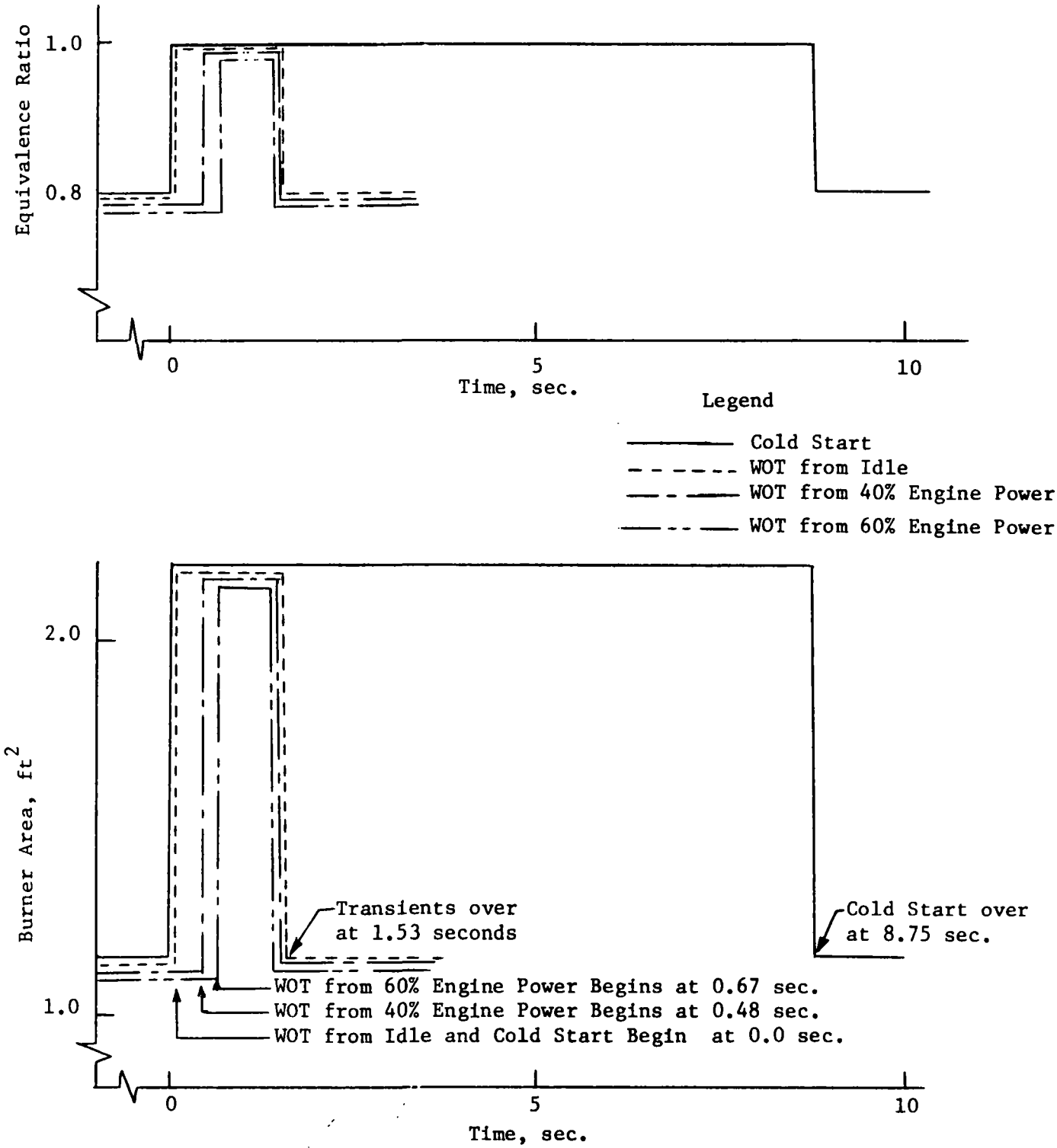

Figure 52. Schedule of Burner Area and Equivalence Ratio During the 4 Transients

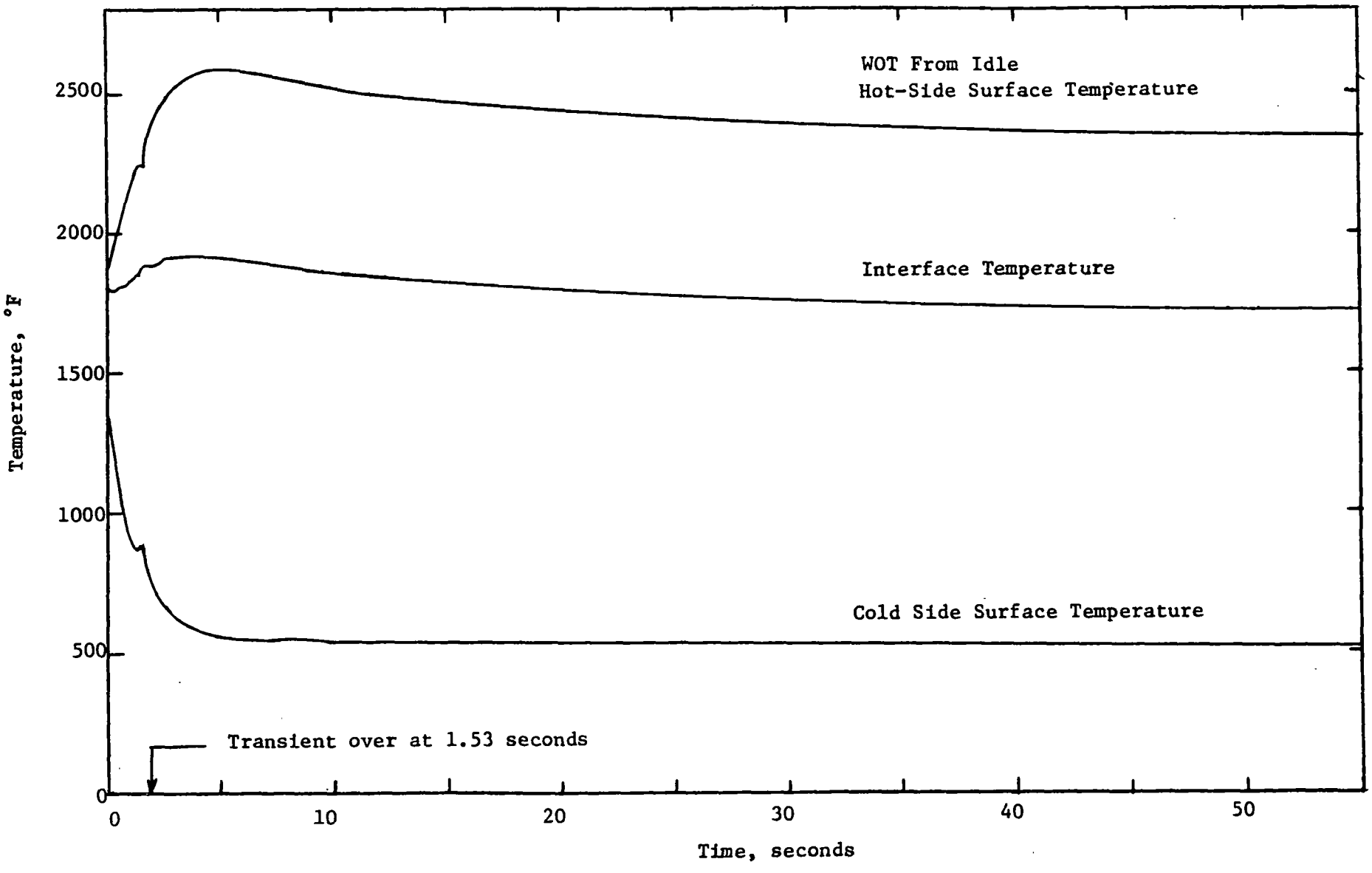

Figure 53. Calculated Thermal Response of the Porous Combustor During WOT From Idle

idle of the Base Line Engine to full gas generator speed. The fuel transient ends after 1.53 seconds. Figure 54 shows the undiluted burned gas temperature during this transient. From the theory of the porous combustor, only the superficial gas velocity, V_{25}, and the equivalence ratio, R, determine the flame temperature; hence, the burned gas temperature remains constant after the transient is over at 1.53 seconds because both V_{25} and R remain constant.

To examine the time-dependent behavior of the hot-side surface temperature during the WOT, Figure 55 is shown in which the time rate of change of temperature of the hot-side surface node as well as the hot-side surface temperature for the first 8 seconds of the WOT transient are plotted. Similarly, Figure 56 shows the time-dependent behavior of the three surface fluxes as defined earlier: Q_{Air}/A_{Burn}, Q_{Fl}/A_{Burn}, Q_{RAD}/A_{Burn}. When the burner finally reaches steady state after approximately 80 seconds for this transient, the equality holds that:

$$Q_{RAD} = Q_{Fl} \tag{10}$$

For this transient, the value of Q_{Air}/A_{Burn} is about 10 times as large as Q_{RAD}/A_{Burn} for most of the transient. The overshoot in temperature above the final steady-state value for this transient occurs because the dT/dt of the surface node is still a large positive number when the hot-side burner temperature first goes through the value that corresponds to the final steady-state value. Because of the selected schedule of burner area, the flux that heats the incoming air, Q_{Air}/A_{Burn}, undergoes a step increase at 1.53 seconds, which is a large disturbance in the flux boundary condition at the surface; the burner is unable to instantaneously conduct

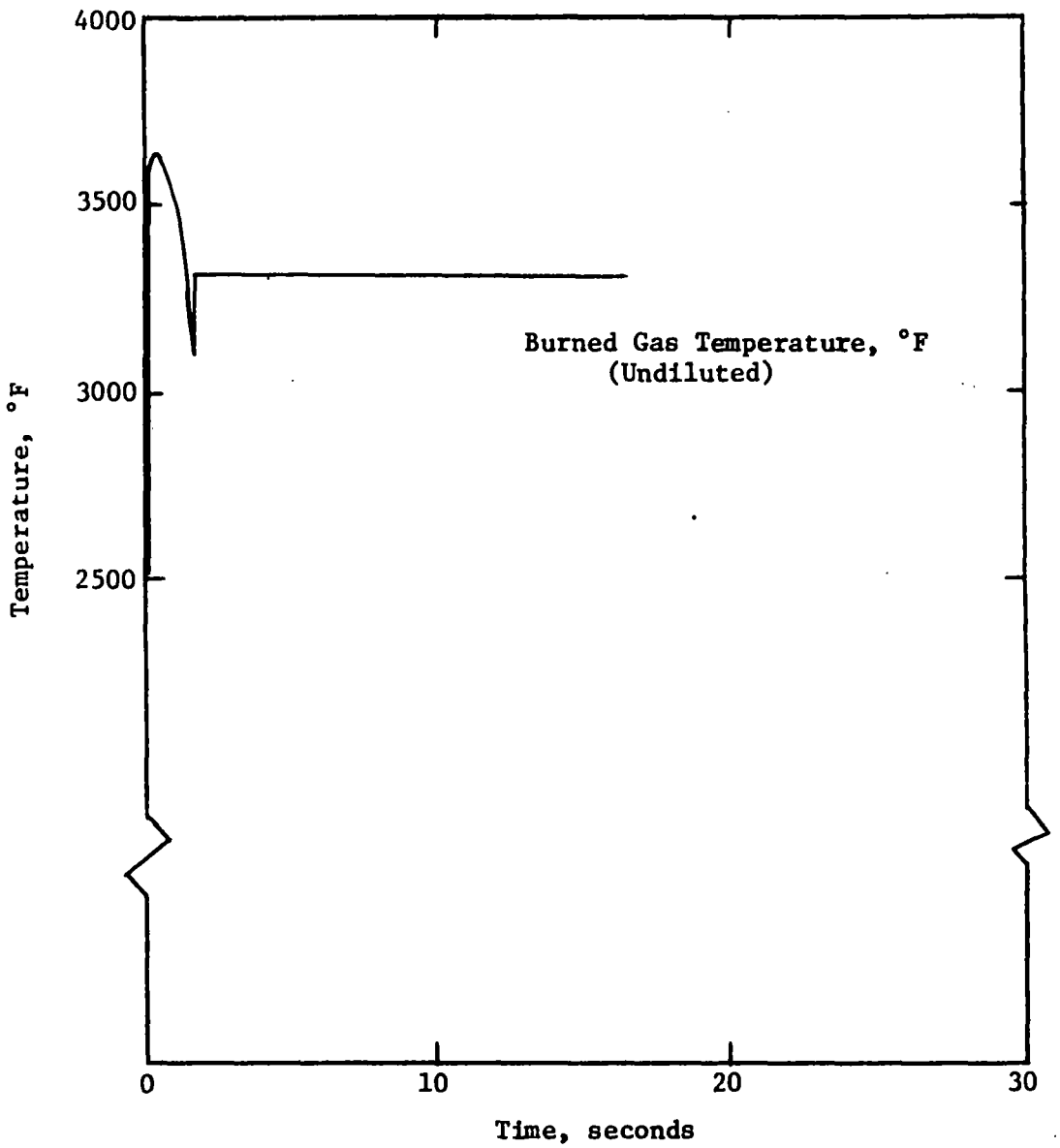

Figure 54.. Undiluted Burned Gas Temperature During the WOT Transient From Idle to 100% Gas Generator Speed of the Base Line Engine

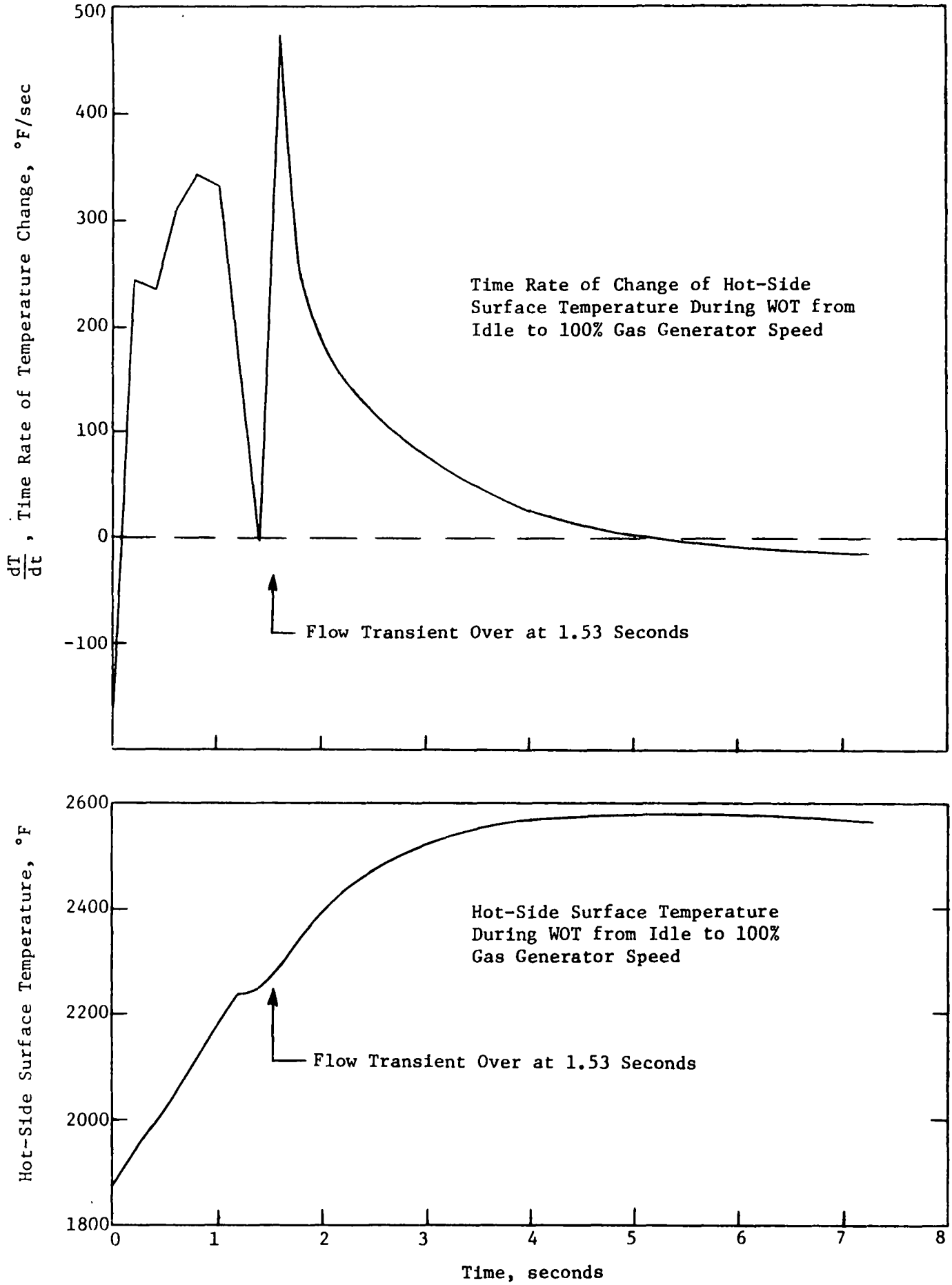

Figure 55. Conditions at the Burner Surface During WOT From Idle to 100% Gas Generator Speed

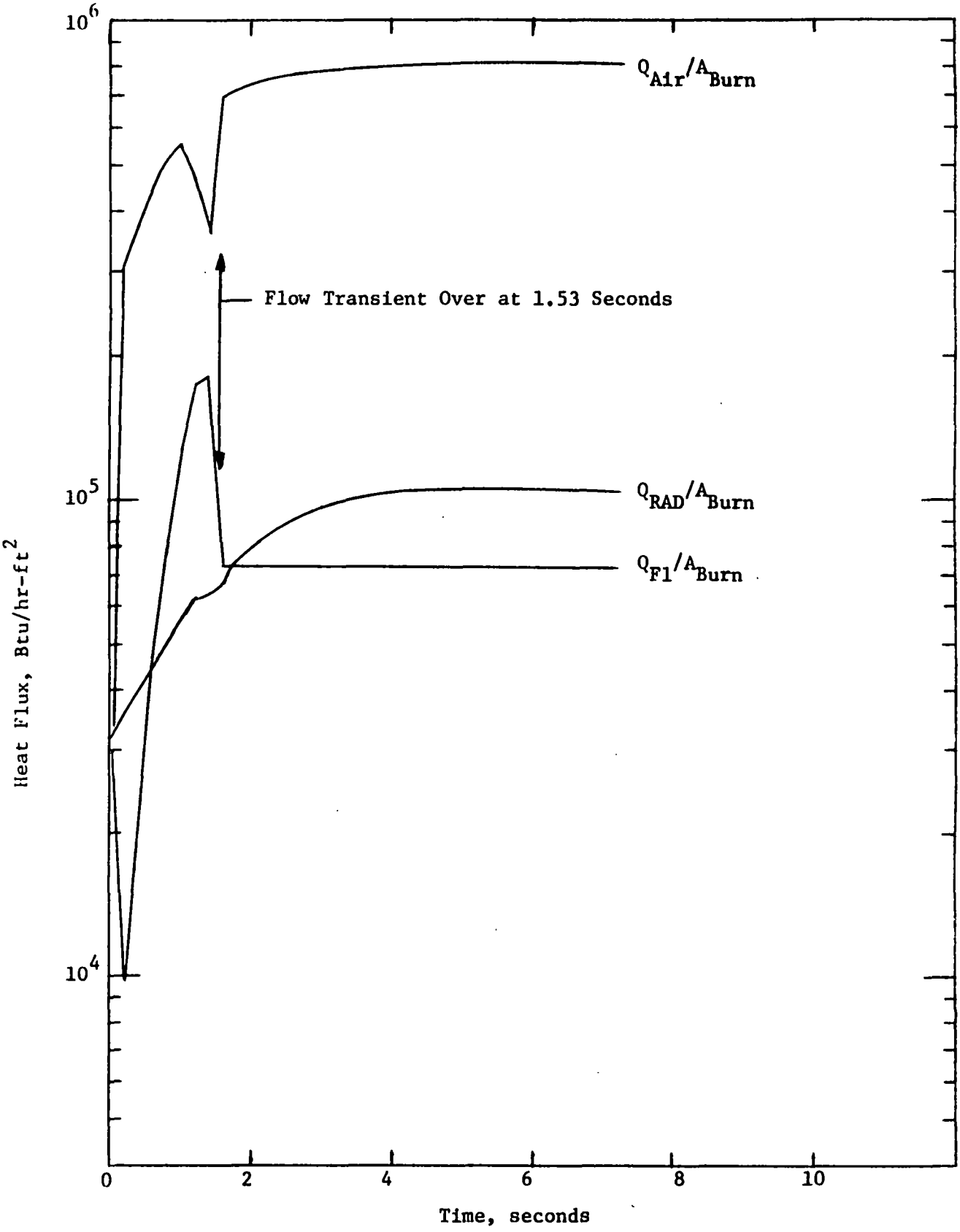

Figure 56. Heat Fluxes Back to the Burner Surface During WOT from Idle to 100% Gas Generator Speed

away this step increase in heat flux with the current gradient, so the surface node begins to heat up in order to provide the necessary temperature gradient to conduct away the heat flux.

A hypothetical transient was run to investigate the calculated thermal response further. For this case, the initial temperature profile was selected such that the temperature gradient in the solid was comparable to the final steady-state value of the WOT transient; the initial temperatures were selected at about 200°F lower than the final steady-state values. The results of this transient calculation are shown in Figure 57. There is no overshoot of the hot-side surface temperature, and the time-rate of change of the hot-side surface temperature is an order of magnitude lower than that of the real WOT shown above in Figure 55 because the initial temperature profile is steep enough to conduct away the incoming heat flux. The transient temperature is asymptotically approaching the steady-state value without overshoot because the time rate of change of the hot-side surface temperature is asymptotically approaching zero.

The transient burner temperatures and the undiluted burned gas temperature for the WOT transient from 40% engine power are shown in Figures 58 and 59. The corresponding information for the WOT transient from 60% engine power is given in Figures 60 and 61, while the corresponding information for the Cold Start transient is given in Figures 62 and 63.

Estimates of NO_2 produced by the hot-air mechanism during the 4 transients are shown in Figure 64, as a function of gas generator speed. Estimates of CO decay are shown in Figure 65. The calculations are quasi-steady-state; the NO_2 calculations are made using the NO_2 production rate

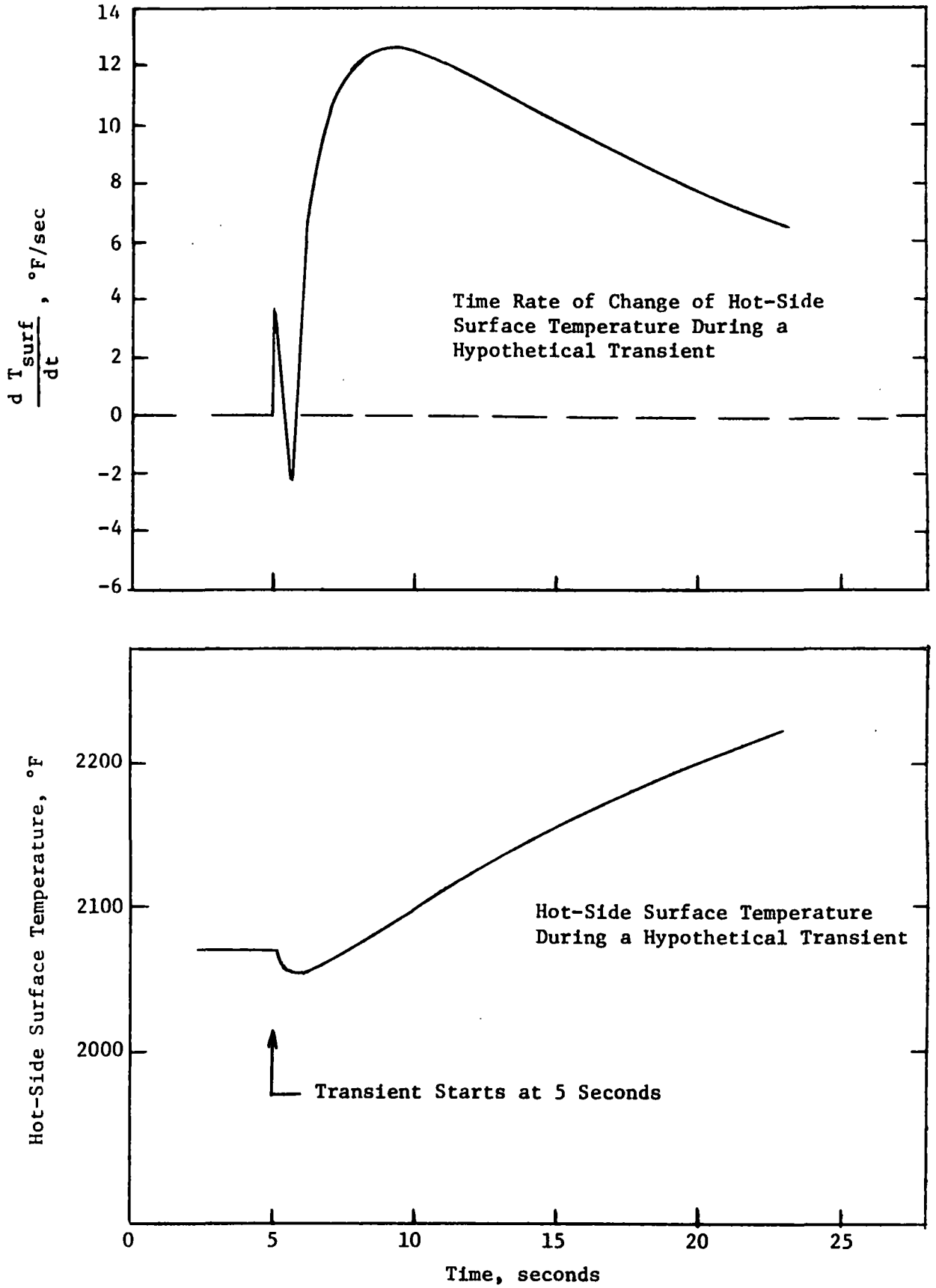

Figure 57. Thermal Response of Porous Combustor to a Hypothetical Transient

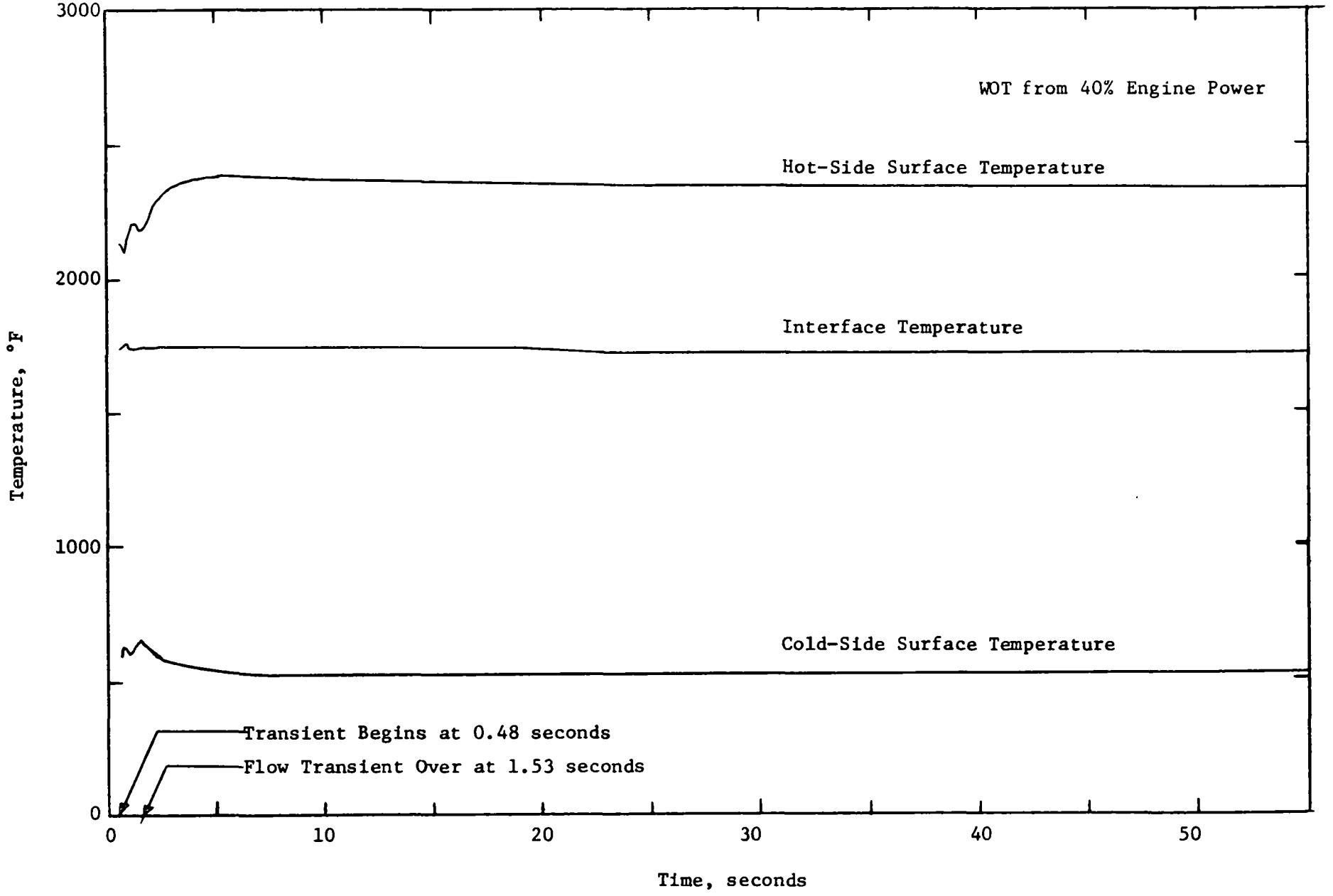

Figure 58. Calculated Thermal Response of the Porous Combustor During the WOT Transient from 40% Engine Power

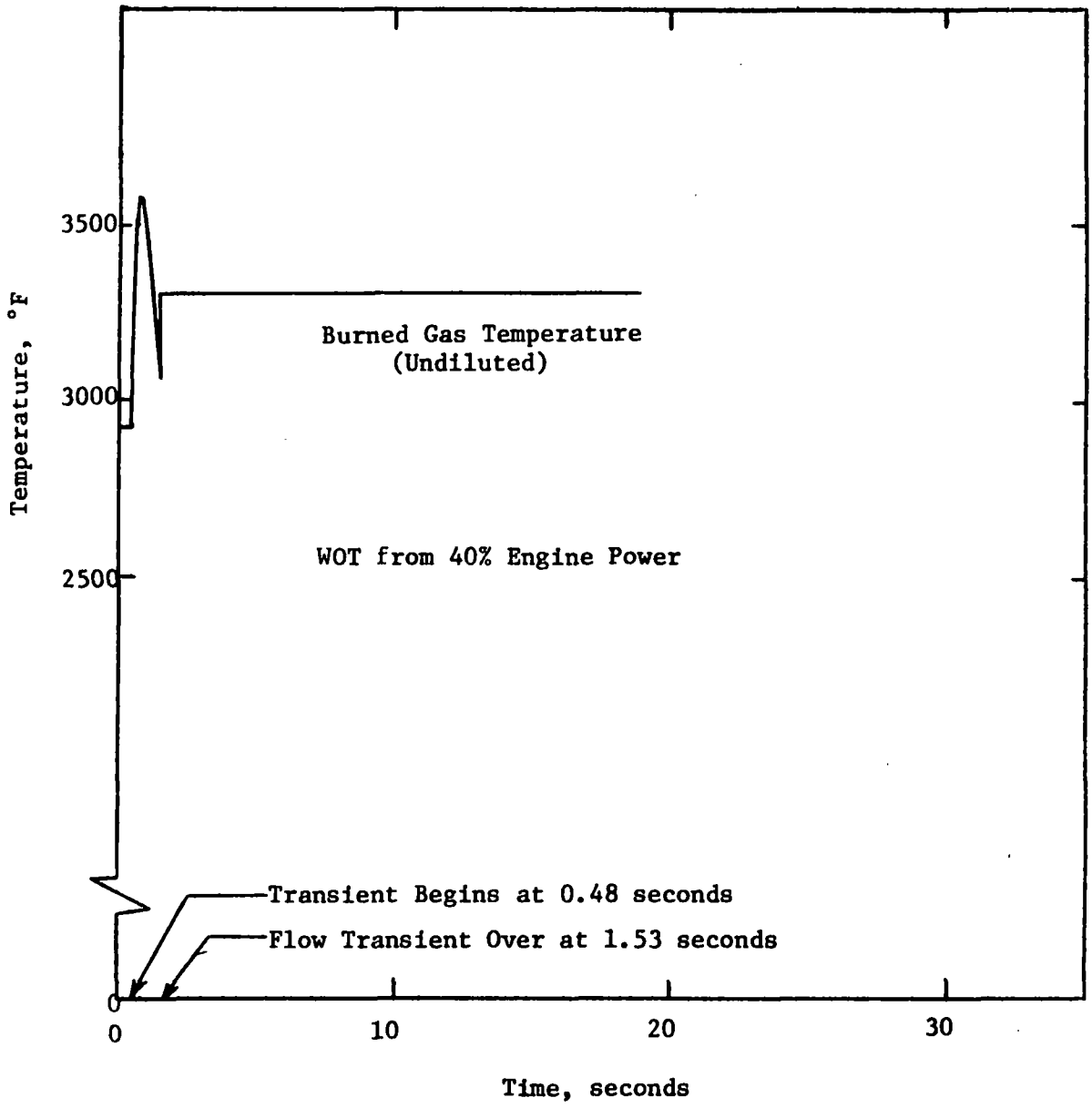

Figure 59. Burned Gas Temperature During the WOT Transient from 40% Engine Power of the Base Line Engine

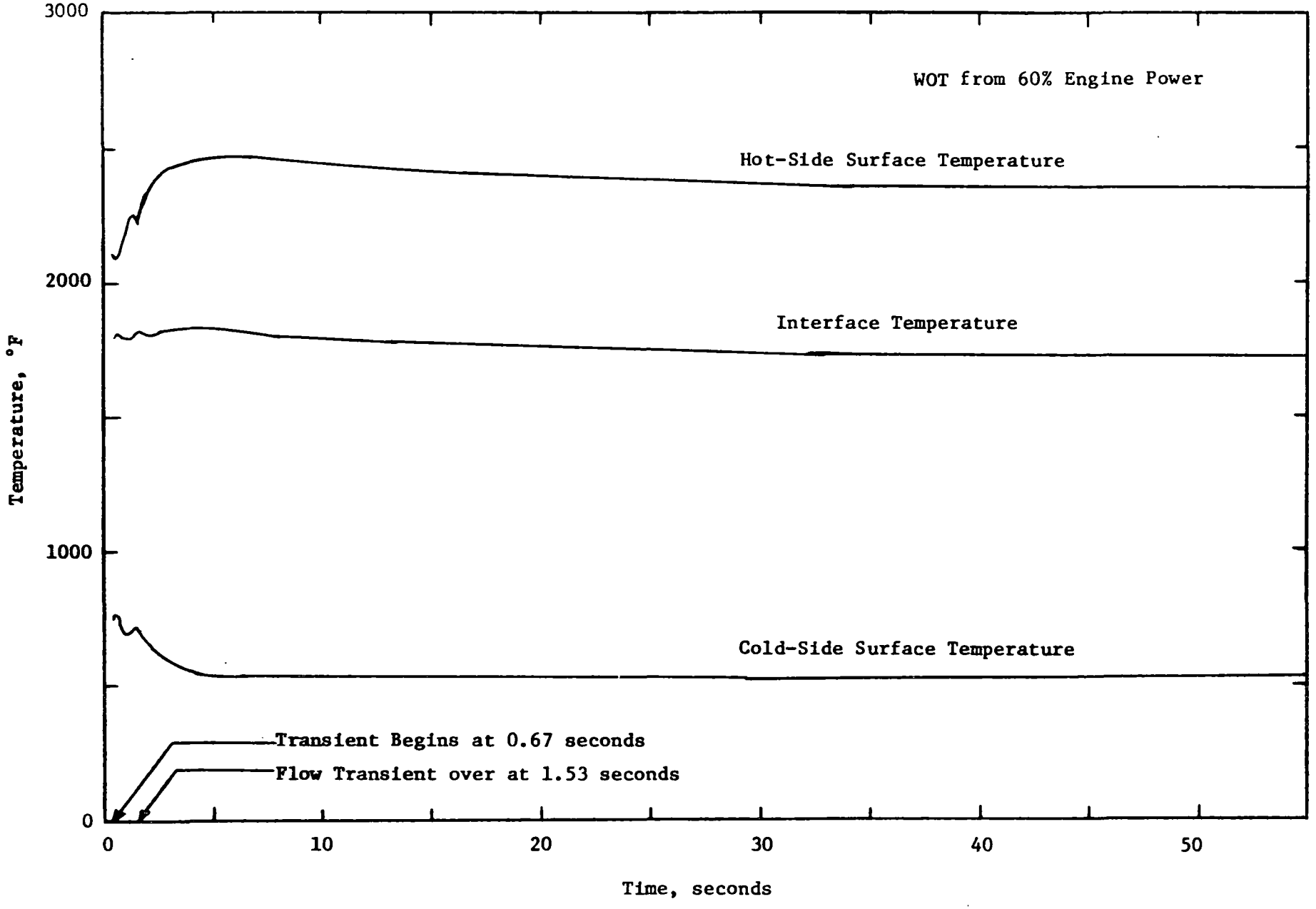

Figure 60. Calculated Thermal Response of the Combustor During the WOT Transient from 60% Engine Power of Base Line Engine

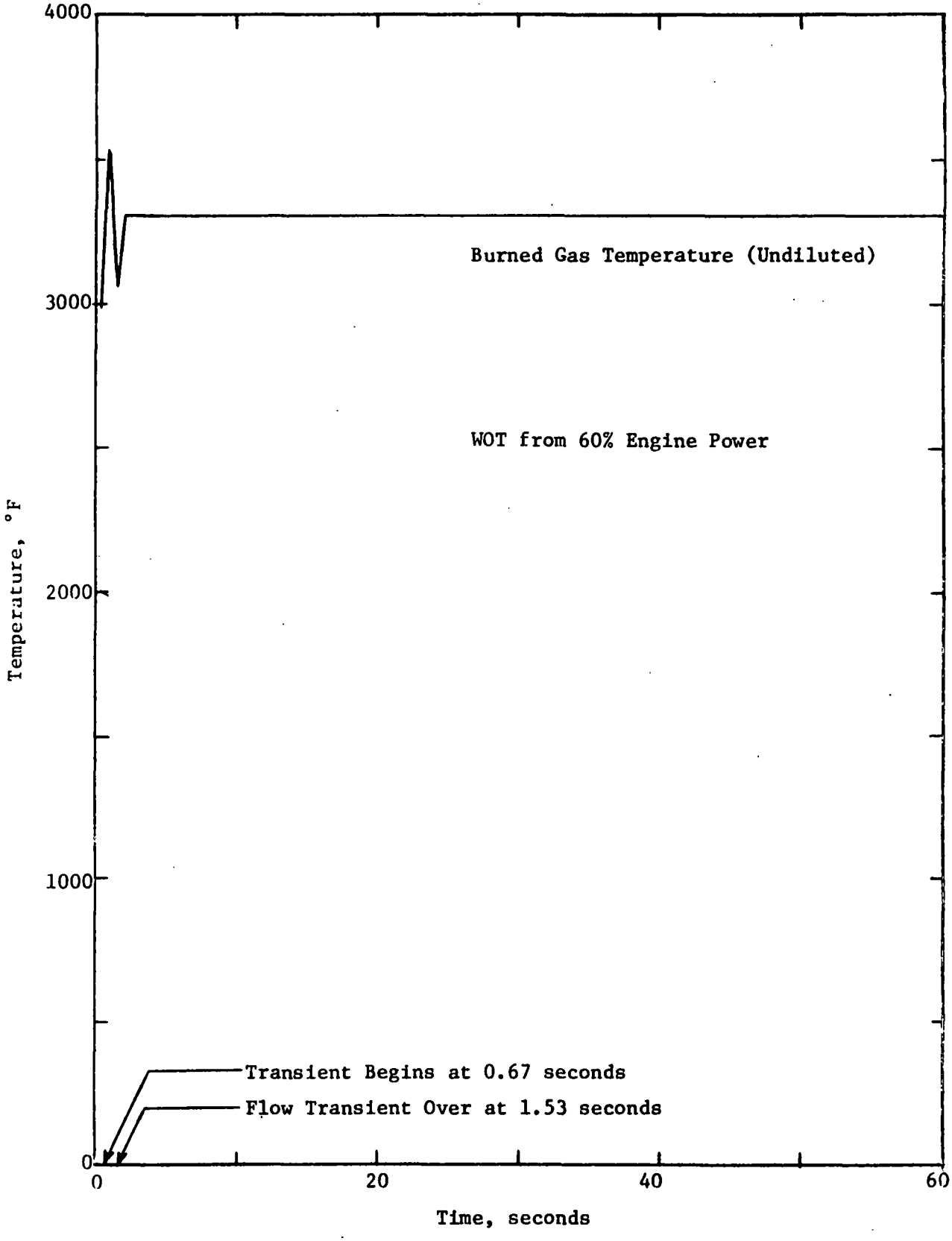

Figure 61. Burned Gas Temperature During the WOT from 60% Engine Power of the Base Line Engine

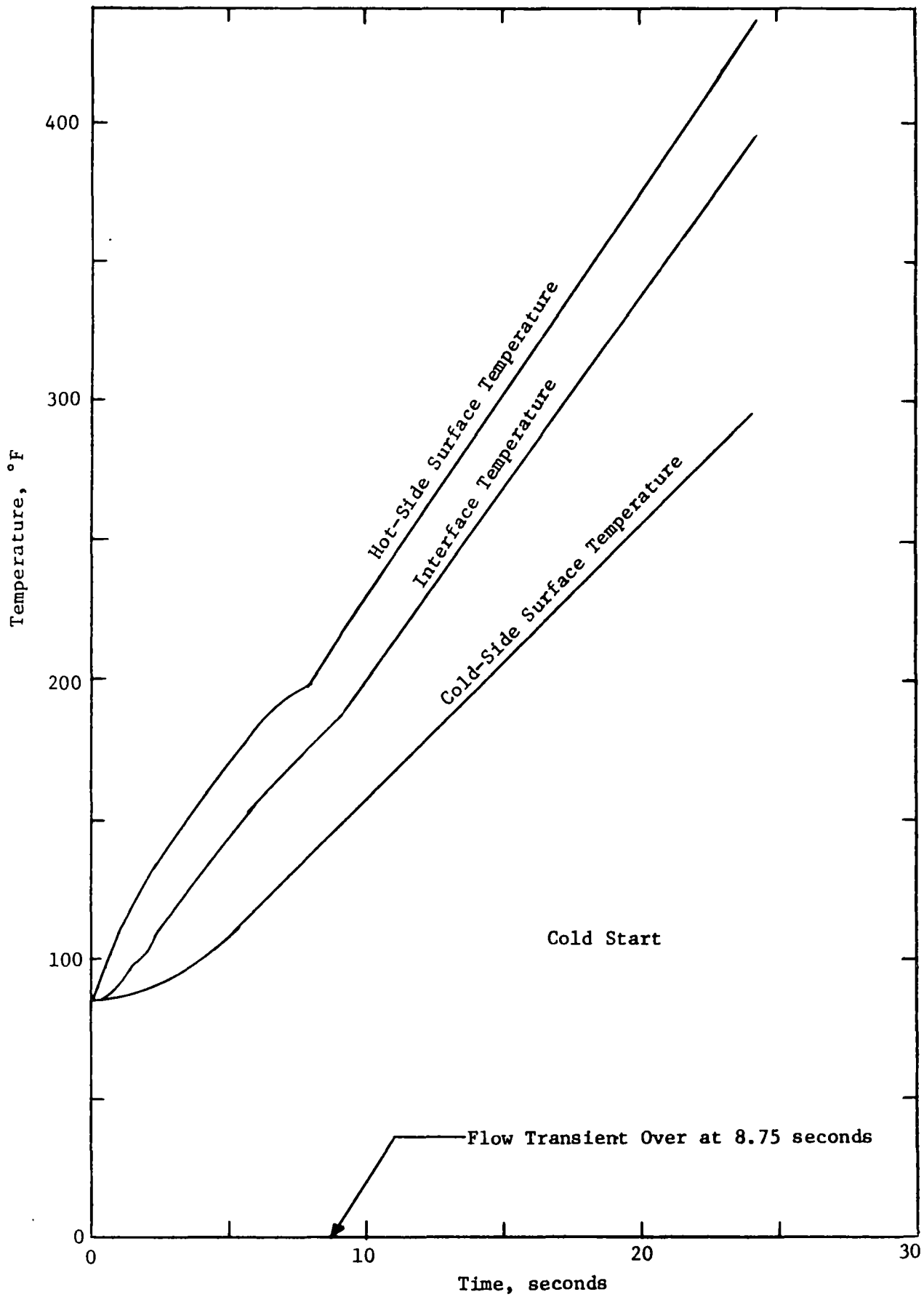

Figure 62. Combustor Response to Cold Start Transient

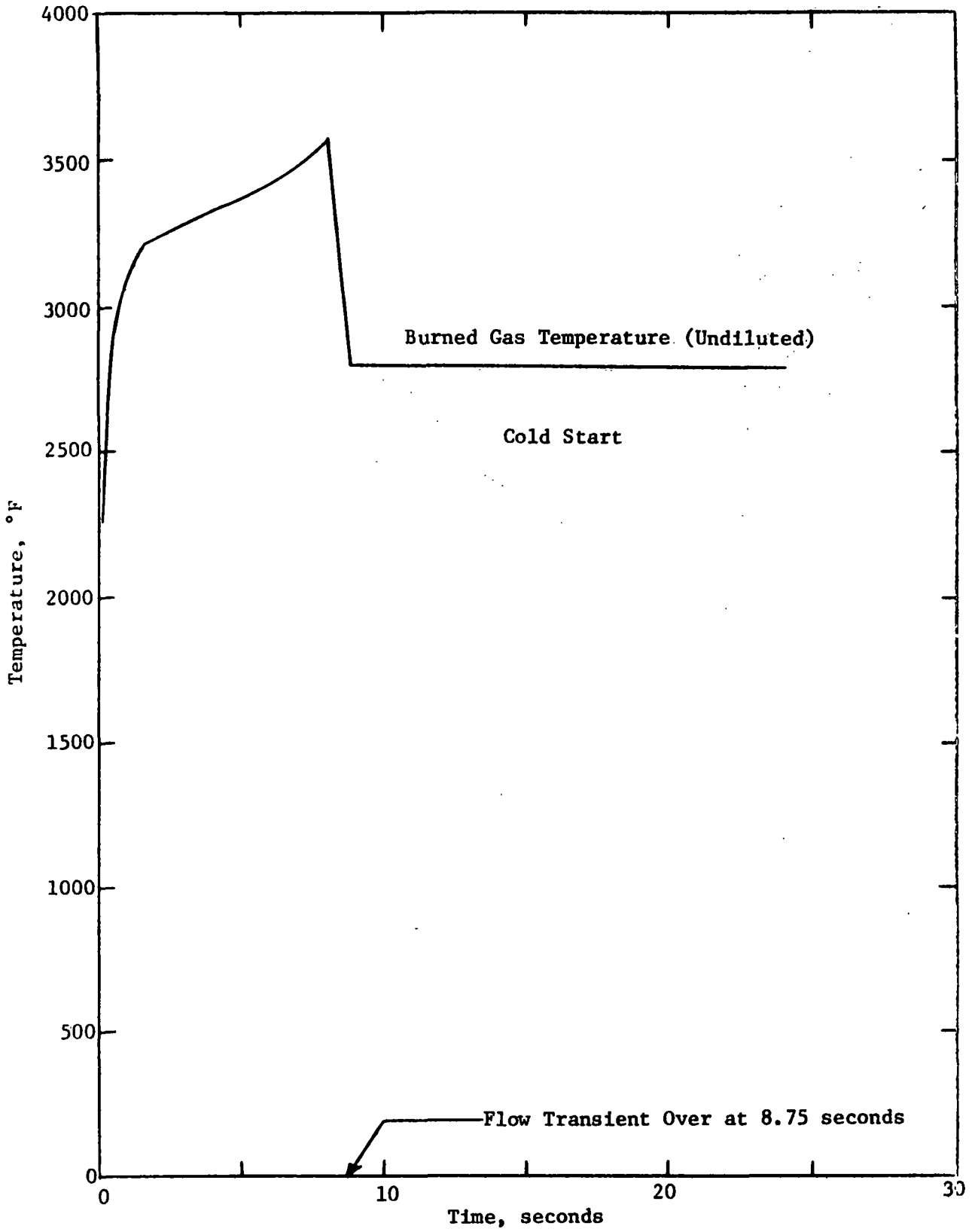

Figure 63. Burned Gas Temperature During Cold Start Transient of Baseline Engine

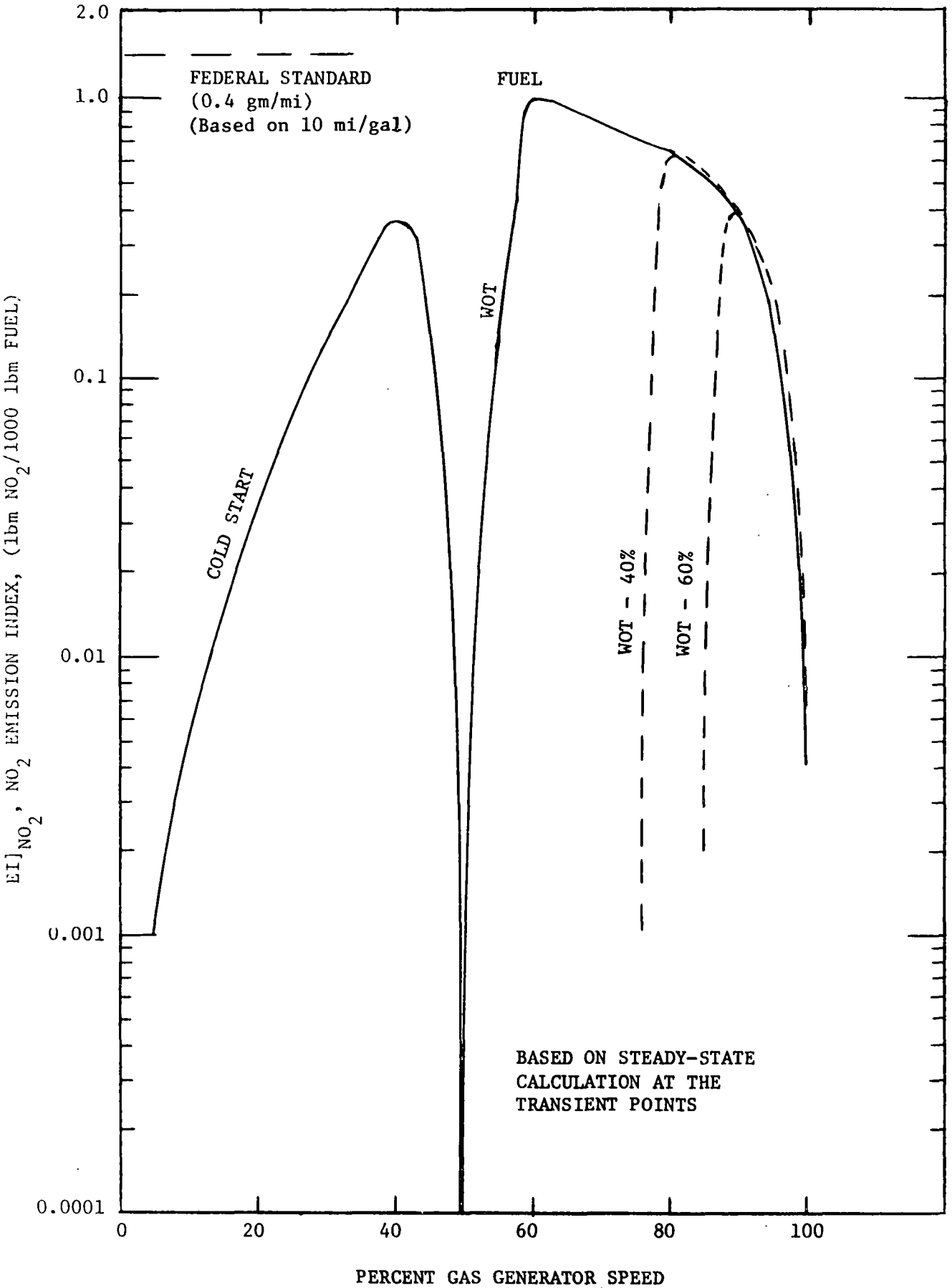

Figure 64. Predicted NO_2 Emissions Index Based on the Hot Air Mechanism

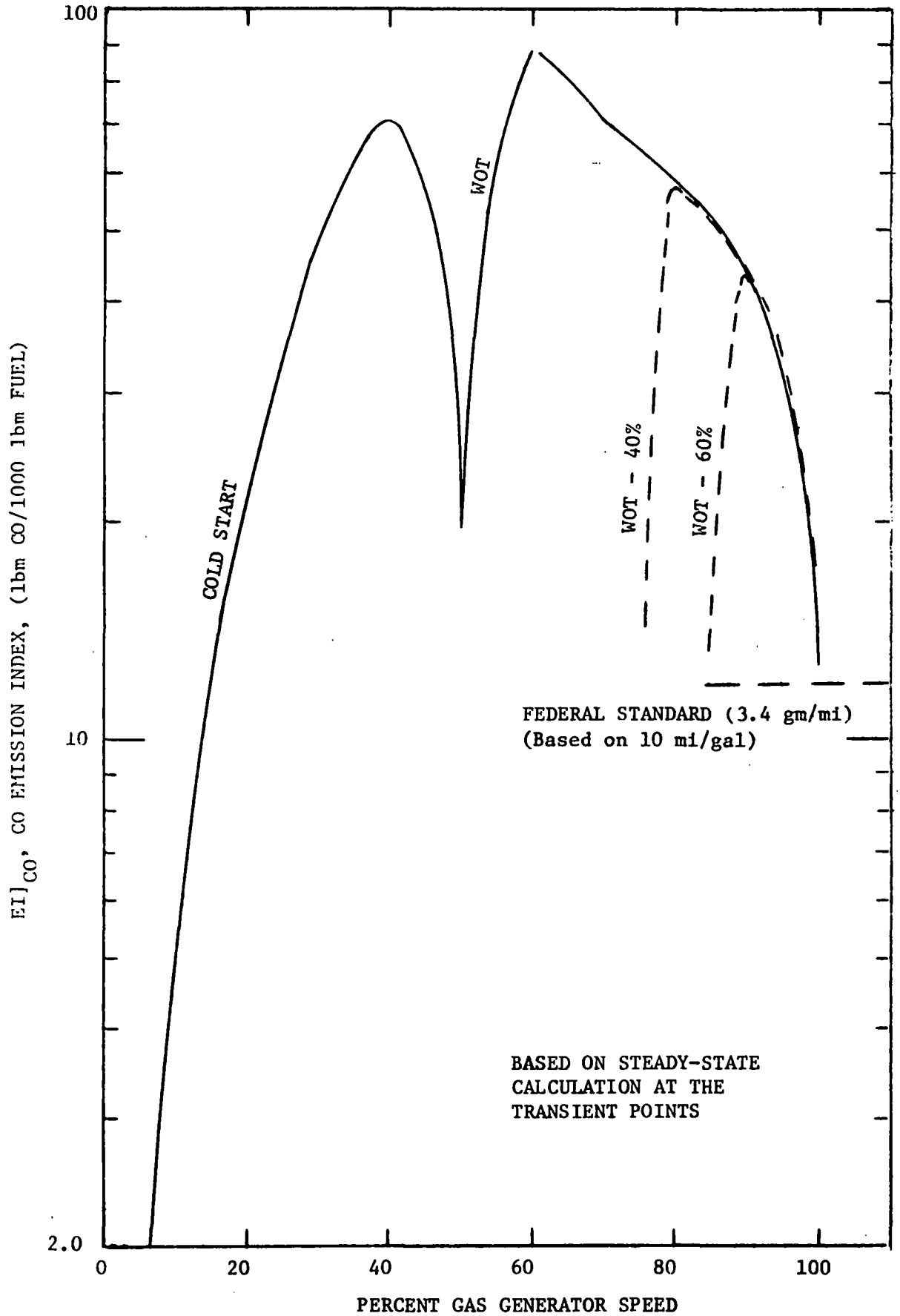

Figure 65. Predicted CO Emissions Index

with the "hot-air" mechanism shown in Figure 3 and are made with flame temperatures based on the instantaneous values of superficial gas velocity, V_{25}, and of equivalence ratio, R. The stratified plug-flow model was used to estimate residence times in the combustors. Also shown for comparison in Figures 64 and 65 are the Federal Standards.

COMBUSTOR CONCEPT FEASIBILITY DEVELOPMENT

The object of this task was to fabricate a porous plate burner model (approximately 1/5 size) which could be run over the combustor operating conditions of the Base Line Engine and to fully test this burner so as to obtain emissions and operational data.

First, initial screening work on radiation-cooled geometries was done. However, cracking and preignition occurred a number of times, and tests to examine this phenomenon were conducted. Because of the occurrence of preignition, attention was turned to air-cooled combustors. A design analysis of air-cooled combustors was done, and several were built and tested.

Initial Screening of Radiation-Cooled Combustors

Screening tests of various porous plate combustor configurations were carried out with models one-fifth the size of the combustor for the Base Line Engine application. The combustor configurations tested included porous ceramics, porous metals, and burners made up of layers of screens and insulating materials. These configurations are radiation-cooled geometries.

The combustor test rig used for these screening tests is shown in Figure 66. The primary air-fuel mixture enters the test rig through the pipe at the left. The secondary or diluent air enters through the fitting

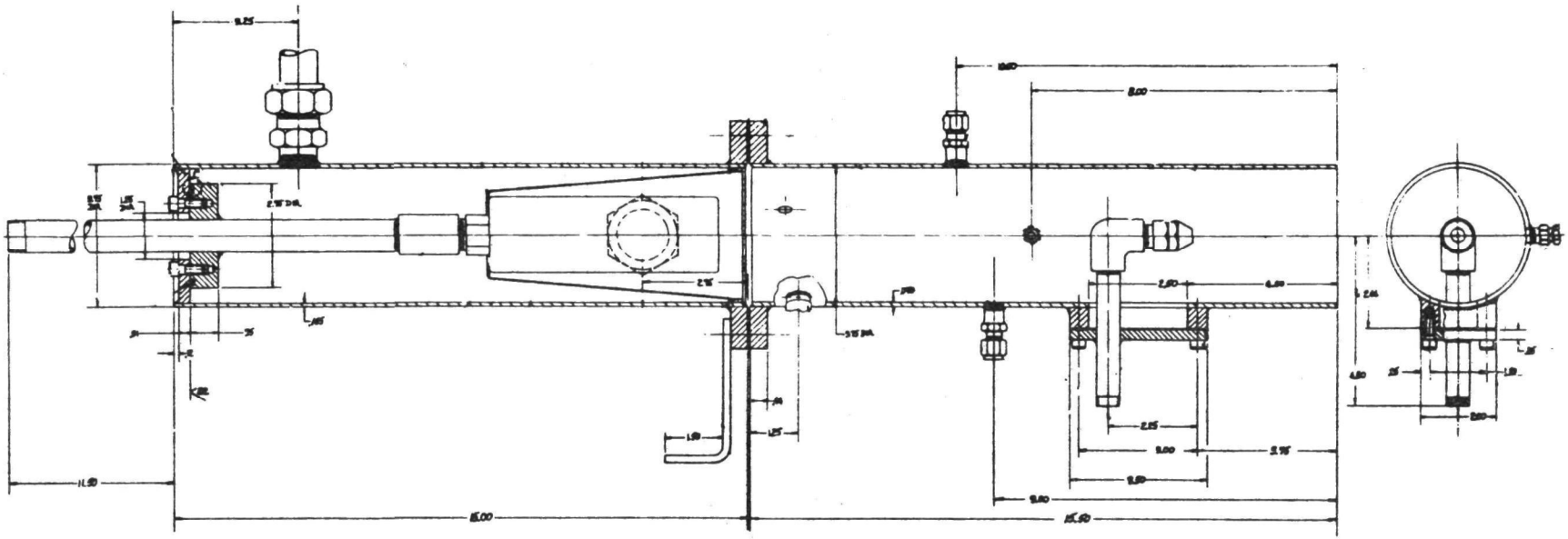

Figure 66. Gas Turbine Porous-Plate Combustor Test Section

at the top left of the drawing. The cylindrical burner (about two inches in diameter and six inches long) is surrounded by a conical screen which is a radiation sink for the burner and which is cooled by the secondary flow. The hexagonal shape is a view port which permits visual observation of the burner during testing. Another view port downstream of the flange is used to detect the presence or absence of flames or plumes from the burner. Farther downstream is the water injection nozzle which is used to cool the gas stream ahead of the valve which controls the pressure level in the system.

Ceramic Combustors - The first screening tests were done with porous silicon carbide cylinders in a typical configuration shown in Figure 67. Since it was recognized prior to the present contract that high service temperatures were required for the porous plate, SiC cylinders were procured with the largest porosity (15 to 20%) commercially available. In a combination of bench and rig testing, all 4 of the cylinders tried were fractured with each cylinder having a different test history. It was tentatively concluded that the fractures were related to non-uniform density (porosity). The silicon carbide tests are summarized in Table 3.

Metallic Combustors - A porous stainless steel burner is shown in Figure 68. During the first test with a metal burner, the surface of a bare porous stainless steel burner became too hot at high heat fluxes and was damaged. To increase the temperature capability, the burner was wrapped with a layer of Kanthal wire screen, but preignition was still a problem. Ignition inside the burner did not occur until the temperature of the Kanthal screen on the outside of the burner was in excess of 2100°F, as indicated by an optical pyrometer. The results indicate that a higher temperature differential between the burner surface and the inside surface

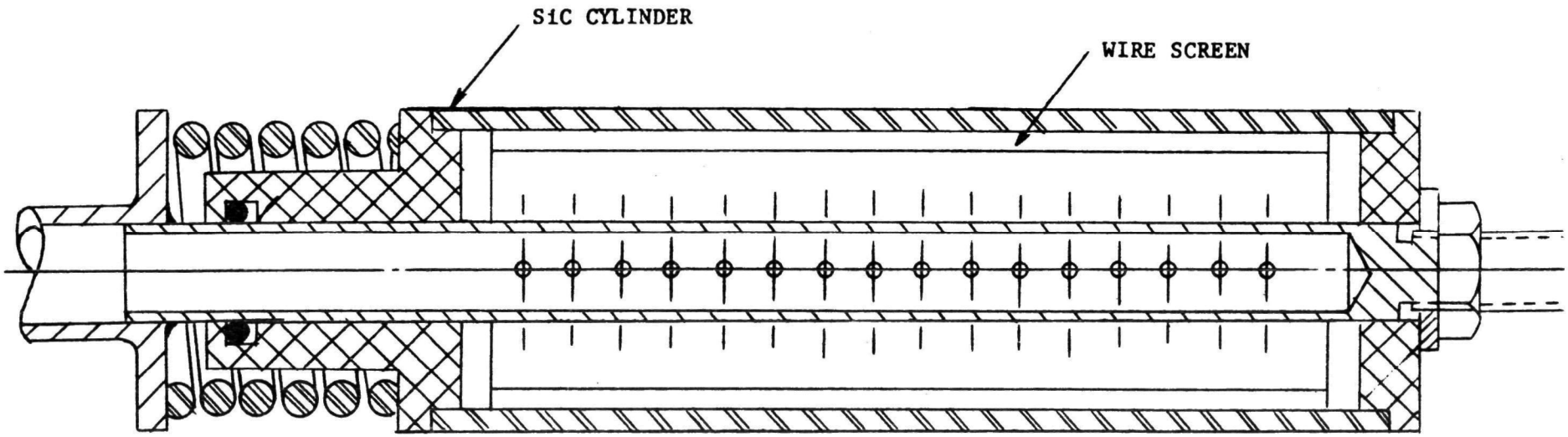

Figure 67. SiC Spring Loaded Configuration

Table 3. SILICON CARBIDE COMBUSTOR CONFIGURATIONS

Description	Results
• Lavite End Caps • High Temp. Gaskets • Spring Loaded	• Two hours of operation • Atmospheric lift-off data • Shattered next day after 30 min. operation
• Bolt Loaded • No Diluent Screen	• Burner shattered as soon as ignited
• Bolt Loaded • Flat Steel End Caps • High Temp. Gaskets	• 8 cycles in shop vise 1200-1400°F to room temp. • 6 cycles in test rig
• Attached TC's Inside Burner • Flat Inconel End Plates	• Burner shattered after 15 min. operation
• Bolt Loaded • Flat Inconel End Caps • High Temp. Gaskets	• Temperature gradients observed during vise tests • Stress relieved at 1800°C, 1 hour. • Burner shattered while being fired up

DESCRIPTION

- POROUS STAINLESS STEEL BURNER

RESULTS

- AT PEAK HEAT FLUX AND AT PRESSURE POROUS PLATE EXCEEDS ALLOWABLE TEMPERATURE (2000°F)

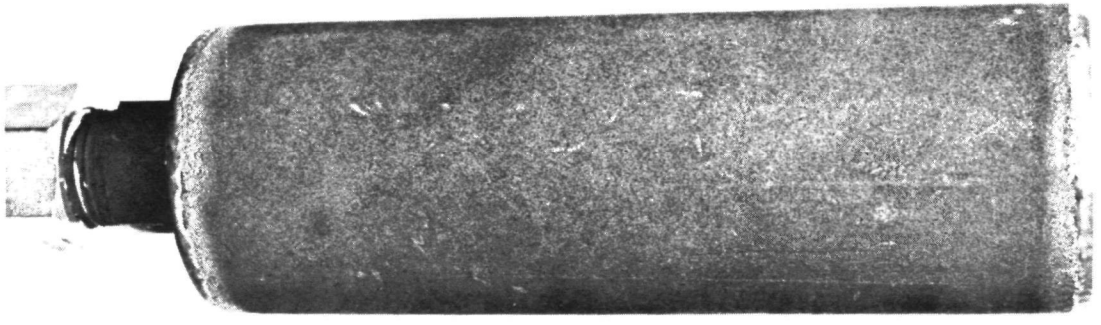

Figure 68. Metallic Combustor Configurations

is needed to avoid internal ignition.

Hence, a layer of ceramic high-temperature porous insulation was placed between the Kanthal screen and the porous steel burner in an attempt to provide this temperature differential. A sketch of this configuration is shown in Figure 69. Tests were run with exit gas velocities up to 200 ft/sec. In most cases, the reason for termination of the test was the presence of a hot spot on the outer stainless steel cover pipe. Post-test inspections revealed that the burners had melted opposite the hot spot.

Several multi-layer burner configurations were constructed of porous metal with various types of insulation and Kanthal screening. In most cases, the burner would function satisfactorily for about 10 to 15 minutes with a uniform red glow and no plume, and then the burner would fail due to hot spots, and/or holes in the insulation.

A burner shown in Figure 70 was assembled of Kanthal screen, four layers of Cerapaper and two layers of zirconia cloth insulation and Kanthal screen. The burner ran successfully for about two hours at 8 psig and V_{25} around 10-15 cm/sec. Three days later, the burner was restarted to measure NO_x, but the burner did not operate properly and a hot spot was observed. Disassembly revealed that the burner end cap on the inlet side had failed.

This burner was rebuilt and tested in the rig. At a typical FDC condition, the NO was measured at 15 ppm with low diluent flow. After further testing,the burner deteriorated, and disassembly revealed that the insulation had shrunk away from the end plates.

The metallic combustor screening tests are summarized in Table 4.

DESCRIPTION

- POROUS STAINLESS STEEL BURNER
- TWO LAYERS OF CERAPAPER INSULATION
- ONE LAYER OF KANTHAL SCREEN

RESULTS

- NO PREIGNITION AT OUTSIDE TEMPERATURE OF 2150°F (OPTICAL PYROMETER)
- FLAME NOT EXTINGUISHED AT AS HIGH AS 130 FPS AXIAL VELOCITY

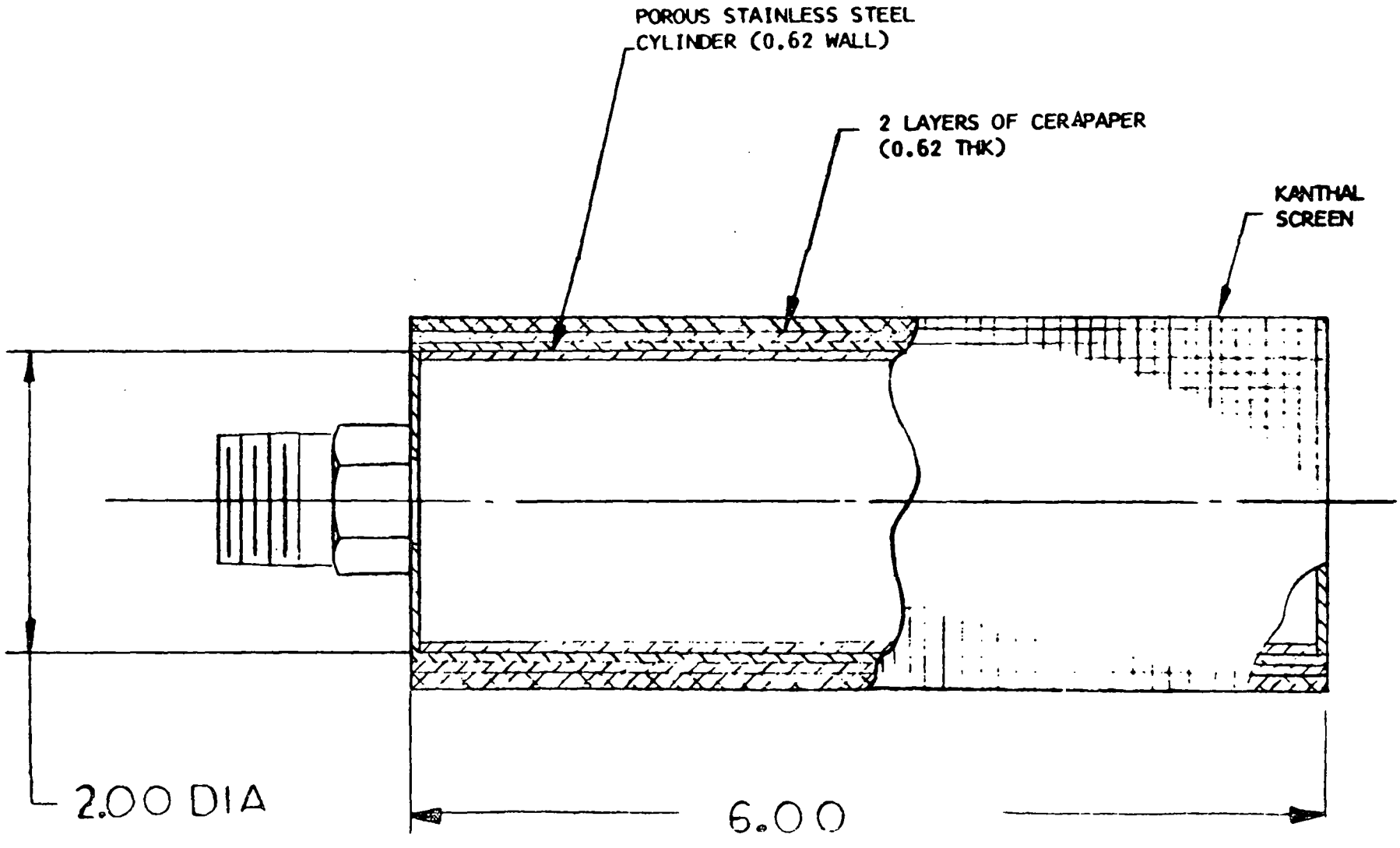

Figure 69. Kanthal-Wrapped Burner

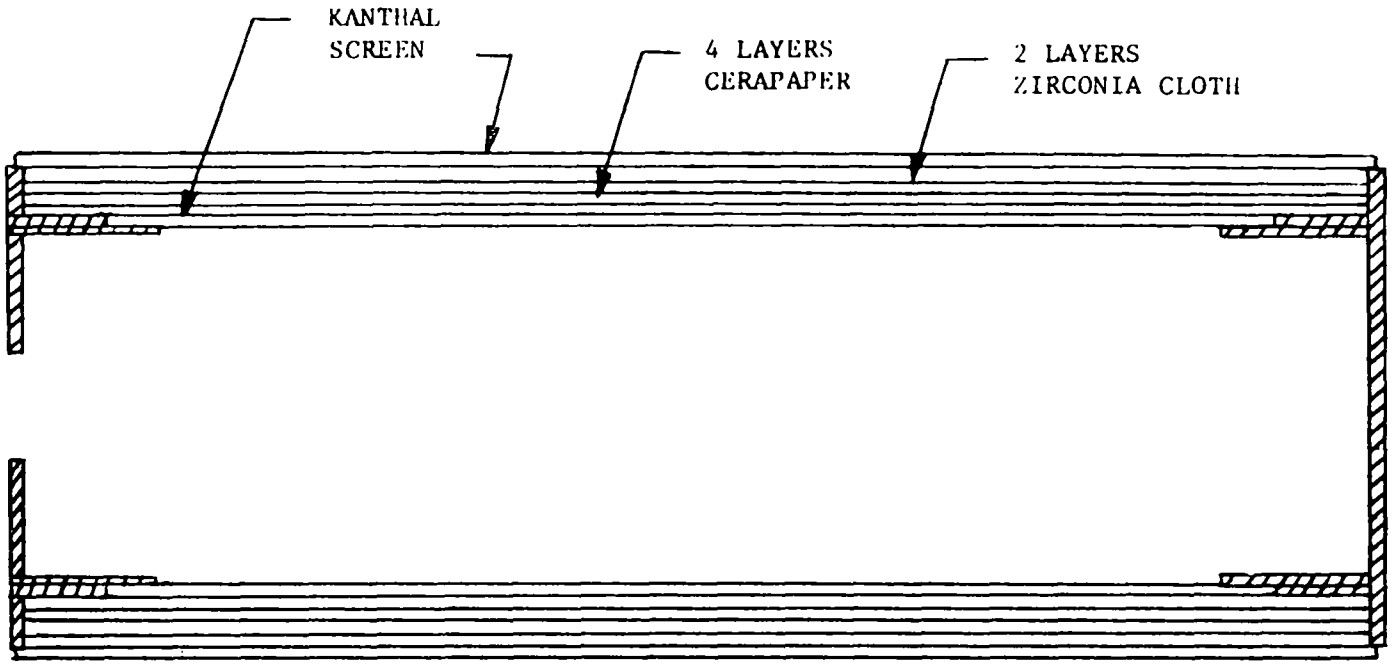

RESULTS: Ran well for about two hours at 8 psig, and superficial velocity of 15 cm/sec. Burner was restarted 3 days later to measure NO_x emissions but hot spot appeared. Burner end cap at inlet had failed.

Figure 70. Kanthal-Wrapped Burner with Zirconia Cloth and Cerapaper Insulation

Table 4. METALLIC COMBUSTOR CONFIGURATIONS

Description	Results
• Porous Stainless Steel Burner	• At peak heat flux and at pressure porous plate exceeds allowable temperature (2000°F)
• Porous Stainless Steel Burner • One Layer Kanthal Screen Around Burner	• Porous plate runs cooler • Preignition at high heat flux • Kanthal raises allowable temperature (2400°F)
• Porous Stainless Steel Burner • Two Layers of Kanthal Screen Around Burner	• Operation unchanged
• Porous Stainless Steel Burner • Two Layers of Cerofelt Insulation • One Layer of Kanthal Screen	• No preignition at outside temperature of 2150°F (Optical Pyrometer) • Flame not extinguished at 130 fps axial velocity
• Porous Stainless Steel Burner • Two Layers Cerofelt Insulation • One Quarter Inch High Fences; Spacing: 0.25 and 0.5 Inches	• Fences shield flame from axial velocity • Cerofelt fails due to required pressure drop
• Porous Stainless Steel Burner • Two Layers of Cerofelt Insulation • Two Layers Kanthal Screen 1/8 Inch Apart	• Flame not extinguished at 200 fps axial velocity • Inner Kanthal screen operating temperature raised

Table 4. METALLIC COMBUSTOR CONFIGURATIONS
(Cont'd.)

Description	Results
• Porous Inconel Burner • Two Layers Cerapaper • One Layer Kanthal Screen	• Ran well for 10-15 min., then "clink" sound, large plume • Downstream end of burner failed
• Porous Inconel Burner • Two Layers Cerapaper • One Layer Kanthal Screen • Better End Cap Design	• Ran well for 30 min. • Burner operation changed, plume appeared • Inconel was intact, Kanthal and stainless steel diluent screen had few holes
• Porous Inconel Burner • Two Layers Irish Refrasil • One Layer Kanthal Screen	• Developed hot spot after 10-15 min. • Insulation had split and there were large holes in Inconel and Kanthal screen, small hole in diluent screen
• Kanthal Screen • Three Layers Cerapaper • Kanthal Screen	• Ran well for 10-15 min., then chugging sound and plume • Outside of burner like new • Inside Kanthal screen melted • Five or six small holes in insulation
• Same as above	• Ran well for 15 min. • Developed hot spot • Inner Kanthal screen melted • Multiple holes in insulation • Several holes in diluent screen
• Kanthal Screen • Four Layers Cerapaper • Two Layers Zirconia Cloth • Kanthal Screen	• Ran well for 2 hours • Burner was restarted after weekend but hot spot appeared • Burner end cap at inlet had failed
• Same as above	• Ran well for about 30 min. Measured NO = 15 ppm at typical FDC condition with low diluent flow. Then observed high NO and plume. • Insulation had moved away from end cap

Emission Measurements on Burner 102 - Burner S/N 102, which consisted of a porous inconel matrix with ZrO_2 cloth insulation on the inside diameter, was tested on the bench and in the test rig. Tests on the bench were run at equivalence ratios of 0.7 and 0.8 over the full range of unburned gas velocities. A few test points were obtained at an equivalence ratio of 0.9. The burner was then installed in the test rig. Emission measurements (CO and NO_x) were made at atmospheric pressure for an equivalence ratio of 0.7 over the full range of unburned gas velocities. The Emission Index (EI) as calculated from the ppm measurements is shown in Figure 71. The data is not corrected for water content. Also shown are estimates of NO_2 production from the "hot-air" mechanism and CO decay which use a residence time calculated from a stratified plug-flow model.

Composite Ceramic Burner - A ceramic burner of SiC rings over a mullite cylinder shown in Figure 72 was run on the bench for about thirty minutes over a range of V_{25}. Then the burner became cooler on the downstream end and the cooler area gradually increased as the pressure drop through the burner decreased from 15 to 7 psi. Disassembly revealed that the SiC rings were intact but the mullite cylinder had multiple cracks.

Preignition Tests

During the initial screening tests of the cylindrical radiation-cooled burners described previously, a number of occurrences of preignition were observed. In these instances, the fuel-air mixture was ignited upstream of the burner by the hot inner surface of the burner. In order to determine the operating conditions which lead to preignition in this type of burner, a special test fixture was designed and built. Figure 73 is a sketch of the fixture and Figure 74 shows the completed

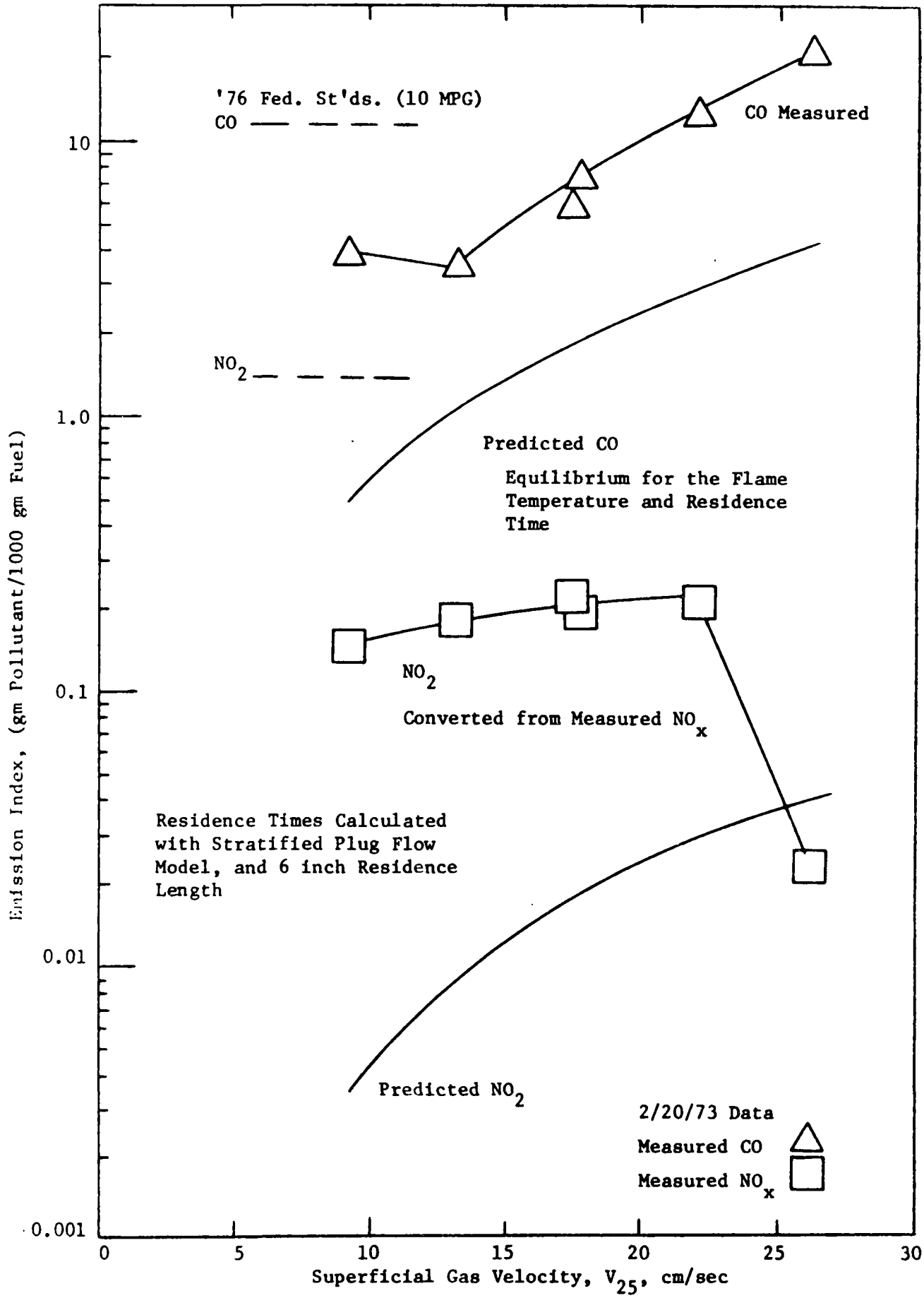

Figure 71. Emission Measurements from Burner S/N 102

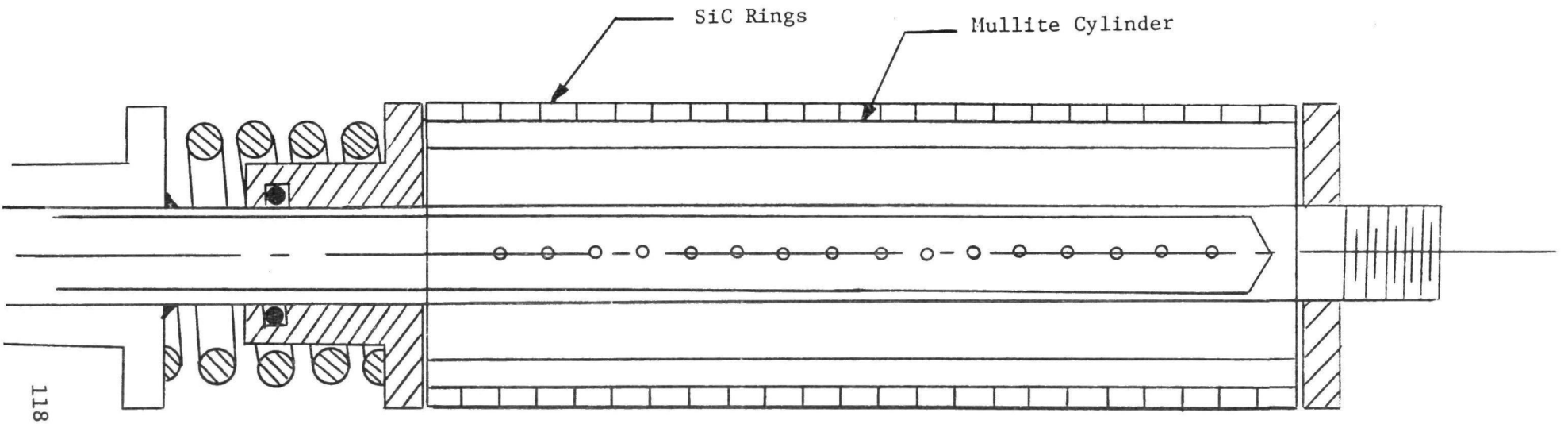

Figure 72. Configuration With SiC Rings Over Mullite Cylinder

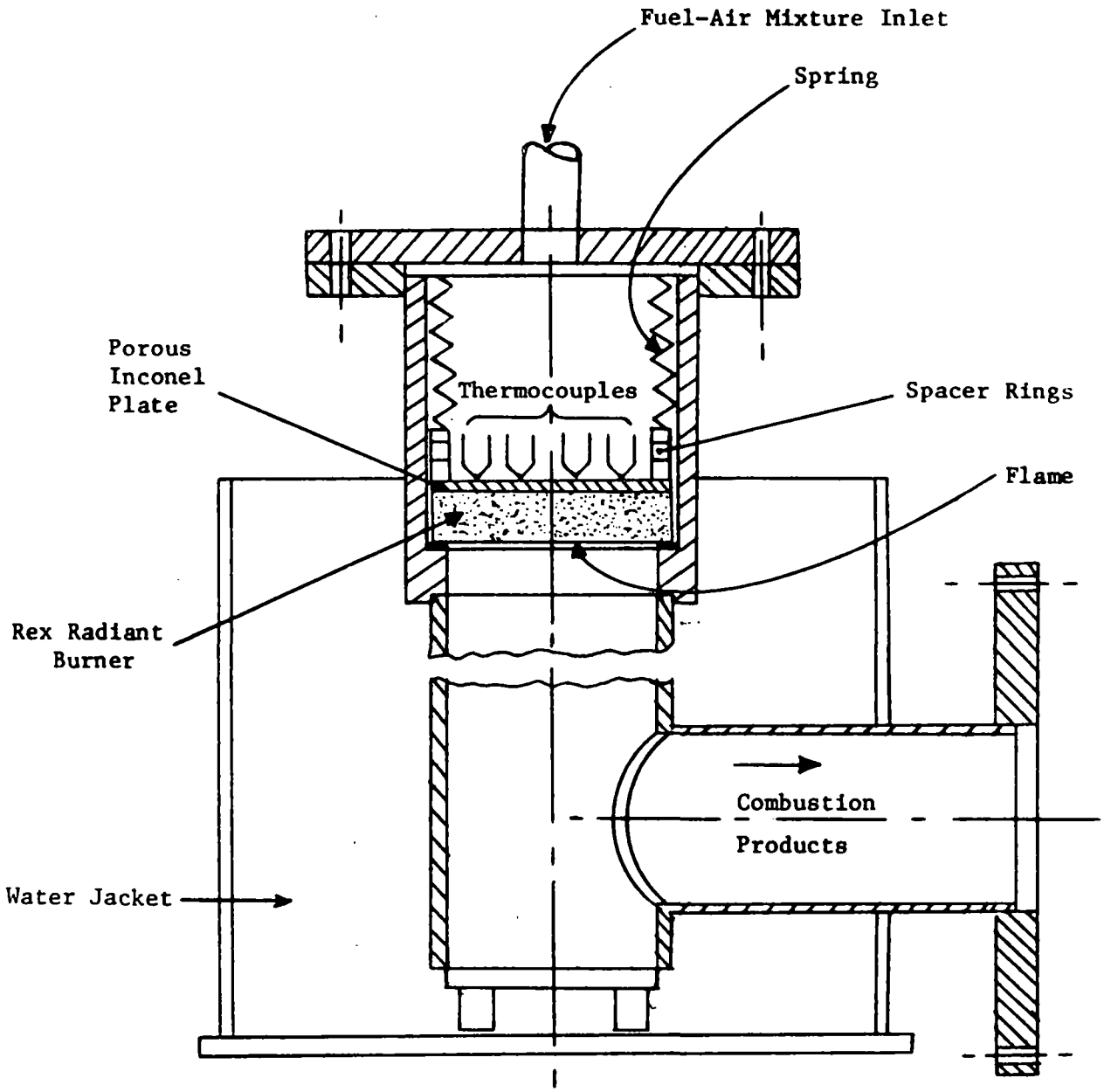

Figure 73. Schematic of Preignition Test Setup

Figure 74. Preignition Test Rig Hardware

parts. The test burner was a commercial product of Rex Radiant Company and consisted of a flat, circular 3-inch-diameter disc with an overall thickness of 0.6 inches. The disc was a composite in which the layer at the burning surface was composed of 0.1 inch thickness of porous SiC, backed by mullite which performed the function of a thermal insulation in order to keep the upstream surface cool while the burning surface was running at high temperature. A porous Inconel plate was installed at the upstream face of the ceramic burner and four thermocouples were attached to the plate in order to measure the upstream surface temperature. These thermocouples were used as a measure of impending preignition. The fuel-air mixture was fed into the plenum upstream of the burner as shown. After passing through the porous burner, the mixture was burned near the downstream surface and the combustion products flowed out through a water-cooled passage to the exhaust. A water cooled valve in the exhaust was used to control the burner operating pressure. Table 5 summarizes the tests performed in the preignition rig.

Tests were completed on the bench at one atmosphere pressure and an equivalence ratio of 0.9 over a range of unburned (superficial) gas velocities (V_{25}) from 15 cm/sec to 40 cm/sec. In these tests, the upstream surface temperature remained essentially at the temperature of the incoming fuel/air mixture and no preignition occurred. The test section was then installed in the pressurized rig and the same tests were conducted at one and at two atmospheres pressure. No preignition was observed.

The system pressure was next increased to three atmospheres with R = 0.9 and $V_{25} \approx 10$ cm/sec. The measured upstream surface temperature of the

Table 5. PREIGNITION TESTS

Test	Section	R	Inlet Temp. °F	Press, Atmos	V_{25}, cm/sec	Result
FB-1	Rex Radiant burner	0.9	55	1	15 - 40	No preignition
		0.9	55	2	15 - 40	No preignition
		0.9	46	3	40-32	Preignition
FB-2	Rex Radiant burner backed with two layers of ZrO_2 cloth	0.9	60	3	40 - 32	Preignition
FB-3	Rex Radiant burner backed with two layers of ZrO_2 cloth plus two layers fiber-chrome	0.9	45	3	40 - 32	Preignition
FB-4	Rex Radiant burner	0.7	65	1	15 - 40	No preignition
			65	2	15 - 40	No preignition
			65	3	15 - 40	No preignition
			65	4	40 - >15	Preignition

burner began to rise rapidly and when the temperature reached about 1400°F, preignition occurred and the fuel was immediately shut off. Another attempt was made to establish this point with the same result. It was then decided to set three atmospheres pressure and 40 cm/sec. At this high velocity, the flame was near liftoff and little heat was transferred from the flame to the burner. The objective was to reduce the unburned gas velocity (and increase the heat flux to the burner) in steps until the preignition condition was established. This plan was successful and a preignition point was established. Figure 75 is a plot showing the temperature recorder behavior as the preignition condition was established. In order to determine the effect of insulation on the preignition condition, two layers of ZrO_2 cloth were installed between the upstream face of the burner and the inconel plate. This had no effect on the preignition results. An additional two layers of 1/8 in. thick Fiberchrome insulation were installed with no effect on the preignition results. Examination of the ceramic burner used in the above tests revealed that it had hairline cracks extending from the outer edge along generally radial lines.

Based on the above results it was concluded that operation at four atmospheres pressure would be possible only if the equivalence ratio were reduced. A new SiC/Mullite burner was installed and tests were conducted at R = 0.7. No preignition occurred at a pressure of three atmospheres over the full velocity range. At a pressure of four atmospheres, the upstream face temperature increased to about 950°F and stabilized for $V_{25} \sim 15$ cm/sec. Figure 76 is a recorder chart trace showing this condition. At this condition, very slight changes in fuel-

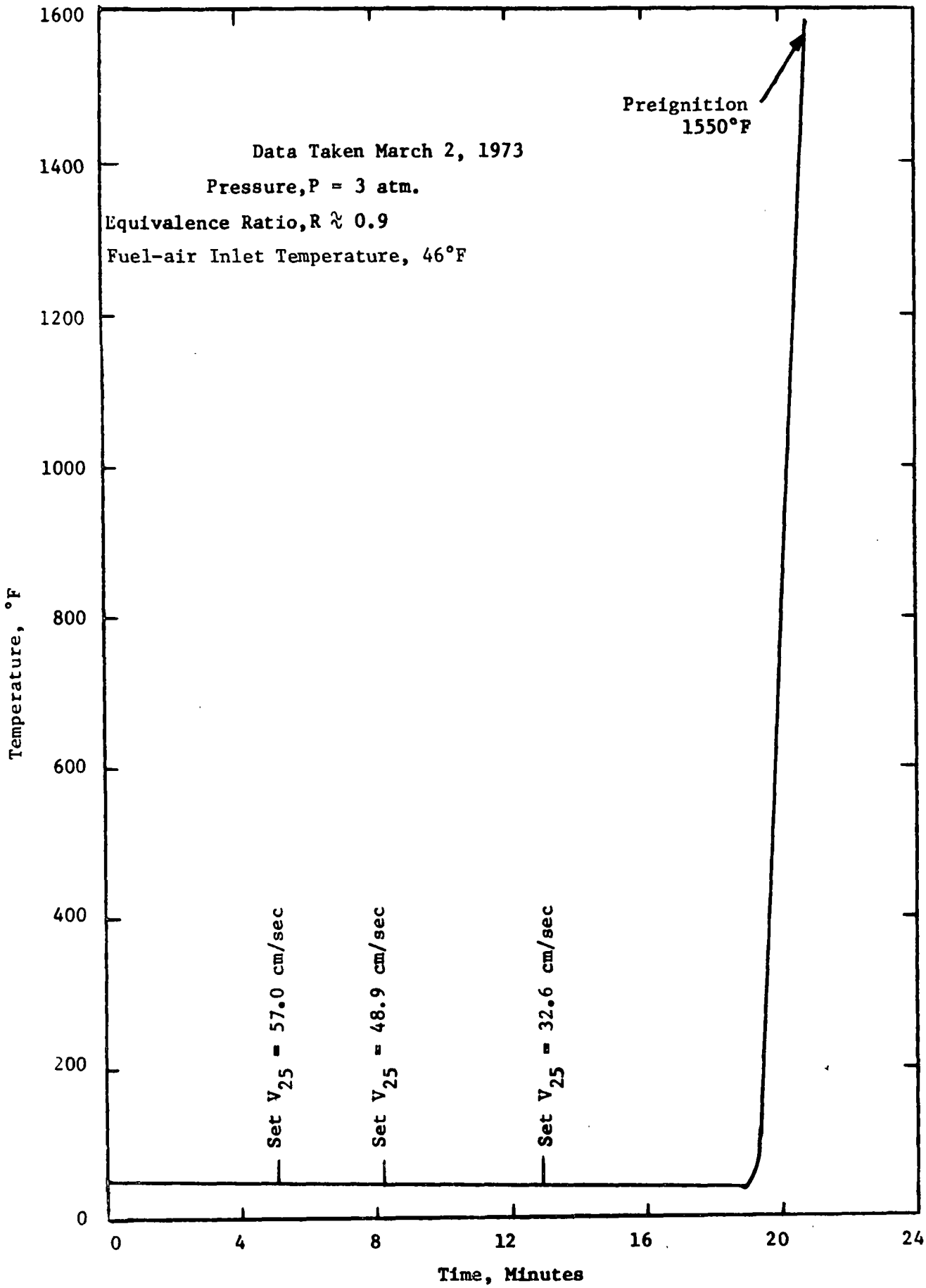

Figure 75. Upstream Face Temperature Leading to Preignition at 3 Atmospheres

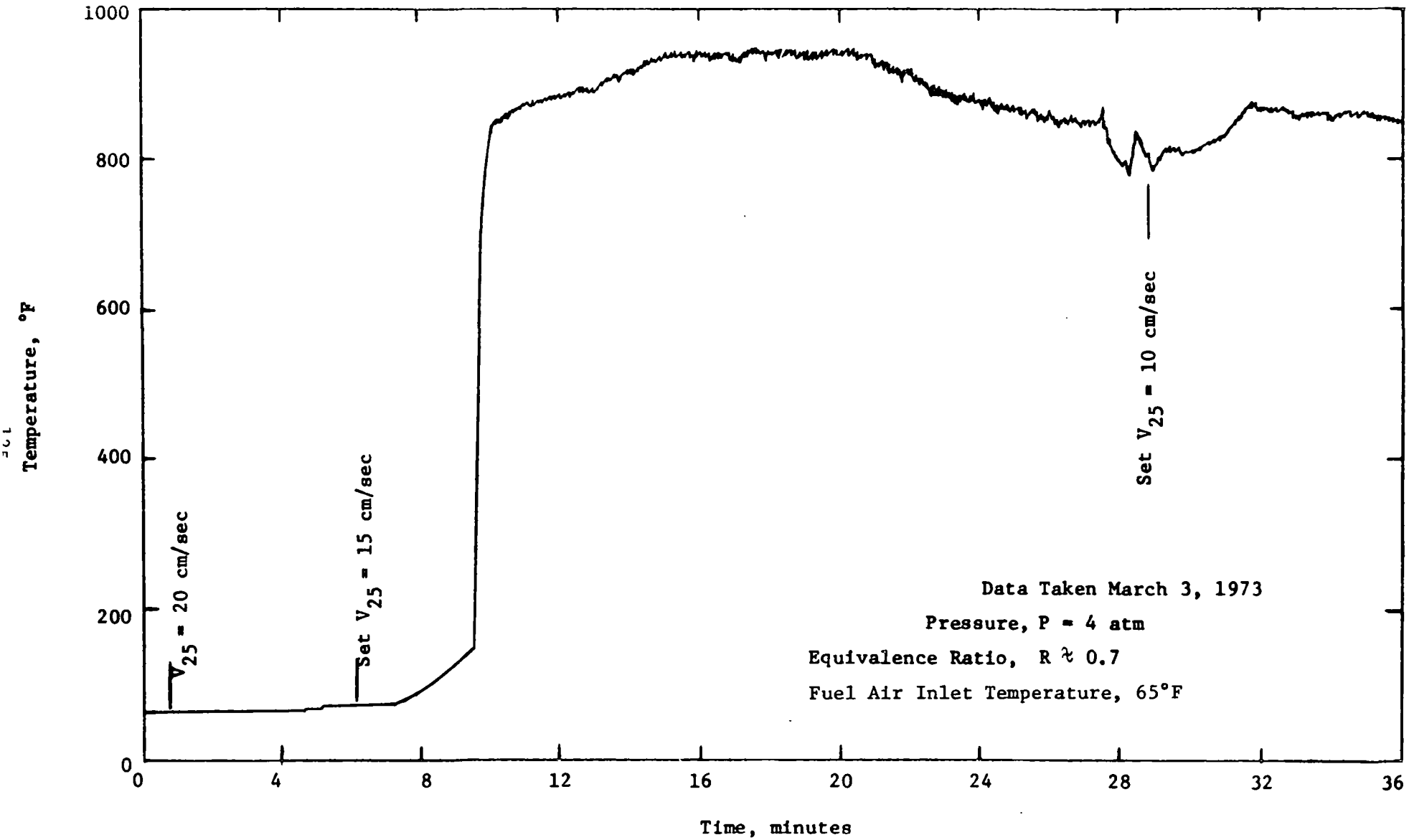

Figure 76. Impending Preignition at P = 4 Atmospheres

air ratio caused large effects on the upstream face temperature. Post-test examination of this second burner revealed the same type of hairline cracks as those observed in the first burner.

The temperature of the downstream surface (combustion side) of the burner was not measured during the preignition tests. However, using the theoretical heat flux from the flame to the burner, a surface temperature required to radiate this heat away can be calculated. For a pressure of 3 atmospheres and an equivalence ratio of 0.9, the calculated surface temperature is 2120°F. For a pressure of 4 atmospheres and an equivalence ratio of 0.7, the calculated temperature was about 2050°F. The emissivity was taken as 0.9. Within the accuracy of the measurements and the uncertainties in the calculations, these two temperatures can be considered equal. A tentative conclusion is that at a certain hot-side surface temperature, the flame propagates against the flow of fuel-air mixture in the porous plate and eventually reaches the upstream surface igniting the fuel air mixture prematurely. The phenomenon labeled "flashback" is postulated to occur at a fixed hot-side surface temperature which probably depends on such things as porosity and pore size of the porous material.

Air-Cooled Combustor

Design Analysis - In order to solve the problem of preignition or flashback experienced in radiation-cooled burners, some preliminary calculations were performed to determine the effect of air cooling on the temperature of a metallic burner. The configuration examined had cooling tubes embedded in the porous plate matrix, using air as the cooling medium. With the temperature limitations of a metallic burner, neither radiation cooling alone nor air cooling alone could reject the heat load from the

flame at all operating conditions. The calculations were made to determine if the combination of radiation and air cooling could reject the heat. Some available combustor loading calculations indicated that the maximum steady state heat flux from the flame to the porous plate was on the order of 70,000 Btu/hr-ft^2.

Figure 77 is a plot of the radiation heat flux between two long concentric cylinders. The inner cylinder (surface 1) represents the burner surface radiating to a heat sink (surface 2). At a burner surface temperature of 2000°F, the radiant heat flux ranges from about 28,000 Btu/hr-ft^2 to 37,000 Btu/hr-ft^2, depending upon the sink temperature. Thus for an air cooled combustor, the difference between the heat flux of 70,000 Btu/hr-ft^2 and the radiated flux must be removed by cooling, or the burner temperature will exceed 2000°F. An analysis was performed to determine the temperature distribution in a burner with embedded cooling tubes. It was assumed that the heat flux from the flame to the burner surface is uniform and that there is no temperature variation through the thickness of the burner. The resulting nonlinear differential equation describing the burner temperature distribution was solved numerically for a number of possible operating conditions. For each of these cases, the solution yielded the axial temperature distribution in the burner. The maximum calculated temperature for each case was used as a measure of cooling effectiveness. The cooling air fractional pressure drop ($\Delta P/P$) was held constant at 5%. Figure 78 shows the calculated maximum wall temperature as a function of heat flux from the flame to the burner with burner operating pressure as the parameter. The cooling air inlet temperature was taken as 400°F which is about the maximum compressor discharge temperature. Figure 79 is the corresponding result for a cool-

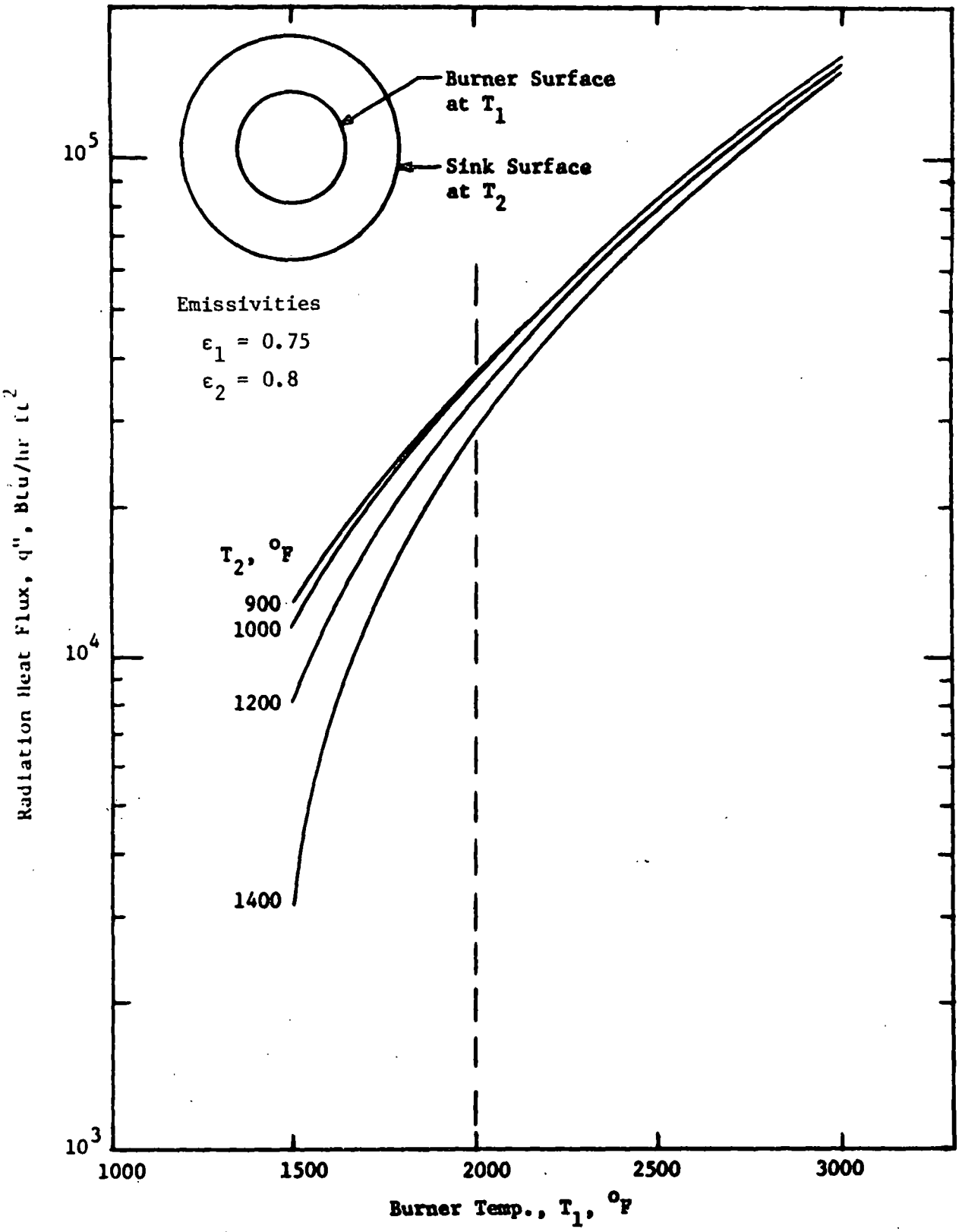

Figure 77. Radiant Heat Flux From A Burner

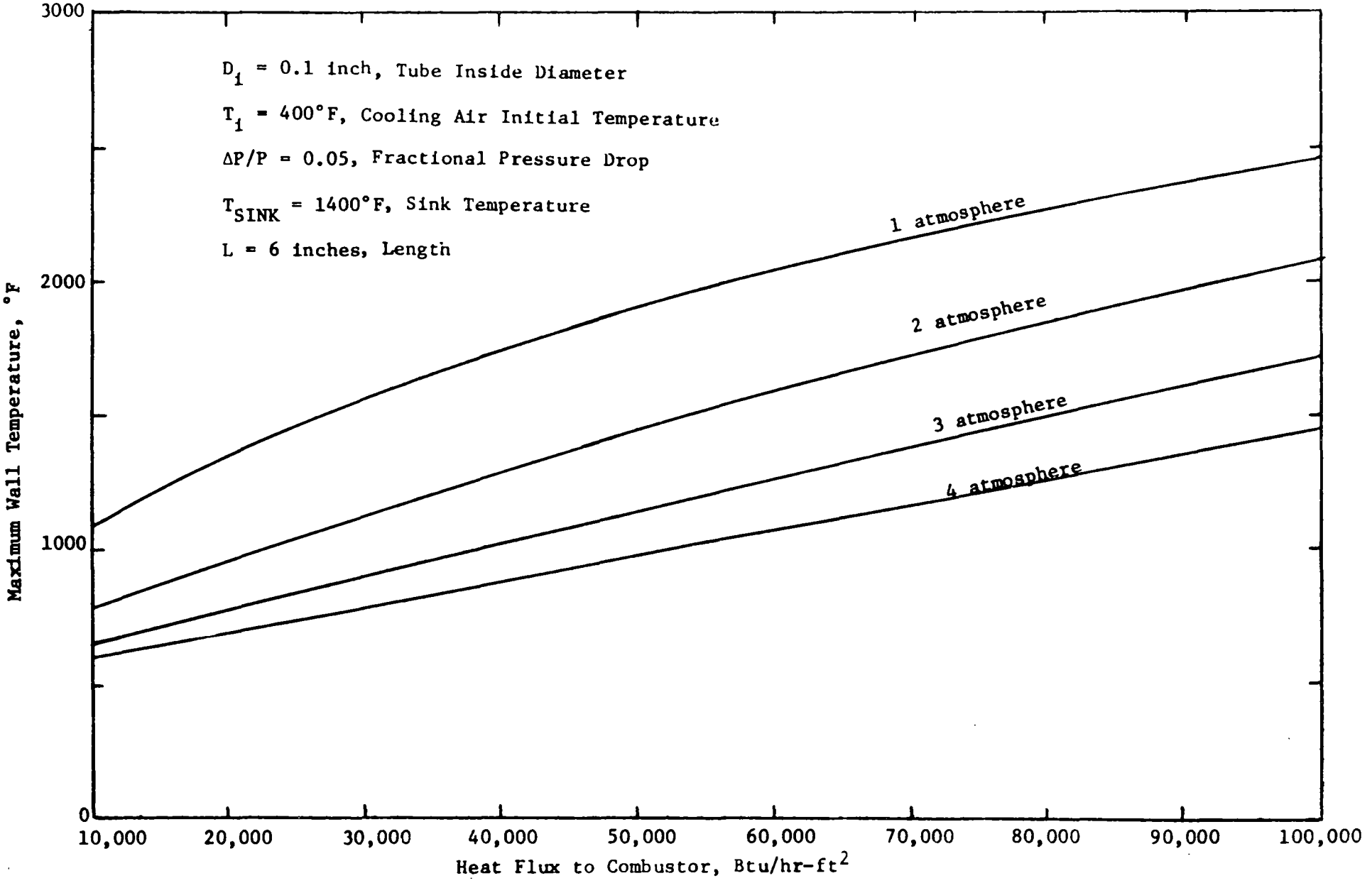

Figure 78. Calculated Maximum Wall Temperatures for Air-Cooled Burner for Cooling Air Initial Temperature, 400°F

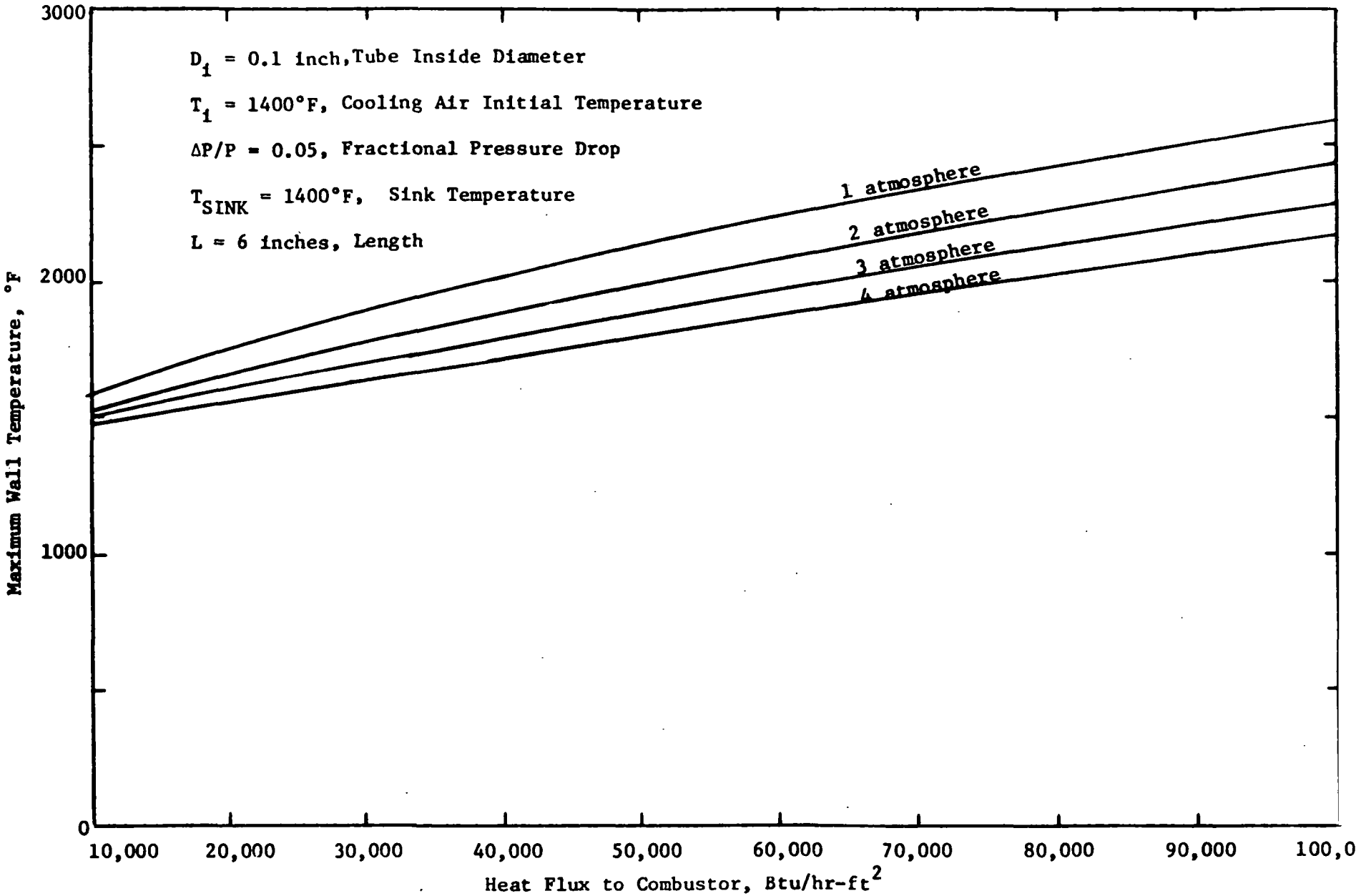

Figure 79. Calculated Maximum Wall Temperatures for Air-Cooled Burner for Cooling Air Initial Temperature, 1400°F

ing air inlet temperature of 1400°F which is about the maximum regenerator discharge temperature. In order for these plots to have meaning, the heat flux from the flame to the combustor porous surface must be known. Figure 80 is an estimate of that flux as a function of superficial gas velocity for several burner pressures and an equivalence ratio of 0.9. Taking the peak heat flux for 4 atmospheres, namely 108,000 Btu/hr-ft^2, results in maximum combustor surface temperatures of 1520°F and 2200°F for cooling air temperatures of 400°F and 1400°F, respectively. Based on these encouraging results, the decision was made to fabricate an air-cooled burner made up of sintered nichrome powder with 1/8 inch OD cooling tubes embedded in the matrix. Design of this burner was completed and fabrication development work was done. That development work is described in the Section on Porous Plate Fabrication Development.

Mechanical Design - Figure 81 shows the design of the first air-cooled burner which was designated as 106. Table 6 is a Parts List for this burner. The basic burner is a porous cylinder with a 2.25 inch outside diameter (O.D.) and 1.75 inch inside diameter (I.D.). The porous matrix is made up of nichrome powders bonded together by brazing as described in the Section on Porous Plate Fabrication Development. A total of 24, 1/8 inch O.D. cooling tubes are embedded in the porous matrix and run parallel to the burner centerline. Insulation held in position by a screen is installed on the inner cylindrical surface of the burner. The end plate is insulated with a disc of insulation. The fuel-air mixture enters the burner through the large tube at the center, passes through the screen, the insulation, and the porous nichrome and is ignited on the outer cylindrical surface. Cooling air discharges from four inlet tubes into a cooling air manifold. From this manifold, the cooling air enters the cooling tubes where it is

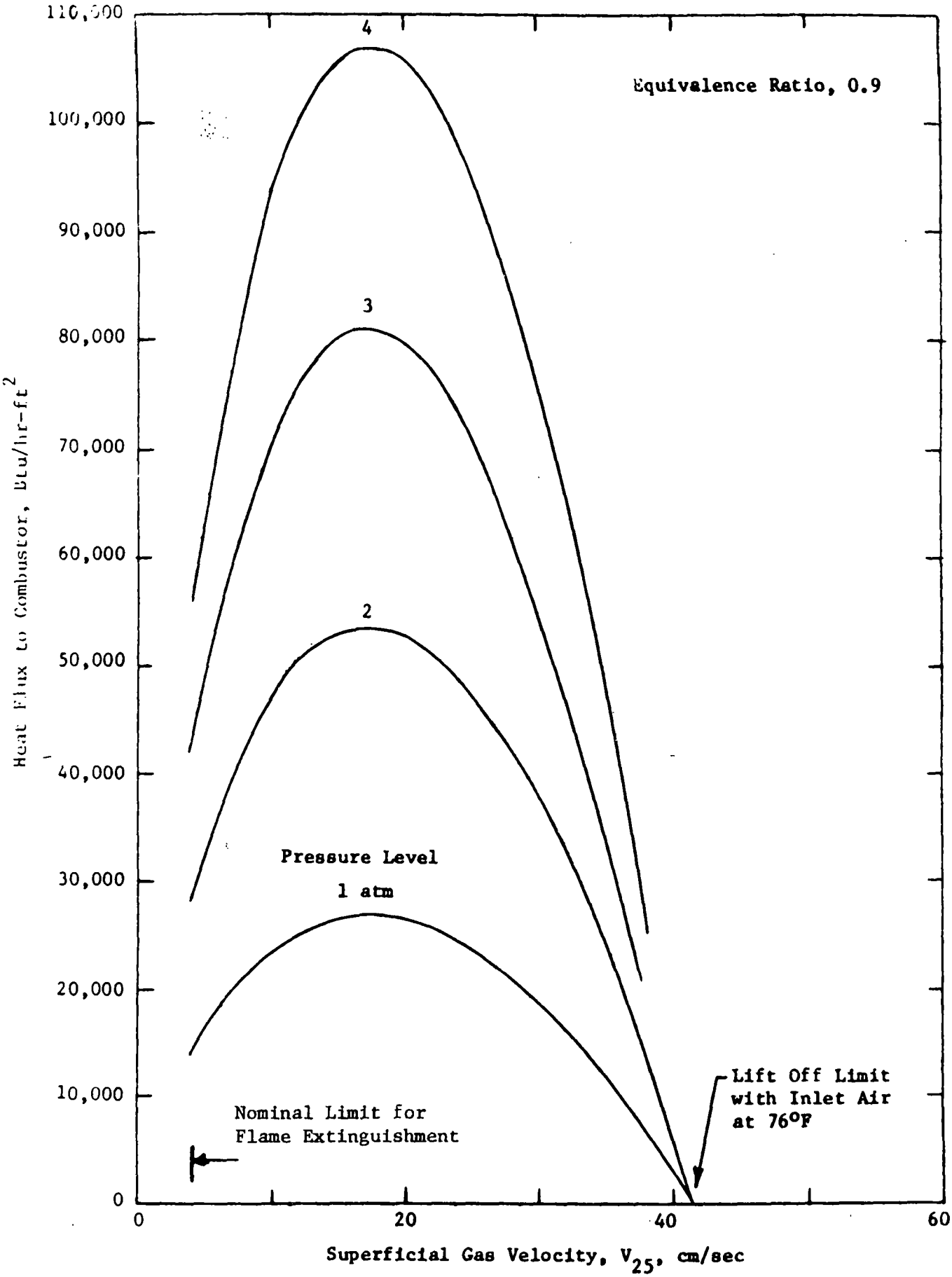

Figure 80. Heat Flux Back to the Porous Burner as a Function of Pressure and of Superficial Gas Velocity (V_{25})

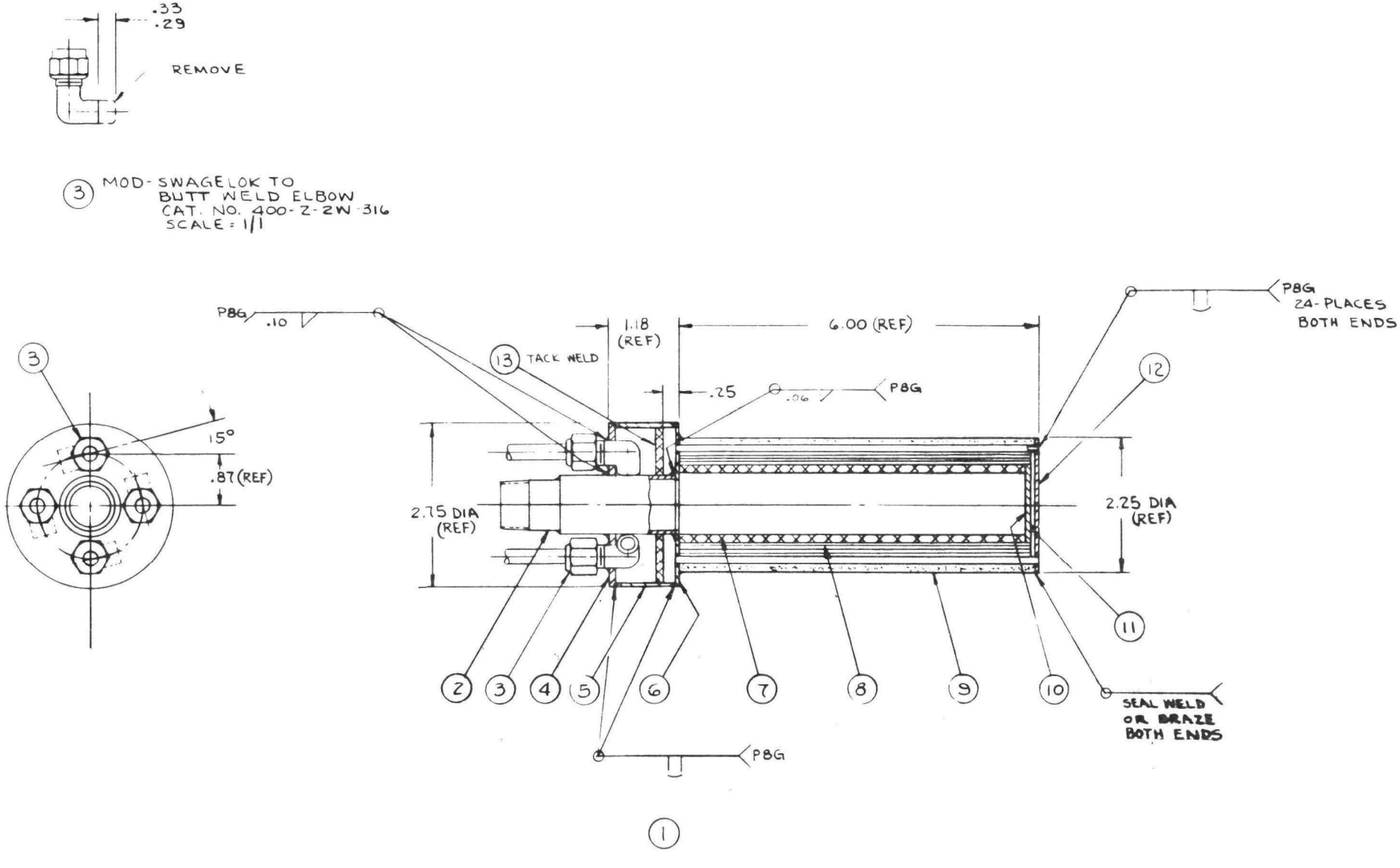

Figure 81. Design of Air-Cooled Porous Burner 106

Table 6. PARTS LIST OF AIR-COOLED POROUS BURNER SHOWN IN FIGURE 81

Item 1.	Assembly
2.	Fuel-Air Inlet Tube
3.	Cooling Air Fitting
4.	End Plate
5.	Side Wall of Cooling Air Manifold
6.	Upstream End Plate
7.	Insulation Retainer Screen
8.	Zirconium Oxide Insulation
9.	Porous Burner
10.	Insulation Retainer Plate
11.	Zirconium Oxide Insulation
12.	Downstream End Plate
13.	Flow Distribution Screen

heated by the heat transferred from the flame back to the burner. The heated cooling air discharges from the cooling tubes at the end of the burner and mixes with the combustion products. Figure 82 is a photograph of burner 106 during fabrication.

Table 7 is a list of the air-cooled burners which were tested on this program. Burner 107 was a modification of 106 in which the porous matrix was made thicker and the tubes were embedded in the center of the matrix instead of at the inner surface. Burner 107 has an outside diameter of 2.5 inch and an inside diameter of 1.75 inch and contains 27 cooling tubes. All of the air-cooled burners had a burning surface length of 6 inches.

Air-Cooled Burner Tests

Tests of air-cooled burners were made to map their operational range, determine their emission characteristics and establish their durability.

Test Procedures and Facilities - The general procedure for testing model burners was to perform a bench checkout test followed by tests in the pressurized rig. The purpose of the bench test was to observe the flame uniformity and to check for defects such as leaks. During the bench tests, the pressure drop across the porous matrix was measured as a function of superficial velocity (V_{25}).

Figure 83 is a schematic diagram of the gas turbine burner test rig. The burner being tested is installed in the pressure cylinder as shown. Separate streams of primary, secondary and cooling air are supplied from a plant air system at 100 psig pressure. The fuel used in the burner development tests was propane. The primary air passed through a rotameter and then through an electrical heater where it could be heated to temperatures simulating the compressor discharge temperature

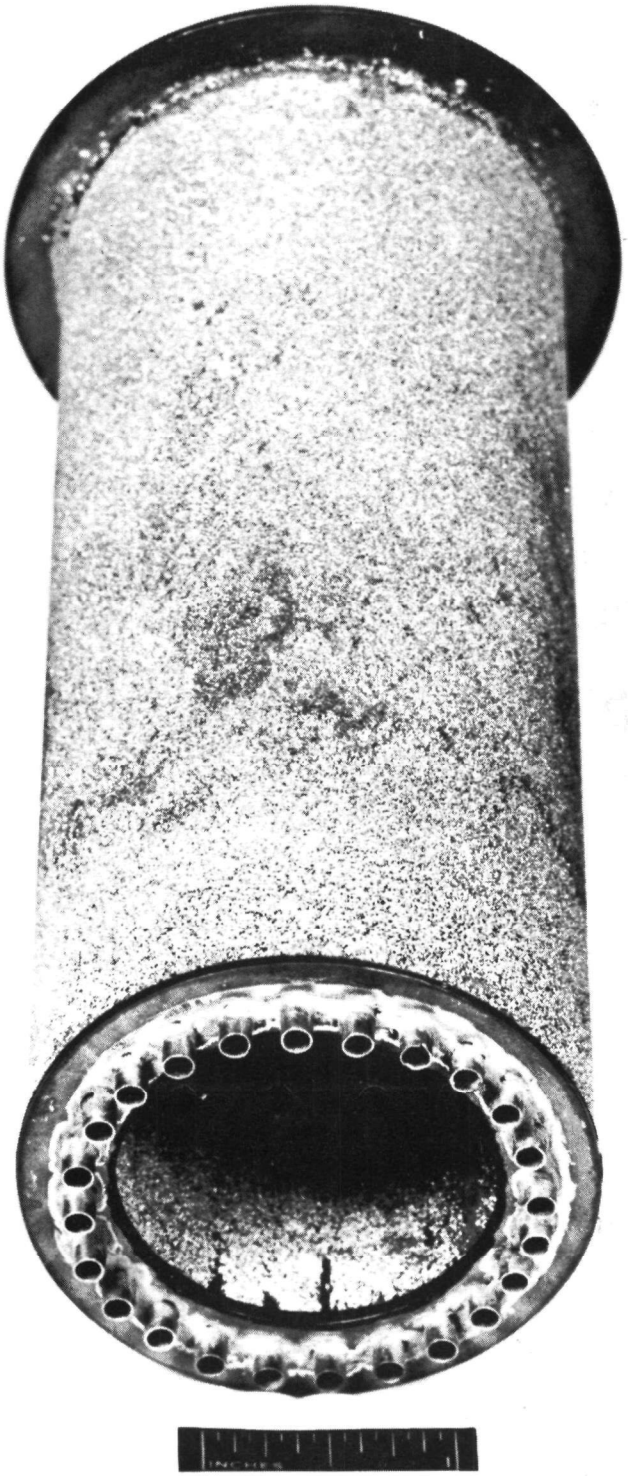

Figure 82. Air-Cooled Burner #106 During Fabrication

Table 7. AIR-COOLED BURNERS (CYLINDRICAL)

Burner	Description	Tests
106	Brazed nichrome, 2.25" O.D. x 1.75" I.D. 24 cooling tubes	Bench tests Pressure rig tests
107	Brazed nichrome, 2.50 O.D. x 1.75" I.D. 27 cooling tubes	Bench tests Pressure rig tests
108	Same as 107	Bench tests only
109	Same as 107 except with slotted surface.	Bench tests Limited pressure rig tests.
108M	Burner 108 modified with insulation and screen on outer surface.	Bench tests Pressure rig tests with heated combustion and cooling air.

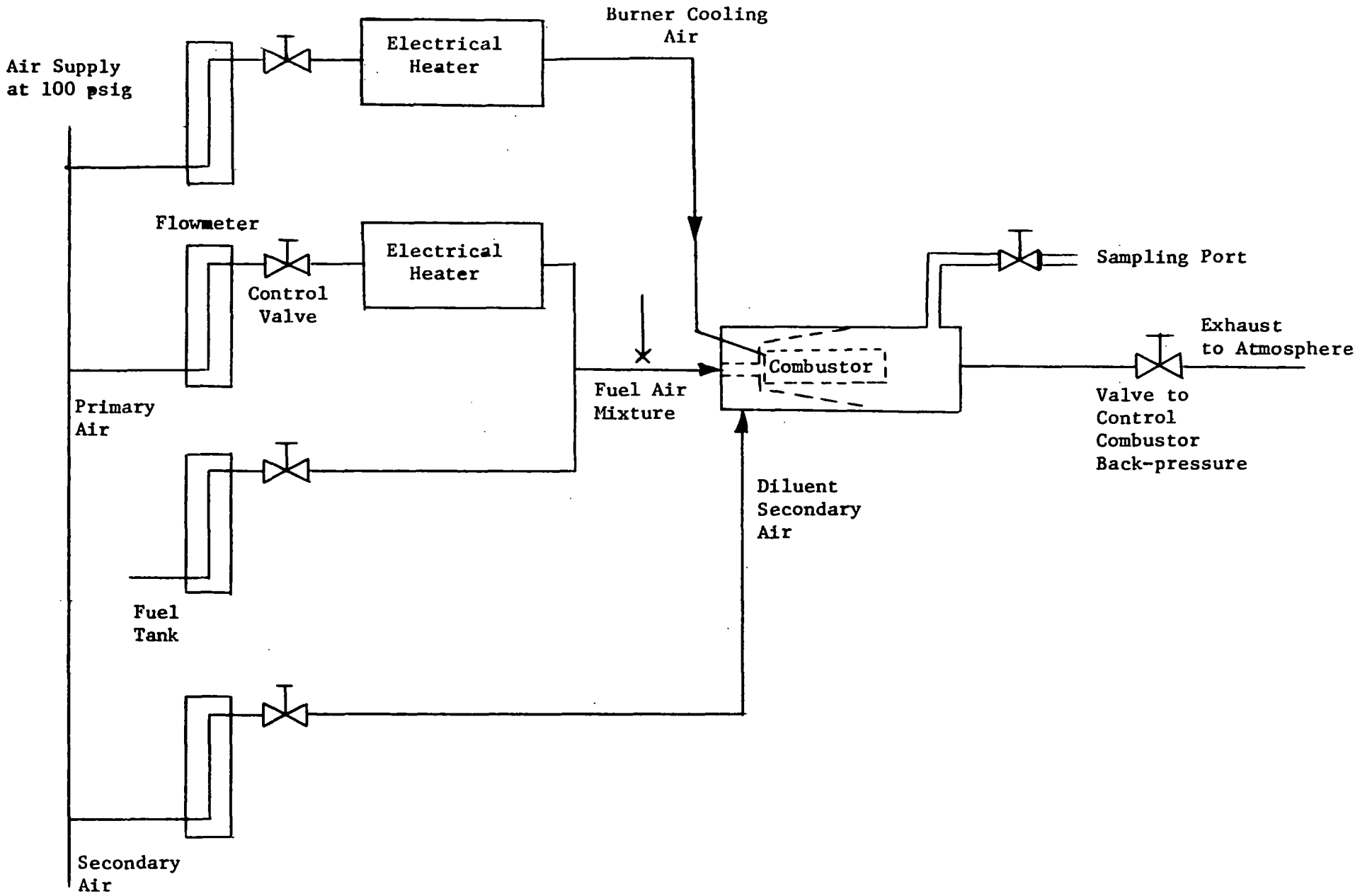

Figure 83. Schematic of Gas Turbine Combustor Test Facility

(about 400°F) of the gas turbine. Fuel flow was measured with a rotameter and was then injected into the primary air stream. The fuel-air mixture then entered the burner where it was burned. Surrounding the burner was a conical screen which served as a heat sink for radiation from the burner surface. The heat sink screen was cooled by the secondary air which flowed radially inward through the screen and mixed with the combustion products. Cooling air passed through a rotameter and an electrical heater, where it could be heated to about 400°F, and into the cooling air manifold in the burner. After passing through the cooling tubes, the cooling air mixed with the combustion products and the diluent secondary air. The combined burner exhaust then flowed out through a water-cooled valve used to control the burner operating pressure level. Samples of the exhaust gases were taken through a sampling line downstream of the burner. Measurements of CO, CO_2, NO, NO_2 and unburned hydrocarbons were made with a Scott Research Laboratories, Inc., Model 108H Exhaust Gas Analysis System which was purchased by the General Electric Company. Figure 84 is a photograph of the Scott equipment.

Burner 106 - This was the first of the air-cooled burners to be tested in the pressurized rig. Before installing the burner in the rig, a bench checkout was performed. The equivalence ratio was held constant at 0.8 and the superficial gas velocity (V_{25}) was varied from 10 cm/sec to about 45 cm/sec. During this operation, several small hairline cracks appeared on the surface. The cooling air flow rate was set equal to the combustion air flow rate. No flashback was observed.

The burner was then installed in the pressurized rig in order to measure emissions and to determine the effectiveness of the air cooling.

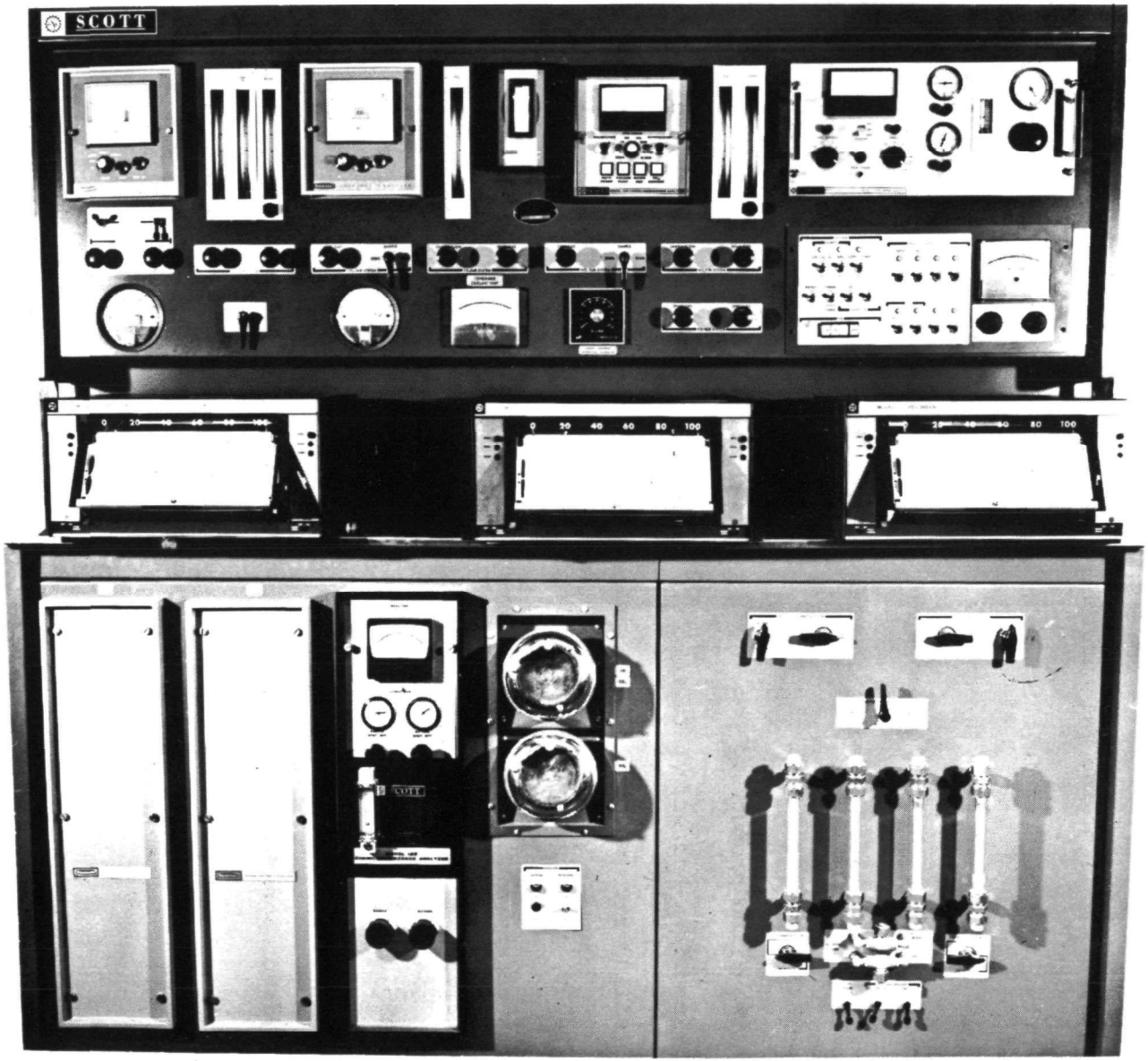

Figure 84. Scott Exhaust Gas Analyzer

Tests were conducted with room-temperature air at burner pressure of one, two, and three atmospheres before a flashback occurred and the test was stopped. These tests imposed the most severe conditions, in terms of heat flux to the burner, of any burner tested to that time.

Figure 85 is a plot of the emission index for the measurements of CO and NO_x from burner 106 as a function of superficial velocity. The solid points are the measurements and the open points are the corresponding prediction; for NO_x, the calculation uses the "hot-air" mechanism. All of the measured NO_x values were well below the 1976 Federal Standard. The CO values exceeded the standard at a V_{25} of around 20 cm/sec.

Figure 86 shows the measured NO_2 emission index for the tests at pressures up to four atmospheres. No definite trend with pressure is evident.

Post-test examination of the burner revealed the existance of several cracks. The appearance suggested that the flashback probably occurred through one of these cracks. The pressure surge associated with flashback split the burner along four axial cracks located approximately 90° apart. A new air-cooled burner (designated as burner 107) was designed and built, This burner was 50% thicker (0.375 in. wall) and placed more of the sintered powder behind the tubes.

Burner 107 - Air-cooled burner 107 was tested on the bench, both for pressure drop and for uniformity of flame. Figure 87 is a plot of the measured pressure drop as a function of unburned gas velocity, V_{25}. Measurements were made both with and without burning. The increased pressure drop during burning is probably due to changes in burner porosity due to heating and reduced gas density.

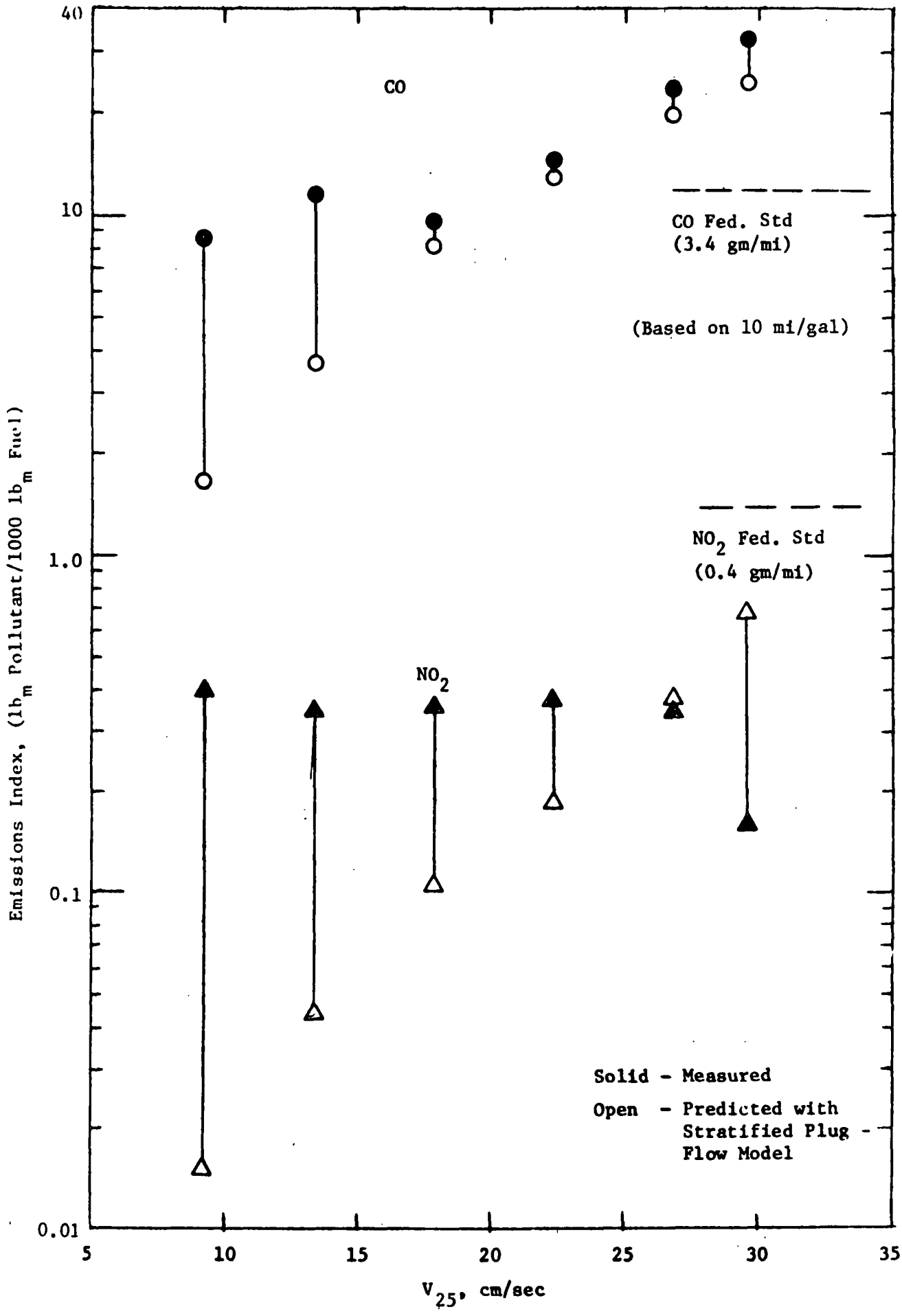

Figure 85. Emissions from Air-Cooled Burner S/N 106 at 1 Atm. Pressure

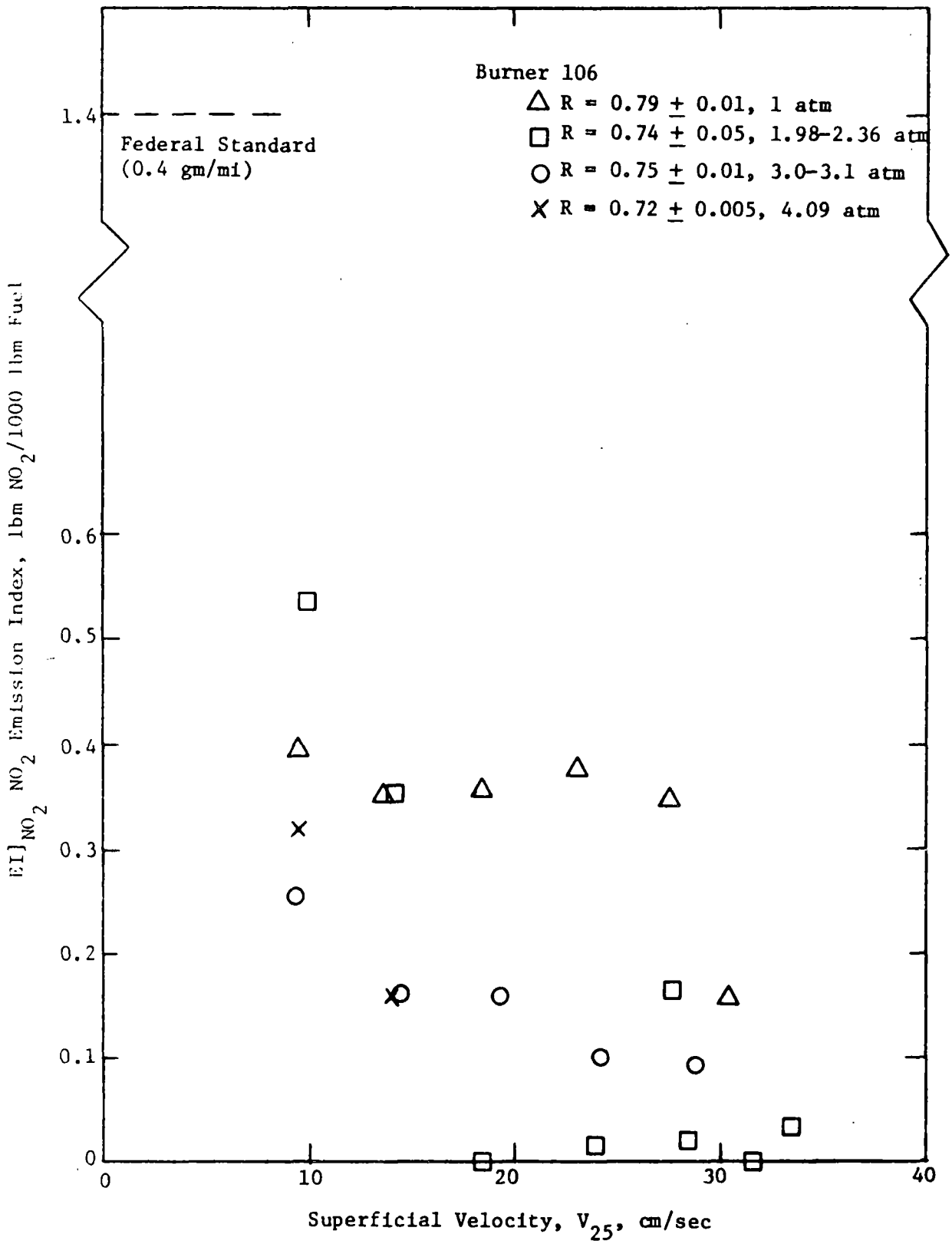

Figure 86. NO_2 Measurements at 1 to 4 Atmospheres on Air-Cooled Burner

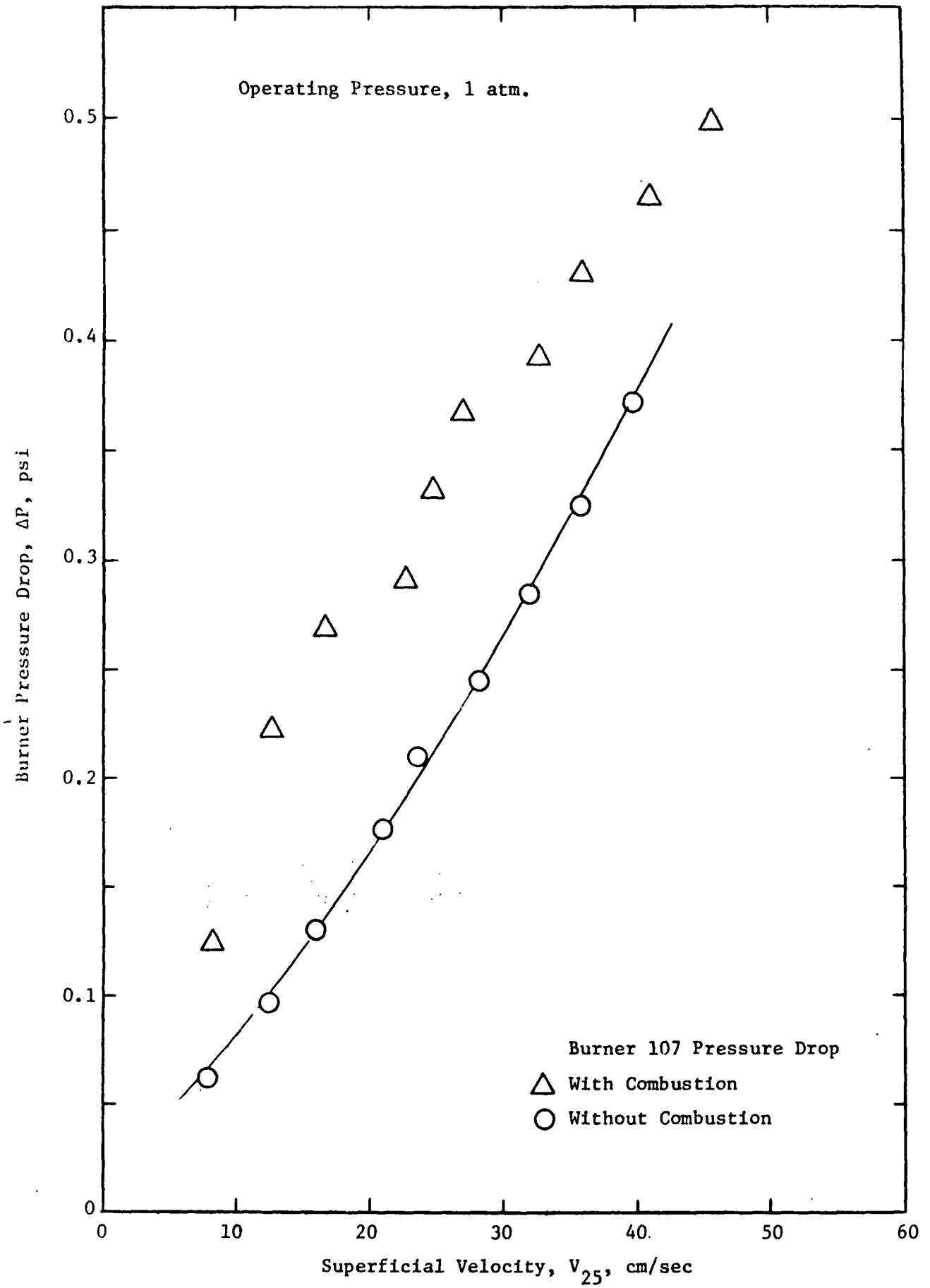

Figure 87. Burner 107 Pressure Drop

Figure 88 shows the CO and NO_2 measurements for burner 107. The NO_2 values were below the Federal Standard over the full range of superficial gas velocity. The CO values exceeded the standard above about 15 cm/sec. This is probably due to the relatively cool exhaust temperature associated with unheated inlet air. Subsequent tests with heated inlet air with burner 108M described below tend to confirm this hypothesis.

Tests with these burners showed that the unburned hydrocarbons (HC) emissions were essentially zero when the burner was intact. It was soon learned, in fact, that indications of unburned HC was a definite indication of a burner defect. Testing with burner 107 was terminated when there were indications of hydrocarbons. Post-test examination of the burner revealed longitudinal cracks similar to those observed with burner 106. The cause of the cracks was hypothesized to be due to hoop stresses associated with the radial temperature gradient through the burner.

Burner 108 - This burner was identical to burner 107. Since 107 cracked during tests, 108 was checked out on the bench only.

Burner 109 - In order to avoid the problem of cracking, the decision was made to machine longitudinal slots in the burner extending radially inward from the outer surface of the burner to the top of the tubes (one slot for each tube). This slotted burner was designated as 109 and was checked out on the bench. During preliminary tests in the pressurized rig, the burner cracked and this test was terminated before any emissions data was obtained.

Burner 108M - Burner 108 was modified into burner 108M by wrapping the cylindrical surface with a layer of Fiberchrome insulation held in position with a Kanthal screen. Tests were conducted in the pressurized rig first with unheated combustion and cooling air and later with these air

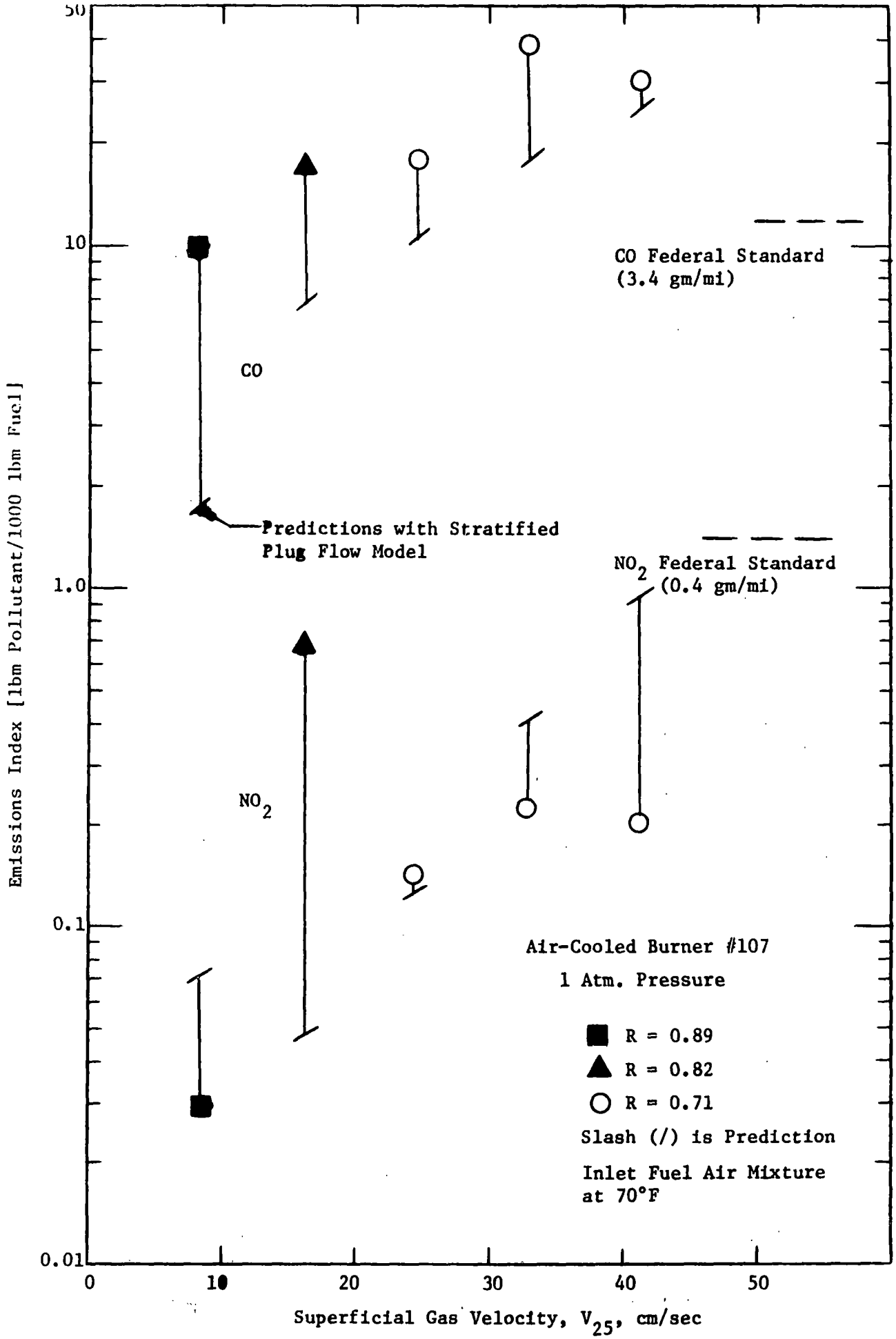

Figure [illegible]. Measurements of CO and NO_x Emissions on Burner 107

streams heated to temperatures approximating compressor discharge temperature (400-600°F). Figure 89 shows the CO emissions and Figure 90 shows the NO_x data. The CO emissions are lower with heated air (open points) than with unheated air (solid points), as would be expected with the higher exhaust temperatures associated with the heated air; with the higher exhaust temperatures, the CO decay rates are higher which result in reduced CO. For the same reason, it is not surprising that the NO_x values increased with the air heating, since higher exhaust temperatures also mean higher NO_x production rates. However, all the data were below the Federal Standards.

FUEL-AIR MIXTURE SUPPLY DEVELOPMENT

Because the porous plate combustor requires a uniform mixture of fuel and air upstream of the porous plate, it was necessary to design, fabricate and test a fuel-air mixture supply system.

Design and Fabrication

The technical literature indicated that, within reasonable geometrical restraints, complete vaporization of the required quantities of gasoline could be accomplished only if more than one of the following vaporization mechanisms were used:

1. Preheating the fuel prior to injection into the airstream.
2. Pressure atomization.
3. Air atomization, including shearing and sonic atomization.
4. Evaporation of droplets by the heat of the primary airstream.
5. Evaporation of droplets centrifuged onto a plate heated by heat losses from the combustion zone.

All of the above mechanisms could be utilized when combustion is in progress. The cold starting problem dictated that a sonic air atomizer

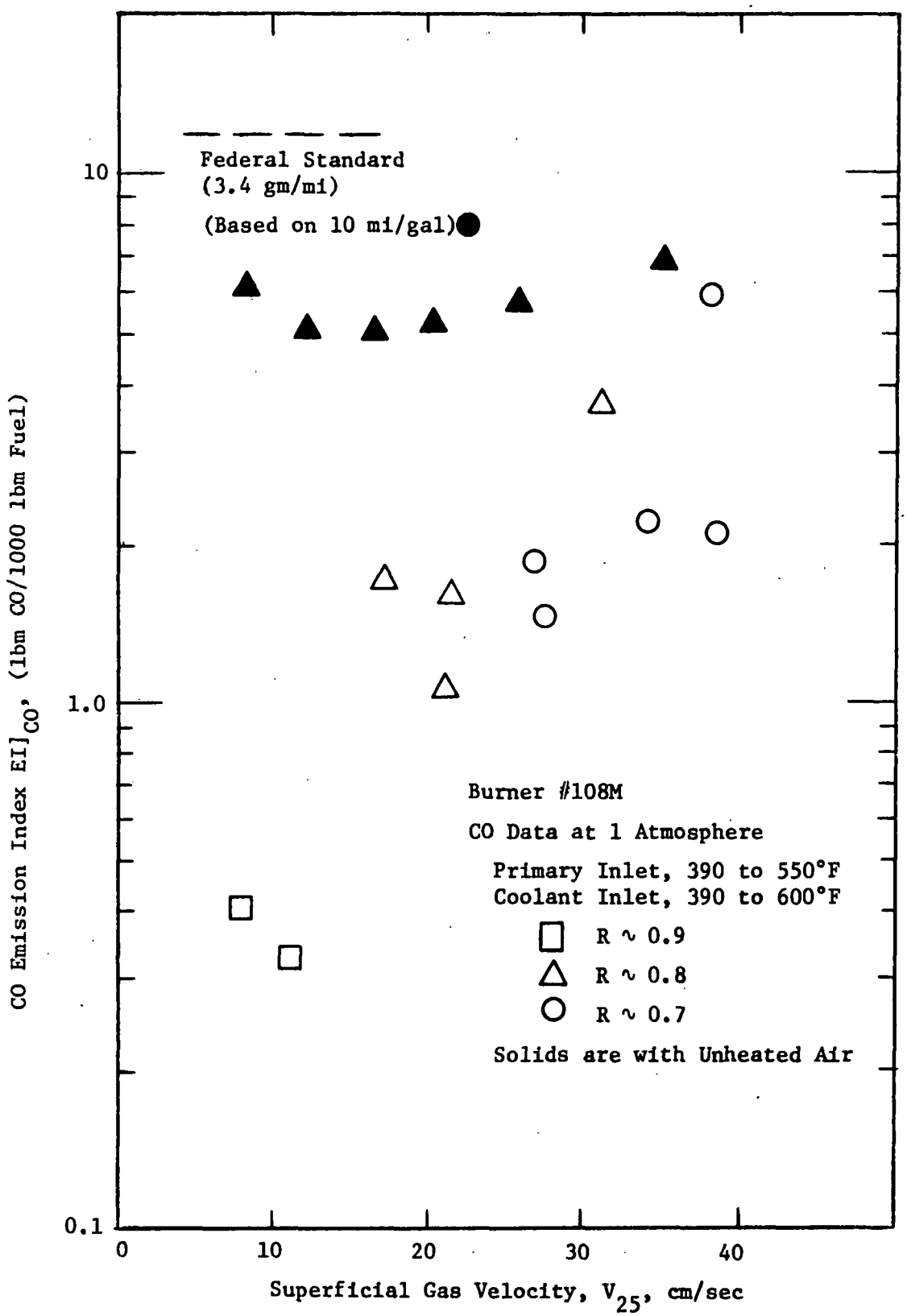

Figure 89. Measured CO Emissions on Burner 108M with Both Heated and Unheated Air

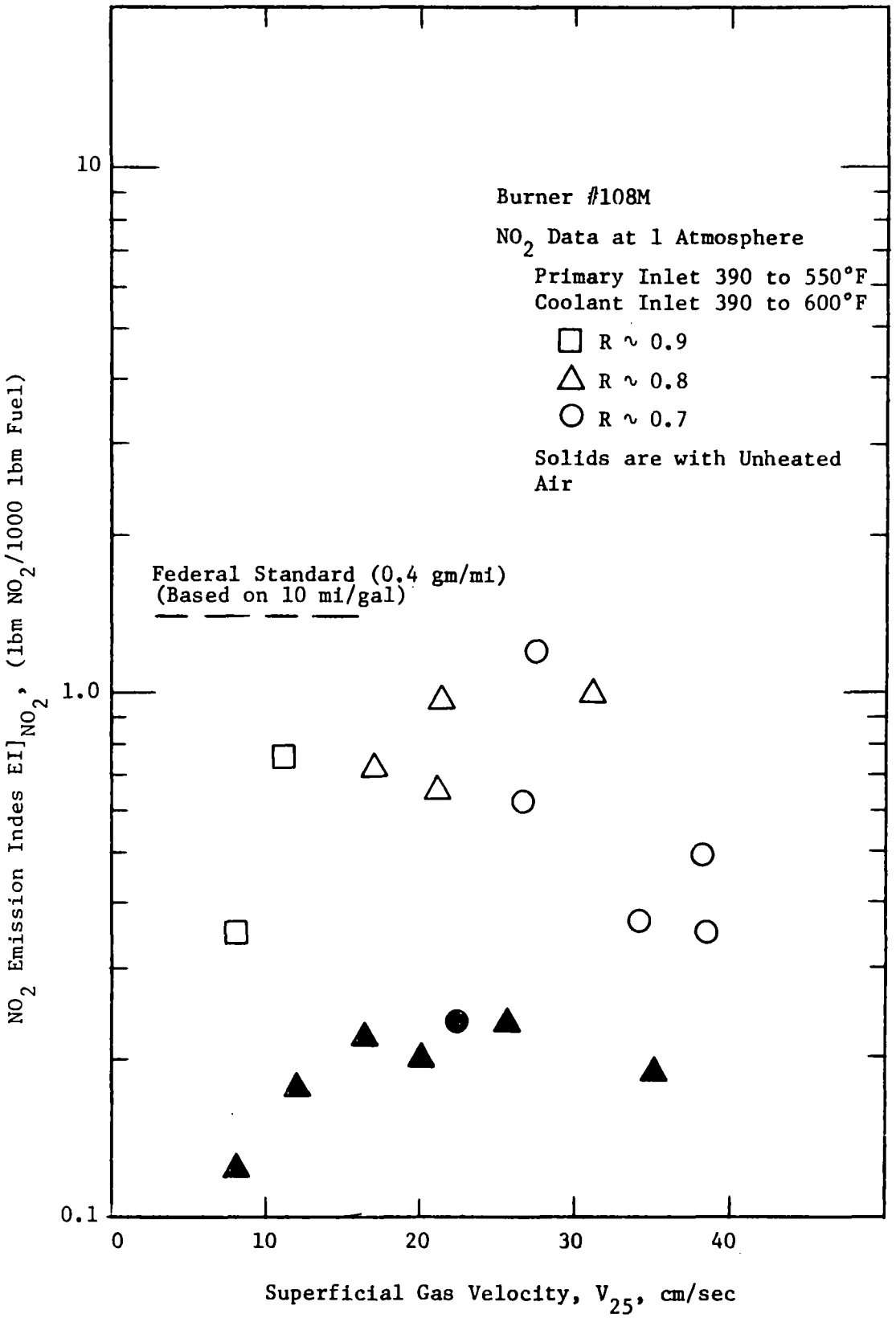

Figure 90. Measured NO_x Emissions on Burner 108M with Both Heated and Unheated Air

be utilized to produce the fuel spray. This type of injector is also capable of meeting the high turndown ratio required with reasonable airflow and air and fuel pressure requirements.

Fuel-Vaporizer Test Assembly - A gas turbine fuel vaporizer test assembly shown in Figure 91 was fabricated, instrumented, and tested. This assembly comprises the following elements.

Burner Model - The cylindrical surface is provided with sixteen 0.04 in. inner diameter tube fittings, and the end is provided with one of the same. These fittings are used to pass the thermocouple wires through, to control the flow area and thus model the porosity of the porous matrix; and the tubes attached to the fittings are used for pressure taps. The cylinder and end outer surfaces are wrapped with electric heating wire to partially model the operating temperature of the porous matrix. The end plate contains a centerbody and flow director to assist the fuel-air mixture in making a 180° turn. Three thermocouples are staggered within the model of the porous matrix to measure its inside wall temperature.

Vaporizer Plate - An internal heated cylinder enclosed within a cone acts as a vaporizer plate. The cylinder is closed on one end except for a hole through which the fuel nozzle protrudes and six flow-directing louvers. When used with the louvers, the air flow area is variable in order to produce a constant fuel-air ratio. A high tangential velocity is produced, which effectively creates an airflow path much longer than the axial length of the cylinder. The vaporization of the fuel is enhanced by the longer exposure of the fuel droplets to the sensible heat of the air. Also, the larger droplets are vaporized by the heated cylinder wall when they contact it either by impaction of the

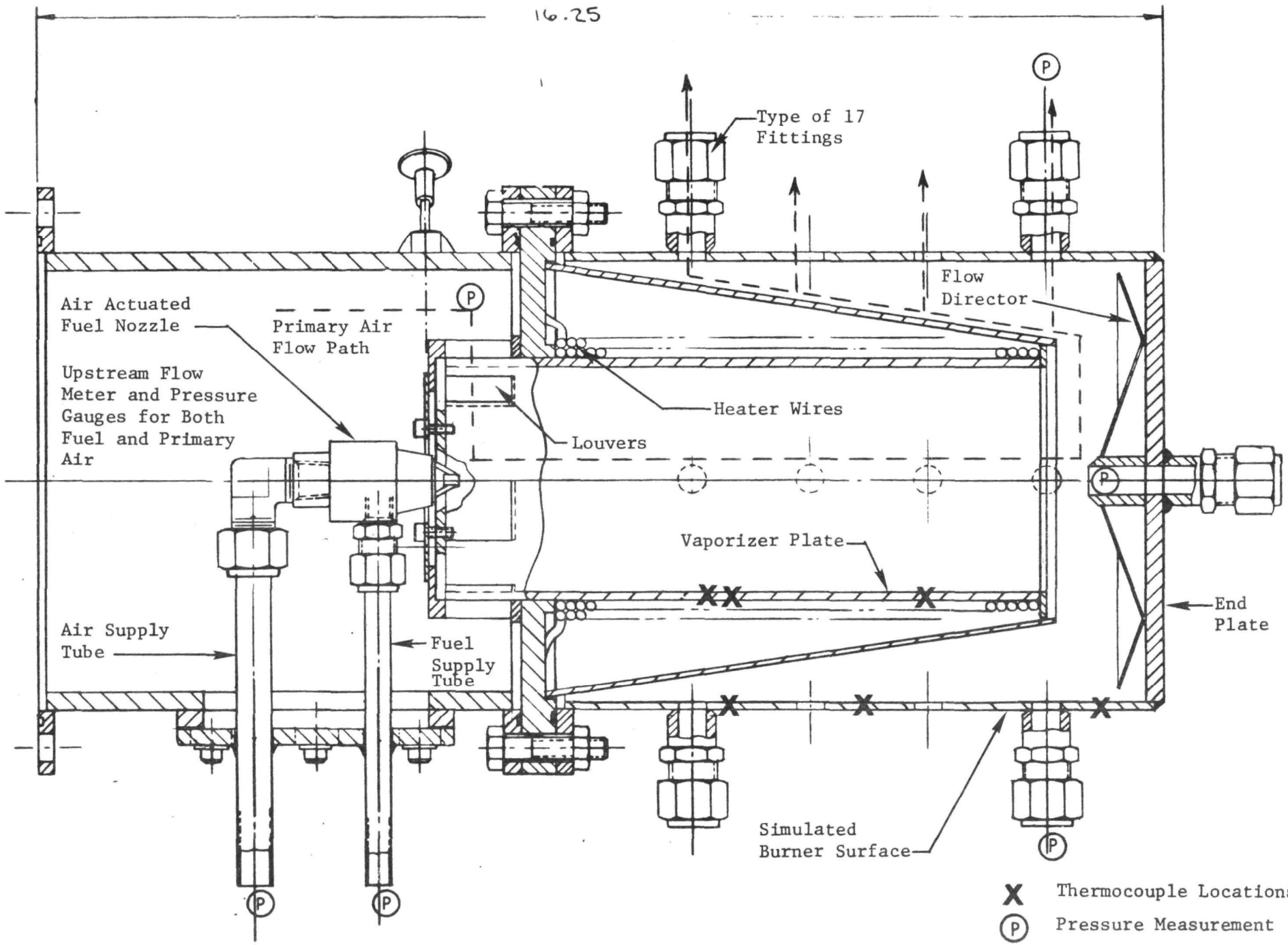

Figure 91. **Fuel Vaporizer for Gas Turbine Combustor**

spray or by centrifuging. The cone acts as a flow director and as a radiation barrier between the model of the porous matrix and the vaporizer cylinder. Two thermocouples measure the vaporizer cylinder wall temperature.

Fuel Nozzle - Sonicore 156K and 125K atomizer nozzles made by the Sonic Development Corporation have been tested. The actuating air as shown in Figure 92 enters the center of the nozzle through a 1/4 in. pipe ell. The fuel enters a chamber surrounding the air chamber through a 1/8 in. pipe connector. It is injected into the airstream through fixed orifices of 0.032 in. diameter. The spray immediately enters a zone wherein a resonator cup creates soundwaves which break the spray into a soft mist of droplets which are expected to be about 20 microns or less under most operating conditions.

Thus, the assembly utilizes the principles of low-pressure atomization, air shearing and sonic atomization, evaporation of droplets by the heat of the airstream, and evaporation of droplets centrifuged onto a plate heated by combustion zone heat losses. Other methods which can be incorporated into this assembly include preheating of the fuel, the insertion of a device into the vaporizer cylinder which will increase the passage length and time of exposure of the fuel to the hot air, and inserts around the nozzle tip to create more turbulence or change the quantity of air passing through the spray.

Summary of Fuel Nozzle Tests - The fuel nozzles were assembled in a rig which contained an air supply with electric heater, flowmeter and gauge which read the pressure at entry into the nozzle. The fuel system contained a pressurized tank, flowmeter, and gauge which read fuel pressure at entry into the nozzle. The spray was exhausted into atmospheric air and was observed visually.

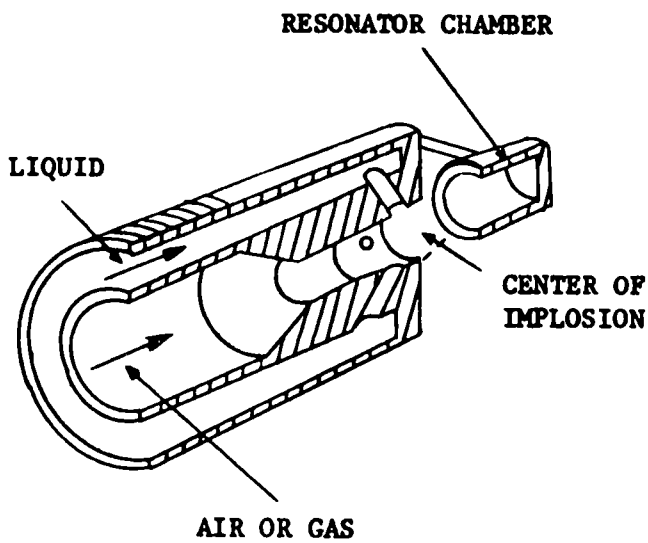

Figure 92. "Sonicore" Fuel Vaporizer

Since the air orifices were nozzles of fixed throat diameters, the air flow rates could be set at any given level below choked flow by varying the air supply pressure. At low fuel supply rates, the presence of the fuel had no appreciable effect. At fuel supply rates above 50 lb/hr, the air flow rates decreased.

Since the fuel orifices were of fixed number and diameter, the fuel flow rates could also be controlled by varying the fuel supply pressure. Low fuel supply rates could be achieved by the aspiration of the air-stream, with greater aspiration achieved at a given air flow rate by the smaller 125K nozzle.

The intent of the nozzle calibrations was to determine whether the spray from either nozzle was satisfactory and what combinations of air and fuel flows were best. Since the greatest amount of energy available for atomization was supplied by the air, smaller droplets are produced by larger air flow rates at constant fuel flow rates, and by smaller fuel flow rates at constant air flow rates. A "wet" spray - "dry" spray boundary was established by varying the fuel flow at constant air flows and temperatures. The boundary was a straight-line variation with pressure, being about 7 lb/hr for the 125K nozzle and about 6 lb/hr for the 156K nozzle, both at 15 psi air pressure differential and essentially invariant with air temperature.

A criteria which showed more distinction between the two nozzles was the stable combustion limit. By setting the nozzle air flow and increasing the fuel flow, a point was reached at which a flame would not blow out after the ignition source was removed. At 10 psi air pressure differential, the stable combustion limit was about 34 lb/hr fuel flow for the 156K nozzle and about 10 lb/hr fuel flow for the 125K nozzle. The appearance of the

flames also favored the 125K nozzle, since its flames could be made to appear virtually invisible, indicating good vaporization very close to the nozzle. The 125K nozzle appeared to have a distinct advantage with respect to quick vaporization because it produced smaller drops.

The distribution of the 125K nozzle was also superior, since under most operating conditions the spray angle was larger than that of the 156K nozzle. The larger spray angle and the softer spray assists in distributing the spray into the high tangential swirl of the combustion air and in impacting the larger drops onto the vaporizer hot plate.

The 125K nozzle was chosen for further testing.

Summary of Vaporizer Fluid Flow Tests - By varying the setting of the movable louvers and the air pressure differential across them, the effective louver flow area and the tangential swirl velocity could be calculated. The effective burner flow area was variable by closing some of the seventeen Swagelok fittings of the burner model. Pressure was measured through one of the nozzle supply tubes and the port on the end of the burner model. The supply air was at ambient temperature and the conditions at the burner model exit were ambient. A fuel injector was not installed during the tests.

With a louver air pressure differential of 1 psi (tangential velocity, 270 fps) and the louvers nearly completely closed, a choked air flow of 160 lb/hr was delivered with a model burner flow area of 1 to 2 in^2. With the louvers fully open, an air flow of 1080 lb/hr was delivered (variable with burner area).

Calculations of Degree of Vaporization - The test conditions used for tests of the fuel-air mixture supply were those specified for the Base Line Engine in Table 1. Using the data summarized by Graves and Bahr[10] and the most severe air conditions specified in Table 1 as far as high flow rate/low air temperature conditions are concerned (the Federal Driving Cycle point with a fuel flow of 65 lb/hr), estimates were made of the degree of vaporization which could be achieved by the sensible heat of the air alone. The contact time and length of air flow path given in Figure 93 were based upon the vectorial path length using tangential swirl velocities and axial through-flow velocities.

It was expected that droplet sizes would be produced by the sonic injector which would be at least as good as those of a simple orifice at 300 psi fuel pressure differential, and that 300 ft/sec tangential velocity would be achievable with reasonable air pressure differential. Therefore, it was expected that 93 percent vaporization could be achieved through air sensible heat alone. All other test points except the one with a fuel flow of 65 lb/hr require less tangential velocity and could tolerate coarser sprays to achieve the same degree of vaporization.

A thermal analysis has shown that the vaporizer plate would operate at about 1200°F inside an operating porous burner if it were not shielded from radiation. With the present shielding, its operating temperature would be closer to 200°F. Therefore, by proper design of the shielding, the vaporizer plate could be designed to operate between these extremes. The heating wires within the vaporizer plate allow the vaporizer plate temperature to be controlled as a test variable.

A plot of the heat required to heat the required quantities of fuel from 100°F to 425°F and to vaporize 100% of the fuel can have superimposed

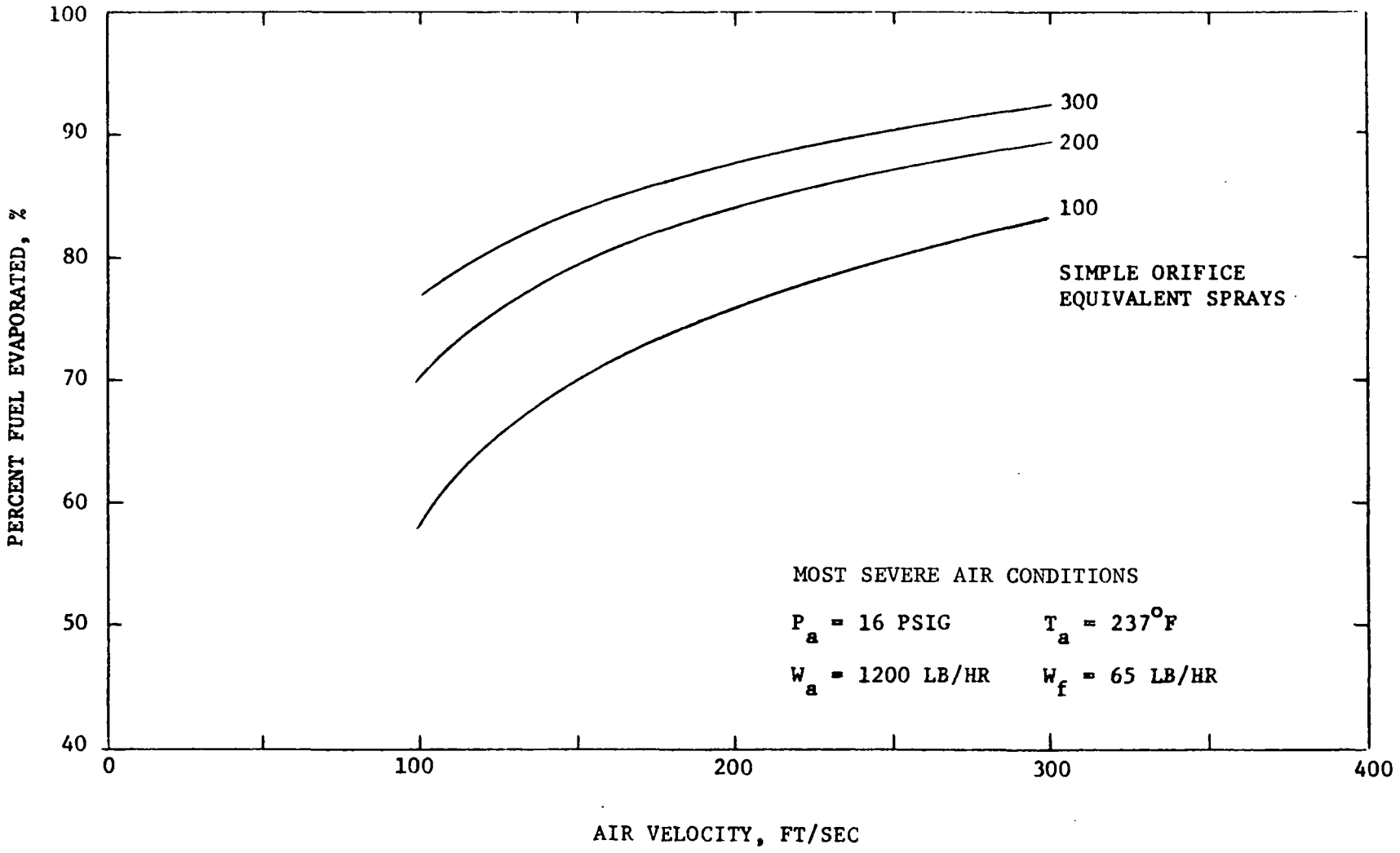

Figure 93. Estimated Performance of Fuel Vaporizer for Gas Turbine Combustor

upon it the heat provided by convection from the plate to the combustion air at constant equivalence ratio. The heat required rises linearly with the amount of fuel while the heat provided decreases hyperbolically. The net result is that 100 percent of the fuel can be vaporized by the plate up to a fuel flow of 20 lb/hr (provided it is placed upon the plate). The vaporized fraction decreases to 50 percent at a fuel flow of 30 lb/hr, 11 percent at 65 lb/hr, 8 percent at 85 lb/hr, and 2 percent at 160 lb/hr.

The 11 percent vaporized at 65 lb/hr by the plate plus the 93 percent vaporized by the sensible heat of the air exceeds 100 percent. Also it is not expected that as much as 10 percent of the fuel will be present on the vaporizer plate.

Fuel Vaporizer Tests - The objective of the tests was to determine the degree of fuel vaporization for typical combustor operating conditions.

Test Apparatus - The test apparatus shown in Figure 91 is shown installed in the test facility in Figure 94. The combustion air comes from the left into the vaporizer which is covered with insulation. The injector (heated) air and fuel lines are shown at the location where they enter the test device. Four manifolds can be seen leaving the vaporizer. Each manifold collects the fuel mixture from four fittings along an axial line on the simulated porous surface (see Figure 91). Three of these lines simply discharge the fuel-air mixture. The fourth discharges to a 15-inch diameter porous-plate, water-cooled combustor. The line to this burner is water cooled to arrest further vaporization. Thermocouples to the inside of the simulator/combustor surface, the cylindrical vaporizer tube, and the lines used to carry pressure signals to the manometers are also shown.

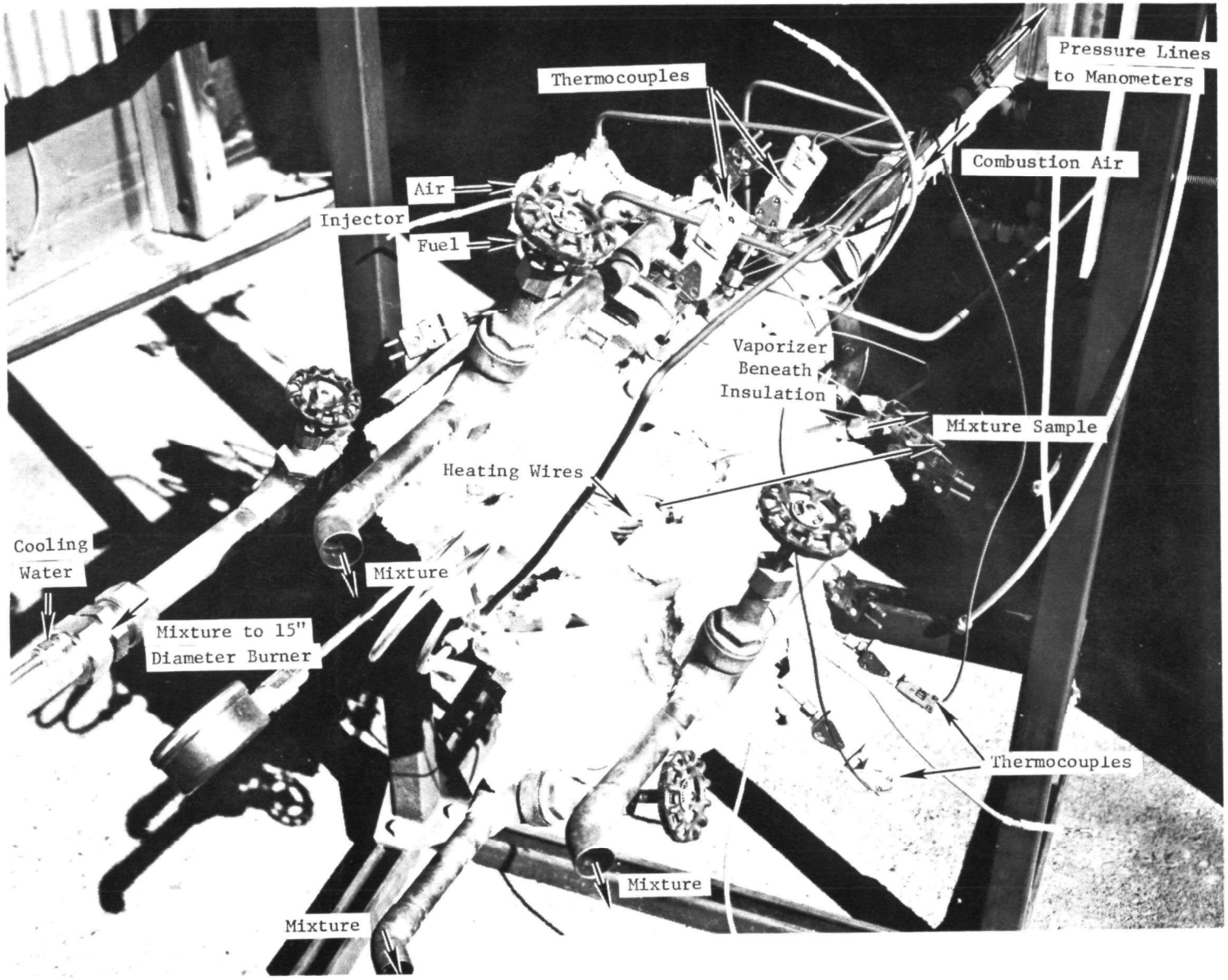

Figure 94. Vaporizer and Inlet and Exhaust Lines

Figure 95 is another view of the vaporizer. Shown on the figure are the heater wires around the simulated porous surface and on the downstream end of the test piece. Also shown are the mixture sampling ports located approximately 1.75 and 5.25 in. from the closed end of the simulated combustor surface. Samples were taken from the 1.75 in. location (open in the figure).

Shown in Figure 96 is the apparatus upstream of the vaporizer. Shown are the flow meters and pressure gauges for the fuel, injector air and combustion air. Pressure lines to the manometers are shown on the right. The injector air and combustion air heaters and insulated lines are shown in the lower part of the figure. The fuel tank and the pressurized ambient-temperature air line are shown at the lower left.

In order to analyze the fuel-air mixture in the vaporizer, a Scott Model 108-H Dilute Exhaust Emission Measurement System purchased by the General Electric Company was used. This console has provisions for measuring total hydrocarbons, NO, NO_2, CO, and CO_2.

Testing Technique - In order to measure the fraction of the fuel that was vaporized, two samples were taken through the total hydrocarbons analyzer, an isokinetic and a non-isokinetic sample. The former determines the total hydrocarbon content by sampling all of the mixture in a given streamline; the latter the amount of unvaporized fuel by allowing the vapor to spill out of the streamline because the sample is extracted at lower velocity.

In order to provide low pressures to the Scott analyzer because it was feared that the existing pressure regulator was not capable of with-

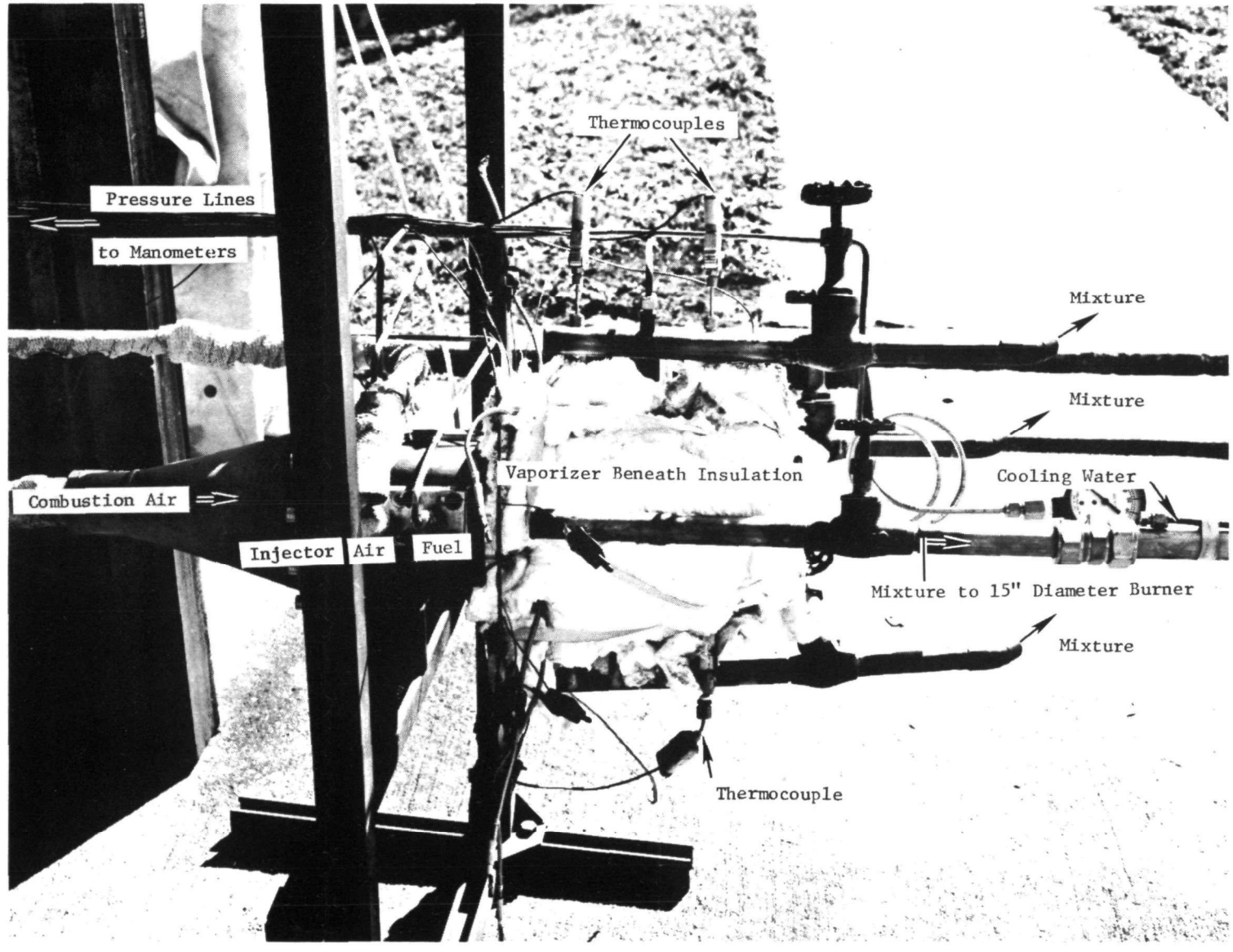

Figure 95. Vaporizer and Inlet and Exhaust Lines

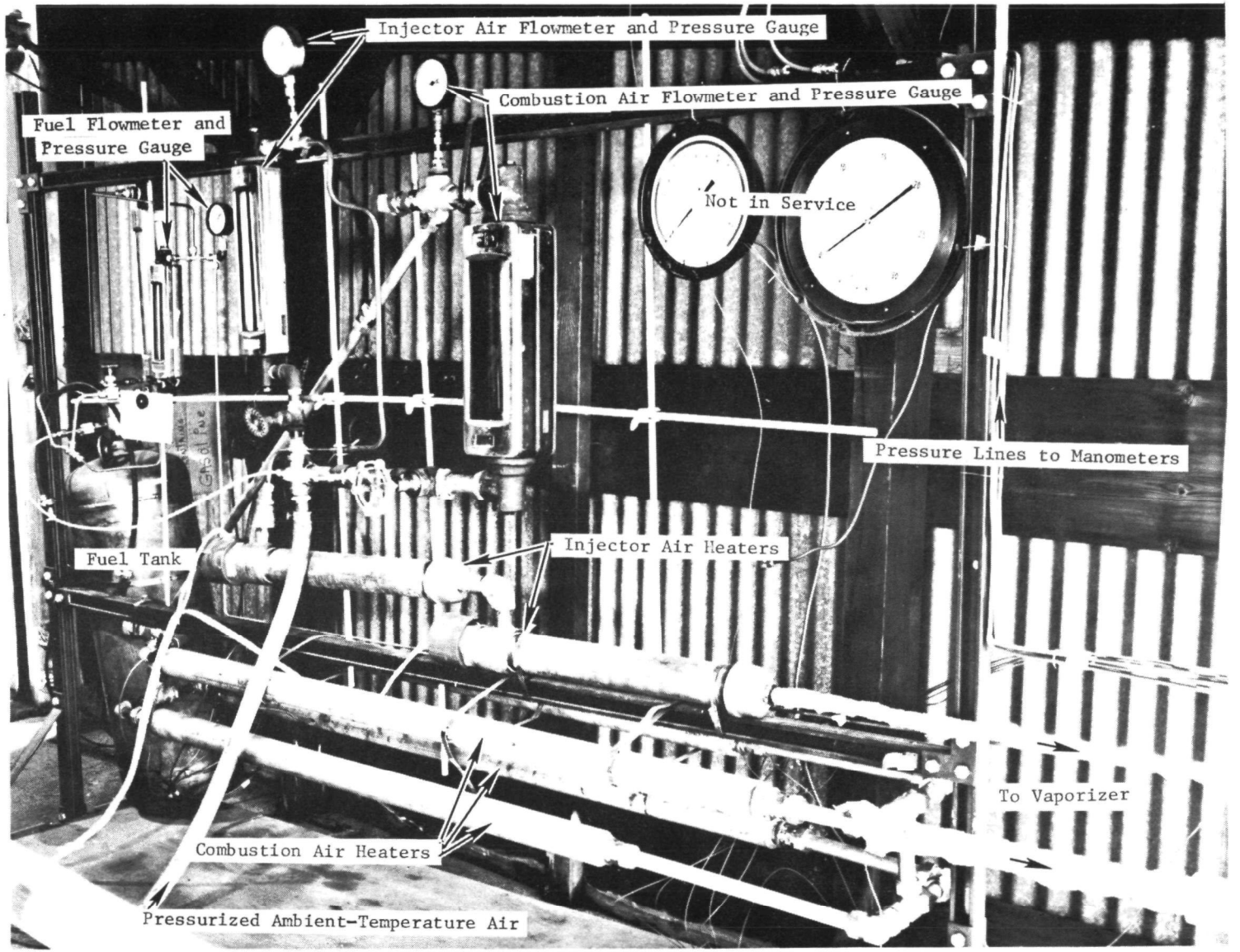

Figure 96. Vaporizer Air and Fuel Supply System

standing the full compressor discharge pressures, the combustor air was maintained at about 1 psig. It was assumed that the combustion air pressure effect on vaporization was small, and anticipated that this could be checked later. The injector air and combustion air temperatures and flow rates and the fuel flow rate were held at the conditions specified for each engine operating point.

Although the vaporizer outer diameter and closed end were insulated to prevent heat loss, the vaporizer heaters were not activated. All of the vaporization tests were run with the primary air louvers fully open, which gave the minimum amount of tangential swirl at each combustion air flow setting. The conditions tested, therefore, represented approximately the most severe expected as far as providing vaporization energy to the spray and heat from the combustion process were concerned.

Test Points - The points 1-6 for the fuel-air mixture supply simulate the six Federal Driving Cycle points in Table 1. Test points 7 and 14-18 simulate the steady speed mode:

Test Point	Vehicle Speed (MPH)
14	70
15	80
16	90
17	100
18	108
7	119

The operating conditions at steady state speeds of 30-60 MPH almost duplicated the conditions of test points 3, 4, 5, and 14.

Fuel flow rates of both 69 and 84 lb_f/hr were run under test point 7. The lower figure represents the most air flow (at R $\approx$ 0.8) which could be heated to the desired temperature. The higher figure represents the desired fuel flow rate at the maximum air temperature which could be achieved. For each of the test points, the injector air and combustion air temperatures were set approximately equal to the calculated compressor discharge temperature. For any given engine condition, an equivalence ratio of about 0.8 was set using the appropriate air and fuel flow rates. The vaporizer pressure was set at approximately 1 psig and the air pressure differential across the nozzle was varied to give a reasonable range of calculated mean droplet sizes. The injector air flow rates were those which resulted from the air pressure differentials.

Test Results - The test data are presented in Table 8 and plotted in Figure 97. In the figure the vaporization quality in percent is plotted against a group parameter similar to that of Graves and Bahr[10] and which relates all of the pertinent terms associated with spray droplet evaporation. The group parameter is:

$$B = \left(\frac{T_a}{1000}\right)^{4.4} \left(\frac{U_a}{100}\right)^{0.8} \left(P_i\right)^{-1.2} \left(\Delta P_f\right)^{0.42} \qquad (11)$$

where T_a combustor primary air inlet temperature, °R

U_a primary air velocity in mixing region, ft/sec

P_i pressure of air leaving injector, psia

ΔP_f equivalent fuel pressure drop through a 0.030-inch orifice, psi

The fuel pressure drop ΔP_f is the equivalent drop in the Graves and Bahr[10] apparatus. Most of the data fall between 93 and 99 percent of the fuel vaporized, although some data were as low as 87 percent. The data seem

Table 8. GAS TURBINE FUEL VAPORIZER TEST DATA

Test Point	Hr	W_α lb_f/hr	P_2 psig	T_1 °F	Wa_{tot} lb_a/hr	Wa/W_f -	R -	ΔP_{ai} psi	$SMD_{0.1}$ μ	Vap. %	1000 B -
1	1428	6.043	1.01	320	119.4	19.76	0.748	1.01	45	-	20
	1450	↓	1.00	310	↓	↓	↓	1.03	41	93.5	19
	1500	5.944	1.15	286	128.7	21.66	0.683	9.26	1	95.3	68
2	1003	10.01	1.09	176	189.5	18.93	0.781	3.83	1	-	50
	1040	↓	1.01	177	187.7	18.76	0.789	2.28	25	96.5	15
3	1054	11.94	1.01	175	221.4	18.54	0.798	3.05	22	97.9	19
4	1117	12.88	1.07	164	241.5	18.75	0.789	3.51	21	93.9	18
	1125	↓		↓	↓	↓	↓	0	∞	90.8	0
	1135	↓	↓	↓	↓	↓	↓	3.51	21	87.7	18
5	1234	15.85	1.22	177	292.1	18.43	0.802	4.72	23	94.8	22
6	0943	64.99	0.84	237	1210	18.62	0.794	17.7	97	96.8	61
	0955	↓	0.85	241	1215	18.70	0.791	24.4	26	97.0	105
7	1407	69.25	1.00	411	1234	17.81	0.831	22.9	80	94.6	176
	1438	↓	1.15	390	1330	19.20	0.770	22.6	100	96.3	154
	1448	↓	1.10	401	1282	18.52	0.799	29.5	23	97.3	280
	1458	↓	1.15	393	1307	18.88	0.784	15.4	∞	96.3	0
	1507	84	1.16	376	1366	16.26	0.910	21.2	∞	93.7	0
14	1320	30.71	2.18	269	518.3	16.88	0.876	9.60	23	97.1	59
	1334	↓	2.18	267	523.2	17.04	0.868	14.9	9	99.0	87
15	1352	38.73	3.68+	300	680.4	17.98	0.823	12.3	29	93.8	77
		↓		312							
	1403	↓	3.42	314	695.6	17.96	0.824	19.9	9	94.5	128
16	1020	48.05	0.56	323	915.2	19.05	0.777	15.2	30	97.1	131
	1037	47.75	0.57	321	908.3	19.02	0.778	20.5	14	97.1	174
	1047	↓	0.58	316	932.0	19.52	0.758	24.1	10	97.2	199
	1057	↓	0.56	323	897.5	18.80	0.787	9.65	∞	95.8	0
17	1130	58.94	0.76	354	1024	17.38	0.851	17.4	125	97.1	96
18	1154	69.25	1.04	373	1269	18.31	0.808	21.8	130	-	125
	1315	68.85	1.01	367	1221	17.73	0.834	23.3	85	90.4	137
	1332	↓	0.94	377	1189	17.27	0.856	30.8	18	87.4	258
	1340	↓	1.01	371	1219	17.71	0.835	15.1	∞	88.3	0

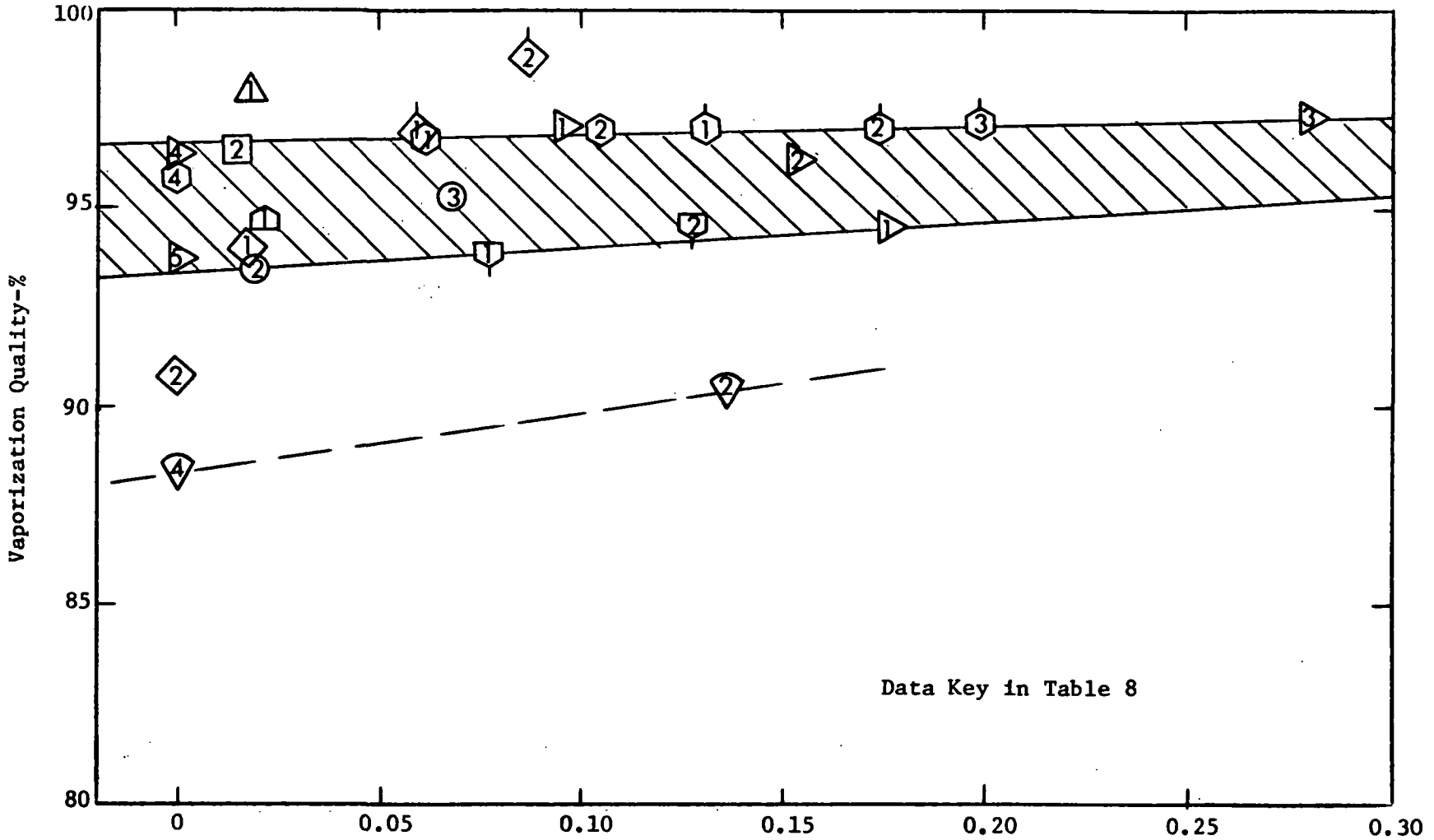

B Group Parameter $B = \left(\frac{T_1}{1000}\right)^{4.4} \left(\frac{U_1}{100}\right)^{0.8} \left(P_2\right)^{-1.2} \left(\Delta P_f\right)^{0.42}$

Figure 97. Experimental Vaporization Quality as a Function of the B Group Parameter

to fall in a band which increases in vaporization quality as the group parameter B increases, indicating the correct influence of the individual variables in the parameter. Except for some extraneous points it appears that the fuel mixing device developed produces a mixture with a high degree of vaproization.

POROUS PLATE COMBUSTOR FABRICATION DEVELOPMENT

Introduction

The basic combustor material considerations are that the material must: (a) have structural and chemical stability at the maximum-use conditions which includes the temperature of use and the ability to withstand the anticipated thermal cycling, (b) be suitable for fabrication into the desired design for the engine, (c) be compatible with other materials of the engine design, and (d) be economically feasible for mass production as a combustor component.

The materials which are presently available and feasible for use in a porous combustor for an automobile gas turbine are outlined in Table 9, which shows the usable temperature range and the reasons for the temperature limitation. The final resolution of material selection will require more detailed test data than are available at the present, both from the design requirements and from material behavior measurement.

These material considerations are outlined below in more detail in terms of the metals and the ceramics. Most of these are available commercially but need more detailed crucial laboratory tests to more accurately define the behavior characteristics for this porous combustor application. The initial selection for detailed development was a com-

Table 9. POROUS COMBUSTOR MATERIALS

Material	Probable Use Temp. °F	Limitations
Ni Alloys	1600-1800	Sintering, Oxidation
Fe-Cr-Al Alloys	1800-2200	Oxidation
Al_2O_3-SiO_2 Glass Fibers	1700-1900	Sintering[a], Devitrification[b]
SiO_2 Glass Fibers	1800-2000	Sintering[a], Devitrification[b]
SiC	2200-2700	Oxidation[c]
$3Al_2O_3$-$2SiO_2$	2400-2700	Sintering
Al_2O_3	2400-3000	Sintering
ZrO_2	2400-3200	Sintering

a. Sintering of glass structures is obviously a liquid phase phenomenum and may be accelerated by pressure due to contact surface increase as a result of plastic deformation at the higher temperatures where the viscosity is decreasing.

b. Devitrification is simply crystallization of the glass(which is, of course, a supercooled liquid) with the result in loss of glass fiber structure.

c. The oxidation of SiC is complex because of the presence of fuel and air which means that SiC, SiO, SiO_2, hydrocarbons, H_2, H_2O, (OH), CO, CO_2 and O_2 are all present. This could mean, for example, that if the SiO species is formed in preference to CO, there may be a high rate of oxidation at temperatures above 2400°F. Also, the oxidation of SiC also can conceivably cause loss of permeability due to pore blocking by the SiO_2 formed. The resolution of this problem probably will depend on measuring the oxidation kinetics in the various temperatures of interest.

bustor using a silicon carbide (SiC) burner face backed with mullite ($3\ Al_2O_3$-$2SiO_2$) to provide the necessary thermal insulation to keep the temperature of the cold side of the burner (which faces the incoming fuel-air mixture) below the ignition temperature. However, after limited testing of commercially available materials in radiation-cooled burners, it became obvious that additional cooling was required at higher loading and that an air-cooled design was essential which would have to be based on a metal system; the preignition tests which lead to the air-cooled design were described earlier.

Metals

The candidate alloys for combustor components are shown in Table 10, which lists compositions of both the Ni-base alloys and the Fe-Cr-Al alloys. These listed alloys were selected primarily on the basis of their excellent oxidation resistance at elevated temperatures. For the stainless steels, in which chromium is the only alloying element, a generalized relationship has been established between the Cr content and the maximum use temperature in standard combustion gases. This relationship is shown in the following tabulation:

% Cr	Max. Service Temperature in Combustion Gases, °F
0	1050
4	1200
8	1300
12	1400
16	1450
20	1650
24	1900
28	2100

Table 10. CANDIDATE ALLOYS FOR COMBUSTOR COMPONENTS

ALLOY	CRYSTAL STRUCTURE MATRIX	COMPOSITION, % Fe	Cr	Ni	Co	Mo	W	Al	Ti	Si	Y
AISI 442	BCC	Bal	20	-	-	-	-	-	-	-	-
AISI 446	BCC	Bal	27	-	-	-	-	-	-	-	-
GE-1541	BCC	Bal	15	-	-	-	-	4	-	-	1
Hoskins 875	BCC	Bal	23	-	-	-	-	6	-	-	-
Armco 18SR	BCC	Bal	18	-	-	-	-	2	0.4	1	-
AISI 310	FCC	Bal	25	20	-	-	-	-	-	-	-
Incoloy 800	FCC	Bal	20	32	-	-	-	0.4	0.4	-	-
Inconel 601	FCC	14	23	Bal	-	-	-	1.4	-	-	-
Rolled Alloys 333	FCC	18	25	Bal	3	3	3	0	-	1.2	-
Hastelloy X	FCC	19	22	Bal	1.5	9	0.6	-	-	0.5	-
Kanthal A-1		Bal	22	-	0.5	-	-	5.5	-	-	-

On this basis, the recommended maximum service temperatures under cyclic conditions for AISI 310 SS (24Cr-20Ni) and AISI 446 SS (27Cr) have been reported as 1900°F and 2100°F, respectively.

Significant improvement in oxidation resistance of iron-chromium and nickel-chromium alloys can be achieved by the addition of Al or Al and Y (yttrium) as exemplified by the 1541 iron base alloy developed by General Electric and the nickel-base Inconel 601 alloy (Table 10). In the Fe-Cr-Al system, one of the main advantages of increased Cr content is to reduce the amount of Al required for the selective oxidation to form the protective Al_2O_3 film; 15-25% Cr has been found to be optimum.[11] A minimum of 2% Al is required to produce the Al_2O_3 layer in the 15-25% Cr-Fe alloy. Al content above 5% result in alloys that are brittle and difficult to fabricate. It was found that additions of yttrium to Fe-Cr-Al alloys result in improved oxidation resistance under cyclic conditions because of increased oxide adherence. The mechanism by which yttrium improves oxide adherence has been postulated that it may result from subscale formation of Y_2O_3 which either promotes sintering of the surface oxide Al_2O_3 or provides a locking affect for the surface oxide. A form of a locking mechanism of the surface oxide layer by a uniform network of internally penetrating oxides has also been suggested as playing a role in achieving the excellent oxidation resistance in the Al containing nickel base alloy Inconel 601.[12] Spalling resistance of the oxide layer is credited to the similar coefficients of thermal expansion of the alloy and the surface oxide.

The oxidation resistance of the Fe-Cr-Al-Y alloys is such that a 0.020 inch thick sheet can resist destructive oxidation for more than

2000 hours at 2300°F, 1400 hours at 2400°F, and 400 hours at 2500°F. The Fe-Cr-Al-Y alloys are as oxidation resistant at 2300°F as the nickel base non-aluminum containing Hastelloy X is at 2000°F. The use of nickel base alloys requires that they be resistant to hot gas corrosion due to sulfur containing environments. For this reason, it is necessary that the Cr content be in excess of 15%. Hastelloy X (22% Cr),for example, shows rather good resistance to hot gas corrosion. However, high Cr plus aluminum additions (Inconel 601) provides still further improvement to hot gas corrosion.

The strength properties of the ferritic (BCC) stainless steels and the more oxidation resistant ferritic iron base alloys at temperatures approaching 2000°F are very low (Table 11). If strength requirements for the structural components exceed the limits of the ferritic iron alloys, it will be necessary to utilize the higher strength austenitic (FCC) iron or nickel base alloys. It is well known and documented that the face centered cubic lattice (FCC) is more resistant to creep than the body centered cubic lattice. Limited testing data on these Fe-Cr-Al alloys are shown in Figure 98 for typical oxidation curves at temperatures of 2000°F to 2600°F, and loss in permeability of porous plates at 1800°F and 2000°F shown in Figure 99.

Ceramics

The most promising ceramic materials for the porous combustor are SiC as the burner face and mullite as an insulator immediately adjacent to the SiC. The crucial thermal properties of these and other potential ceramic materials are shown in Table 12. Since high thermal conductivity and low thermal expansion improve resistance to thermal shock, the selection of SiC is obvious. This selection is further supported by the high emittance factor which enhances radiation heat transfer. The choice of

Table 11. TENSILE PROPERTIES OF CANDIDATE ALLOYS FOR COMBUSTOR COMPONENTS

	TENSILE PROPERTIES			
Alloy	Temp., °F	0.2% Y.S., ksi	Ult, ksi	El, %
AISI 446	RT	51.5	83.0	29.0
	1800	-	2.9	-
	2000	-	1.5	-
GE-2541	RT	50.8	76.7	14.0
	1800	2.2	3.5	135.0
	2000	1.2	2.0	154.0
	2200	1.0	1.8	161.0
Armco 18SR	RT	65.0	85.0	29.0
	1800	-	2.0	-
	2000	-	1.1	-
AISI 310	RT	36.5	84.0	50.0
	1800	8.0	14.0	52.0
	2000	5.0	8.0	35.0
	2200	3.0	6.0	35.0
Incolor 800	RT	47.7	87.7	42.0
	1800			
	2000			
RA 333	RT	50.0	100.0	50.0
	1800	15.4	18.4	53.0
Inconel 601	RT	49.0	107.0	45.0
	1800			
	2000			
Hast. X	RT	52.2	114.0	43.0
	1800	16.0	22.5	45.0
	2000	8.0	13.0	40.0
	2200	3.7	5.4	31.0

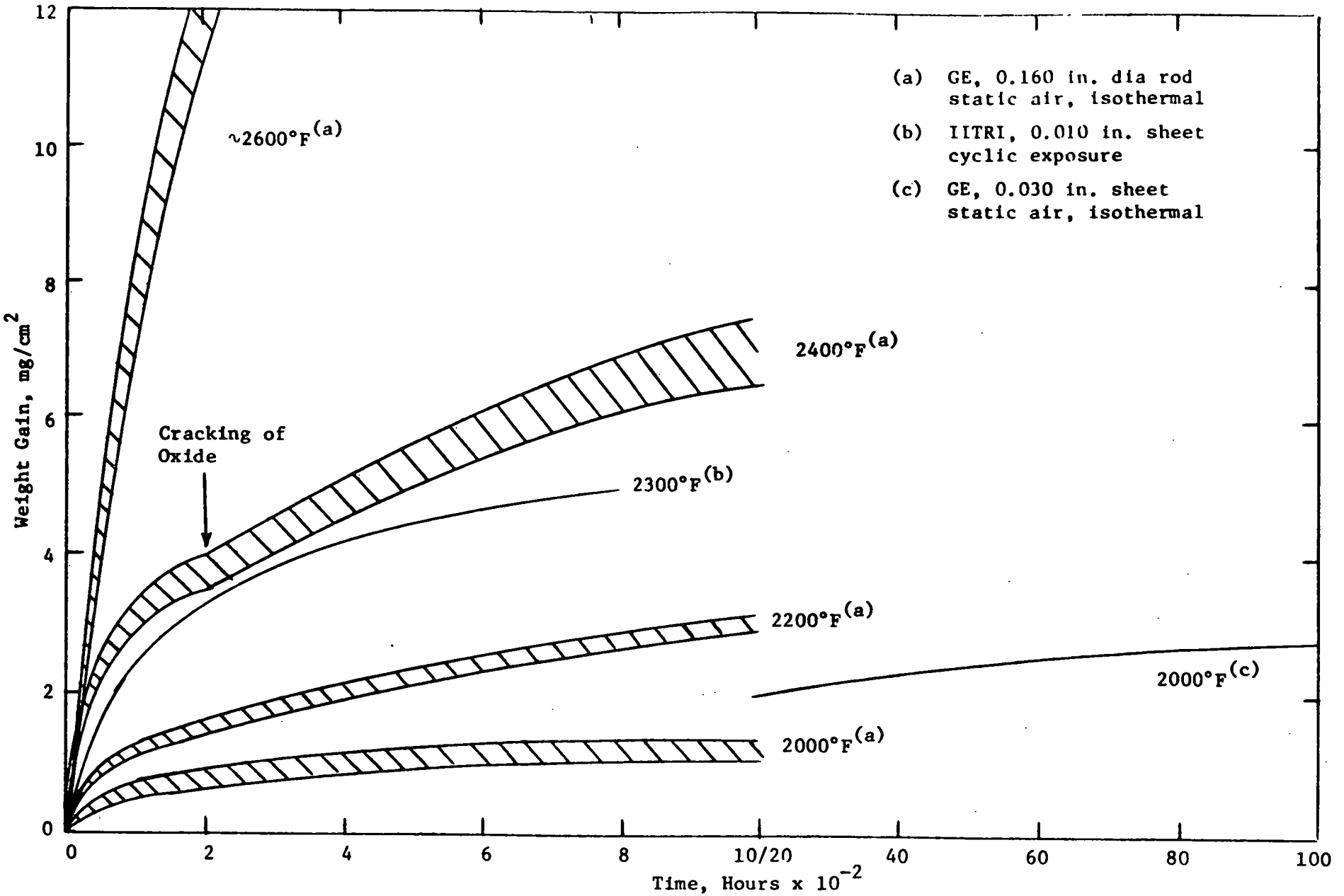

Figure 98. Weight Gain of Fe-25Cr-4Al-Y Alloy During Oxidation Testing in Air

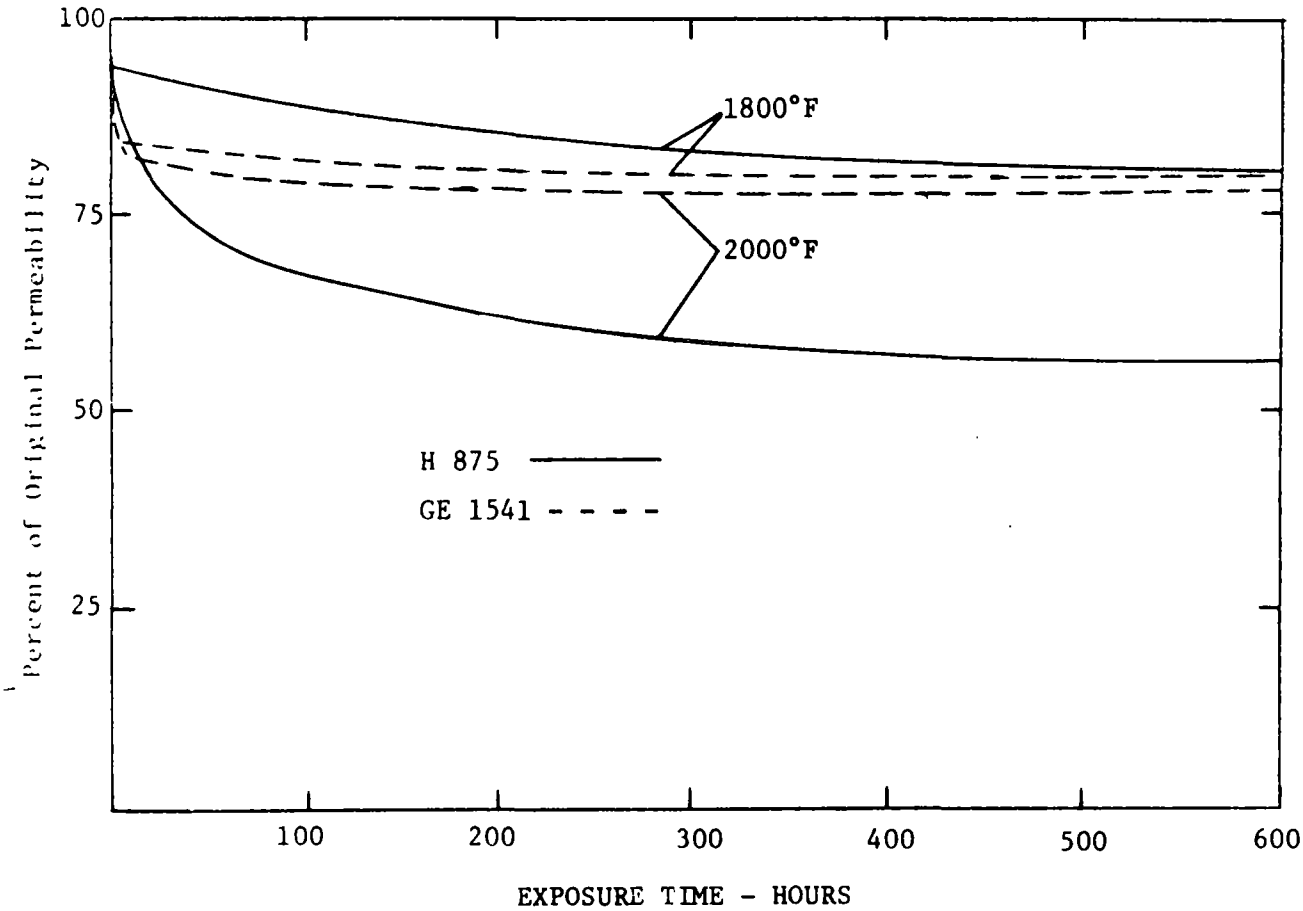

Figure 99. Poroloy Permeability Retention After Exposure at 1800 and 2000°F (982 and 1093°C) in Air. Alloys GE 1541 and H 875[13]

Table 12. CRITICAL THERMAL PROPERTIES OF SELECTED CERAMICS

MATERIAL	THERMAL CONDUCTIVITY IN BTU/(hr)(ft)(°F) 200°F	2000°F	THERMAL EXPANSION COEFFICIENT x 10^{-6}/°F (to 2000-2200°F)	NORMAL TOTAL EMITTANCE AT 2200°F
Al_2O_3	18	3.4	5.0	0.41
MgO	35	3.5	8.8	0.3
ZrO_2	1.0	1.0	6.7	0.5
ZrO_2-SiO_2	3.8	2.5	3.1	
SiC	90	10	2.7	0.85
$3Al_2O_3$-$2SiO_2$	3.5	2.4	2.9	0.6

mullite as an insulator for SiC is based on (a) the close match of thermal expansion plus (b) the fact that SiC forms SiO_2 upon oxidation and the film of this material will bond the SiC to $3Al_2O_3$-$2SiO_2$. It is to be noted, however, that the possibilities of using mullite alone or the use of Al_2O_3 may become economically attractive by using a Cr_2O additive to increase the emittance factor.

The thermal stability of SiC at very high temperatures may impose undesirable limitations on its use as a porous combustor as compared to, for example, Al_2O_3. The oxidation of SiC is not known in sufficient detail to make an accurate prediction at this time. For example, the published data on oxidation[14,15] are not readily applicable to the porous combustor because these data were measured on powders of unknown ratios of surface area to volume. As noted in Table 9, there is need for more detailed test data to apply to this specific application.

The readily available fabricated ceramic materials which were used entirely or in part to construct porous combustors for testing are as follows:

1. ZrO_2 (Y_2O_3 stabilized) cloth is made by Union Carbide Corporation. This material is reported to be made by saturating an organic fiber cloth with suitable zirconium - yttrium salts and then thermally removing the organic accompanied by converting the zirconium-yttrium salts to the oxides. Initial tests on this material show that it begins to become stiff after about one hour at 2400°F, suggesting that sintering and/or crystallite growth is occurring.
2. SiC - mullite porous combustor plates are available from sources such as Rex Radiant. These plates are about 1/8" of SiC bonded

to about 1/2" of mullite. Both substances are of about 16 mesh particle size, probably bonded with some Al_2O_3-SiO_2 substance. Heating to 2600°F for 4 hours shows an increase in grain-to-grain bond.

3. Porous SiC-bonded SiC cylinders are available from the Norton Company. Tests on the cylinders have resulted in fracturing presumably because of non-uniformity in the porosity and/or non-homogeneity in fuel injection; however, limited testing of 1/4" rings shows no evidence of fracture.

4. Porous Al_2O_3-SiO_2 cylinders are available from Coors Porcelain Company. Initial tests were on a "P-6" type porosity which has a $1Al_2O_3$-$1SiO_2$ composition with a thermal expansion similar to Al_2O_3.

In addition to the above, limited studies were undertaken to develop porous ceramic parts of SiC and Mullite in which four fabrication approach were considered. The first technique studied was to use coarse particles of SiC and of mullite made from fine grained powders. These particles are composed of fine grains (i.e., generally below 10 microns); this composition gives much higher strength than the commercially available single crystal particles (such as Rex Radiant uses in their porous combustor). A second approach was to use a volatile organic particle in fine grain compacts to produce the desired porosity. This process will result in a fine grain structure of optimum strength for the high porosity. A third method was to use large single crystal particles and sinter these much the same as the Rex Radiant porous material. The reason for this latter approach was that there may be a porosity loss in use because of sintering at the use temperature which will be minimized by the large grains. A

fourth possibility was to use a material with high emissivity for radiation heat transfer, for example, one of the above ceramics incorporating a high emissivity material such as chromium oxide (Cr_2O_3) or cerium oxide (CeO_2).

However, porous metal materials for combustors were selected as the main effort when it became obvious heat removal by cooling air was essential. Initially these were commercially available alloys in a sheet or plate form. Subsequently, the most crucial work was directed to fabrication of porous metal combustors with air cooling tubes using 80Ni-20Cr powders and 310 stainless steel tubes.

Fabrication of Porous Air-Cooled Burner

The initial porous-plate air-cooled burner designed for development tests was 2.25 inches in outside diameter and 1.25 inches in inside diameter and 6 inches long with 24 coolant tubes 0.125 inch in diameter imbedded on the surface of the inside wall of the porous surface. The porous-plate material was 80% Ni-20% Cr alloy in the form of coarse powder in a particle size range of 25 to 50 mesh which was procured as the only readily available powder in this size range. By making sample pieces, it was found that coarse particles could be sintered in hydrogen at 2400°F to form a soft porous surface. The mixing of 5 to 10 percent of GE-81 braze material with powder was found to improve the strength of the sintered plate and permitted the use of a lower sintering temperature.

A total of nine porous cylinders of approximately the aforementioned dimensions were made and tested on this program. Problems that had to be solved included mold design to minimize the effects of differential expansion between mold and part, mesh size, elimination of density variations in the porous structure by vibration of the mold during filling,

the choice of the correct proportion of braze powder to be added, uniformly mixing the braze powder with the powdered metal. Shown in Figure 100 is the sixth porous cylinder after sintering. Some disproportionate braze distribution areas can be seen on the surface. Shown in Figure 101 is the same porous cylinder with the tube sheets brazed on. This porous combustor (No. 6) was fabricated with an outer diameter increased to 2.50-inches and the 27 coolant tubes located on a 2.125-inch diameter ring so as to be imbedded in the 0.375-inch thick frit wall. This required a new mold design with the 27 coolant tubes held in position by temporary tube sheets of GE-1541 alloy which was pre-oxidized to prevent bonding to the porous material. The coolant tubes were coated with braze to improve the bond with the porous material. The -35 mesh NiCr powder was pre-treated in hydrogen at 2000°F to reduce the oxygen content and improve sinterability and then mixed with 5 percent of GE-81 braze. This assembly was initially sintered at 2300°F and after removal from the mold was resintered at 2370°F for 4 hours. The dimensions of this porous-plate unit were 2.45-2.80 inch outside diameter, 1.70-inch inside diameter, with a wall thickness of 0.35 to 0.40-inch. Radiographic examination of this porous cylinder revealed that considerable improvement in uniformity of density was achieved by vibrating the mold during loading of the NiCr powder, although some layering effect was noted as a result of incremental additions of the powder. This cylinder was fitted with tube sheets and the joints were brazed at 2250°F using GE-81 braze powder.

COMBUSTOR CONFIGURATION AND ENGINE INTEGRATION DESIGN

The accomplishments on the several tasks described above have produced results which can be synthesized into a porous-plate burner design

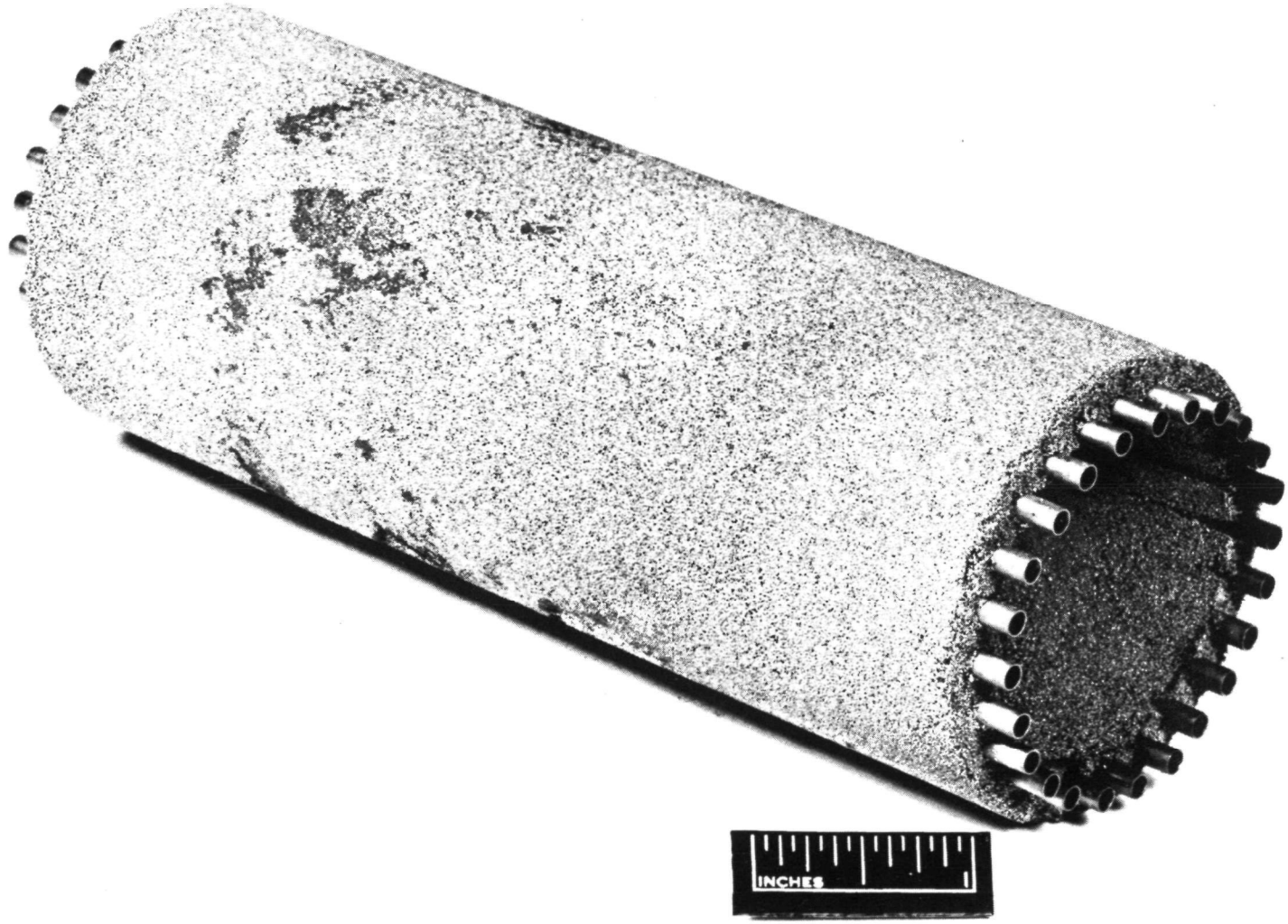

Figure 100. Nichrome Porous Cylinder No. 3 As Sintered at 2350°F

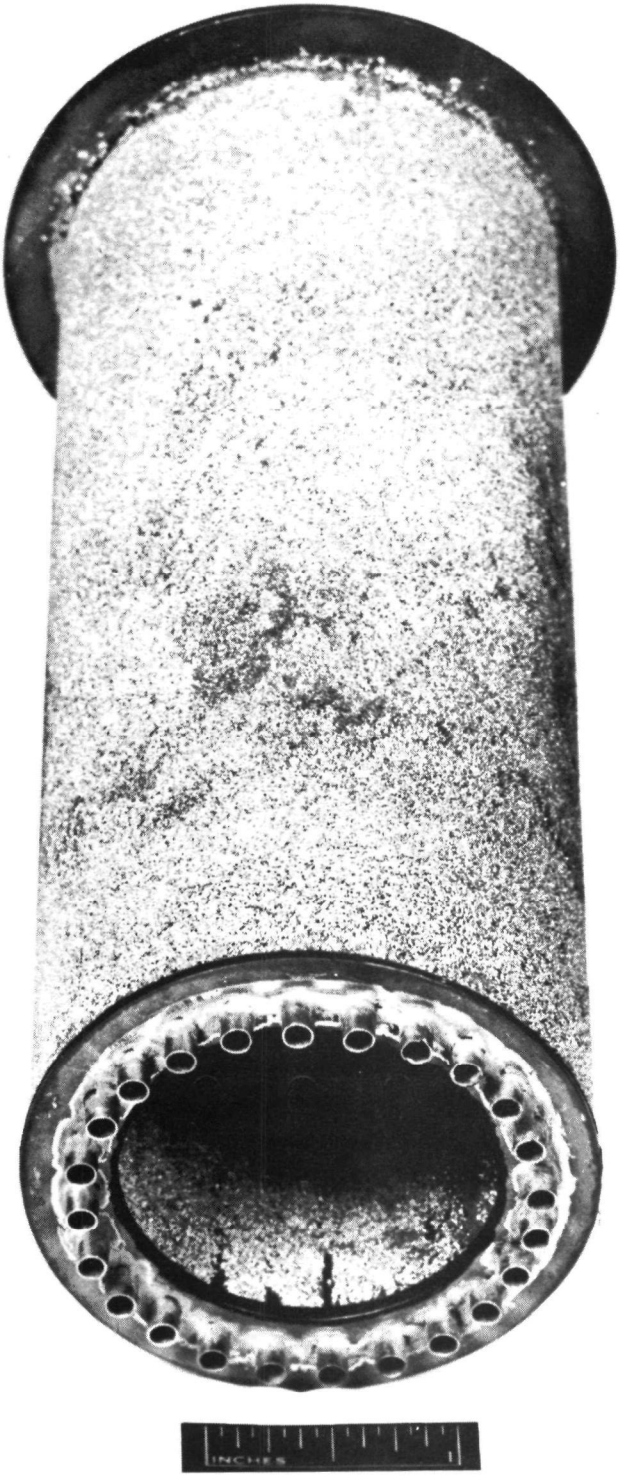

Figure 101. Porous Cylinder No. 3 With Tube Sheets Brazed on Each End

concept for the Base Line Engine. An important result stemming from the Combustor Loading and Emission Analysis is that the porous plate area must change from 1.15 ft^2 for operation along the vehicle level road-load line to 2.2 ft^2 for wide open throttle accelerations in order for the combustor to operate between values of superficial velocity (V_{25}) which correspond to flame extinguishment and to lift-off at the two limits. During such operation, the equivalence ratio must be varied to help limit superficial velocity and to limit porous-plate hot side temperature within the temperature capabilities of available porous materials. Because of the excessive heat flux conducted back to the porous plate from the flame at elevated pressure levels (4 atm.) which heat results in surface temperatures beyond available material limits, it is necessary to cool the burner porous plate by means of embedded air-cooling tubes. The thermal stresses in the air-cooled porous material must be reduced for part integrity by employing a series of flat plates instead of a hollow cylinder. Adequate fuel atomization and vaporization can be obtained by spraying the fuel into compressor discharge-temperature air with an air-assisted nozzle while at the same time avoiding preignition of the fuel. Emission testing with propane indicated that NO_x emission index values were below the Federal Standards. CO emission index values were below the Federal Standards at superficial velocity (V_{25}) levels corresponding to low engine load and slightly above at conditions corresponding to high loads. The unburned hydrocarbon emissions were barely detectable and, therefore, adequately low. Prompted by these results, a design concept for a porous-plate combustor for the Base Line Engine was formulated and is described below.

Combustor Conceptual Design

Figure 102 illustrates the air-cooled porous plate burner concept which is proposed for application to the gas turbine Base Line Engine. Figure 102 was prepared using a drawing of the Base Line Engine. The porous plate combustor shown extends vertically above the engine center line only 2 inches more than the standard combustor for this engine and provides the full 2.2 ft^2 of porous-plate surface required for wide open throttle acceleration. The flat-plate porous burner elements made of sintered nichrome are grouped in five rings of V-shaped burners arranged inside a circular shell which is enclosed within the combustor outer casing. Passages for the flow of primary air,bled from the compressor discharge, and of secondary air from the regenerator discharge are provided in the annular space between the burner support shell and the outer casing. Primary air entering the top of the combustor is admitted through sixteen controllable (on-off) butterfly valves to the vaporization tubes. In each of the vaporization tubes, an air atomizing fuel nozzle is located immediately downstream of the air valve. Vaporization and fuel-air mixing occur during passage of the fuel and air down the length of the 6-inch vaporization tubes. The fuel is vaporized in these tubes by heat from the primary (compressor discharge) flow and from the secondary flow (regenerator discharge) which surrounds the vaporization tubes. At the end of these tubes, the fuel air mixture reverses flow direction and passes down channels formed between the V-shaped burners and the burner support shell. From these channels the fuel-air-mixture flow is admitted to the upstream faces of the porous burners.

Secondary air flowing oppositely to the primary air passes between the vaporization tubes and is admitted to the porous burner cooling tubes.

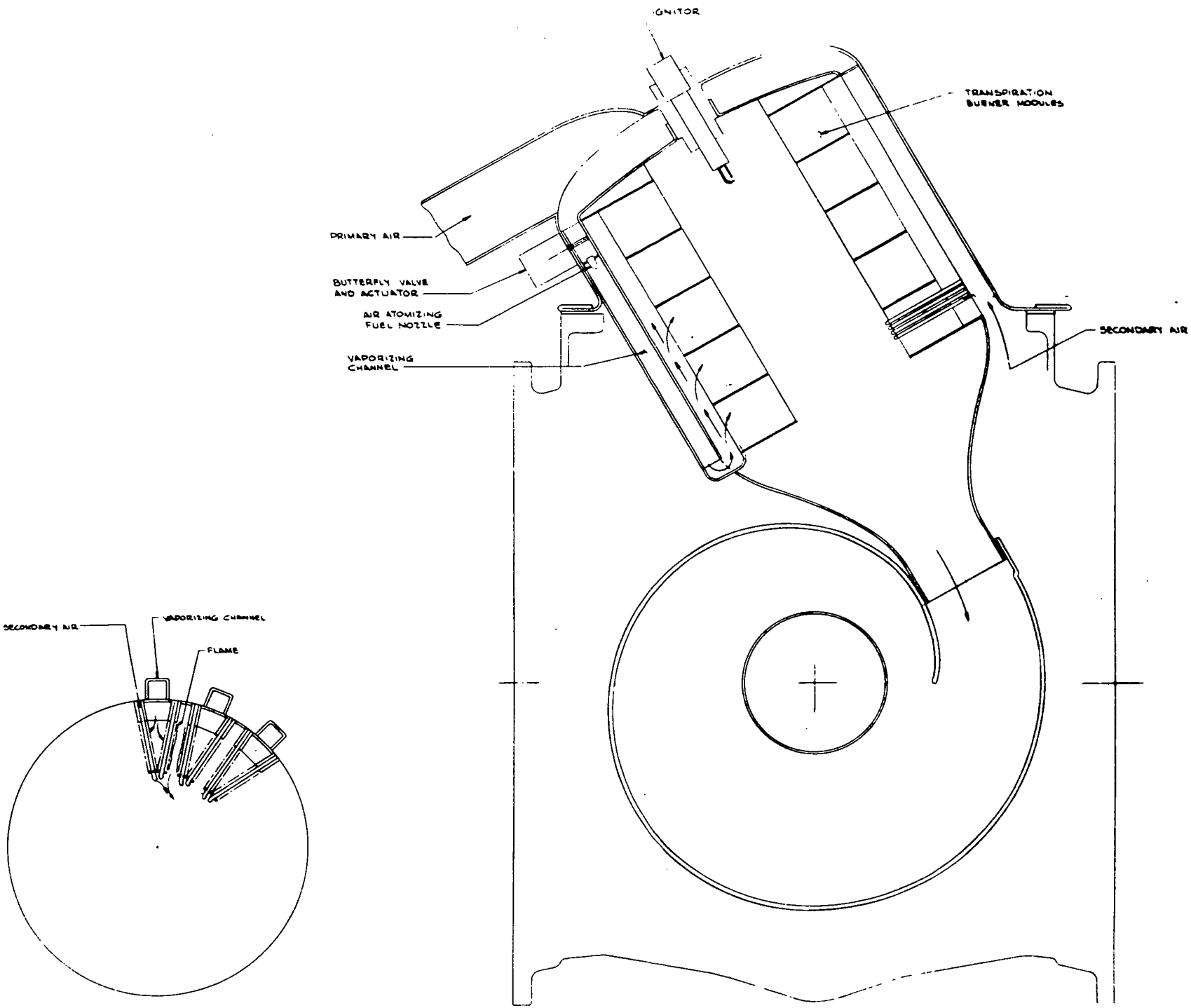

Figure 102. Air-Cooled Porous-Plate Burner Concept

The V-shaped burners are axially segmented into short sections which are sealed by end plates. This prevents severe distortion under the radial temperature gradient existing in the burner porous surfaces. All of the burners in a given line are attached to the sides of one of the fuel-air mixture distribution ducts.

Burning occurs on the outer surfaces of the wedge-shaped burners in the space between opposing burners. Power modulation involves variations in air flow rate and equivalence ratio and in addition involves shutting burners on and off by means of the butterfly air valves. Only the most extreme transient operating condition requires all burners in operation. Non-operating burner surfaces continue to be cooled by secondary air flow through the embedded tubes, and thus serve as radiation heat sinks for the opposing operating burners.

Because of the short length and close spacing of the embedded air-cooling tubes the cooling effectiveness will be quite high. Since this burner concept employs both radiation and air cooling, the surface will run cooler than the values reported in the Section on Loading and Emission Analysis.

Combustor Concept Development

As reported above, cylindrical porous nichrome burner models with embedded air-cooling tubes have been run, mostly at one atmosphere, and have indicated favorable emission results. It is expected that the use of flat plate segments instead of complete cylinders of porous material will alleviate the cracking problem experienced at elevated pressure levels where the heat release rates are increased over the atmospheric case. The sintering parameters must be optimized and the joining methods must be specified which will assure a good product.

The design concept shown in Figure 102 has the flexibility of varying the active area of the burner in eight steps between 1.15 ft^2 and 2.2 ft^2 or in as few as one step. This flexibility will be useful in transient operation because when more than half of the burner area is being used at least some of the wedge-shaped segments will have no radiation sink. By controlling the active area and the equivalence ratio, the superficial velocity (V_{25}) can be made high enough so as to limit the heat flux back to the porous plate to a value that can safely be removed by cooling air alone. This, of course, will have to be balanced against the increase in NO_x because of the smaller reduction in flame temperature.

It is desirable to use regenerated air instead of compressor air for the primary flow from the standpoint of engine fuel mileage. In previous work[16] an analysis of an engine with and without regenerator bypass for the combustor primary air flow was made for the case of a constant equivalence ratio of 0.9. For the Federal Driving Cycle the fuel mileage values with and without regenerator bypass were 10.6 and 12.8 mpg. There is some evidence, for example[2,3] that the atomization and vaporization of gasoline can be carried out in a time interval smaller than the ignition delay using regenerator air, thus eliminating the regenerator bypass. A compromise would be mixing compressor and regenerator discharge flow for the combustor primary flow, thus reducing the fuel mileage penalty without using an extreme temperature that might lead to preignition. For the porous-plate combustor, since the flame temperature is set by the superficial velocity (V_{25}) independent of the burner inlet temperature, no adverse effect on NO_x emission index would be expected with the elevated primary air temperature.

Another means for improving fuel mileage is to use advanced sintered materials having higher operational temperatures. By so doing, the equivalence ratio of the burner could be increased, thereby reducing the regenerator bypass; this bypass could be zero, in the limit. To utilize materials with higher operational temperatures than nichrome, materials processing methods must be worked out which avoid producing the protective oxide coating of the sintering material before sintering.

In light of the present status of the air-cooled porous plate burner for the gas turbine automobile engine, it is important to fabricate a full-size combustor and test it on gasoline over the expected operating range it would have in the Base Line Engine. Because of at least partial success with the nichrome air-cooled burners, nichrome should be utilized in the full size burner. This will require finalizing the sintering parameters for this material and establishing the joining techniques to be used between the porous material and the remainder of the combustor structure.

RANKINE CYCLE COMBUSTOR

DISCUSSION

When any fuel is burned with air, some nitric oxide is almost inevitably formed in the hot product gases; of the contributors to air pollution from combustion processes, it may be the most difficult to eliminate or control. The principal mechanism of its formation is that of the hot-air reaction; and until recent years, this was thought to be the only important process. It is now known that in some circumstances NO can evidently be made in hydrocarbon-air flames by other processes[7,17] and in amounts that are significant in terms of the low source emission goals now established.

The main problem in NO_x reduction is still that of controlling the high temperature ("thermal or hot-air") production of NO. The rate of the process unfortunately becomes appreciable just in the range of burned gas temperatures common to most combustion processes. It has a very large temperature dependence; the rate is approximately doubled by a 90°F increase in temperature so that any preheating (for example, by precompression in an engine cycle) drastically increases NO_x emissions. Conversely, any effective scheme for reduction of the maximum temperature, as well as the residence time at that temperature, can result in substantial decrease in NO_x emission, for which various approaches have been conceived and are being pursued.

The work described here is based on one such idea: limiting the

maximum temperature of a premixed flame by heat removal from the unburned gas, in effect, before the mixture is burned, so that it is equivalent to precooling the mixture. The concept is derived essentially from the cooled porous-plug burner or flameholder, first investigated by Botha and Spalding[5] and by Kaskan[6]. Burners of this kind have since been used extensively in flame studies, and have also been applied in various forms in practical combustion devices.[18,19,20] The background and rationale of the concept were discussed above.

For the combustor boiler in a Rankine-cycle automotive engine, the porous plate combustor is attractive for three general reasons:

1. It appears certain to be readily controllable to yield products low in NO_x and hydrocarbons and acceptable in CO content.
2. It is conceptually well matched to such a cycle, since its required coolant can simply form part of the working-fluid path, with complete recovery of the heat necessarily absorbed by the burner prior to its passage to the boiler.
3. Although it requires a reasonably uniform premixture, the preparation of the fuel-air mixture in this application should be fairly straightforward.

The approach taken is a combination of analytical and detailed experimental work to determine the feasibility of the porous-plate combustor for the Rankine Cycle engine. Furthermore, since the porous-plate combustor requires the fuel and air to be premixed, concepts of a fuel vaporizer were examined.

It was the purpose of the work described here to examine experimentally porous plate combustion particularly with respect

to emissions, and to obtain test data that is relevant to the design of this combustor for a Rankine Cycle engine. Preliminary designs of both the combustor and the vaporizer suitable for the Rankine Cycle were first made.

While the approximate distribution of heat absorption between the burner and the rest of the boiler system can be roughly estimated from available data, it is desirable to determine this with some accuracy for the anticipated range of flame conditions. Many such burner heat flux measurements were made for this purpose, as well as for indirectly estimating or checking the actual burned gas temperature.

Further, measurements of oxides of nitrogen, carbon monoxide, and unburned hydrocarbons were made over the range of operating conditions at the atmospheric pressure of the Rankine Cycle. These measurements were made on flames with air and five different fuels (EPA gasoline, AMOCO, propane, toluene, and n-heptane).

PRELIMINARY BURNER-VAPOR-GENERATOR DESIGN

Preliminary Rankine Combustor Design

Figure 103 shows the conceptual design of the Rankine Engine burner and vapor-generator. Combustion air from the blower passes through a preheater where it is heated by the hot exhaust gases. The preheated air flows through a mixing device where the fuel is injected and atomized. Vaporization of the fuel takes place in the flow ducts leading to the transpiration burners.

The specifications and preliminary design of a porous Rankine burner-vapor-generator with the configuration of Figure 103 are summarized in Table 13. This component has an overall diameter of 18 inches; there is

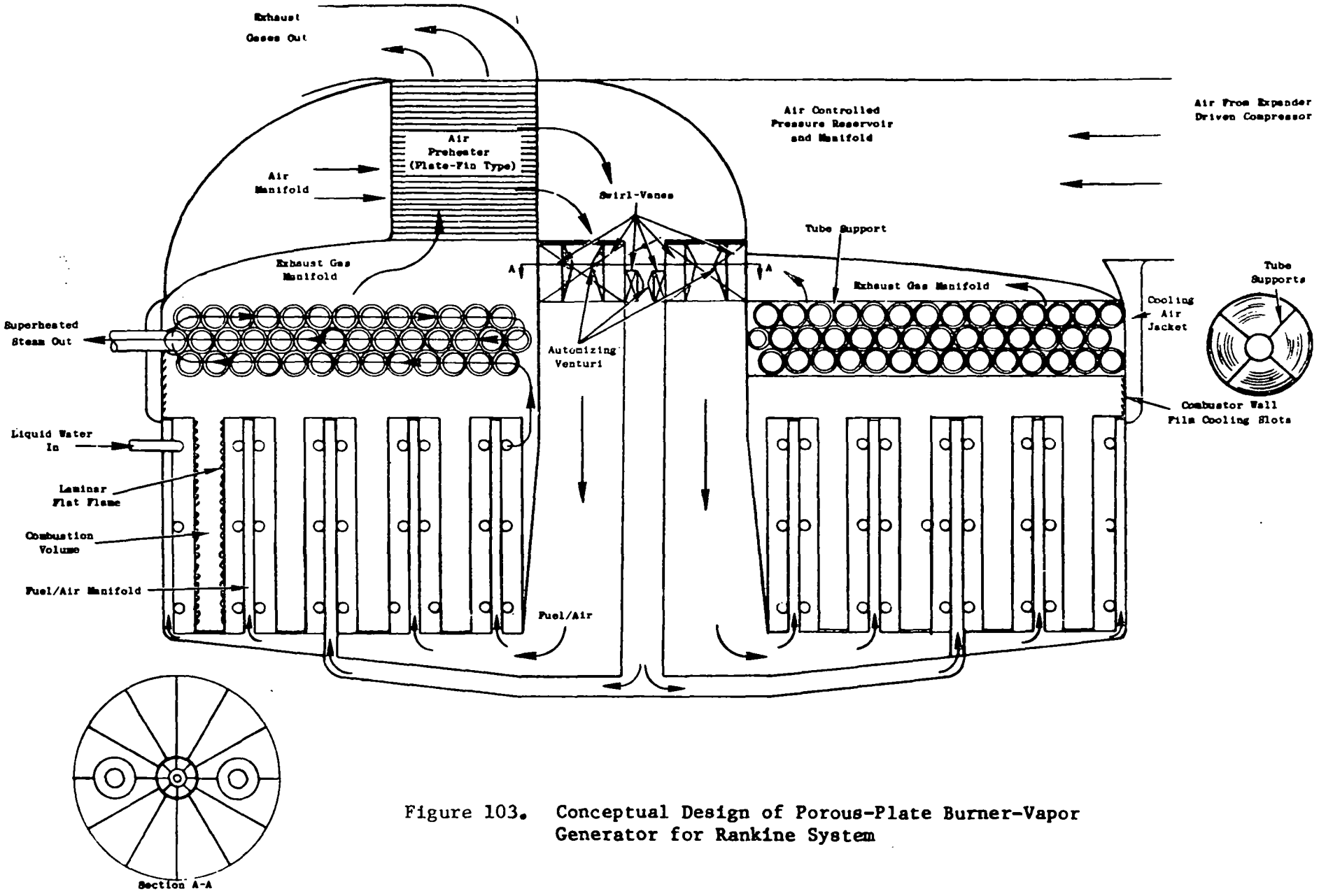

Figure 103. Conceptual Design of Porous-Plate Burner-Vapor Generator for Rankine System

Table 13. POROUS RANKINE COMBUSTOR

SPECIFICATIONS	
Combustor Heat Load	1.87×10^6 Btu/hr
Feedwater Temperature	200°F
Steam Flow	Max. 1296 lbm/hr Min. 40 lbm/hr
Fuel Flow	101 lbm/hr
Feedwater Pressure	1200 psi
DESIGN	
Equivalence Ratio	0.9
Fuel/Air Flow Rate	1801 lbm/hr
Burner Area	5 ft^2 with $V_{25\ Max}$ = 40 cm/sec
Minimum Area to Avoid Lift-off at Maximum Flow	3.9 ft^2
4 Concentric Burner Plates	1/2 in. Thick
Overall Diameter of Burner	18 in.
Burned Gas Exit Velocity with 1/2" Radial Gap for Each Exit Plate	65 ft/sec
Pressure Drop at Design Condition (215 Microns Pore Size, 35% Porosity)	105 psi

3 Stages Required to Meet Turndown Requirement of 32.4:1 with Individual Burner Turndown of 5:1

a 1/4 in. radial gap for each of the 4 concentric burner plates, which gap results in a burned gas exit velocity of 65 ft/sec. Three stages are required to supply an overall turndown ratio of 32.4:1, since the maximum turndown of the individual burners is approximately 5:1. The package shown in Figure 103 has a porous burner area of 5 ft^2.

Preliminary Fuel Supply Design

In conventional combustors using liquid fuel, the fuel is typically injected into the combustion zone in the form of small liquid droplets which are subsequently vaporized and burned. The porous-plate burner requires that the fuel be vaporized and well mixed with air before entering the porous structure of the burner.

Figure 104 shows the fuel-air mixer and fuel vaporizer concept which is similar to that used in a current advanced aircraft engine development program. The fuel enters the mixer through the central tube and is injected radially into the primary air stream through the small orifices. The primary vanes impart a swirling motion to the air which then passes through a venturi section. Additional air is introduced through a radial inflow counter-rotating secondary swirler. The intense shear region between these counter-rotating flows provide good atomization of the fuel which is then vaporized on the downstream duct.

The turndown ratio compatibility of a single burner is in the order of 5:1 for constant pressure and equivalence ratio. In order to achieve the required 20-30 turndown ratio, staging is required.
Figure 105 shows two possible installation configurations for the fuel/air mixers. Preliminary calculations were made to estimate pressure drop as a function of cup dimensions and degree of fuel vaporization as a function of air velocity, air preheat temperature and length of vaporizer.

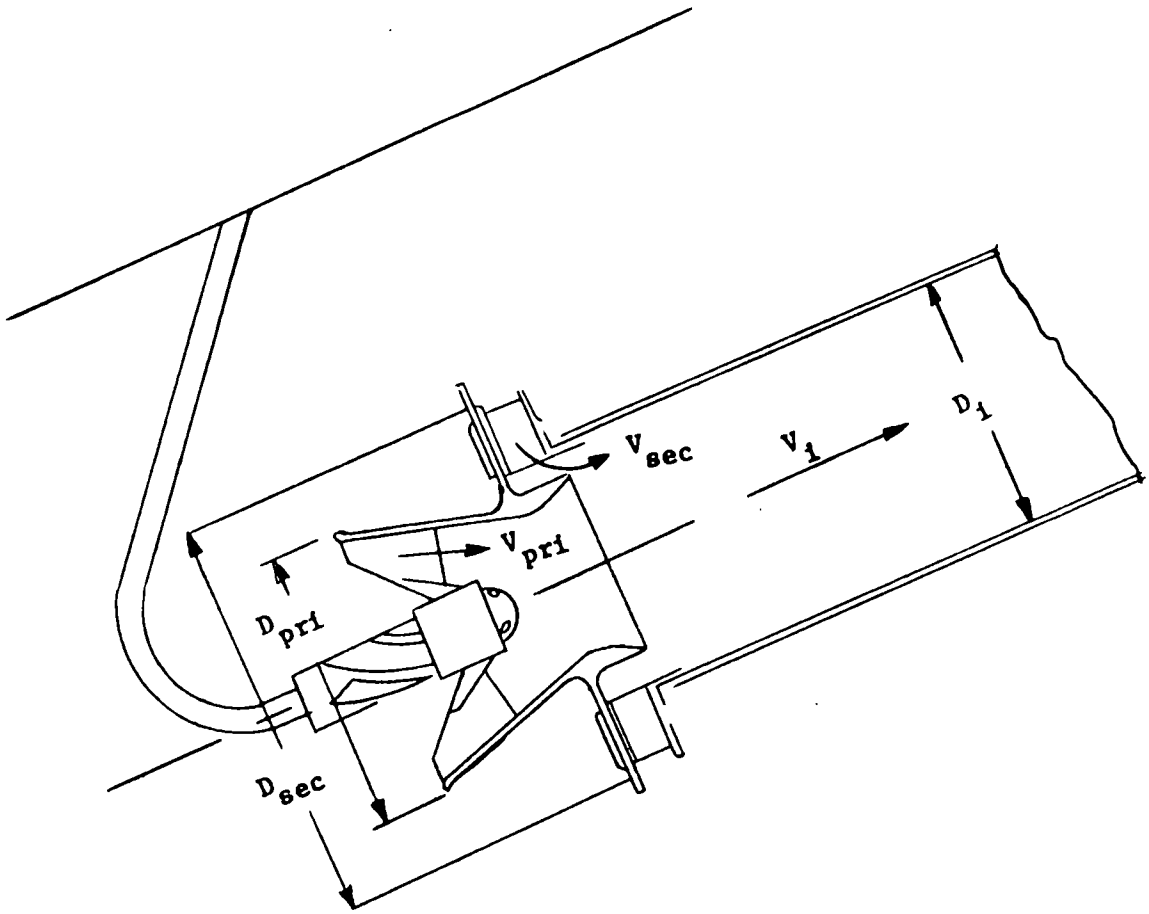

Figure 104. Fuel-Air Mixer and Fuel Vaporizer Double-Swirl Carbureting Concept

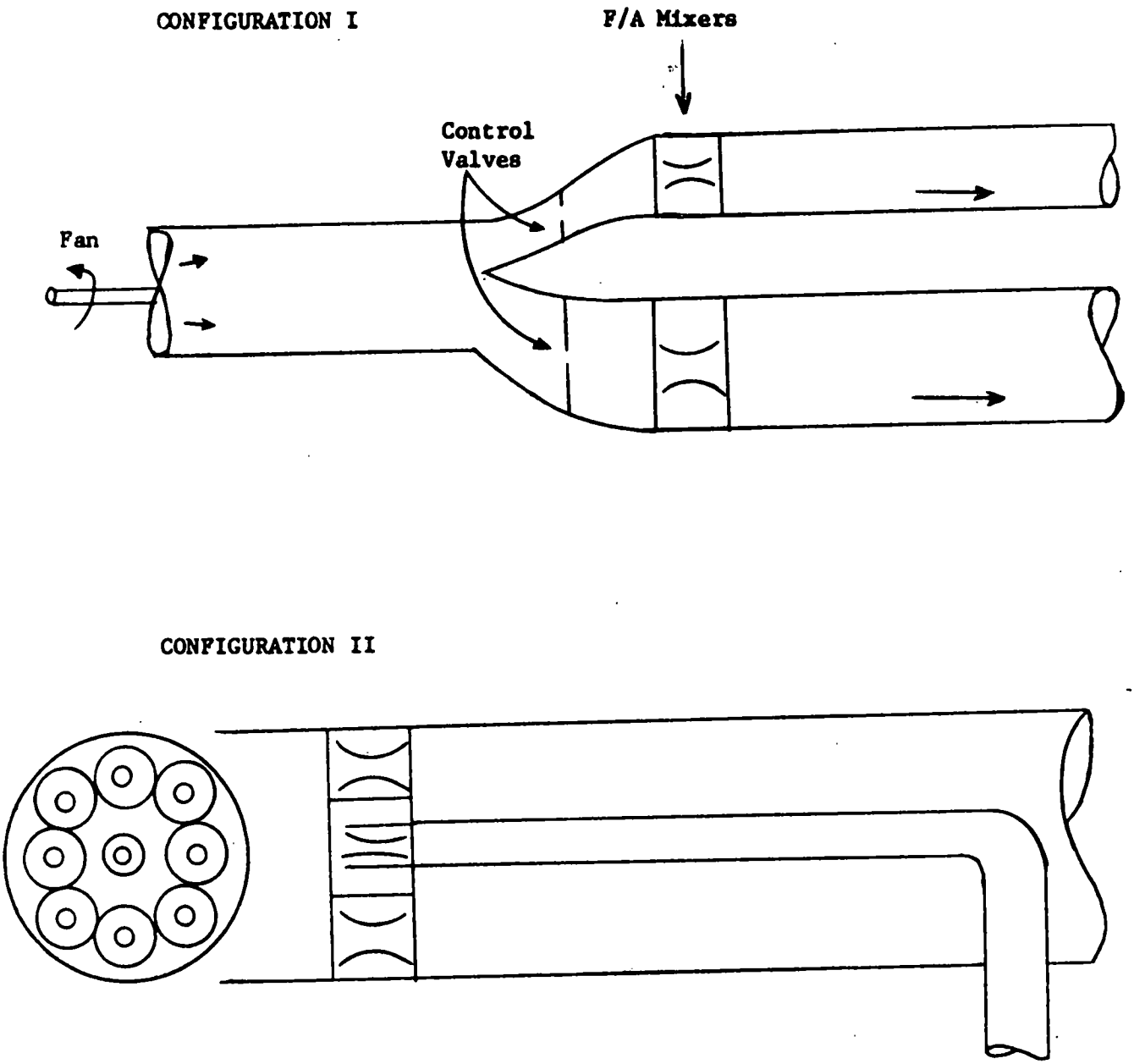

Figure 105. **Preliminary Installation Configurations**

The pressure drop results for the design point are shown in Figure 106 and the degree of fuel vaporization is shown in Figure 107. The fuel vaporization predictions are based on the correlation[21] previously developed. Since the liquid droplets in those experiments were relatively large, the predictions for this mixer (in which the droplets will be small) are believed to be conservative.

After completing the above analyses, the vaporization tests were run on the gas turbine combustor fuel-air mixture supply reported above. As indicated in Figure 97, most of the data indicated 93% or above of the fuel was evaporated. The tests were run at atmospheric pressure similar to Rankine burning conditions. The inlet air temperature was in the range of 164 to 411°F. These temperatures are easily attainable in a Rankine cycle air preheater required for an efficient engine. The equivalence ratio of the data was 0.8, only slightly lower than contemplated for the Rankine combustor. Thus, the test data can be seen as applicable to the Rankine fuel-air mixture supply.

Reference to Figure 91 indicates that a tangential flow of primary air is created in a central tube by variable louvers around the inlet end. A "Sonicore" air-actuated fuel nozzle sprays gasoline in a 90° conical spray down the center line of the central tube. The spray nozzle creates a spray with a 20-50 micron mean drop diameter which quickly evaporates due to the warm primary air introduced into the central tube.

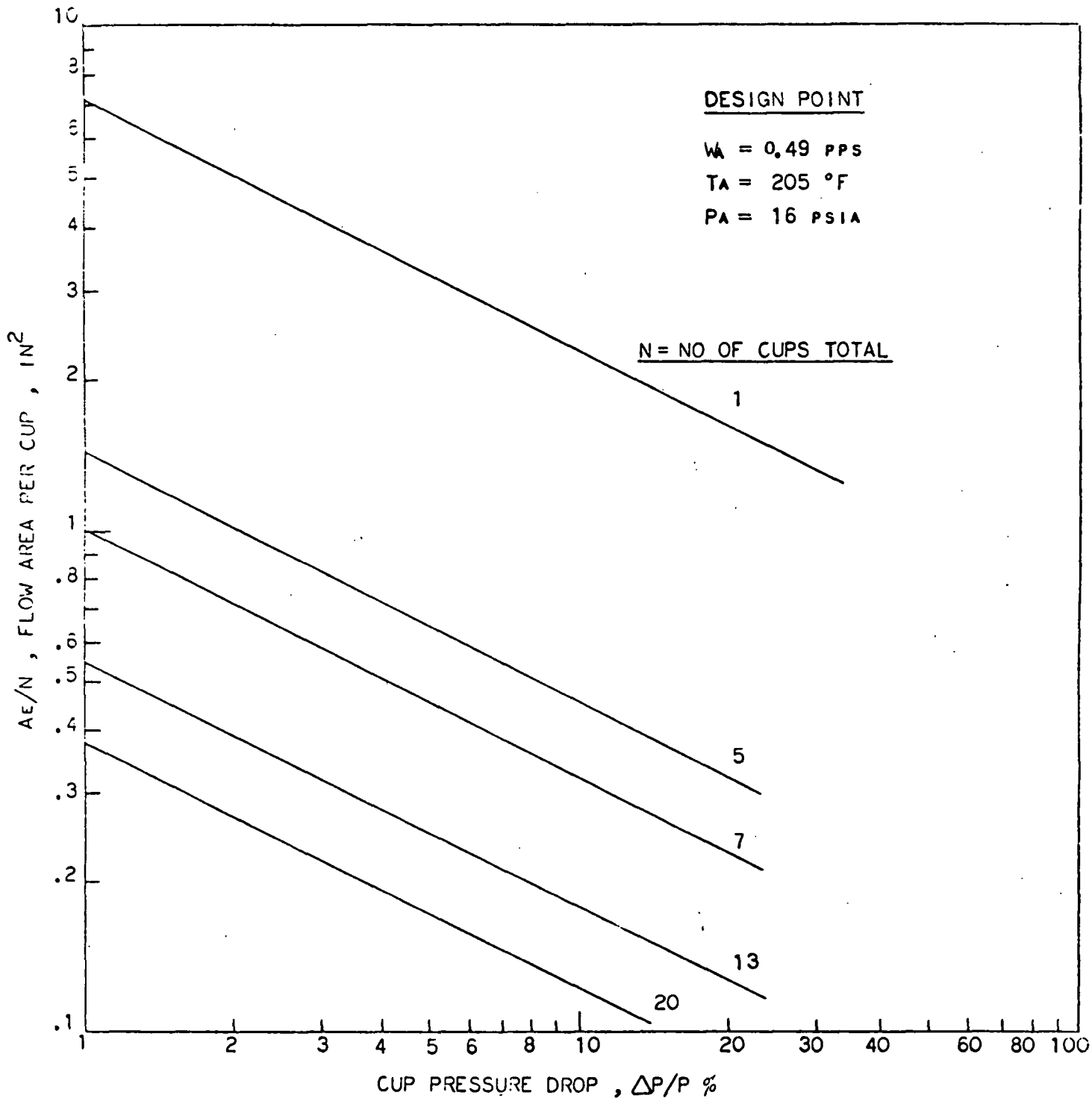

Figure 106. Rankine Engine Fuel-Air Mixer Cup Flow Characteristics

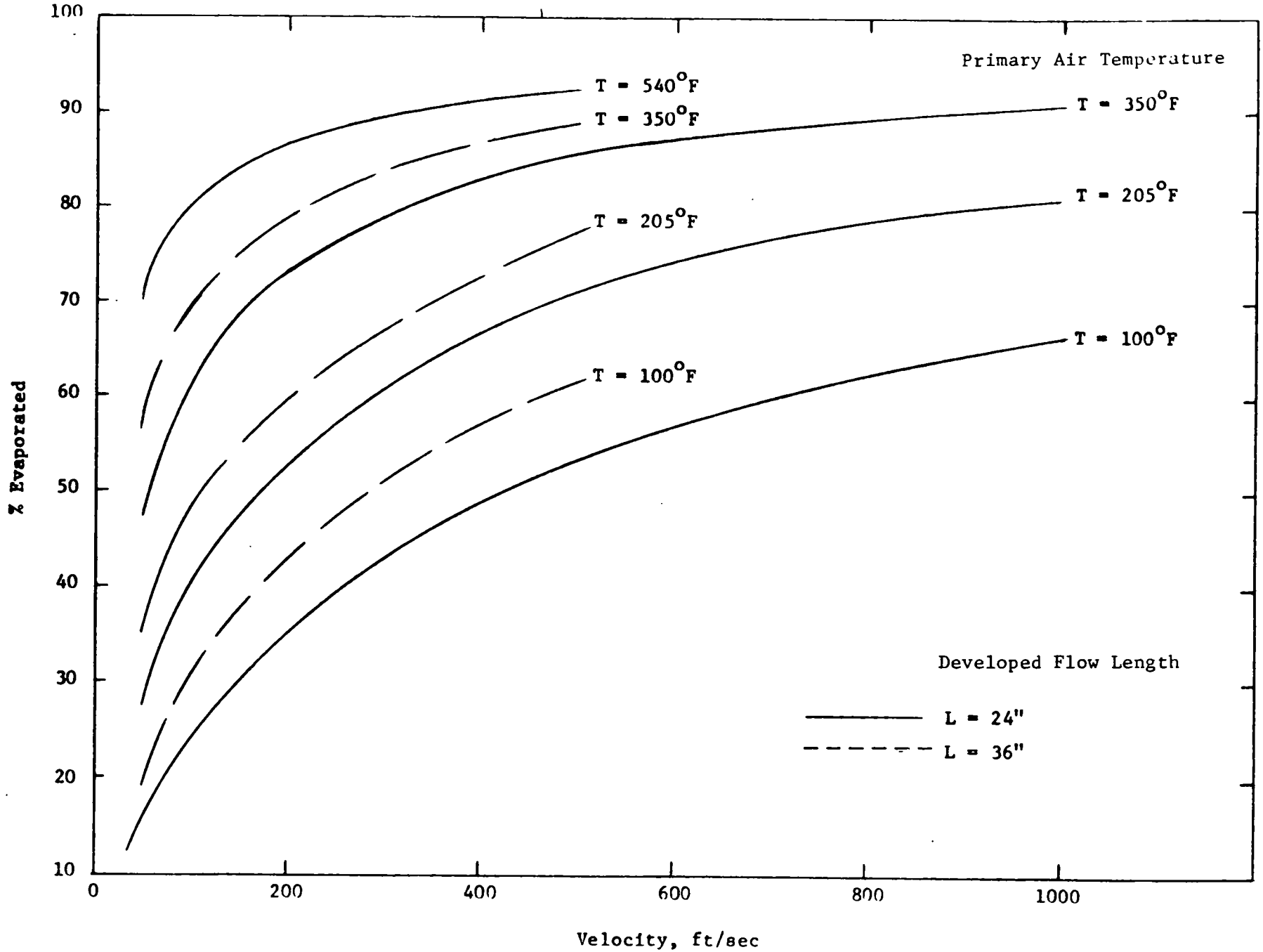

Figure 107. Estimated Vaporizer Performance

The smaller drops follow the streamlines and are evaporated due to the presence of the warm air. It takes only a configurational study to adopt this tested concept to the Rankine combustor

BENCH TESTS

Test Apparatus

Burner and Auxiliary Equipment - To meet the design requirements of a real engine, the individual modular burners will probably have to be other than flat, but a satisfactory evaluation of the quantities of interest here can equally well be made with a flat burner. An available unit made of sintered copper shot and with a 5.5 in. x 5.5 in. burner surface, about 0.4 in. thick and with about 35% porosity, was used in this work; the burner area of 30.3 in^2 is reasonable for laboratory bench tests and is large enough for adequate precision in the desired measurements. The scale factor relative to the specified engine parameters is approximately 1/30. Figure 108 shows an essentially identical sample unit, made only half-filled with the sintered copper shot to illustrate its construction.

A schematic diagram of the test set-up is shown in Figure 109. The burner is secured to a flanged plenum, primarily to reinforce the rectangular water manifolds of the burner which had been made entirely of copper and thoroughly annealed during the sintering of the copper shot. (The manifolds had to sustain a water pressure of as much as 120 psi to suppress boiling, with the preheating required to avoid condensation of pre-vaporized fuels.) The water preheater (Figure 109) is an identical sintered copper burner, and both have manifolded parallel water tubes as in Figure 108, rather than the monotubes in some of the proposed engine designs.

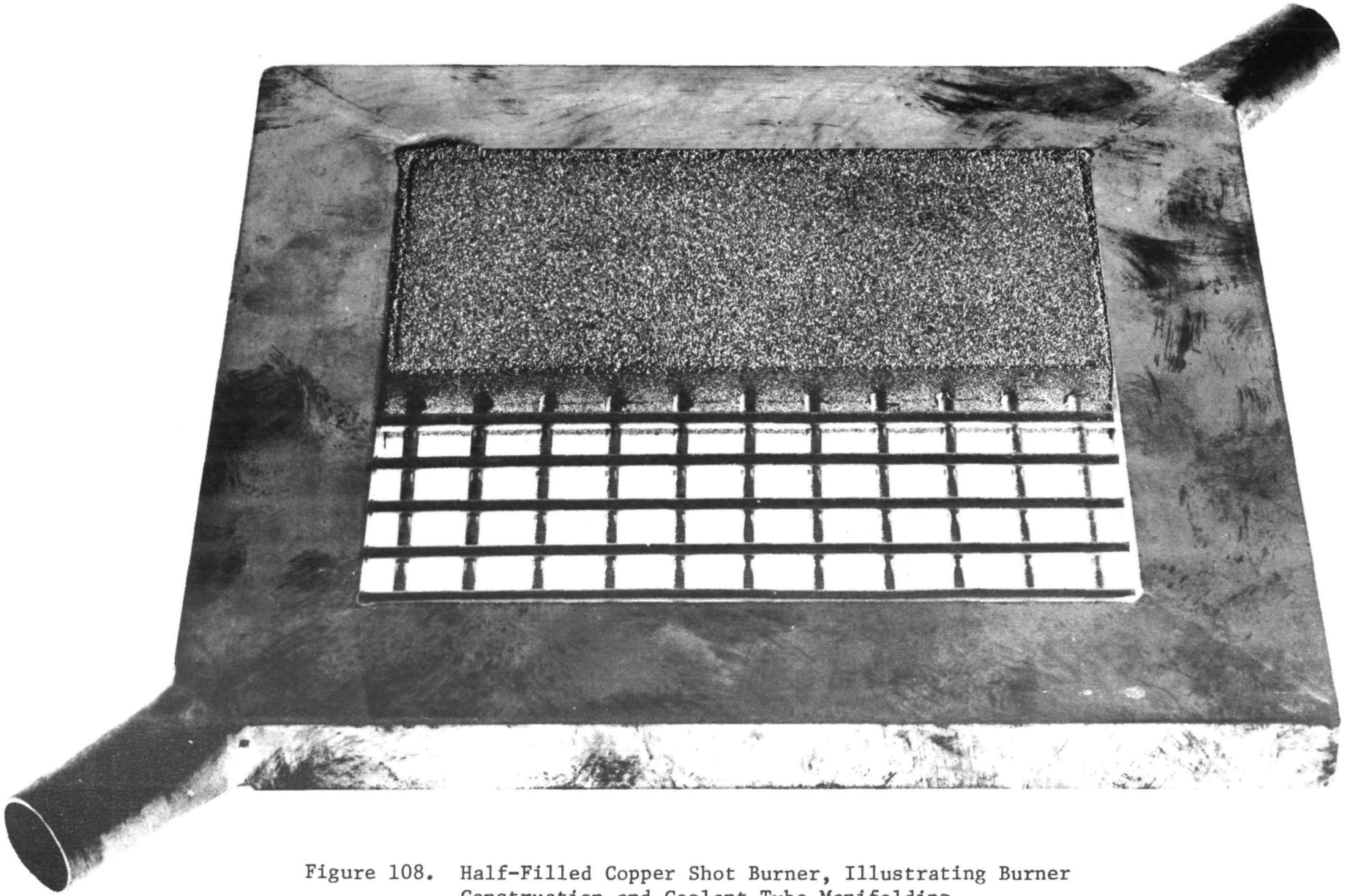

Figure 108. Half-Filled Copper Shot Burner, Illustrating Burner Construction and Coolant Tube Manifolding

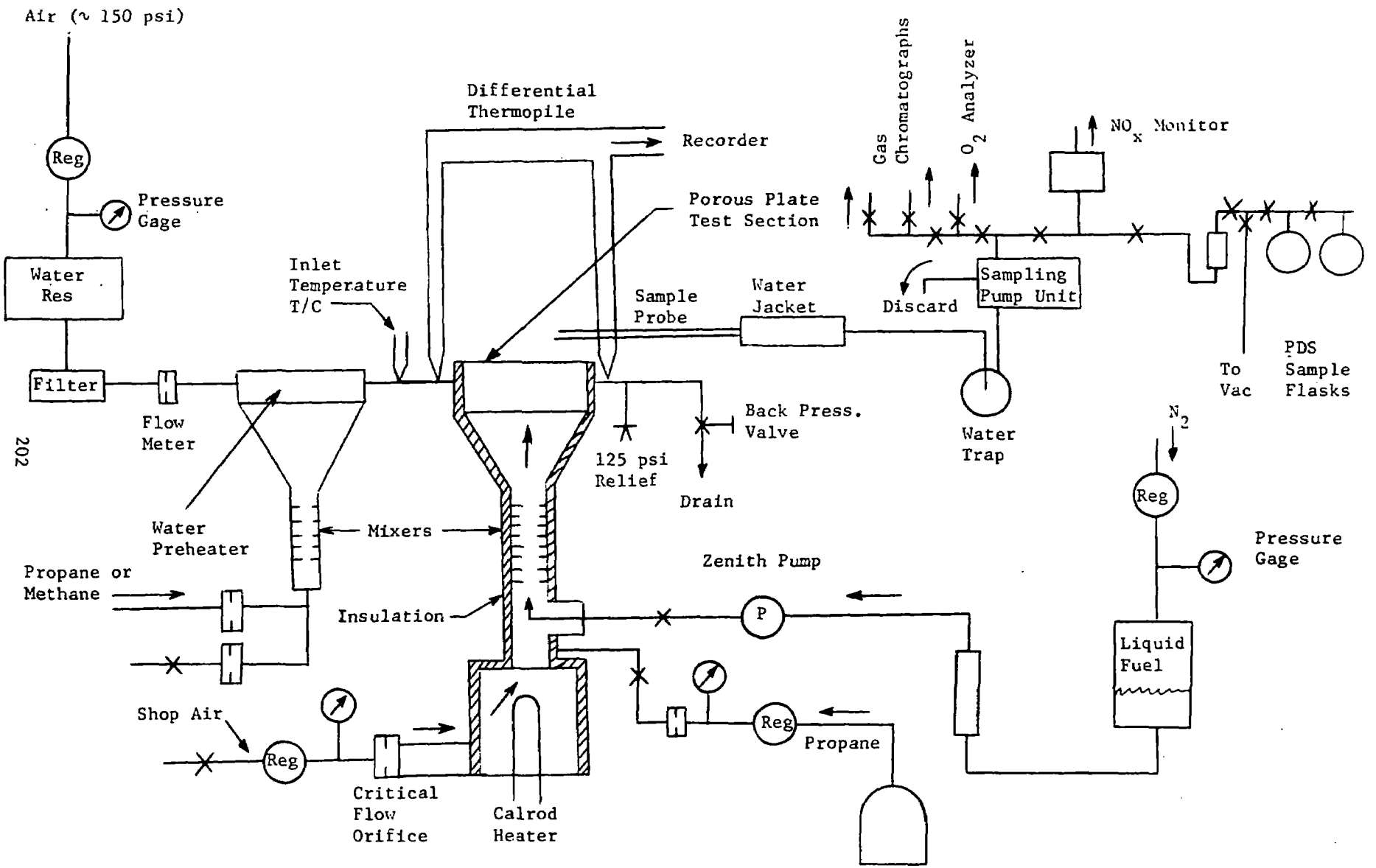

Figure 109. Schematic Diagram of Burner Test and Gas Sampling Arrangement

The water flow appropriate to this scale is about 1.1×10^{-2} lbm/sec; it was metered with a calibrated differential pressure orifice, and delivered from the pressurized reservoir shown. On the preheater, a methane (or propane)-air mixture is burned at a composition and flow adjusted to give the temperature rise required (up to 180°F) to match approximately the preheated air temperature and to avoid condensation of the prevaporized liquid fuel (for example, gasoline) in the burner pores. The air preheater is a Variac controlled 1 KW Calrod immersion heater in about 2 feet of 2-inch pipe. It can heat a steady flow of 1.76×10^{-4} ft^3 (STP)/sec of air to 230°F.

The combustion air was fed from the 150 psi plant supply and metered with a calibrated critical flow orifice meter; when propane was used as the fuel, it was taken from a regulator on a standard container of chemically pure (CP) propane. It was metered with a critical flow orifice, as were also the fuel and air to the preheater when used.

When a liquid fuel was used, it was taken from the reservoir, pressurized to a few psi above system pressure with N_2, through a rotameter and delivered by the adjustable Zenity metering pump to a simple spray nozzle (Monarch or Delavan; 0.6 gallons per hour). The rotameter was calibrated with each of the three liquids used.

Many earlier attempts had been made to operate the system with prevaporized fuel at temperatures up to 306°F, using the single spiral coolant tube in another small porous-plug burner as the heater; it appeared to be a satisfactory and readily adjustable source of the vaporization heat, but pulsations seemed to be very difficult to avoid with any reasonable feed-system modification, and steady flames were seldom obtained with this arrangement. It was finally abandoned for the simpler arrangement

discussed below. To ensure complete vaporization of the liquid fuels, the air was usually preheated to about 212°F, as measured at the entry to the plenum (Figure 109). All of the apparatus downstream of the fuel injection was well insulated with glass wool, and the water temperature at the burner inlet was maintained at about 212°F or higher to avoid possible condensation of the fuel. The spray nozzle, (facing downstream), mounted in the center of the pipe, discharged into the preheated air stream ahead of the mixer. Satisfactory performance of the burner was thus obtained; ignition was prompt and reliable to a steady flame of uniform appearance, which extinguished promptly when the pump was stopped with no evidence of residual unvaporized fuel.

The heat flux to the burner was obtained from the water flow, its specific heat and the temperature rise; calibration of the ten-element thermopile* with which the temperature rise was measured agreed well with standard copper-constantan tables. One of the 1/8 inch diameter stainless steel sheathed junctions of this device contains a separately wired single-junction thermocouple. This end was mounted at the burner inlet to monitor the water temperature as delivered by the preheater. The temperature rise across the main burner was frequently as much as 144°F, so that the exit water was usually flashing to steam beyond the back pressure valve (Figure 109). When a steady flame could be established quickly (for example, with propane-air mixtures), the system would come to equilibrium in a few minutes.

Burned-gas temperature measurements were made with 0.005 in. butt-

*Virtis Corp., Gardiner, N.Y.

welded platinum platinum-(10 percent) rhodium, silica cooled thermocouples; the methods used in their preparation and in computing the radiation correction were those described by Kaskan[6]. In the case of the EPA gasoline, such gas temperature measurements were made for the entire range of conditions of interest. For a few flames, the thermocouple was placed at many locations above the burner surface to learn whether there were significant lateral variations in temperature attributable to velocity nonuniformity; none larger than about 18 to 36°F were found even though the appearance of near-lifted flames that occur with weak mixtures, for example, did show an observable effect of the proximity of the cooling tubes to the surface of the sintered copper. In all the reported measurements, the thermocouple was located at or as close as possible to the point of maximum temperature in the direction of the hot gas flow, usually about 0.2 to 0.4 in. above the burner surface.

Some of these conditions, particularly wherein the burned gas temperature exceeds the melting point of platinum, are rather severe for the survival of these thermocouples, and it is fairly tedious to make them. The gas temperature was frequently obtained from the heat flux and a careful enthalpy balance; when it was measured in both ways, there was good agreement between them and with previous data[6].

Gas Sampling and Analysis - The burned gas was withdrawn through a quartz probe 0.04" I.D. x 0.12" O.D. x 1.18" long; it was joined to a 1.18 in. length of 0.4 in. O.D. quartz tubing, which was connected and sealed to a 10 in. length of 1/4 in. O.D. thin-walled metal tubing. The height of the probe tip above the burner could be adjusted and measured; its lateral position could also be varied, keeping the quartz-to-metal seal outside the flame gas column. From the dimensions and approximate temperature of the probe and the sample flow rate, it was estimated that the sample

cooling rate was approximately 1800°F/msec. The metal tube was jacketed with plastic tubing and fittings for water-cooling, and was connected by polyethylene tubing to a glass trap (to remove liquid condensed from the sample), and to the inlet of the sampling system. By placement of the probe at various distances from the burner, the hot-gas residence time of the sampled gas could be varied and computed from the burned gas velocity (which was calculated from the mass velocity and the burned gas density) and the distance from the probe to the burner.

The sample could be pumped to the various analytical devices as shown in Figure 109, using a small diaphragm compressor in the Stack Sampling Unit that accompanied the NO_x monitor referred to later. Typically, the probe sampling rate was about 0.2 in^3/sec. This unit also contained an aftercooler for the compressor, a gas distribution manifold and a small rotameter which monitored the flow actually delivered for analysis. This flow was generally about 0.1 in^3/sec, the balance of the sampled flow being discarded beyond the compressor.

The O_2 content of the gas was measured with a Beckman E-2 analyzer. It was done primarily to confirm the actual equivalence ratios, for example, when the input fuel flow was uncertain. The O_2/N_2 ratio was also determined by gas chromatography together with carbon monoxide using a 13-X column, helium carrier and a thermal conductivity detector. It had been calibrated with $CO/O_2/N_2$ mixtures prepared from metered flows of the gases.

A second gas chromatograph was used to examine the gases for hydrocarbons, employing a Poropak-N column and a flame ionization detector. It had been calibrated with a number of light hydrocarbons; the sensitivity was equivalent to 1 ppm or less of, for example, CH_4, C_2H_2 or C_2H_4.

For nitrogen oxide measurement by the phenol-disulfonic (PDS) acid procedure, the pumped samples were taken into 180 in^3 or 300 in^3 evacuated flasks containing the required hydrogen peroxide - sulfuric acid solution. The gas sample pressure was brought to 0.5 atmosphere and the pressure was then raised to 1 atmosphere with oxygen. The analysis was made by the PDS procedure[22].

Measurements of total NO_x were also made with an electrochemical NO_x monitor* that was available. The calibration or span gas used was stated to be 196 ppm NO in N_2. The instrument is convenient since it gives a result in a few minutes and is far less tedious to use than the well-accepted PDS procedure. The sample pumping and conditioning assembly (provided for passing the sample continuously to the monitor) could also be used for all of the other analytical sampling as well.

The instrument is supposedly immune to interferences from other gas components including possible hydrocarbons. In the course of earlier work, it was noted, however, that the electrochemical monitor does respond strongly to both acetylene and ethylene, and if present they will seriously interfere. In a few experiments with unintentionally rich flames in the present work, this effect could be quite clearly seen. Therefore,

---

*Dynasciences Corp., Chatsworth, Calif.; model NX-130

it was used only as a guide in confirming trends. Though its indications generally did not grossly disagree with the PDS determinations, they did tend to be higher by about 20 percent. This could not have been due to hydrocarbons, since they were eventually shown to be entirely negligible; it now seems likely that the calibration or span gas used was in error (low in NO) by this amount, since a subsequent PDS analysis of this gas suggested that its NO content in N_2 was only about 150 ppm. It is, therefore, possible that the instrument itself was performing satisfactorily.

Emissions measurements of practical interest would actually be made on the engine exhaust, or in this case at least downstream of the boiler, and therefore on gas which has been quenched to some extent at a rate not easily determined. Such quenching should be very effective on the NO formation process owing to its large temperature dependence, and the result will be close to what is actually present in the hot gas before the boiler, and also to what is measured by the sampling method used here. Freezing the CO concentration is much less likely[23], and a measurement on the boiler exhaust is certain to be lower than on samples obtained with much faster cooling, such as that in the sampling procedure used here. But in any case, the measured concentration may well be low.

It was not feasible nor considered essential to provide a cooler equivalent to the boiler for the present work, so the [CO] determinations no doubt represent levels intermediate between the true values at the high temperature and the values of ultimate practical interest. Thus, they represent upper limits to the emissions levels that would be observed in practice, but lower limits to what is actually present at the burned gas conditions.

Fuels - CP propane was taken from a standard 100 lb liquified petroleum gas container and the toluene was also CP reagent. Prior to receipt of the specified EPA gasoline, some work was done with AMOCO Super Premium (no lead, no phosphate). Its specific gravity was 0.76 at 76°F suggesting a considerable content of aromatic material; it was not analyzed for hydrogen-carbon (H/C) ratio, but based on a subsequent inquiry of the manufacturer's representative, it was taken to be about 50% toluene, 50% paraffins, with a gross composition equivalent to C_7H_{12} for approximate stoichiometry estimates. Similarly, the specific gravity of the EPA gasoline was 0.755, and though its aromatic content is specified to be lower, its allowable olefin content is much higher (about 30%), so its combustion stoichiometry was expected to be very close to that of AMOCO, which also accords with subsequent O_2 analyses of the combustion products.

These three liquid fuels were analyzed for bound nitrogen with these results:

AMOCO Super Premium	11 $\pm$ 5 ppm N
Toluene	24 $\pm$ 5 ppm N
EPA Gasoline	33 $\pm$ 5 ppm N

This N content could account for at most a few ppm of NO_x in the burned gases[17], which would be within the likely error of the analysis and was ignored in considering the emission results.

Near the conclusion of this work, some NO_x formation measurements, also reported here, were made with one other liquid fuel (CP n-heptane) using a smaller (15.5 in^2) but similar water-cooled burner, in which the burned-gas temperature was directly measured. The intent was to examine

for NO_x formation some flames of a fuel with H/C ratio near that of propane, but of molecular weight in the range of the other fuels.

Data Reduction and Correction - Where preheated air was used, a correction to the measured heat flux was applied to obtain the values presented which are referred to an initial condition of 76°F. This correction can be shown to be:

$$\delta F = 2.13\ V_{25}\ (T_{Air} - 76)\ \text{Btu/hr-ft}^2 \qquad (12)$$

with sufficient accuracy. The unit of the terms in Eq. 12 are V_{25} in cm/sec and T_{Air} in °F. For example, with T_{Air} = 230°F and V_{25} = 25 cm/sec, δF = 8200 Btu/hr-ft^2. Although it is at most only a few percent of the total enthalpy flux, it is a significant fraction of the measured heat flux. (The burner heat flux, F, is only 10 to 30% of the total combustion flux, but it must contain all of the effect of the preheat, so long as the burned gas temperature depends only on the mass velocity (V_{25}); $\delta F/F$ can therefore be as high as 25%.)

The heat-balance calculation of the burned gas temperature from the heat flux thus corrected was done as follows. For the calculated adiabatic flame temperature (T_a) of the mixture initially at 76°F, a value of the enthalpy of the mixture was obtained, from which was subtracted this correction, Δh:

$$\Delta h = (F_b/V_{25}) \times \frac{44{,}100}{\bar{m}} = h_{T_a} - h_{T_b}\ \text{(Btu/lb gas)} \qquad (13)$$

in which F_b is the corrected burner heat flux, $\bar{m}$ is the average molecular weight of the burned gas and the constant is a conversion factor to obtain the result in the engineering units usually tabulated. The enthalpy at the calculated adiabatic flame temperature is h_{T_a}, while the enthalpy

at the burned gas temperature is h_{T_b}. These tables[24] have been compiled for various fuel-air mixtures which generally do not correspond exactly to the fuels and compositions encountered here. But we are only interested in enthalpy differences which do not vary significantly with the H/C ratio of the fuel for a given equivalence ratio, R, and temperature interval, and it is readily shown that the temperature decrement is obtained in this way with ample accuracy. Thus, with the quantities h_{T_a} and Δh, h_{T_b} is obtained and the corresponding burned gas temperature, T_b, is read or interpolated from the table.

In view of the fairly low H/C ratios of toluene and the two gasolines, some attention was given to estimates of the adiabatic flame temperatures, or at least how much they should differ from that of propane-air for a given equivalence ratio. The difference (mainly due to the stoichiometry) would not be expected to be large; but owing to the great sensitivity of NO_x formation rate to temperature and the way in which T_a was used when the actual gas temperature was estimated from the heat flux, it seemed desirable to compute the difference with some care. The unit heating value of the stoichiometric mixture of air with the vapors of each of the three liquid fuels was computed to be 94.5 Btu/ft^3 $\pm$ 0.11 (76°F, 1 atm) for all of them, or 4.5% higher than the corresponding value for propane-air (90.6 Btu/ft^3).

A correlation can be made between the trends of these unit heating values with accurately calculated adiabatic flame temperatures, for various classes of hydrocarbons of varying H/C ratio and molecular weight. It shows that the 4.5% difference should result in a 45 to 54°R higher value of T_a; for stoichiometric propane-air (R = 1), T_a is 4091°R, so for the three liquids at R = 1 in air, a value of 4140°R is estimated.

There are also available a few calculated values for toluene, benzene, cyclohexane, etc., mostly for various rich mixtures (R = 1.05 to 1.17)[25] that can be compared with the corresponding values for propane-air; this comparison also indicates a difference of about 45°R. The value of 4140°R for R = 1 was therefore assumed, and with similar estimates of the difference for lean mixtures, a plot of T_a vs. R was made from the computed values for propane-air mixtures. In no case is the estimate believed to be in error by more than ± 9°F.

Measurements of Heat Flux and Burned Gas Temperatures

Figures 110 and 111 summarize the heat flux data, corrected to 76°F in the manner previously described, for propane-air mixtures and for EPA gasoline-vapor air mixtures.

The burned-gas temperatures, largely computed from the heat flux data, are shown in Figure 112 for propane and EPA gasoline, and other data derivable in part from these plots are also summarized in Table 14. Similar data summaries for the toluene and AMOCO gasoline-air mixtures are also shown in Table 14. In the case of the EPA gasoline, direct measurements of the gas temperature by thermocouple, as well as the indirect measurements from the heat flux data, were generally made; on the whole, these were in very good agreement (within 54°R) and the lines shown in Figure 112 average these temperatures.

The data for propane-air mixtures in Figure 112 can be compared with those of Kaskan[6] and the agreement is excellent. There are no data in the literature with which the results for the other fuels could be compared. The heat flux data were in this case extended further toward the adiabatic flame condition, well beyond the range of interest for this application. Although it has no practical consequences in the present

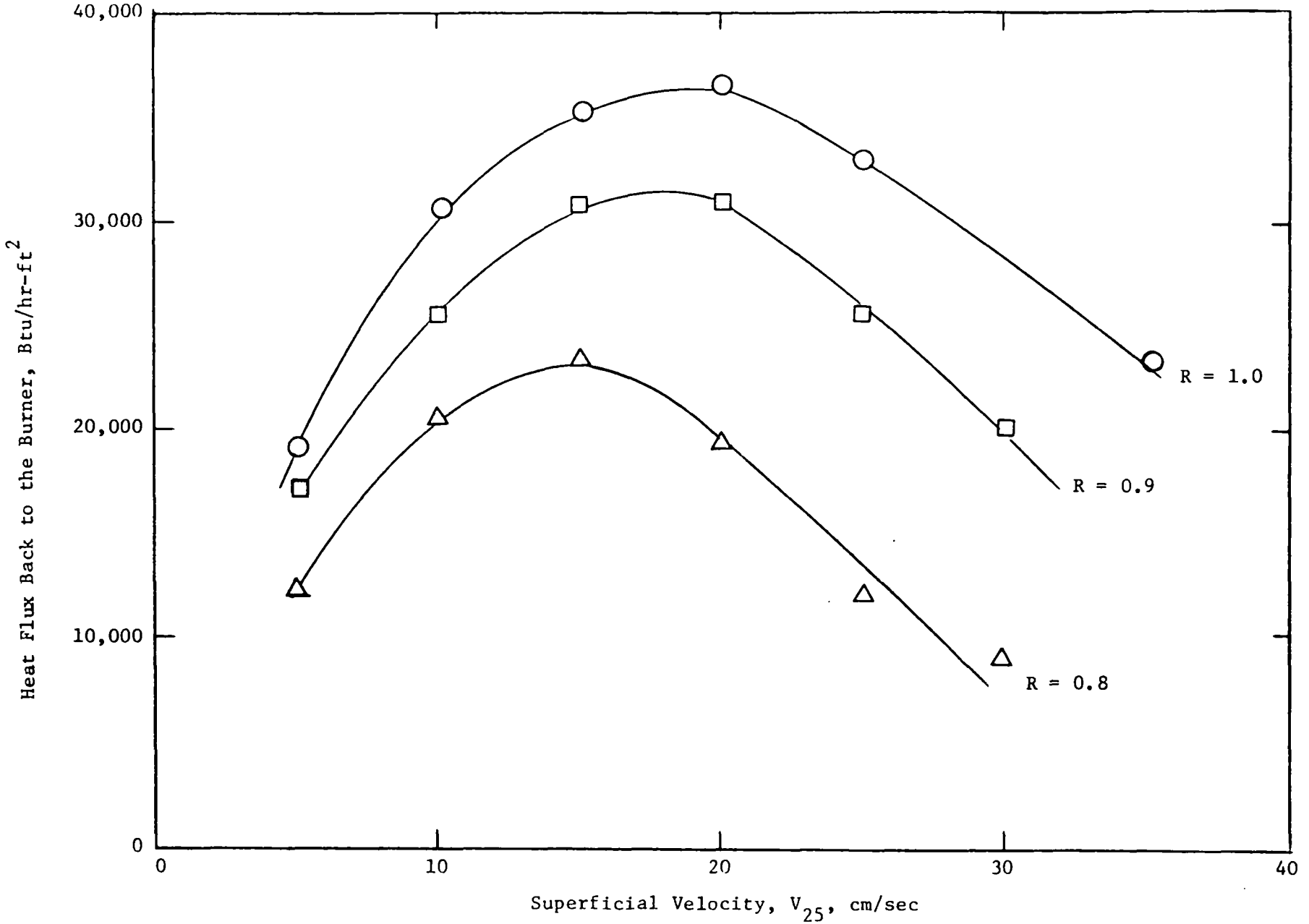

Figure 110. Burner Heat Flux Back to the Burner from the Flame; Propane-Air Mixtures

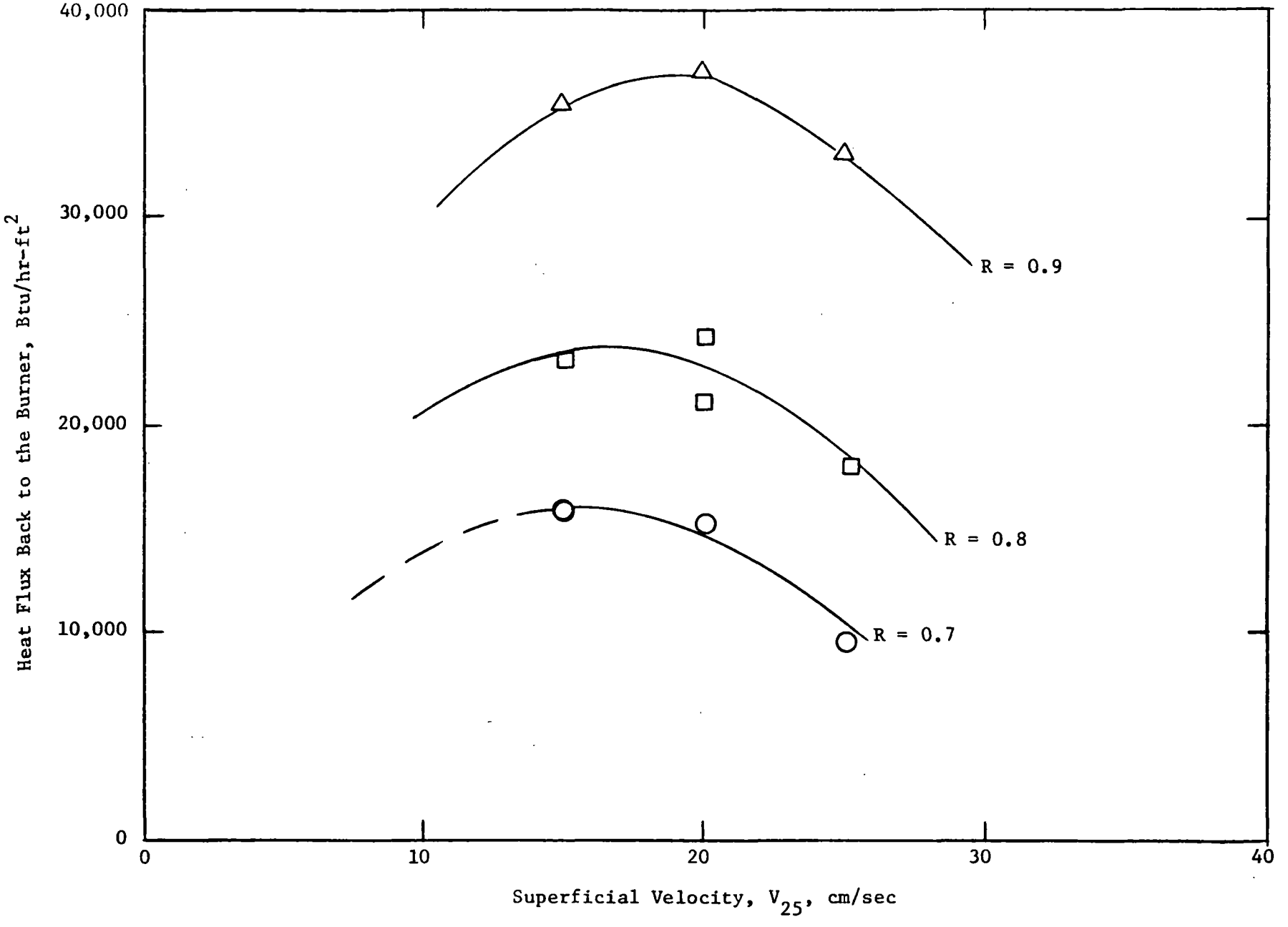

Figure 111. Burner Heat Flux Back to the Burner from the Flame; Gasoline (EPA)-Air Mixtures

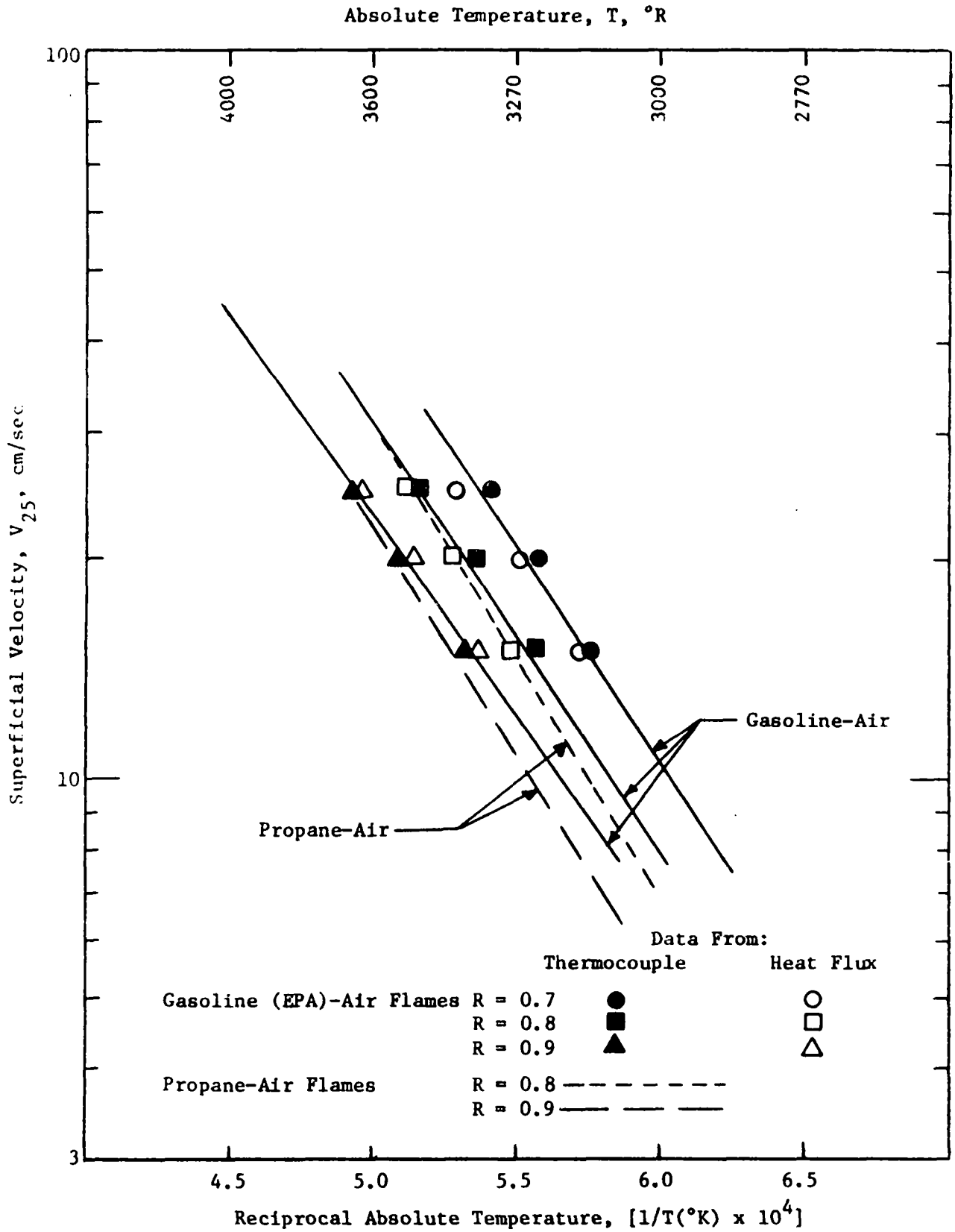

Figure 112. Comparison of Gasoline (EPA) and Propane-Air Burned Gas Temperatures

Table 14. RANKINE MODEL BURNER TEST RESULTS

Fuel	R	h Btu/ft^3	F_{max} Btu/hr-ft^2	$V_{25,m}$ cm/sec	β_m	$T_{F_{max}}$ °R	T_a °R	S_u cm/sec	E Btu / (lbm-mole)
C_3H_8	0.83	76.1	23200	15	0.18	3330	3760	37	99000
	0.95	86.0	31500	18	0.17	3550	4010	42	97200
	1.0	90.6	36500	20	0.17	3640	4090	43	95400
Toluene	0.68	64.4	15900	12	0.18	3060	3330	24	108000
	0.78	73.7	23900	16	0.18	3310	3710	35	110000
	0.86	81.3	34500	18	0.20	3490	3890	38	97200
AMOCO	0.88	83.1	27900	17	0.17	3510	3940	41	108000
	1.0	94.5	41800	19	0.20	3600	4140	43	89100
EPA Gasoline	0.70	66.2	19200	15	0.17	3130	3440	30	99000
	0.80	75.6	25200	17	0.17	3310	3730	39	97200
	0.90	85.1	37200	19	0.20	3492	3960	43	93100

Stoichiometric (R = 1.0) F/A ratios by weight:

Propane 0.0641 (0.0420 by volume)

Toluene 0.0740

Gasolines 0.0703

context, an interesting incidental observation is that the heat flux apparently does not tend toward zero as V_{25} approaches the adiabatic burning velocities for these mixtures. There would evidently be a residual heat flux of about 8200 Btu/hr-ft^2 which is no doubt due mainly to radiation from the flame to the cold burner surface. From the emissivity of such flames (estimated as about 0.03), the radiative flux in such a geometry should be approximately of this magnitude. If it is computed for each condition and subtracted from the measured values, the remainder then does tend to zero as the unburned gas velocity, V_{25}, approaches the adiabatic burning velocity, S_u.

In Table 14, h is essentially the lower heat of combustion of the (gaseous) fuel per unit volume of the mixture (76°F, 1 atm). $F_{b,max}$ and $V_{25,m}$ are respectively the maximum heat flux and the unburned mixture velocity at which it occurs. The fraction β_m ($F_{b,max}/h_{V_{25,m}}$) is the fraction of the enthalpy flux rejected to the burner at the maximum heat flux. The maxima, as seen in Figures 110 and 111, are of course rather flat, so that the designation of $V_{25,m}$ and β_m are somewhat arbitrary; they are included as possibly useful for design purposes. $T_{F_{max}}$ is the flame temperature at which the heat flux back to the burner is a maximum.

T_a is the calculated adiabatic flame temperature and S_u is the normal burning velocity of the mixture (that is, Su is the value of V_{25} which occurs at the temperature, T_a) obtained by extrapolation (Figure 112) and noted as a matter of general interest. E is the apparent "activation energy" indicated by the slopes of these lines: $E = -4606\ \bar{R}\ (d(\log_{10}V_{25})/d(1/T))$. $\bar{R}$ is the universal gas constant, $\bar{R}$ = 1.9859 Btu/°R lbm-mole. The last three columns would suffice to determine the temperature de-

pendence of V_{25}. For a given V_{25} and R, there is little difference in the actual burned-gas temperature for a given fuel. At least, for the hotter flames (near R = 1), the higher initial enthalpy content (h) of the higher molecular weight fuels seems mostly to enhance the burner heat flux rather than the burned gas enthalpy.

It is worth noting that, where both were measured, comparison of the directly measured temperatures and those computed from the heat flux shows little, if any, of the kind of disagreement noted by Kaskan[6] in comparing his results with other data computed from heat flux measurements[5]. To the extent that combustion is not entirely complete in the flame itself, it might be expected that those temperatures calculated from the heat flux would be somewhat higher; but if there is such a consistent difference here, it appears to be no more than about 54°R which is about the expected uncertainty in the temperature anyway. Similarly, any calorimetric losses associated with the heat flux measurements would also result in a higher computed gas temperature. It appears that neither source of error could have been significant.

Emissions Measurements

Carbon Monoxide - The analytical results are given in Table 15 as the measured concentrations in samples taken about 20 msec from the flame. Many of them are at or below the equilibrium concentrations corresponding to the burned gas conditions. Some analyses were also made on samples taken closer to the flame where [CO] was found to be considerably higher than equilibrium, and the expected decay behavior could be qualitatively observed as shown for a few cases in Figure 113.

No quantitative interpretation or kinetic analysis of the measurements was attempted for reasons discussed below; but the measurements do

Table 15. RANKINE MODEL BURNER EMISSION RESULTS

	R Dim.	V_{25} cm/sec	T_b °R	$R_{NO} \equiv \frac{d[NO]}{dt}$ ppm/msec R_{NO} Meas.	R_{NO} Calc.	ppm Prompt [NO] Meas. (Approx.)	Pred. Est.	[Measured] ppm [NO] 20M sec PDS a)	(DYN) b)	ppm [CO] 20M sec	[CO]$_{eq.}$ (T_b)
C_3H_8	0.93	25	3690	0.95	0.64	25	15	44	(38)	500	1100
	0.93	20	3570	0.25	0.26	15	12	20	--		
	0.93	15	3430	0.17	0.05	10	10	14	--		
	0.83	25	3540	0.56	0.22	7	5	19	--	150	700
	0.83	20	3440	0.27	0.10	6	5	12	--	---	
	0.83	15	3330	0.05	0.03	5	5	6	--	---	
AMOCO	0.96	25	3780	8.0	1.2	--	25	160	--	1500	3000
	0.88	25	3690	7.5	0.86	--	20	150	--	---	
Toluene	0.95	--	--	--	--	--	--	--	--	1500	1200
	0.86	20	3470	1.8	0.23	30	15	65	(69)		
	0.78	20	3370	1.0	0.07	15	~ 5	35	(31)		
	0.68	20	3260	0.3	0.02	10	~ 0	15	(31)		
Gasoline (EPA)	0.89	25	3650	3.4	0.47	25	20	90	(77)	1200	1200
	0.88	20	3560	--	--	--	--	--	(77)	800	720
	0.86	15	3380	--	--	--	--	--	(51)	400	300
	0.77	25	3490	1.0	0.19	35	~10	55	(59)	600	600
	0.78	20	3350	--	--	--	--	--	(38)	400	350
	0.76	15	3200	0.06	0.02	15	~ 5	18	(25)	< 100	145
	0.78	15	3130								
	0.70	25	3420	--	--	--	--	--	(38)	200	200
	0.68	20	3220	--	--	--	--	--	(21)	~ 100	65

a) Phenol disulphonic acid method

b) Dynasciences electrochemical NO_x monitor

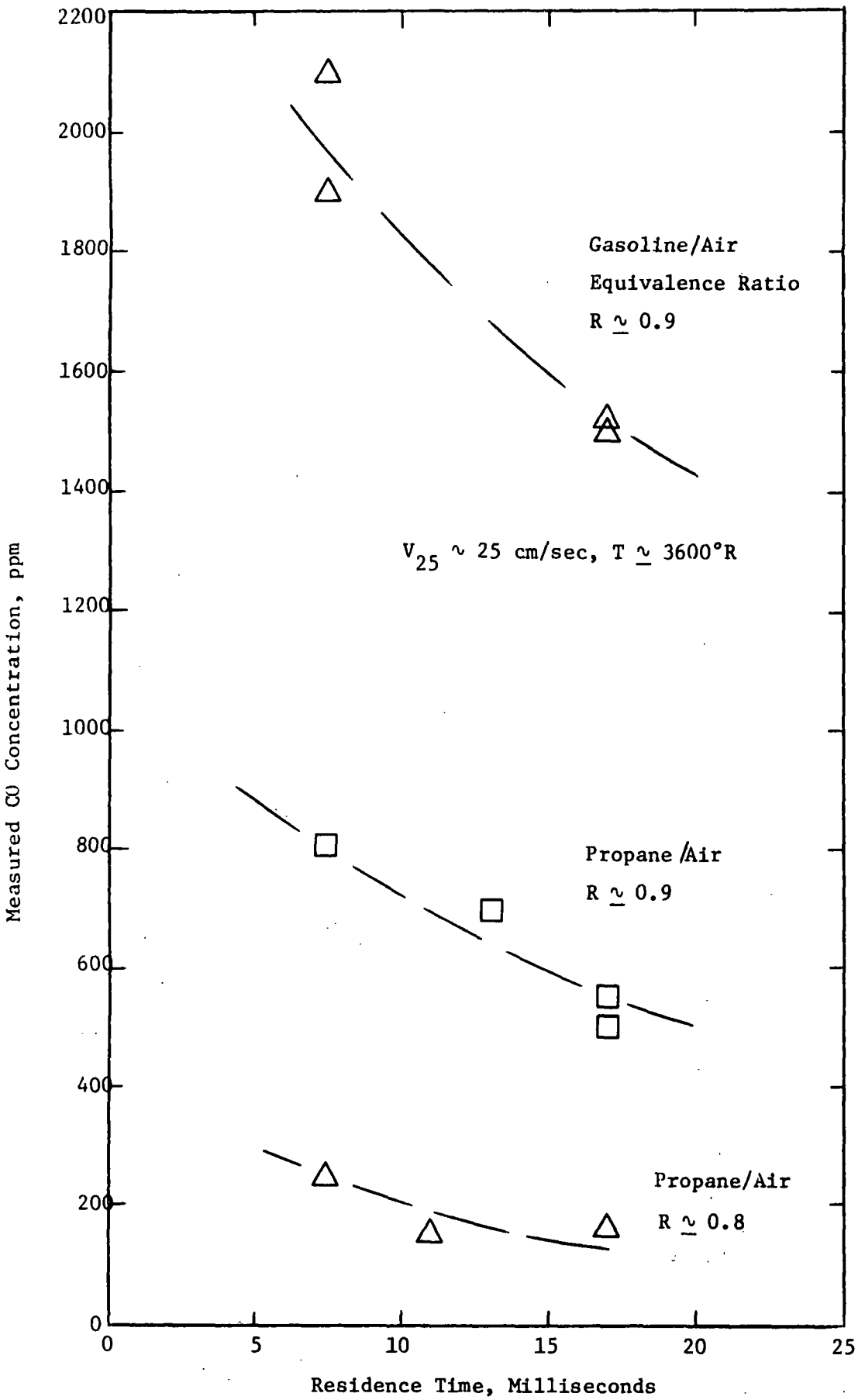

Figure 113. CO Analyses from Two Flames

adequately show that, with this hot gas residence time, and a practically attainable quenching or cooling rate in the boiler, the CO emission would be less than the specified level, which is equivalent for the average operating condition to about 800 ppm. A few of the measured values in Table 15 apparently exceed this level, but they too would certainly fall below 800 ppm in the boiler; the values given represent an upper limit to what can be expected of the engine.

In this connection, it has been shown in other work[26] with a geometrically similar burner system, that a large reduction in [CO] does occur across such a downstream heat exchanger; it was found to decrease by more than an order of magnitude to values typically corresponding to equilibrium at temperatures lower than 3240°R. Whatever the analysis or interpretation of this process may be, as a practical matter, a similar reduction must occur in any similar device.

The CO data given in Table 15 was converted to the Emission Index and is plotted for all the fuels tested in Figure 114. The bulk of the data falls below the level corresponding to the original 1976 Federal Standard, especially at the lower values of superficial velocity (V_{25}) or lower power levels. At some of the higher values of superficial velocity (V_{25}) and hence higher power levels, the measurements are above the level of the Standard for gasoline burned at an equivalence ratio of 0.9. However, it is expected that the CO emissions averaged over a duty cycle would be below the Standard since a large fraction of the duty cycle occurs at the lower power levels.

Hydrocarbons - Most of the sampling for this purpose was done at residence times of 10 to 20 msec; in no case with any of the fuels was any hydrocarbon detected; it is concluded that with any reasonable excess air there will be essentially zero (<1 ppm) emission of hydrocarbons from

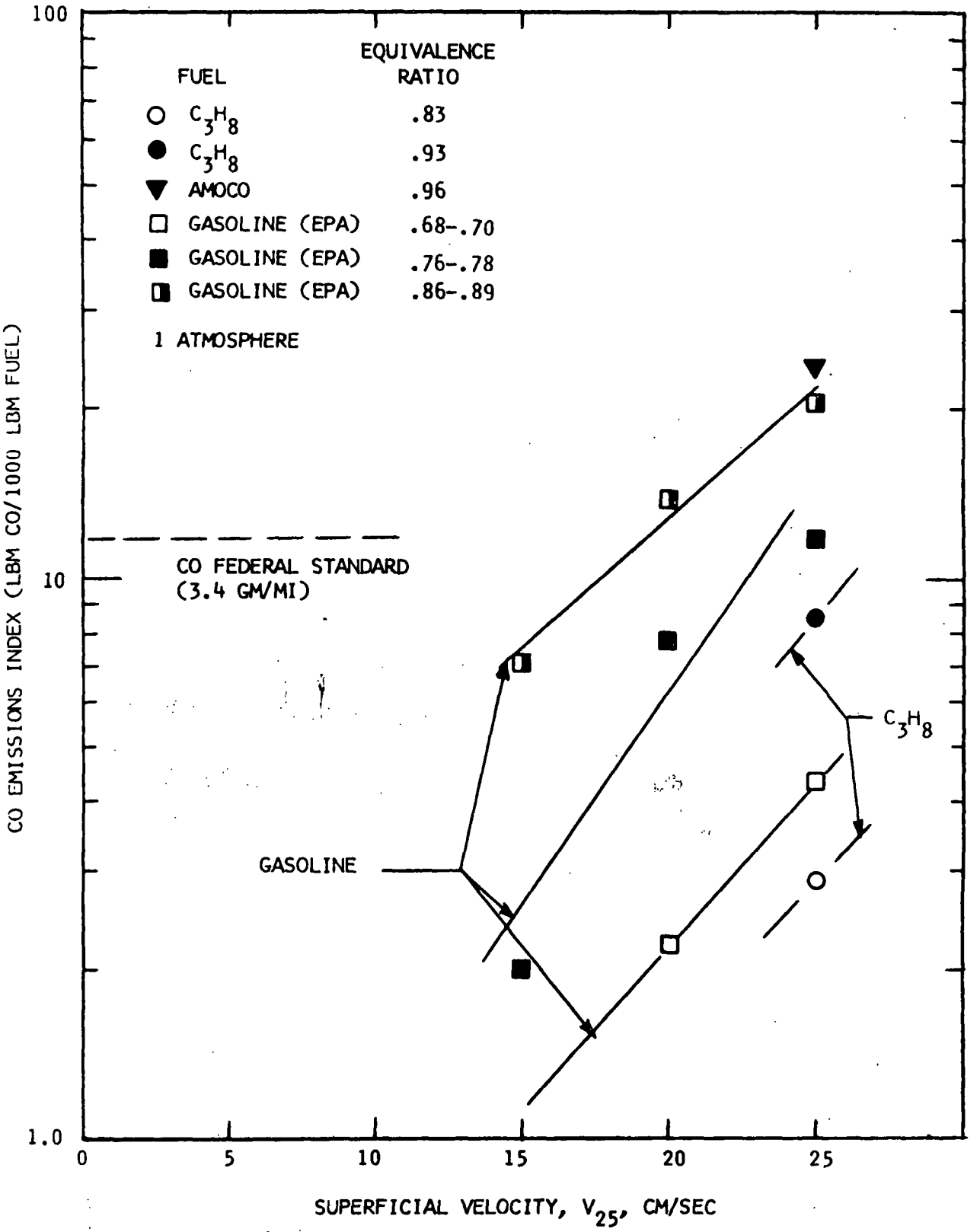

Figure 114. CO Experimental Measurements on Water-Cooled Burners with 20 Milliseconds Residence Time

burners of this kind. In fact, it was generally observed that the normal background CH_4 concentration (1.0 to 1.2 ppm) was, if anything, decreased by the flame.

Oxide of Nitrogen - Most of the results summarized in Table 15, were obtained at conditions similar to but not necessarily identical with those in the thermal tests just described, since they were not usually done simultaneously. The main interest here is in the NO_x formation data, compared in Table 15 and Figure 115 with the computed values to be expected by the thermal or hot-air mechanism; with the assumption of $[O] = [O]_{eq}$, the equation of the solid line was obtained; for combustion products at 1 atm with O_2 mole fraction (N_{O_2}):

$$R_{NO} \equiv d[NO]/dt = \frac{3.3 \times 10^{18}}{T} e^{\frac{-136,500}{RT}} (N_{O_2})^{1/2} \text{ (ppm/millisec)} \quad (14)$$

from the same basic kinetic data used by Fenimore[7]. The present estimate of the NO formation rate in Eq.14 is about 30% higher than the original estimate given in Figure 3; this correction was made after more careful consideration of the relevant kinetic data. The line (practically straight in this temperature interval) was calculated for an oxygen mole fraction, $N_{O_2} = 0.02$, and the data were adjusted or normalized to this oxygen content to facilitate comparisons at a fairly representative excess air condition. This oxygen content corresponds to an equivalence ratio of R = 0.91.

The individual rates were obtained from the slopes of linear plots of the analytical results versus the time from the burner, and the "prompt NO" was obtained from the intercept at zero time in essentially the manner described by Fenimore[7]. The "predicted estimate" of the prompt NO was made from Fenimore's data with the assumption that it would be the same for all hydrocarbon fuels at the same equivalence ratio.

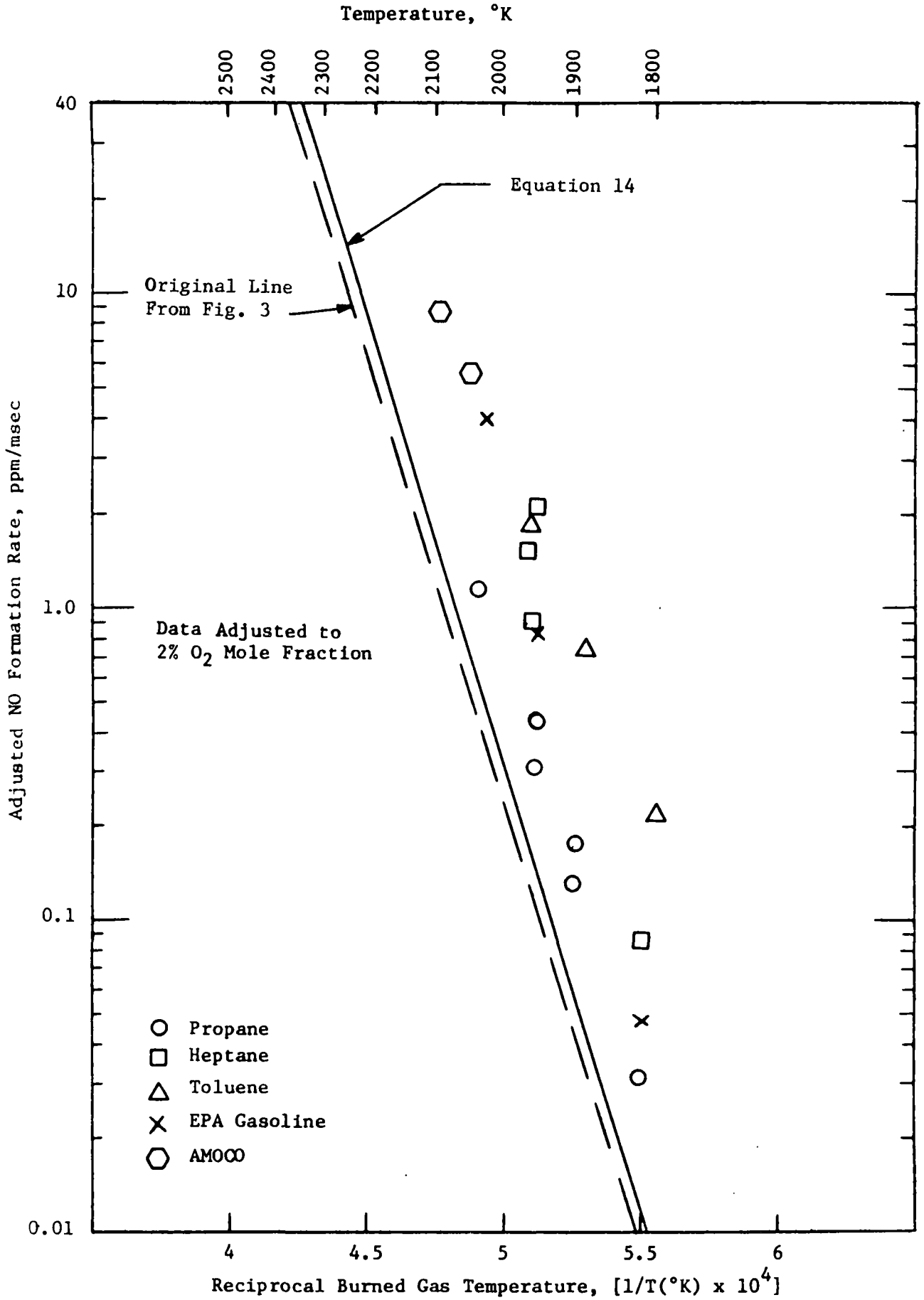

Figure 115. Variation of NO Formation Rate from "Hot-Air" Mechanism as a Function of Reciprocal Absolute Temperature. NO Formation Rate Adjusted to 2% Molar O_2.

The errors in both the thermal NO_x derived from the slopes, and in the intercepts are no doubt large. There were usually too few observations to warrant any assumption other than linearity or constant R_{NO} at a given condition; in no case were there more than three sampling positions (for example, at 1.0, 2.0 and 3.0 cm from the burner) and frequently only two were taken. The uncertainty in R_{NO} may be as much as 50% and the intercepts may be in error by 5 or 10 ppm, (though there was no case in which there appeared to be no intercept at all), but the tabulated values at 20 msec in Table 15 would be in reasonable accord with a measurement at that residence time (taken as appropriate for the present application and representing what would be found in the engine exhaust), whatever the distribution between prompt and thermal NO_x may be. The uncertainty in these values of $[NO_x]$ at 20 msec is estimated as no more than 30%.

With these reservations concerning their accuracy, the data may be compared with the calculated line, bearing in mind this also has a likely uncertainty of about $\pm$ 30%. The data for propane-air flames may be said to agree reasonably well; they lie within a factor of two of the calculated values, and this may be little outside the combined errors.

For the other four fuels, a single line could represent well enough all the data, but everywhere it would be just about an order of magnitude higher; alternatively, the disagreement with the predicted line is equivalent to about 270°R for a given rate, or by 180°R relative to the propane data. In any case, it is too large to be accounted for by experimental errors in either the analyses or in the temperature measurements. (The possible contribution of fuel nitrogen had been anticipated, but the analyses mentioned earlier showed that it could account for at most only

a few ppm in the burned gases.)

Thus, the measured formation rate of NO, at least for the fuels of high average molecular weight exceeds by about an order of magnitude the rate expected or calculated with the assumption that $[O] = [O]_{eq}$. The conclusion seems inescapable that the actual [O] averaged over the residence time ($\approx$ 20 msec) must in fact be higher by a factor of five or more. Since the oxygen concentration must be decreasing toward equilibrium and would be expected to attain $[O]_{eq}$ in this time, the oxygen concentration nearer the flame would have to be still larger. It should be noted that the plotted data do not include the contributions, shown in Table 15, of the intercepts or prompt NO. Had they been arbitrarily included in averaging the rate, the results would be somewhat higher still. It seemed reasonable to separate its contribution however, since it does appear to be real and generally agrees satisfactorily with data[7] though the possibility that it too results from excess [O] cannot be entirely ruled out by these results.

There have been many investigations of the emission of nitrogen oxides from combustors and engines with a variety of fuels, including some similar to those used in this work; unfortunately, there appears to have been none with premixed flames of hydrocarbons higher than propane, with which the data given here can be directly compared. There has been reported one rather detailed experimental study[26] and analysis of NO formation in a premixed, quasi-one-dimensional propane-air flame system. With near-adiabatic flames of one equivalence ratio (R = 0.8), estimates were made of the variation of the rate with time for up to 15 msec from the main zone of flame reactions. The maximum instantaneous rate a few msec from the flame appeared to be an order of magnitude or

more higher than would be predicted from Eq.14, generally decreasing thereafter.

For the same burned gas temperature, and for roughly comparable burned gas conditions, an average d(NO)/dt computed over a residence time comparable with that considered here (about 20 msec) would be about a factor of two higher than that measured in the present work; it would more nearly agree with the data for higher hydrocarbons (Figure 115 and Table 15). In view of the differences in equipment and approach, the agreement may be reasonable; but from either set of results, it has to be concluded that the NO formation rate is considerably higher than Eq.14 would suggest, whatever the detailed interpretation may be.

The failure of the approximation or assumption that $[O] = [O]_{eq}$ in the burned gases of hydrocarbon flames has been discussed by others in the context of NO formation; it formed the basis for interpretation of the data just mentioned,[26] and in the following generally similar discussion, its connection with CO and its afterburning is considered.[27]

That higher-than-equilibrium concentrations of free radicals do occur in post-flame gas has been shown in many experimental studies. The nature of the chemical processes involved, the partial equilibrium state, and the subsequent relatively slow radical recombinations are well established[28] and need not be elaborated here; but it is worth noting that the slow decay or "afterburning" of CO in lean hydrocarbon-air flame gases is intimately connected with such excess radical concentrations. It is known that the afterburning is really a recombination process[27,29] in which CO is in effect one of the radicals in excess of equilibrium. It is connected with the others through the equilibrium

constant for the balanced reaction:

$$CO + OH = CO_2 + H \tag{15}$$

And through similar relations for the other balanced reactions, in effect:

$$CO + O_2 = CO_2 + O \tag{16}$$

is also balanced. In the products of lean flames [CO] must then be just proportional to [O] or $[O]/[O]_{eq} = CO/[CO]_{eq}$ and will always be greater than unity during the afterburning of carbon monoxide; the rate of formation of NO will then be larger by this ratio also.

For reasons discussed previously, the [CO] measurements summarized in Table 15 may have no really quantitative meaning; the true [CO] in the burned gas must be higher than that measured owing to uncertainties in the sampling procedure. But even from these data it is qualitatively clear that [CO] does, as expected, decrease from levels considerably higher than equilibrium.

There appears to have been only one investigation[29] in which excess radical concentrations were determined and directly related to [CO] and its decay in the burned gas of a lean hydrocarbon flame. It was an ethylene-air flame at 3528°R at an equivalence ratio of 0.82, and $[CO]/[CO]_{eq}$ about 1 msec after the main reaction zone of the flame was approximately 10, decreasing to approximately 5 in the 6 msec period observed. This ratio might have approached unity in roughly the time of interest here (20 msec), during which its average value and therefore $[O]/[O]_{eq}$ evidently would have been about 5.

If it is assumed that this ratio (deduced from only one set of data) applies to the lean burned gases of other hydrocarbons, and that the

ratio has no temperature dependence, a line parallel to the predicted line (Figure 115) could be drawn; the data would generally lie within a factor of two of this adjusted prediction. Within the likely errors of the data, this could then be considered fair agreement.

The fairly consistent difference between the results for propane and the other fuels (Figure 115) is still unexplained. Assuming the validity of and extending the argument above, it would be inferred that $[CO]/[CO]_{eq}$ following the main reaction zone is appreciably higher in flames of these higher hydrocarbons. There is some indication of such a tendency in data obtained here; but it would be worthwhile to investigate this point (using, for example, optical techniques[29,30]) that would permit an unequivocal determination of [CO] or its equivalent in the actual burned gas conditions of such flames.

The NO_x data shown in Table 15 was converted to Emission Index and is plotted for all the fuels in Figure 116, as a function of superficial velocity, V_{25}, and equivalence ratio. Some of the individual NO_2 values for gasoline burned at an equivalence ratio of 0.9 are above the level of Federal Standard at high values of V_{25}; however, the NO_2 values at the lower values of V_{25} (or lower power) are well below that of the Standard, and it is expected that the NO_2 emissions averaged over a duty cycle would be below the Standard since a large fraction of the duty cycle occurs at the lower power levels.

Summary and Conclusions From Bench Tests

The thermal and emissions characteristics of some non-adiabatic hydrocarbon-air flames at 1 atmosphere have been determined for use in the design of a transpiration (cooled porous metal) burner for the combustor boiler of a low-NO_x Rankine cycle engine. Flames of mixtures

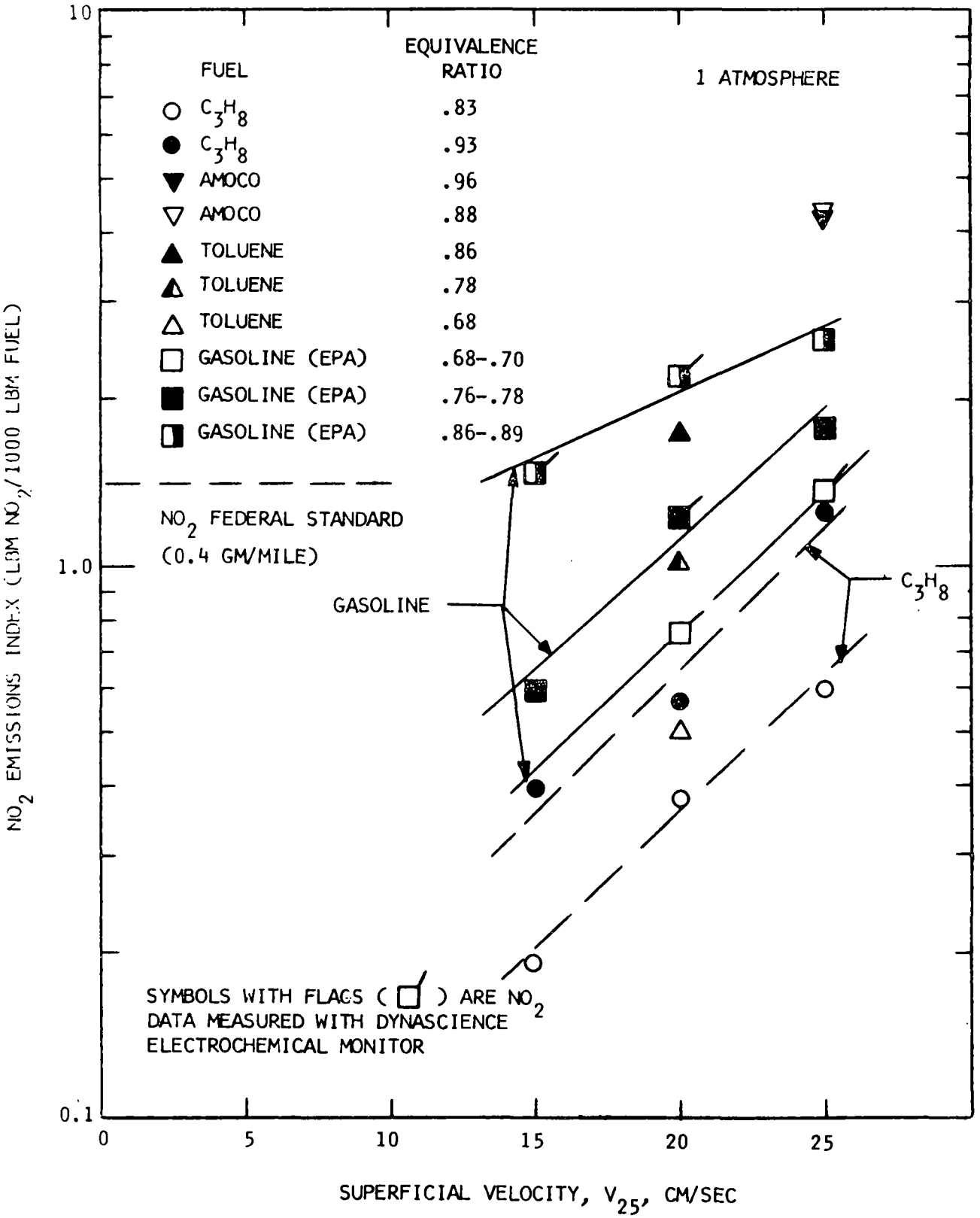

Figure 116. NO_2 Experimental Measurements on Water-Cooled Burners With 20 Milliseconds Residence Time

of air with propane and with prevaporized toluene, heptane and two gasolines were stabilized on a 30.3 in^2 water-cooled porous copper burner. Burned gas temperature as a function of mixture mass velocity and equivalence ratio was determined for each fuel, and other related flame parameters were computed and summarized. The temperature was obtained either from direct thermocouple measurements or from the measured burner heat flux and a heat balance; when both were made on the same flame, they agreed well.

Determinations of NO_x, CO and hydrocarbons were made on probe samples with hot gas residence times up to about 20 millisec. Hydrocarbons were found to be <1 ppm and thus negligible from any flame examined ($R \leq 0.95$). The absolute concentration levels of carbon monoxide as measured are of doubtful significance, but the decay of [CO] from values much higher than equilibrium could be observed. The levels estimated for practical engine exhaust conditions are expected to be satisfactorily lower.

From the measured NO_x concentrations, the rate of the thermal or hot-air formation of NO in the burned gas was estimated and correlated with the measured burned-gas temperatures. It was compared with the prediction from accepted kinetic data, with the assumption that $[O] = [O]_{equ}$; the measured rates are all higher than predicted, and for the fuels of higher molecular weight, by about an order of magnitude at all observed temperatures (3240°R-3780°R).

It is concluded that the average [O] must correspondingly exceed $[O]_{eq}$ and the probable connection between this excess and [CO] is discussed.

REFERENCES

(1) Amann, C.A., W.R. Wade, and M.K. Yu. Some Factors Affecting Gas Turbine Passenger Car Emissions. SAE Paper 720237. 1972.

(2) Wade, W.R., P.I. Shen, C.W. Owens, and A.F. McLean. Low Emissions Combustion for the Regenerative Gas Turbine: Part 1 - Theoretical and Design Considerations. ASME Paper 73-GT-11. 1973.

(3) Azelborn, N.A., W.R. Wade, J.R. Secord, and A.F. McLean. Low Emissions Combustion for the Regenerative Gas Turbine: Part 2 - Experimental Techniques, Results, and Assessment. ASME Paper 73-GT-12. 1973.

(4) Wohl, K. Quenching, Flashback, Blow-off - Theory and Experiment. Fourth Symposium on Combustion. 1953. p. 68-89.

(5) Botha, J.P. and D.B. Spalding. The Laminar Flame Speed of Propane Air Mixtures with Heat Extraction from the Flame. Proc. Roy. Soc. (London). A225; 71-96, 1954.

(6) Kaskan, W.E. The Dependence of Flame Temperature on Mass Burning Velocity. Sixth Symposium on Combustion. 1957. p. 134-143.

(7) Fenimore, C.P. Formation of Nitric Oxide in Premixed Hydrocarbon Flame. Thirteenth Symposium on Combustion. 1970. p. 373-380.

(8) Barnett, H.C. and R.R. Hibbard, (ed.). Basic Considerations in the Combustion of Hydrocarbon Fuels with Air. NACA Report 1300. 1957. p. 135.

(9) Schneider, P.J. Conduction Heat Transfer. Addison-Wesley, 1955. p. 218-221.

(10) Barnett, H.C. and R.R. Hibbard, (ed.). Basic Considerations in the Combustion of Hydrocarbon Fuels with Air. NACA Report 1300. 1957. p. 1-31.

(11) Wukusick, C.S. and J.F. Collins. An Iron-Chromium-Aluminum Alloy Containing Yttrium. Materials Research and Standards. December 1964.

(12) Cundiff, J.W. Superalloy Improves Anti-Smog Devices for Autos. Metal Progress. September 1972.

(13) Madsen, P. and R.M. Rusnak. Oxidation Resistant Porous Material for Transpiration Cooled Vanes. NASA CR-1999. 1972.

(14) Adamsky, R.F. Oxidation of Silicon Carbide in the Temperature Range 1200°F to 1500°F. J. Physical Chemistry. 63: 305-307. 1959.

(15) Jorgensen, P.J., et al. Oxidation of Silicon Carbide. J. Am. Cer. Soc. 42: 613-616. 1959; Effects of Oxygen Partial Pressure on the Oxidation of Silicon Carbide. J. Am. Cer. Soc. 43: 209-212. 1960.

(16) Automobile Gas Turbine-Optimum Cycle Selection Study. General Electric Report GESP 730 FS. June 1972.

(17) Fenimore, C.P. Formation of Nitrogen Oxides from Fuel Nitrogen in Ethylene Flames. Combustion and Flame, 19: 289. 1972.

(18) Siegler, M. and G.E. Moore. Flame Recombination of Oxygen and Hydrogen. Chem. Engrg. Prog. Symp., 66:1. 1970.

(19) U.S. Patent 3,589,184 (1971) (Continuous Flow Gas Calorimeter). G.E. Moore.

(20) U.S. Patent 3,672,839 (1972) (Exothermic Gas Generator). G.E. Moore.

(21) Bahr, D.W. Evaporation and Spreading of Iso-octane Sprays in High Velocity Air Streams. NACA-RME 531.14. November 1953.

(22) Oxides of Nitrogen in Gaseous Combustion Products (Phenoldisulfonic Acid Procedure). ASTM Test Method Specifications Designation D-1608-GO, reapproved 1967.

(23) Halpern, C. and F.W. Ruegg. A Study of Sampling of Flame Gases. J. Res. NBS, 60: 29-37. 1958.

(24) Fremont, H.A. et al. Properties of Combustion Gases - System C_nH_{2n}-Air. General Electric Co., Cincinnati, Ohio. 1955 and Kutzko, G.G. Properties of Combustion Gas-System CH_4-Air. General Electric Company. R68AEG161. 1968.

(25) Fristrom, R.M. and A.A. Westenberg. Flame Structure. McGraw-Hill, 1965. p. 22-23.

(26) Williams, G.C., A.F. Sarofim, and N. Lambert. Nitric Oxide Formation and Carbon Monoxide Burnout in a Compact Steam Generator. Symp. on Emissions from Continuous Combustion Systems. Plenum Press, 1972. p. 141.

(27) Schott, G.L. Comments on Article by Robert F. Sawyer and Trilochan Singh. Co-reactions in the Afterflame Region of Ethylene/Oxygen Ethane/Oxygen Flames. Thirteenth Symposium on Combustion. 1970. p. 403-415.

(28) Fenimore, C.P. Chemistry in Premixed Flames. Macmillan, 1964.

(29) Kaskan, W.E. Excess Radical Concentrations and the Disappearance of Carbon Monoxide in Flame Gases from Some Lean Flames. Combustion and Flame (London). 3:49-60. 1959.

(30) Kaskan, W.E. The Source of the Continuum in Carbon Monoxide-Hydrogen-Air Flames. Combustion and Flame (London). 3:39-48. 1959.

APPENDIX A

COMBUSTOR TEST FACILITY

The combustor test facility is located in the Gas Dynamic Facility No. 1 of Bldg. D and is shown in simplified schematic form in Figure A-1

The facility was designed for 1/5th or full scale automotive gas turbine combustor testing. The design criteria are as follows:

1. Primary Air Flow 0.031 - 0.4 pps to 400°F
2. Secondary Air Flow .75 - 2.25 pps to 1400°F
3. Fuel Flow (Gasoline) - 6 lb/hr to 75 lb/hr ambient temperature

The plant air supply (100 psig) is fed through a filter from which it is split to provide air to both the primary and secondary flow metering stations. Pressure regulating valves ahead of the metering tubes (sharp edge orifice type) control the orifice upstream pressures. The primary metering system consists of three orifice metering tubes in parallel to cover the 13:1 flow range required. Remote operated pneumatic actuated valves are used to direct air flow through the proper orifice. A down stream flow control valve can be used in conjunction with the combustor back pressure valve to control combustor pressure and primary air flow. Shown in Figure A-2 are the test cell flow metering sections and the primary and secondary flow heaters.

The primary heater is electrically powered from an adjacent substation. The power control system consists of ignitions with firing rate varied to control voltage and current to the resistance type air heaters.

The secondary air system is basically the same as the primary, how-

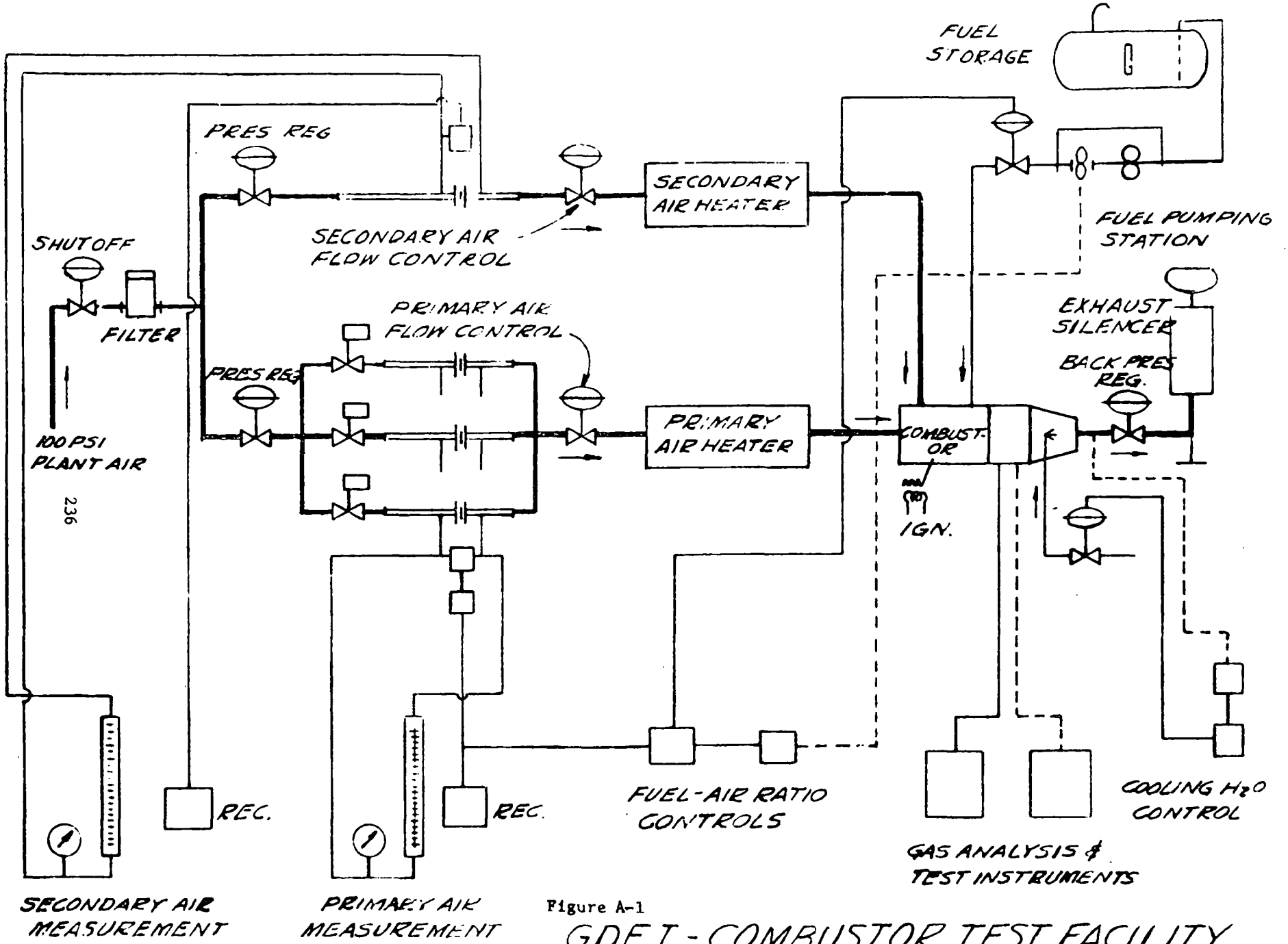

Figure A-1

GDFI - COMBUSTOR TEST FACILITY

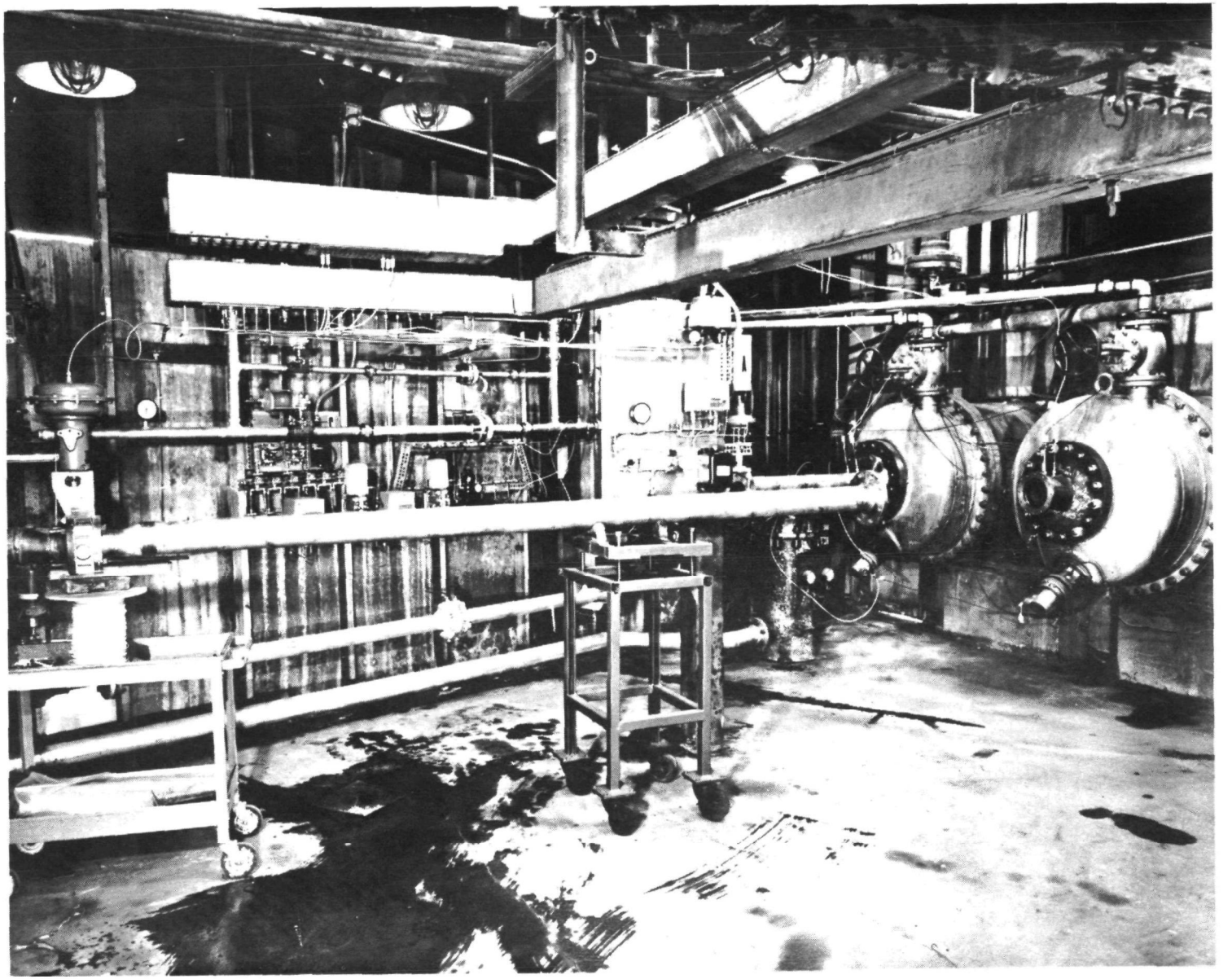

Figure A-2. Test Cell Heaters and Flow Metering Sections

ever only one orifice metering station is required to cover the air flow range.

Cooling water is injected into the combustor discharge gas stream prior to entering the butterfly type back pressure valve. Water flow is automatically controlled to maintain a maximum temperature of 500°F entering the back pressure valve. An exhaust silencer discharges the gases and water vapor vertically to the atmosphere.

The fuel system consists of a 250 gallon storage tank equipped with a float for level indication and located outside of the test area. A small motor driven gear type pump with pressure regulating valve and by-pass return to the tank is located adjacent to the storage tank. Fuel is fed into the test cell to a control station where a remote operated valve controls the flow to the combustor. A turbine type flowmeter senses fuel flow. Shown in Figure A-3 is the fuel storage and pumping system.

The control room houses all controls and instrumentation. Operation is controlled completely from the control consoles in this area. Shown in Figures A-4 and A-5are the heater and facility control consoles respectively. All pertinent parameters are indicated and if necessary recorded. An automatic fuel-air ratio control system is capable of holding a constant fuel-air ratio over a range of primary air flows. The ratio type system also allows changes in the fuel-air ratio to be made. The system will then hold the new fuel-air ratio over a range of air flows.

To operate a combustor of the 1/5th scale size, the inner valves of pressure regulating and control valves are changed and smaller orifice plates are installed in the flow metering tubes. The turbine type fuel flow sensor is also replaced with a smaller unit. The portable Scott Research Laboratory Inc. Model 108H Dilute Exhaust Gas Analysis System

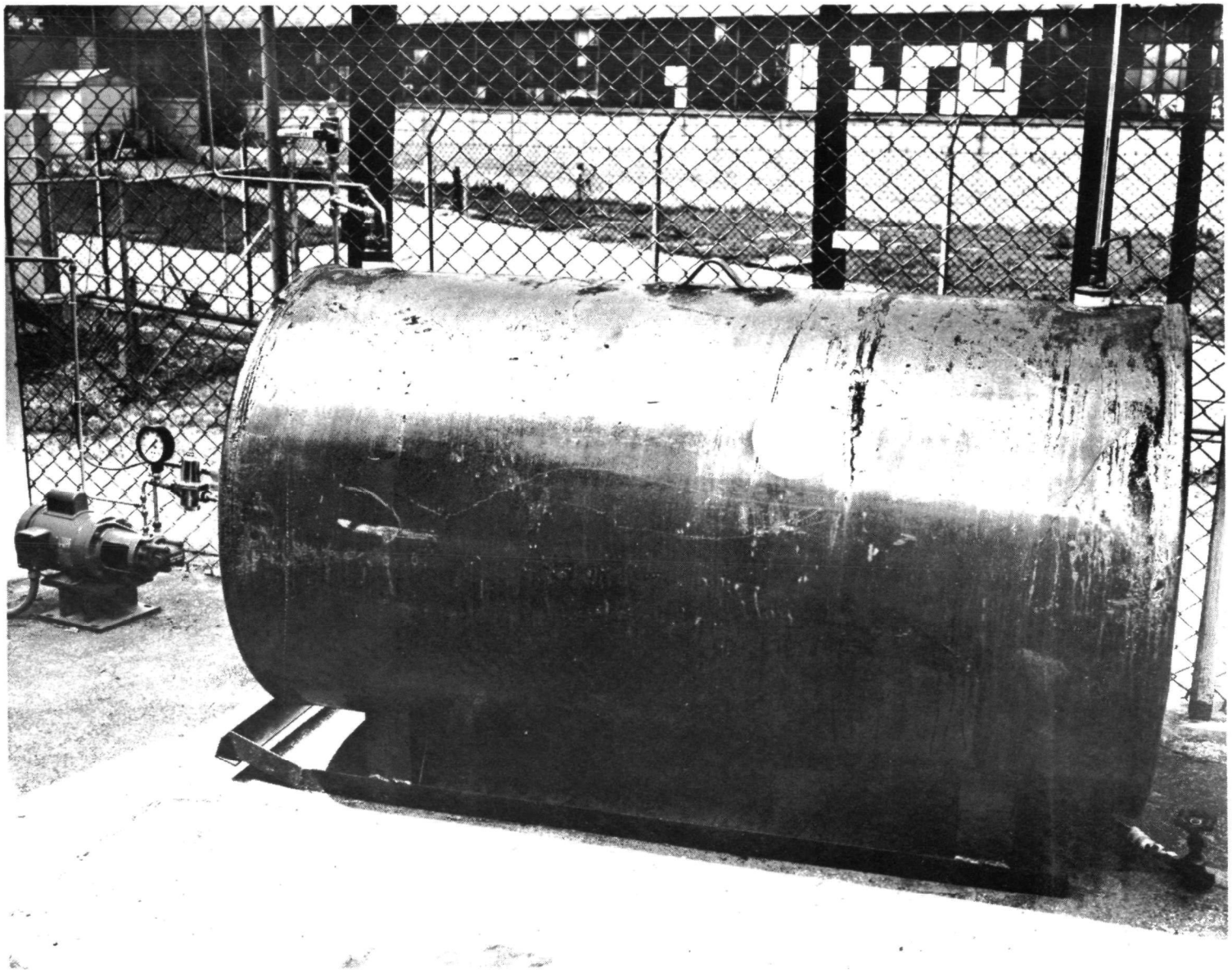

Figure A-3. Fuel Storage and Pumping

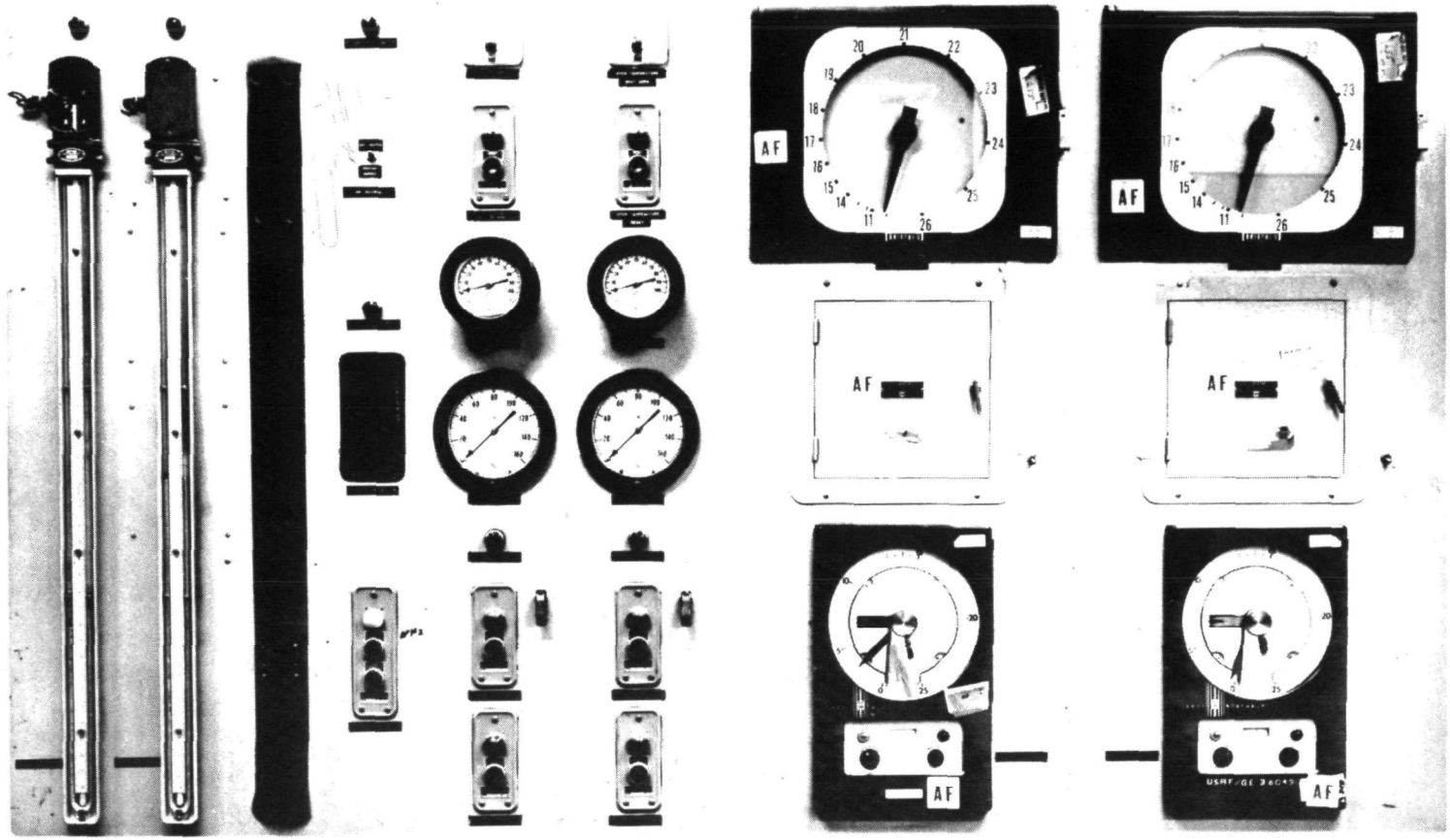

Figure A-4. Heater Control Console

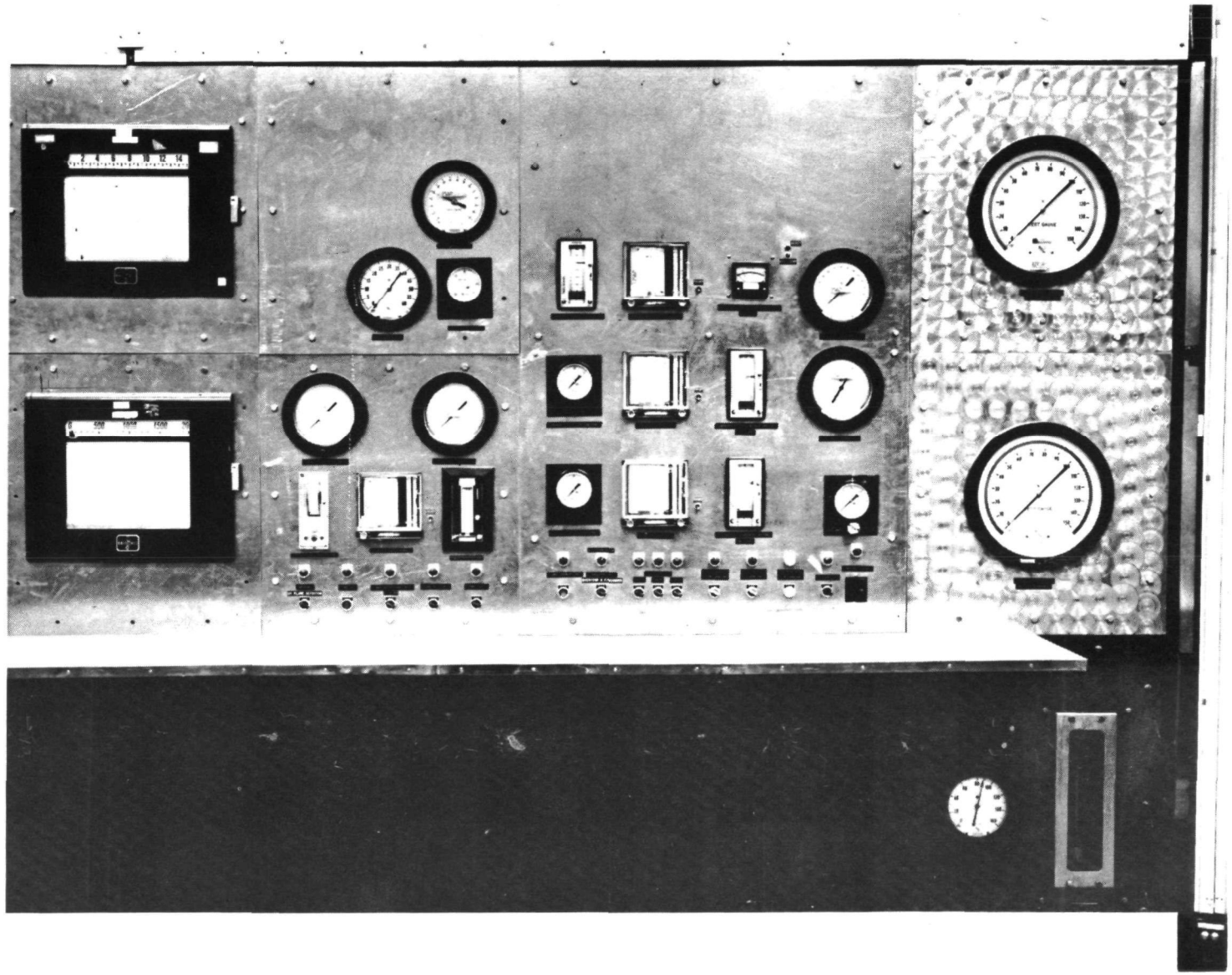

Figure A-5. Facility Control Console

purchased by General Electric shown in Figure A-6 is available for use in the Gas Dynamic Facility No. 1 (GDF-I). It has provisions for measuring NO, NO_2, CO, CO_2, O_2 and total hydrocarbon emissions.

The facility has been given a mechanical checkout. Both heater units have been tested and operate satisfactorily. A complete checkout will be made after the installation of a combustor.

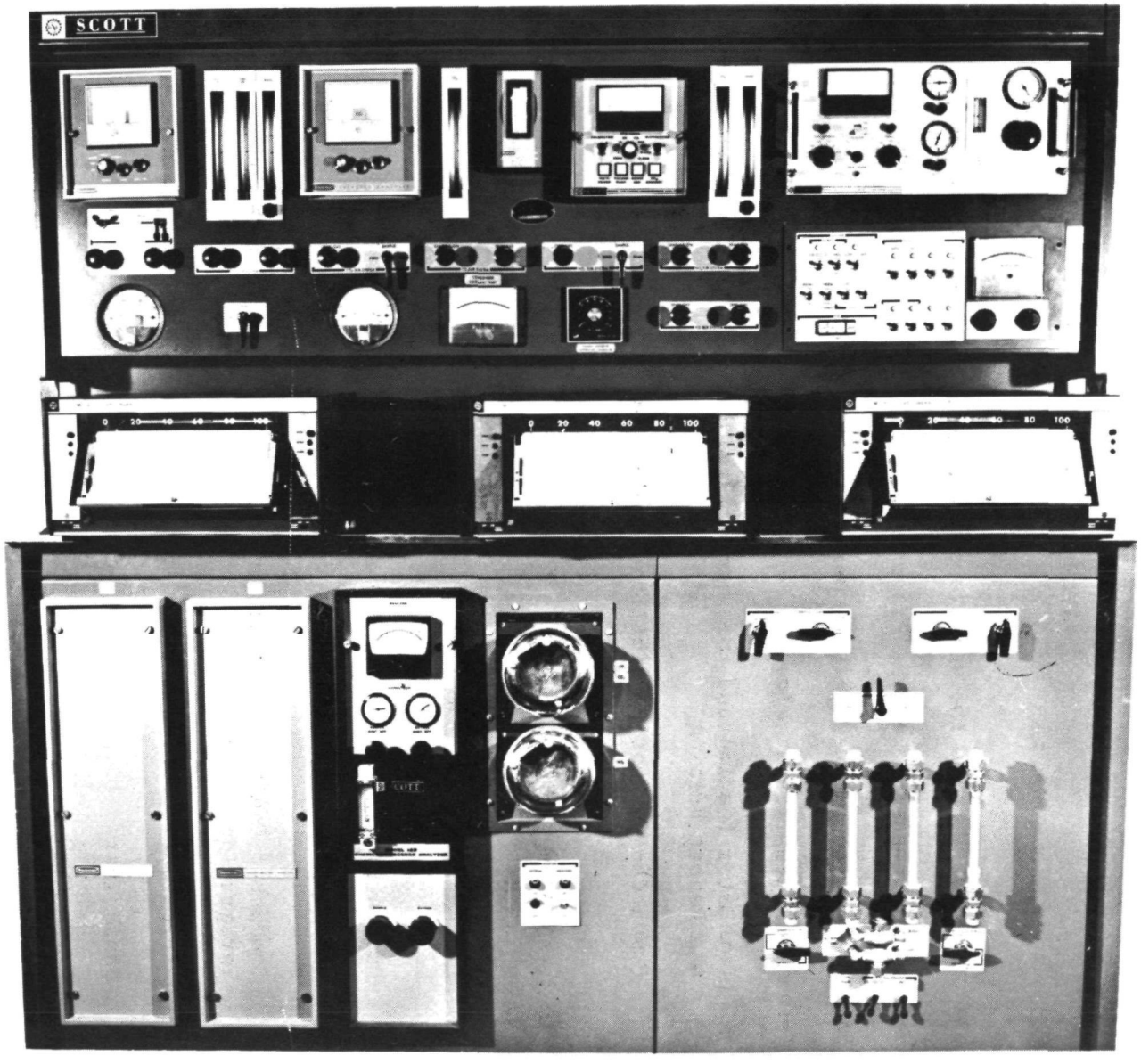

Figure A-6. Scott Exhaust Gas Analyzer

ACKNOWLEDGEMENT

Contributions to the work reported herein were made by a number of people in the Energy Systems Programs and the Corporate Research and Development components of the General Electric Company. The main contributions are listed below:

Combustor Loading and Emission Analysis and Report Editing	C.W. Deane
Combustor Concept Feasibility Development	J.A. Bond G.C. Wesling
Testing Operations	R.A. Fuller H. Bradley
Fuel-Air Mixture Supply Development	J.A. Bond B.L. Moor
Porous Plate Combustor Fabrication Development	R.G. Frank J.F. White J.F. Collins
Combustor Configuration and Engine Integration Design	A.W. Schnacke
Preliminary Burner-Vapor Generator Design	J.R. Peterson
Bench Tests	G.E. Moore B.E. Gans

These contributions are gratefully acknowledged.

The contributions to the program by T.S. Mroz and W.C. Cain, the EPA Project Officers are also gratefully acknowledged.

TECHNICAL REPORT DATA
(Please read Instructions on the reverse before completing)

1. REPORT NO. EPA-460/3-73-001	2.	3. RECIPIENT'S ACCESSION NO.
4. TITLE AND SUBTITLE Development of Low Emission Porous-Plate Combustor for Automotive Gas Turbine and Rankine Cycle Engines		5. REPORT DATE September 1973
		6. PERFORMING ORGANIZATION CODE
7. AUTHOR(S) Richard J. Rossbach		8. PERFORMING ORGANIZATION REPORT NO.
9. PERFORMING ORGANIZATION NAME AND ADDRESS General Electric Company, Energy Systems Programs, P. O. Box 15132, Cincinnati, Ohio 45215		10. PROGRAM ELEMENT NO.
		11. CONTRACT/GRANT NO. 68-01-0461
12. SPONSORING AGENCY NAME AND ADDRESS U.S. ENVIRONMENTAL PROTECTION AGENCY, Office of Air and Water Programs, Alternative Automotive Power Systems Division, Ann Arbor, Michigan 48105		13. TYPE OF REPORT AND PERIOD COVERED
		14. SPONSORING AGENCY CODE

15. SUPPLEMENTARY NOTES

16. ABSTRACT

The purpose of this contract was to evaluate analytically and experimentally the use of the porous-plate combustor for use in the gas-turbine or Rankine-cycle advanced automobile engines to control exhaust emissions. As regards the gas turbine application, this report contains analytical results on the burner area requirements for the various operating conditions of the Baseline Engine as well as exhaust emission predictions. The design concept of an air-cooled, variable-area combustor for this engine is presented. Operational and emissions data on several experimental combustors are presented along with the fabrication development leading to these combustors. Finally the demonstration results for a full-scale fuel-air mixture system are presented. With regard to the automotive Rankine engine application, heat load and emissions data are presented for propane and four liquid fuels. Although the fuel-air mixture system developed for the gas turbine combustor is directly applicable, alternate systems were investigated. Finally recommendations for the development of both gas turbine and Rankine combustors are presented.

17. KEY WORDS AND DOCUMENT ANALYSIS

a. DESCRIPTORS		b. IDENTIFIERS/OPEN ENDED TERMS	c. COSATI Field/Group
Air pollution	Hydrocarbons	Porous plate combustor	
Development	Carbon monoxide	Burner-vapor generator	13B
Combustion chamber	Propane	Fuel atomizer	21B
Automotive engines	Gasoline		21E
Rankine cycle	Nichrome		
Fabrication	Oxides of nitrogen		
Exhaust emissions			

18. DISTRIBUTION STATEMENT Unlimited	19. SECURITY CLASS *(This Report)* Unclassified	21. NO. OF PAGES 254
	20. SECURITY CLASS *(This page)* Unclassified	22. PRICE

EPA Form 2220-1 (9-73)